

MICROFACIES ANALYSIS OF THE EOCENE ÇAYRAZ FORMATION
(HAYMANA BASIN, TURKEY): RESPONSE OF BENTHIC
FORAMINIFERAL COMMUNITIES
TO SEDIMENTARY CYCLICITY

THESIS SUBMITTED TO
THE GRADUATE SCHOOL OF NATURAL AND APPLIED SCIENCES
OF
MIDDLE EAST TECHNICAL UNIVERSITY

BY

NİLYA BENGÜL

IN PARTIAL FULFILLMENT OF THE REQUIREMENTS
FOR
THE DEGREE OF MASTER OF SCIENCE
IN
GEOLOGICAL ENGINEERING

AUGUST 2022

Approval of the thesis:

**MICROFACIES ANALYSIS OF THE EOCENE ÇAYRAZ FORMATION
(HAYMANA BASIN, TURKEY):
RESPONSE OF THE BENTHIC FORAMINIFERAL COMMUNITIES TO
SEDIMENTARY CYCLICITY**

submitted by **NİLYA BENGÜL** in partial fulfillment of the requirements for the degree of **Master of Science in Geological Engineering Department, Middle East Technical University** by,

Prof. Dr. Halil Kalıpçılar
Dean, Graduate School of **Natural and Applied Sciences** _____

Prof. Dr. Erdin Bozkurt
Head of Department, **Geological Engineering** _____

Prof. Dr. Sevinç Altıner
Supervisor, **Geological Engineering, METU** _____

Examining Committee Members:

Prof. Dr. Muhittin Görmüş
Geological Engineering, Ankara University _____

Prof. Dr. Sevinç Altıner
Geological Engineering, METU _____

Prof. Dr. İsmail Ömer Yılmaz
Geological Engineering, METU _____

Assoc. Prof. Dr. Ayşe Özdemir
Geological Engineering, Van Yüzüncü Yıl University _____

Assoc. Prof. Dr. Fatma Toksoy Köksal
Geological Engineering, METU _____

Date: 31.08.20

I hereby declare that all information in this document has been obtained and presented in accordance with academic rules and ethical conduct. I also declare that, as required by these rules and conduct, I have fully cited and referenced all material and results that are not original to this work.

Name, Surname: Nilya Bengül

Signature:

ABSTRACT

MICROFACIES ANALYSIS OF THE EOCENE ÇAYRAZ FORMATION (HAYMANA BASIN, TURKEY): RESPONSE OF BENTHIC FORAMINIFERAL COMMUNITIES TO SEDIMENTARY CYCLICITY

Bengül, Nilya
Master of Science, Geological Engineering
Supervisor: Prof. Dr. Sevinç Özkan Altner

August 2022, 170 pages

The Haymana Basin in central Anatolia (Turkey) formed during the closure of the Neo-Tethys in the Late Cretaceous to Middle Eocene as a forearc accretionary wedge. Middle Eocene aged units in this basin are exposed near Çayraz Village, Haymana. The Çayraz Formation is represented by the package of nummulitic banks and intercalation of calcareous mudstones. The aim of this study to investigate the sedimentary cyclicity and depositional sequences in the Eocene successions of the Haymana Basin. To be able to achieve this objective, the stratigraphic section has been measured. Detailed microfacies analyses of the carbonate succession have been carried out to determine the depositional model of the formation. The data indicate a ramp type depositional model. Fossil assemblages have been determined. These fossils are mainly larger benthic foraminifers; *Nummulites* sp., *Assilina* sp. and *Alveolina* sp., *Orbitolites* sp., *Discocyclina* sp.. Their relative abundances have been analyzed to determine their responses to cyclicity. The fossil associations in the depositional environment, have been used in vertical changes of the facies as in the lateral relationship of the facies. Thus, cyclic relationships in the stratigraphic sequence have been determined. A total of 21 cycles have been determined. A total of

seven boundaries, two possible and five type-2, have been determined and six sequences have been recognized. The age of the stratigraphic sequence has been assigned as Early-early Middle Eocene. The age data has been used for the correlation of the sequence boundaries with the eustatic sea-level curve. The difference between sequence boundaries and the eustatic curve of might have resulted from tectonic activities.

Keywords: Larger Benthic Foraminifera, Microfacies, Cyclicity, Sequence stratigraphy, Eocene Çayraz Formation, Haymana Basin

ÖZ

EOSEN ÇAYRAZ FORMASYONUNUN (HAYMANA HAVZASI, TÜRKİYE) MİKROFASİYES ANALİZİ: BENTİK FORAMİNİFER TOPLULUKLARININ TORTUL DÖNGÜSELLİĞE TEPKİSİ

Bengül, Nilya
Yüksek Lisans, Jeoloji Mühendisliği
Tez Danışmanı: Prof. Dr. Sevinç Altıner

Ağustos 2022, 170 sayfa

İç Anadoludaki (Türkiye) Haymana Havzası Neo-Tethysin kapanması sırasında Geç Kratese ve Orta Eosen döneminde yay önu yığışım kaması olarak oluşmuştur. Orta Eosen yaşlı birimler Haymana, Çayraz köyü yakınlarında yüzeylemektedir. Çayraz Formasyonu Nummulitli bant paketleri ve aralarına giren kalkerli çamurtaşlarıyla temsil edilmektedir. Bu çalışmanın amacı Haymana havzasının Eosen çökellerinin çökelim sekanslarını ve sedimanter döngüsellığı incelemektir. Bu hedefe ulaşmak için stratigrafik kesit ölçülmüştür. Detaylı mikrofasiyes analizleri karbonat çökellerinde detaylı yapılarak çökeltme modeli belirlenmiştir. Data rampa tipi çökeltme modeli göstermektedir. Fosil toplulukları belirlenmiştir. Bu fosiller başlıca iri bentik foraminiferlerdir; *Nummulites* sp., *Assilina* sp. ve *Alveolina* sp, *Orbitolites* sp., *Discocyclina* sp.. Bunların göreceli çoklukları incelenmiş ve döngüsellığı tepkileri belirlenmiştir. Fosillerin birlirleriyle ilişkileri ve bunların gösterdiği ortamlar yanall fasiyes değışimlerinde kullanıldığı gibi dikey fasiyes ilişkilerinde de

kullanılabilmektedir. Böylelikle, stratigrafik sekansta döngüsel ilişkiler belirlenmiştir. Toplamda 21 döngü belirlenmiştir. Toplamda yedi, iki olası ve beş tip-2 sınırı belirlenmiştir ve altı sekans tanınmıştır. Stratigrafik sekansın yaşı Erken- erken Orta Eosen olarak atanmıştır. Bu yaş datası sekans sınırlarının östatik deniz seviyesi eğrisi ile korelasyonu için kullanılmıştır. Sekans sınırlarının östatik eğri ile arasındaki fark tektonik aktiviteler sonucu oluşmuş olabilir.

Anahtar Kelimeler: İri Bentik Foraminifer, Mikrofasiyes, Döngüsellik, Sekans stratigrafisi, Eosen Çayraz Formasyonu, Haymana Havzası

*To my beloved mother Ragibe Arıcıođlu
and her childhood....*

ACKNOWLEDGEMENTS

First of all, I would like to express my gratitude to my supervisor Prof. Dr. Sevinç Altınler for her valuable support, guidance, advices and patience. I am also very grateful for the discussions and guidance, encouragement and support of Prof. Dr. Demir Altınler. Their lectures were very crucial for me while choosing this field of geology. They have been there whenever I felt in doubt; they supported and guided my work.

I am also grateful to Assoc. Prof. Dr. Ayşe Özdemir for her guidance, support and advices.

I would like to express my gratitude to my dear friend and also our research assistant Gamze Tanık for her helps in fieldwork, and support throughout this thesis work. I would like to thank our research assistant Serdar Görkem Atasoy for his support and responding my questions.

I would like to thank to Mr. Orhan Kahraman for the preparation of thin section samples in Sample Preparation Laboratory, and Gonca Alptekin for her helps in Analytical Chemistry Laboratory.

I would like to thank to my friends, Tekin Tekik, Hazal Güldür, Tuğçe Uçar, Zeynep Dayıoğlu, Yalınçe Lal Dikmenli, Ali Uygur Karabeyoğlu, Akın Çil, Meryem Dilan İnce Özkan, Ezgi Vardar, Zeynep Seda Eren Özmen, Can Özmen, Özgün Andaç Doğan, Mufide Ceren Erzin, Nergis Nevra Akalın Yalçın, Aytuğ Meriç, and Orkan İbrahimov for their friendship , support and encouragement and being my side with their tactful actions. I am grateful to them all.

I am also grateful to beloved Tutku Ayata for his helps in fieldworks, support and encouragement and being my side all the time.

At last but not least, I would like to thank to my mother Ragibe Arıcıoğlu for her endless support and encouragement, and my beloved grandmother Aysel Arıcıoğlu for just being there to be my idol, to my dear aunts Gülbahar Hepsağ and Güler Arıcıoğlu

and to my dearest uncle Ahmet Arıcıođlu for their support and to my beloved sister Yasmin Bengül that i would like to thank for being on my side all the time, encouragements and taking care of our family's beloved dog Floki when i needed .

TABLE OF CONTENTS

ABSTRACT.....	v
ÖZ.....	vii
ACKNOWLEDGEMENT.....	x
TABLE OF CONTENTS.....	xii
LIST OF TABLES.....	xv
LIST OF FIGURES.....	xvi
LIST OF ABBREVIATIONS.....	xxi
CHAPTERS	
1. INTRODUCTION.....	1
1.1. Purpose and Scope.....	1
1.2. Geographic Setting of the Study Area.....	3
1.3 Method of the Study.....	9
1.4. Previous Works.....	21
1.5. Regional and Geological Setting.....	26
2. STRATIGRAPHY.....	33
2.1. Lithostratigraphy.....	33
2.1.1. Çayraz Formation.....	33
2.1.1.1 The measured section of the Çayraz Formation.....	39
3. MICROFACIES.....	51
3.1. Microfacies Types.....	52
Lagoon Facies.....	60
3.1.1 MF1, Miliolinid, alveolinid, orbitolitid, bioclastic packstone.....	60
3.1.2 MF2, Orbitolitid, alveolinid, miliolinid, bioclastic packstone to wackestone.....	62
3.1.3 MF3, Nummulitid, alveolinid, miliolinid, bioclastic packstone to wackestone.....	63
3.1.4 MF4, Nummulitid, orbitolitid, bioclastic packstone to grainstone.....	64
Shoal Facies.....	65
3.1.5 MF5, Nummulitid, assilininid, bioclastic packstone.....	65
3.1.6 MF6, Nummulitid, discocyclinid, assilininid, bioclastic packstone.....	66
3.1.7 MF7, Assilininid, nummulitid, bioclastic packstone to grainstone.....	67

3.1.8 MF8, Discocyclinid, nummulitid, assilinid, planktonic foraminiferal, bioclastic packstone to wackestone.....	68
Shallow open marine facies	70
3.1.9 MF9, Discocyclinid, nummulitid, bioclastic grainstone	70
3.1.10. MF10, Discocyclinid, nummulitid, planktonic foraminiferal, bioclastic packstone ..	71
3.1.11 MF11 Grainstone	73
3.1.12 MF12 Small benthic foraminiferal, planktonic foraminiferal wackestone	74
3.1. 6. Microfacies and Depositional Environment.....	74
3.2. Microfacies Analyses dependent on fauna relationship.....	83
3.2.1 Foraminiferal Assemblages used in the detection of the fossil associations.....	83
<i>Nummulites</i> sp. Lamarck, 1801.....	84
<i>Assilina</i> sp. d'Orbigny, 1839	86
<i>Discocyclina</i> sp. Gumbel 1870	87
<i>Alveolina</i> sp. d'Orbigny, 1826.....	89
Miliolid	90
<i>Orbitolites</i> sp. Lamarck, 1801	92
Coralline Red Algae.....	94
3.3 Bio-associations	96
Bio-association A.....	96
Bio-association B	96
Bio-association C.....	96
Bio-association D.....	97
Bio-association E	97
Bio-association F	97
Bio-association G.....	97
Bio-association H.....	98
Bio-association I	98
4. SEQUENCE STRATIGRAPHY	101
4.1. Historical Background of Sequence Stratigraphy	101
4.2. Meter-scale shallowing upward cycles (Parasequences)	101
4.1.1. Types of shallowing upward cycles (Parasequences)	102
4.1.1.1 A-Type Cycles	102
4.1.1.2 B-Type Cycles	108

4.1.1.3 C-Type Cycles	109
4.1.1.4 D-Type Cycles	111
4.1.1.5 E-Type Cycles.....	117
4.1.1.6 F-Type Cycles.....	118
4.1.1.7 G-Type Cycles	122
4.1.1.8 H-Type Cycles	124
4.2. Sequence Stratigraphic Interpretation.....	126
5. DISCUSSION AND CONCLUSION.....	135
REFERENCES	145
APPENDICES	157
A. PLATES	157
PLATE 1	157
PLATE 2	158
PLATE 3	159
PLATE 4	160
PLATE 5	161
PLATE 6	163
B. Stratigraphical distribution of fossil assemblages in the measured section.....	164
1. Stratigraphical & environmental distribution of fossil assemblages in the part of the measured from samples NB0 to NB7	164
2. Stratigraphical & environmental distribution of fossil assemblages in the part of the measured from samples NB-B-1 to NB-B-9.....	166
3. Stratigraphical & environmental distribution of fossil assemblages in the part of the measured from samples NB8 toNB43	167
4. Stratigraphical distribution of fossil assemblages throughout the measured section.....	170

LIST OF TABLES

TABLES

Table 1 Microfacies main groups, Determined microfaces and environment of deposition.	79
Table 1 (Continued) Microfacies main groups, Determined microfaces and environment of deposition.....	80
Table 2 GPS data of the measured section from sample NB1 to NB43, gathered from "BasicAirData GPS Logger" application.....	169

LIST OF FIGURES

FIGURES

Figure 1: Location map of the study area indicated by the blue rectangle, taken from Google Earth.....	4
Figure 2: Aerial photographs of the location of the study area (yellow-white rectangle shows the study area, yellow lines show the measured section parts) taken from Google Earth.	5
Figure 3: A) Çayraz Fm. and Eskipolatlı Fm., the white dashed line indicates an approximate boundary between formations. B) yellow rectangle: sampled lithology, NB0-6. NB2 and NB28 sample locations, white line: shows strata. C) Southeastward profile of the measured section, NB2, NB3, NB4 and NB4-A sample locations.	7
Figure 4: D) yellow line: limestone lithology. E) white line: sampling beds location of the samples NB33, NB34, NB35, NB36.....	8
Figure 5: Field photograph of the studied section with the labeling of the sample numbers of the limestone.	9
Figure 6: The positions of the limestone and sandstone samples that were collected during the first fieldwork phase. These samples are marked with green color.	11
Figure 7: The positions of the limestone and sandstone samples that were collected during the second fieldwork phase. These samples are marked with lilac color.....	12
Figure 8: The positions of the samples were collected during the third fieldwork phase. These samples are marked with pink color.....	14
Figure 9: The positions of the samples that were collected during the fourth fieldwork phase. These samples are marked with yellow color.	16
Figure 10: NB-A section part of the measured section. The positions of the samples that were collected during the fifth fieldwork phase. These samples are marked with orange color.	18
Figure 11: NB-A part the NB stratigraphic sequence	19
Figure 12: Image of the thin section preparation in the laboratory.....	20
Figure 13: Image of washing samples 250-106-63-micron meters fraction and planktonic foraminifera.....	21
Figure 14: Main tectonic units of Turkey and the location of the Haymana Basin (yellow star). Image modified after Okay and Tüysüz (1999).	26
Figure 15: Development of the Haymana Basin as a fore-arc position due to subduction of the Northern Branch of Neo-Tethys beneath the Pontides. Image modified after Okay and Altner (2016).....	27
Figure 16: Sketch cross section of the Haymana Basin (showing the lateral relationships of the same aged units) during the Maastrichtian, Lower Paleocene and Lower Eocene showing the paleogeographical setting (modified after Ünalan et al., 1976)	28
Figure 17: Geological map of the Haymana Region and location of the study area (red square) (Modified after 1/500.000 Map of MTA and Rojay 2013).	29

Figure 18: Generalized columnar section of the Haymana Basin modified from Ünalın et al. (1976) and Okay and Altınır (2016). (red line indicate the approximate location of the measured section covering the Çayraz Formation).....	30
Figure 19: Type locality of the Çayraz formation (NW of the Çayraz Village).	34
Figure 20: Generalized geological map of the Çayraz region with the subunits of the Haymana formation. (The red line shows the approximate location of the measured section, the white/blue rectangle shows the study area) (modified from Çiner, 1996).	35
Figure 21: Çayraz Formation presentation of the columnar and horizontal relationship between other lithostratigraphic units of Haymana Basin (Çiner et al., 1993)	38
Figure 22: Close up view of the study area taken from Google Earth with measured section indicated. NB section showed with yellow lines and NB-B section showed with blue lines	39
Figure 23: The Studied NB and NB-B Sections from the Çayraz Formation.....	41
Figure 24: Detailed columnar section showing the taken samples NB1, NB2, limestone samples and NB-A-2, NB-A-3, NB-A-4, NB-A-5, NB-A-6, NB-A-7, NB-A-8, NB-A-9, NB-A-10, NB-A-14, NB-A-15, NB-A-16, NB-A-17, NB2-14, NB2-15, NB2-16 mudstone samples' location from the measured section.	42
Figure 25: Detailed columnar section showing the taken samples NB3, NB4 location from the measured section.	43
Figure 26: Detailed columnar section showing the taken samples NB5, N6 and NB7 location from the measured section.	45
Figure 27: Detailed columnar section showing the taken samples NB8 and NB9 location from the measured section.	46
Figure 28: Detailed columnar section showing the taken samples NB10, NB11, NB12, NB13, NB14, NB15, NB16, NB17, NB18 and NB19 location from the measured section. .	47
Figure 29: Detailed columnar section showing the taken samples NB20, NB21, NB22, NB23, NB24, NB25 and NB26 location from the measured section.....	48
Figure 30: Detailed columnar sections showing the taken samples NB27, NB28, NB29, NB30, NB31 and NB32 location from the measured section.	49
Figure 31:Original, expanded and revised Dunham classification (Embry and Klovan , 1971) (The ones that were observed in the study have been indicated by red square) (gathered from Flügel, 2010).....	52
Figure 32: Folk's Textural Classification of Carbonate Sediments (The ones that were observed in the study have been indicated by red square) (Flügel,2010, after Folk,1959)....	53
Figure 33: Folk's Textural Classification of Carbonate Sediments (The one that was observed in the study have been indicated by red square) (Flügel,2010, after Folk,1959)....	53
Figure 34: Fossiliferous limestone classification after Dunham (1962) and Folk (1959, 1962). (The ones that were observed in the study have been indicated by red square) (gathered from Flügel, 2010)	54
Figure 35: Distribution of the Standard Microfacies (SMF) types in the Facies Zones (FZ) of the rimmed carbonate platform model (Flügel, 2010) (A: evaporitic, B: brackish). The ones that were observed in the study have been indicated by yellow highlights.	56
Figure 36: Generalized distribution of microfacies types in different parts of a homoclinal carbonate ramp (Flügel, 2010). The ones that were observed in the study have been indicated by yellow highlights.....	57

Figure 37: Early and Middle Eocene depositional platform model for large benthic foraminifera, and the distribution of the fossils over the platform (Flügel, 2010).....	58
Figure 38:Photomicrograph of MF1 (sample NB7).....	61
Figure 39: Photomicrograph of the MF1 (sample NB18).....	61
Figure 40: Photomicrograph of the MF2. (sample number NB31. N: <i>Nummulites</i> sp., R: Rotaliniid, O: <i>Orbitolites</i> sp., Alv: <i>Alveolina</i> sp., L: <i>Lockhartia</i> sp. E: Echinoid fragment.)	62
Figure 41: Photomicrograph of MF2 (sample number NB12. N: <i>Nummulites</i> sp., R: Rotaliniid, O: <i>Orbitolites</i> sp., M: Miliolinid, Alv: <i>Alveolina</i> sp. ,L: <i>Lockhartia</i> sp. E: Echinoid fragment, bf: benthic foraminifera, pf: planktonic foraminifera.)	63
Figure 42: Photomicrograph of the Microfacies 3 (sample NB32. A: <i>Assilina</i> sp., Alv: <i>Alveolina</i> , L: <i>Lochartia</i> sp., M: Milionid, N: <i>Nummulites</i> sp. O: <i>Orbitolites</i> sp., R: <i>Rotaliniid</i> .sp., T: <i>textularina</i> .)	64
Figure 43: Photomicrograph of the microfacies MF4. (sample NB9. A: <i>Assilina</i> sp.,bf: benthic foraminifera, D: <i>Discocyliina</i> sp., pf: planktonic foraminifera, N: <i>Nummulites</i> sp. O: <i>Orbitolites</i> sp., R: <i>Rotaliniid</i> .sp., L: <i>Lochartia</i> sp.).....	65
Figure 44: Photomicrograph of the MF5 (sample NB-B-7. MF7 A: <i>Assilina</i> sp., N: <i>Nummulites</i> sp.).....	66
Figure 45: Photomicrograph of the MF6 (the sample NB5. P: pelecypoda surrounded with calcite crystal, C:LCRA and CRA. N: <i>Nummulites</i> , A: <i>Assilina</i> sp., R: <i>Rotaliniid</i> , pf: Planktonic foraminifera, Di: <i>Ditrupa</i> sp., D: <i>Discocyliina</i> , C: Coralline Red Algae (CRA)).	67
Figure 46: Photomicrograph of the MF7. (the sample NB8. A: <i>Assilina</i> sp., C: Coralline Red Algae, N: <i>Nummulites</i> sp., R: Rotaliniid, sand grains).	68
Figure 47: Photomicrograph of the MF8 (the sample NB6. A: <i>Assilina</i> sp., C: LCRA, CRA. D: <i>Discocyliina</i> sp., N: <i>Nummulites</i> sp., pf: Planktonic Foraminifera, R: Rotaliniid. At upper right: <i>Assilina</i> sp. surrounded by CRA, At lower left : D surrounded by CRA).....	69
Figure 48: Photomicrograph of the MF8 (the sample NB2 , A: <i>Assilina</i> sp., Ac: <i>Actinocyliina</i> sp., D: <i>Discocyliina</i> sp., Di: <i>Ditrupa</i> sp., E: Echinoid plate, pf: Planktonic foraminifera, bf: Benthic foraminifera, N: <i>Nummulites</i> spp., C: Coralline Red Algae).	70
Figure 49: Photomicrograph of the MF9 (the sample NB4. MF11, A: <i>Assilina</i> sp.,B: Benthic foraminifera C: Rotaliniid,, D: <i>Discocyliina</i> sp., E: echinoid fragment, pf: planktonic foraminifera, N: <i>Nummulites</i> sp., P: pelecypods).	71
Figure 50: Photomicrograph of the MF10 (the sample NB1, D: <i>Discocyliina</i> sp., Di: <i>Ditrupa</i> sp. pf: Planktonic foraminifera, P: Pelecypods (Bivalve fragment), o: Ostracoda, bf: Benthic foraminifera, N: <i>Nummulites</i> spp., M: miliolid).	72
Figure 51: Photomicrograph of the Microfacies 11 (sample NB3, A & D: Broken benthic foraminifera fragment, B: echinoid spine, C: Rotaliniid, E: biserial.)	73
Figure 52: Determined RMF types in this study.	78
Figure 53: Early and Middle Eocene depositional platform model for large benthic foraminifera, and the distribution of the fossils over the platform (modified from Flügel, 2010). and determined bio-associations from this work (a, b, c, d, e, f, h, i). Microfacies distribution with bio-associations. The order of the list of fossil in the figure indicates the possibility of the occurrence in the depositional environment is high then the others. The	

preferences of the fossils are depending of the depositional environment condition. (BouDagher-Fadel, 2018a).	81
Figure 54: Composite depositional model of the studied area.	82
Figure 55: Thin section photomicrographs of <i>Nummulites</i> sp.. from sample NB5 (A:axial section; B: oblique section).....	85
Figure 56: Thin section photomicrograph of <i>Assilina</i> sp. from sample NB5 (axial section). 87	
Figure 57: Thin section photomicrograph of <i>Discocyclina</i> sp. from samples NB4 and NB5 (nearly axial / tangential sections)	88
Figure 58: Thin section photomicrograph of <i>Alveolina</i> sp.from sample NB 18 (oblique section).....	90
Figure 59: Thin section photomicrographs of miliolids from samples A&D: NB18, B&C:NB19 (A, B, C: equatorial sections; D: oblique section)	92
Figure 60: Thin section photomicrograph of <i>Orbitolites</i> sp.from sample NB19.	93
Figure 61: Thin section photomicrograph of CRA from samples NB5, NB17.....	95
Figure 62: Distribution of bio-associations in the studied samples.	99
Figure 63: A1 type cycle (Cycle 1) of the measured section and photomicrographs of microfacies deposited within this cycle.	104
Figure 64: A2 type cycle (Cycle 2) of the measured section and photomicrographs of microfacies deposited within this cycle.	105
Figure 65: A2 type cycle (Cycle 3) of the measured section and photomicrographs of microfacies deposited within this cycle.	105
Figure 66: A3 type cycle (Cycle 4) of the measured section and photomicrographs of microfacies deposited within this cycle.	106
Figure 67: A4 type cycle (Cycle 5) of the measured section and photomicrographs of microfacies deposited within this cycle.	106
Figure 68: A5 type cycle (Cycle 6) of the measured section and photomicrographs of microfacies deposited within this cycle.	107
Figure 69: A6 type cycle (Cycle 7) of the measured section and photomicrographs of microfacies deposited within this cycle.	107
Figure 70: B type cycle (Cycle 8) of the measured section and photomicrographs of microfacies deposited within this cycle.	108
Figure 71: C1 type cycle (Cycle 9) of the measured section and photomicrographs of microfacies deposited within this cycle.	110
Figure 72: C2 type cycle (Cycle 10) of the measured section and photomicrographs of microfacies deposited within this cycle.	111
Figure 73: D1 type cycle (Cycle 11) of the measured section and photomicrographs of microfacies deposited within this cycle.	113
Figure 74: D2 type cycle (Cycle 13) of the measured section and photomicrographs of microfacies deposited within this cycle.	114
Figure 75: D3 type cycle (Cycle 15) of the measured section and photomicrographs of microfacies deposited within this cycle.	115
Figure 76: D4 type cycle (Cycle 18) of the measured section and photomicrographs of microfacies deposited within this cycle.	116

Figure 77: D5 type cycle (Cycle 20) of the measured section and photomicrographs of microfacies deposited within this cycle.	116
Figure 78: E type cycle (Cycle 12) of the measured section and photomicrographs of microfacies deposited within this cycle.	117
Figure 79: F1 type cycle (Cycle 14) of the measured section and photomicrographs of microfacies deposited within this cycle.	120
Figure 80: F2 type cycle (Cycle 17) of the measured section and photomicrographs of microfacies deposited within this cycle.	121
Figure 81: G1 type cycle (Cycle 16) of the measured section and photomicrographs of microfacies deposited within this cycle.	123
Figure 82: G2 type cycle (Cycle 19) of the measured section and photomicrographs of microfacies deposited within this cycle.	123
Figure 83: H type cycle (Cycle 21) of the measured section and photomicrographs of microfacies deposited within this cycle.	125
Figure 84: Sequence Structure: TST: Transgressive System Tract, HST: Highstand System Tract, (SB: Generalized Measured Section and Interpreted Sequence Boundaries with MF	130
Figure 85: Generalized measured section showing sequence boundaries and comparison with Sneddan and Liu (2010) eustatic sea level curve.	133

LIST OF ABBREVIATIONS

ABBREVIATIONS

HST: Highstand System Tract

TST: Transgressive System Tract

mfs: Maximum flooding surface

SB: Sequence Boundary

MF: Microfacies

CRA: Coralline Red Algae

LBF: Large Benthic Foraminifera

LCRA: Later Stages of Coralline Red Algae

A: *Assilina* spp.

Ac: *Actinocyclus* sp.

Alv: *Alveolina* sp.

C: Coralline Red Algae

D: *Discocyclus* sp.

L: *Lockhartia* sp.

N: *Nummulites* spp.

M: *Miliolina* sp.

O: *Orbitolites* sp.

a: Agglutinated foraminifera (Agg)

bf: Benthic Foraminifera

pf: Planktonic Foraminifera

E: Echinodacea (plate or spine)

L: *Lockhartia* sp.

Di: *Ditrupa* sp

CHAPTER 1

INTRODUCTION

1.1. Purpose and Scope

Sedimentary cycles have been recognized in the field for centuries (e.g. Steno 1669-1916; de Maillet, 1748; Suess, 1888, 1906, 1918). It has been suggested that cycles of change in accommodation or sediment supply correspond to sequences in the rock record (Catuneanu, et al., 2011). The sequence stratigraphical approach is described originally as an unconformity bounded stratigraphic unit (Sloss et al., 1949; Sloss, 1963, Wheeler 1958, 1959 a, b, 1963). The concept was revised to include "a relatively conformable succession of genetically related strata bounded by unconformities or their correlative conformities" (Mitchum et al., 1977). It continued to develop in time from a concept to a method. In a series of publications in late 1970, Vail et al. established a revolutionary stratigraphic method of basin analysis for what became known as "sequence stratigraphy" (Vail et al., 1977a; Vail, 1987; Wagoner et al., 1987, 1988, 1990, 1991; Posamentier et al. 1988, 1992; Posamentier and Vail 1988; Posamentier and Allen, 1994; Catuneanu, 2006; Catuneanu, 2009). Subsequently, this method of stratigraphic analysis has developed into the fundamental approach for interpreting the distribution of the sediment bodies (Catuneanu, et al., 2011). The concepts of sequence stratigraphy apply to carbonate systems the same way as they do to siliciclastic systems (Sarg, 1988; Schlagher, 1993, 2002, 2005).

The idea that sea-level changes could be global was first proposed by Suess (1906). The eustatic control to the clastic depositions have been suggested by Vail et al., (1977b), Posamentier and Vail (1988) and Posamentier et al. (1988). There is a biotic response to sea-level change and cyclicity (Weber, 2001). Therefore, in carbonate systems either global or local relative sea-level changes control the carbonate deposition similarly to the clastic systems. On the carbonate platforms and ramps the

sediment supply is mainly controlled by the ecology of the carbonate producing organisms (Hottinger, 1998; Catuneanu et al, 2011). These organisms are affected by many parameters; such as water chemistry, sediment influx, light penetration depth, salinity, water temperature, dissolved oxygen and carbon dioxide level of the water, sea-level, etc... These parameters can be recorded locally and/or globally in scale in the rock record. The variations of these parameters control the diversity and density ratio of the biota of the strata, consequently the sedimentary sequences (Hallock, 1981; Hottinger, 1983, 1997; Reiss and Hottinger 1984; Hottinger, 1989; Hallock and Glenn 1986; Hottinger, 1998). One of the main carbonates producing organisms is benthic foraminifera including “larger benthic foraminifera” which have complicated internal structures. Since the benthic foraminifera lives either as attached to a substrate or free of any attachment on the sea floor, at all ocean depths they are very susceptible to sea-level change (BouDagher-Fadel 2018a, Flügel, 2010).

The main objective of this study is to delineate sequence boundaries and to define the types of shallowing upward meter-scale cycles in the studied units of the Çayraz Formation in the Haymana Basin in the Central Anatolia. The early- Middle Eocene aged Çayraz formation represents that one of the youngest marine succession of the Haymana Basin (Ünalán et al., 1976; Çiner, 1996). Since the Çayraz Formation is characterized by a continuous shallow marine carbonate sequence (Ünalán et al., 1976), it is mainly composed of large benthic foraminifera, which is an excellent environmental indicator. To achieve this main objective, the microfacies analysis has been carried out in order to determine the depositional environments of the samples collected from the Çayraz Formation in detail. One of the main tools to investigate sea-level changes is to determine the distribution of benthic foraminifers, in particular, larger benthic foraminifers. Based on these analyses, the sea-level changes have been recorded throughout the studied section, then the types of meter-scale cycles have been set and finally, the sequence boundaries have been delineated.

The Çayraz Formation is the youngest marine sequence deposited in the Haymana Basin. It is composed of two separate shelf systems, including coarsening-upward and shallowing-upward sequences recognized (Çiner et al, 1996a). The shelf systems are

determined as a lower shelf system and an upper shelf system with deep marine marl in between (Çiner et al., 1996a). These peritidal carbonate successions mainly composed of shallowing-upward cycles. In this study lower shelf of the Çayraz formation is studied based on the larger benthic foraminifera associations. The cycles are determined based on the field observations of the facies change and elaborated microfacies analysis in the laboratory. Microfacies studies are conducted for the purpose of determination of the depositional environment model. The depositional history of the studied section is constructed by examining the paleontological and sedimentological characteristics of these microfacies. The sequence boundaries are determined after that point, by using the microfacies study data's indicated environment of deposition, the major rock building fossils' preferred environment characteristics and the change of these parameters spatially. This study also aims to understand the controlling mechanism on the sea-level and the relative sea-level change whether is related to the eustacy or the tectonics. In order to do that, geological age control was made by using planktonic foraminiferal data (identified by Gamze Tanık) from the studied samples and from studies of Özcan et al. (2018, 2020), and Tanık (2017).

Finally, the sequence boundaries have been processed the geological time and compared with the global sea-level data by using the recently revised and modified chronostratigraphic eustatic sea-level chart (Snedden and Liu, 2011).

1.2. Geographic Setting of the Study Area

The study area is located 70 km southwest of Ankara in between the Yeşilyurt and Çayraz villages (Figure 1, Figure 2). It is approximately 2 km northeast of the Yeşilyurt village and 4 km northwest of the Çayraz village (Figure 2).

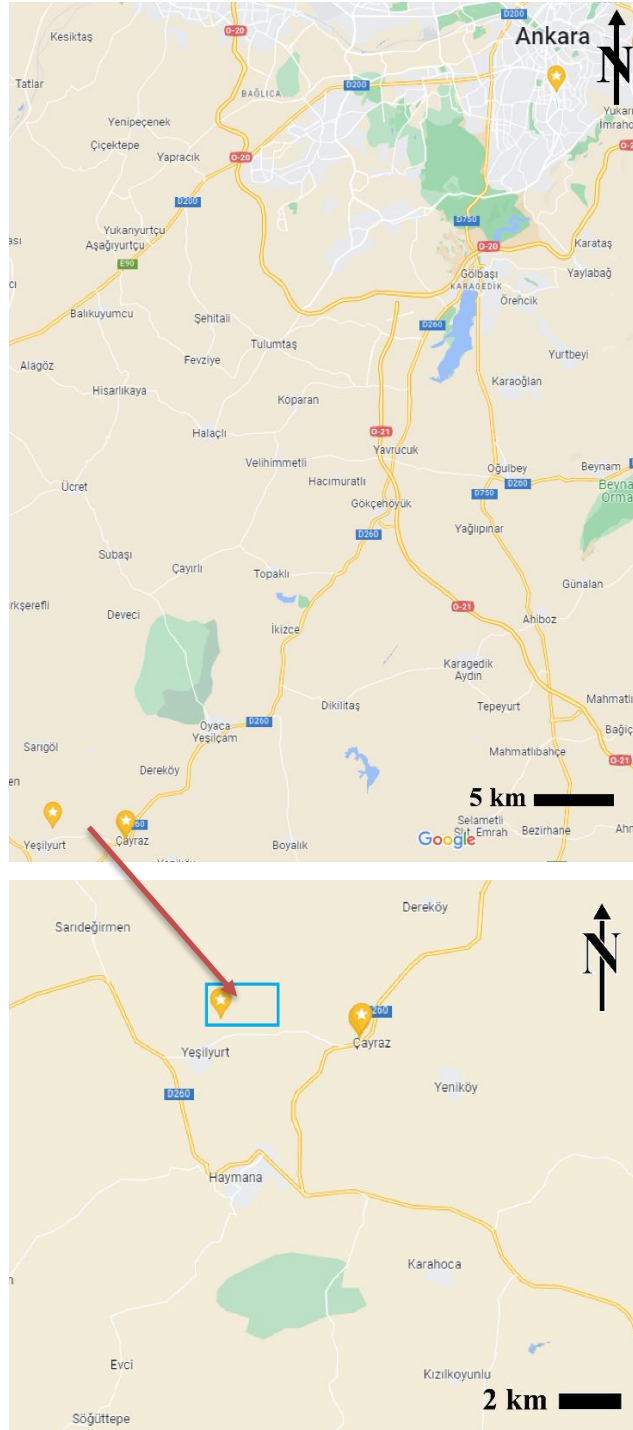


Figure 1: Location map of the study area indicated by the blue rectangle, taken from Google Earth.

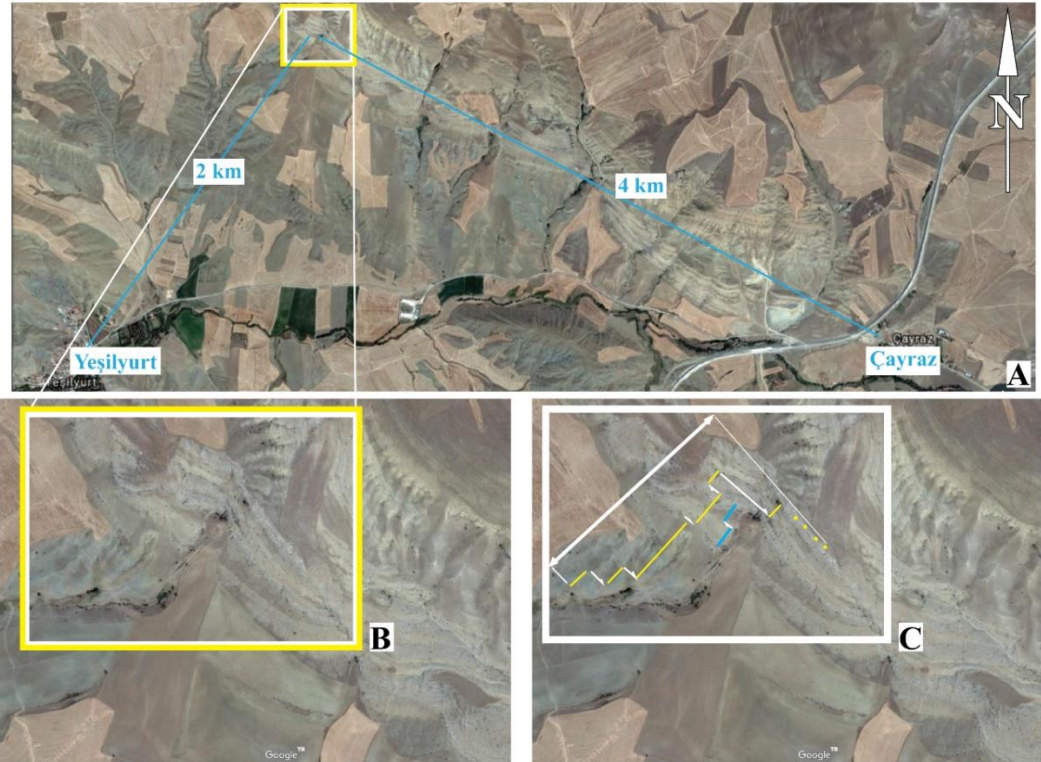


Figure 2: Aerial photographs of the location of the study area (yellow-white rectangle shows the study area, yellow lines show the measured section parts) taken from Google Earth.

The studied area was chosen since the lower shelf units of the Çayraz Formation are widely exposed. The section was measured from the first limestone bed in the monotonous fine-grained units of the underlying Eskipolatlı Formation to the top of the shelf with the stacking pattern of the limestone beds. The studied section was measured from the NW-SE trending hill. Measurement started at the SW side of the hill. It continued up to the top of the hill, and laterally shifting to the SE while tracing the strata.

In order to collect samples during the measurement of the sedimentary sequences, six planned fieldworks have been held along with several exploratory fieldwork. The GPS point data of the collected limestone and sandstone samples are shown in Table 2. The first exploratory fieldwork is made to determine the distribution of the Çayraz Formation of the stratigraphical section started from the Eskipolatlı Formation. At the first planned fieldwork (12.11.2017), 32 limestone samples were collected (Figure 4). The 2nd fieldwork was carried out (22.05.2018) to collect the mudstone samples of the NB-A part of the measured section. The 3rd fieldwork was carried out on 19.10.2018,

in order to collect mudstone samples that intercalated with the appointed limestone packages. Some parts of the mudstone samples (between the samples NB0-1 and NB1) were collected in order to place the Çayraz Formation sequences in the chronostratigraphic chart. The 4th fieldwork was carried out at 07.09.2019, in order to collect the rest of the sequence stratigraphic section the lower shelf of the Çayraz formation (Çiner et al., 1996a). The 5th fieldwork was carried out on 18.09.2019, in order to collect samples for the closed 35 meters part of the NB section. Finally, the 6th fieldwork was carried out at 10.11.2019 for the correlation of all the previously collected data.

The studied stratigraphic section started at the lower part of the hill with the mudstone lithology and continued with the limestone intercalation with sandstone (Figure 3). The sandstone beds turn into sandy limestone lithology and continued with the stacking pattern of the limestone layers up to the top of the hill. The marker bed was laterally traced crossing the valley and additional samples were collected from the southeast of the hill (Figure 4).

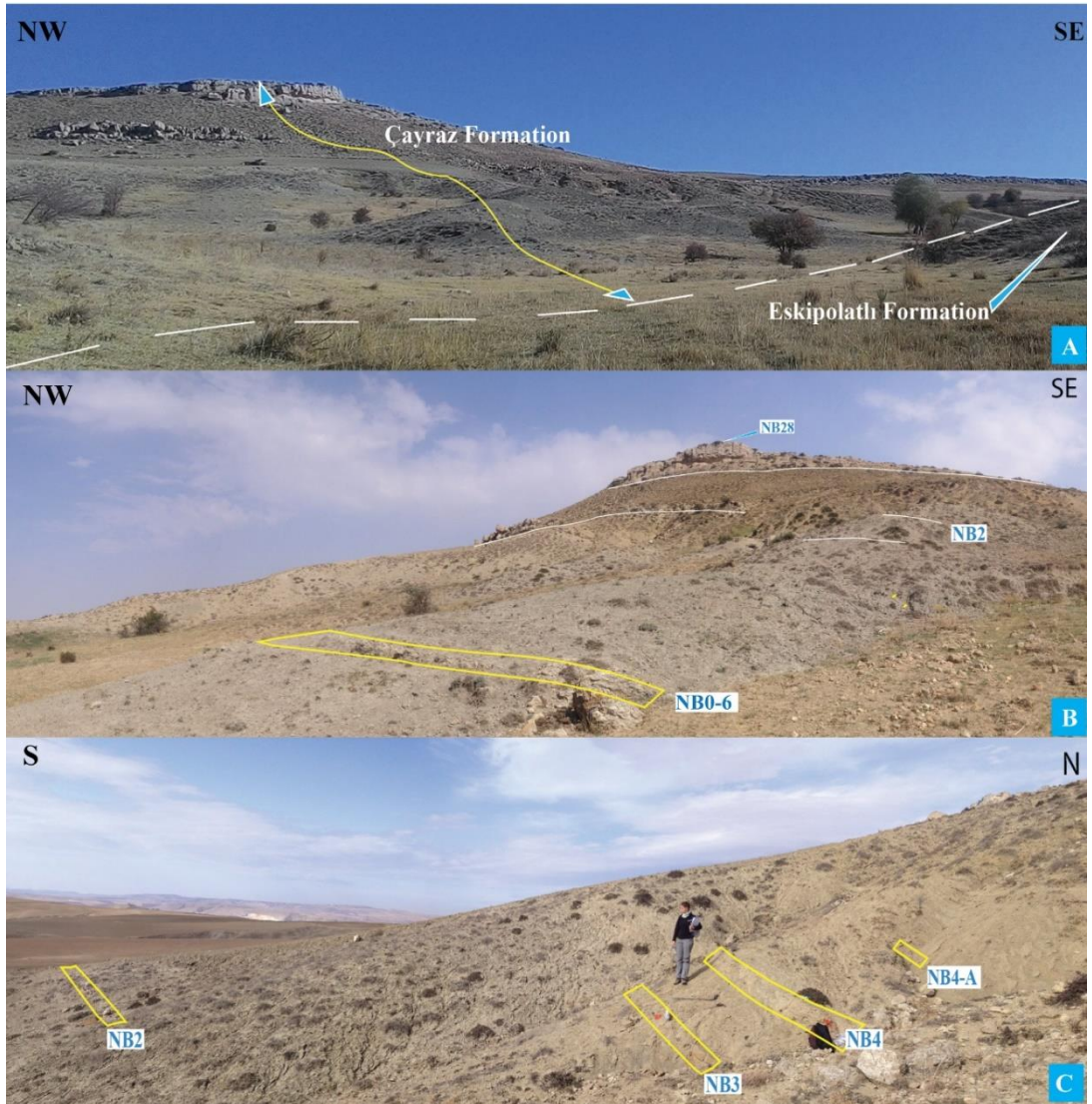


Figure 3: A) Çayraz Fm. and Eskipolatlı Fm., the white dashed line indicates an approximate boundary between formations. B) yellow rectangle: sampled lithology, NB0-6. NB2 and NB28 sample locations, white line: shows strata. C) Southeastward profile of the measured section, NB2, NB3, NB4 and NB4-A sample locations.

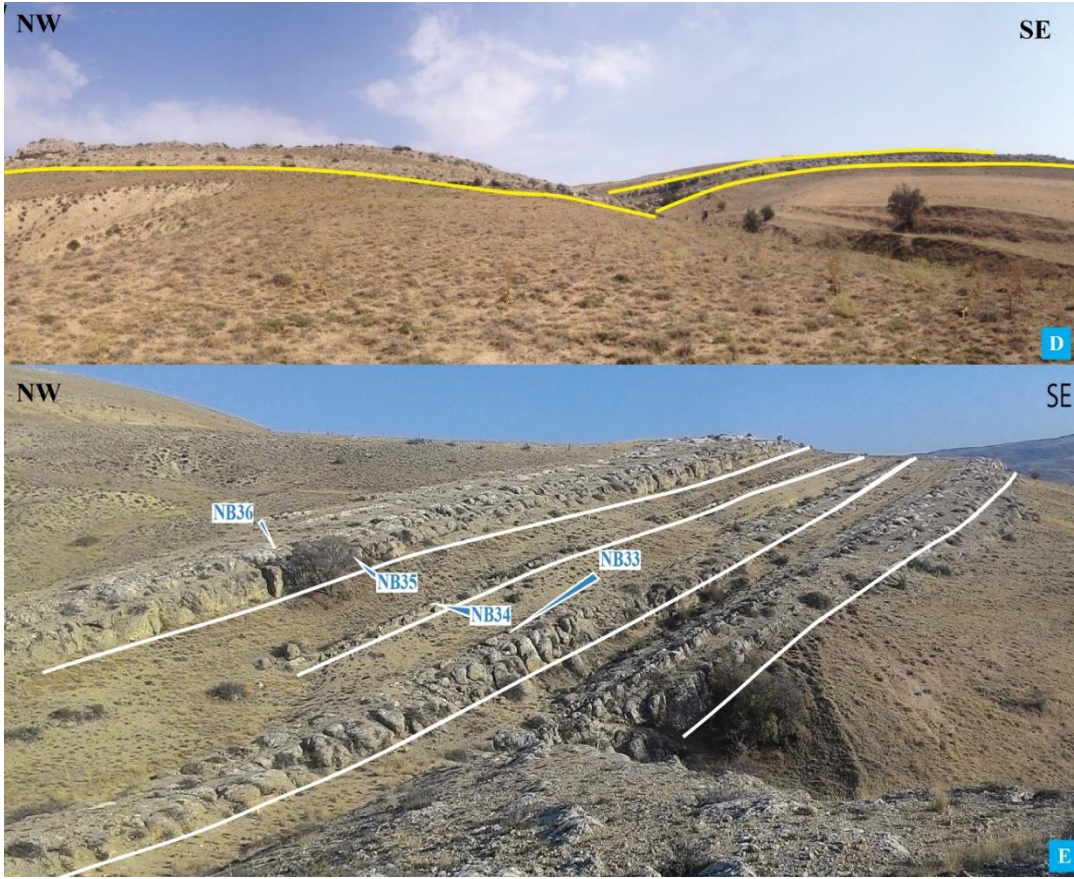


Figure 4: D) yellow line: limestone lithology. E) white line: sampling beds location of the samples NB33, NB34, NB35, NB36

Starting point of the cyclic deposition of the limestone beds corresponds to the early Eocene carbonate cycles of Çayraz Formation (Figure 5). Lower part of the hill shows the intercalation of the fine-grained lithology which is calcareous mudstone to limestone with samples NB1 and NB2.

From sample NB8 to the NB30, which is stay behind the hill, continuous limestone beds are observed with differentiating clastic composition, fossil content, and some also observable features such as; color, hardness etc...

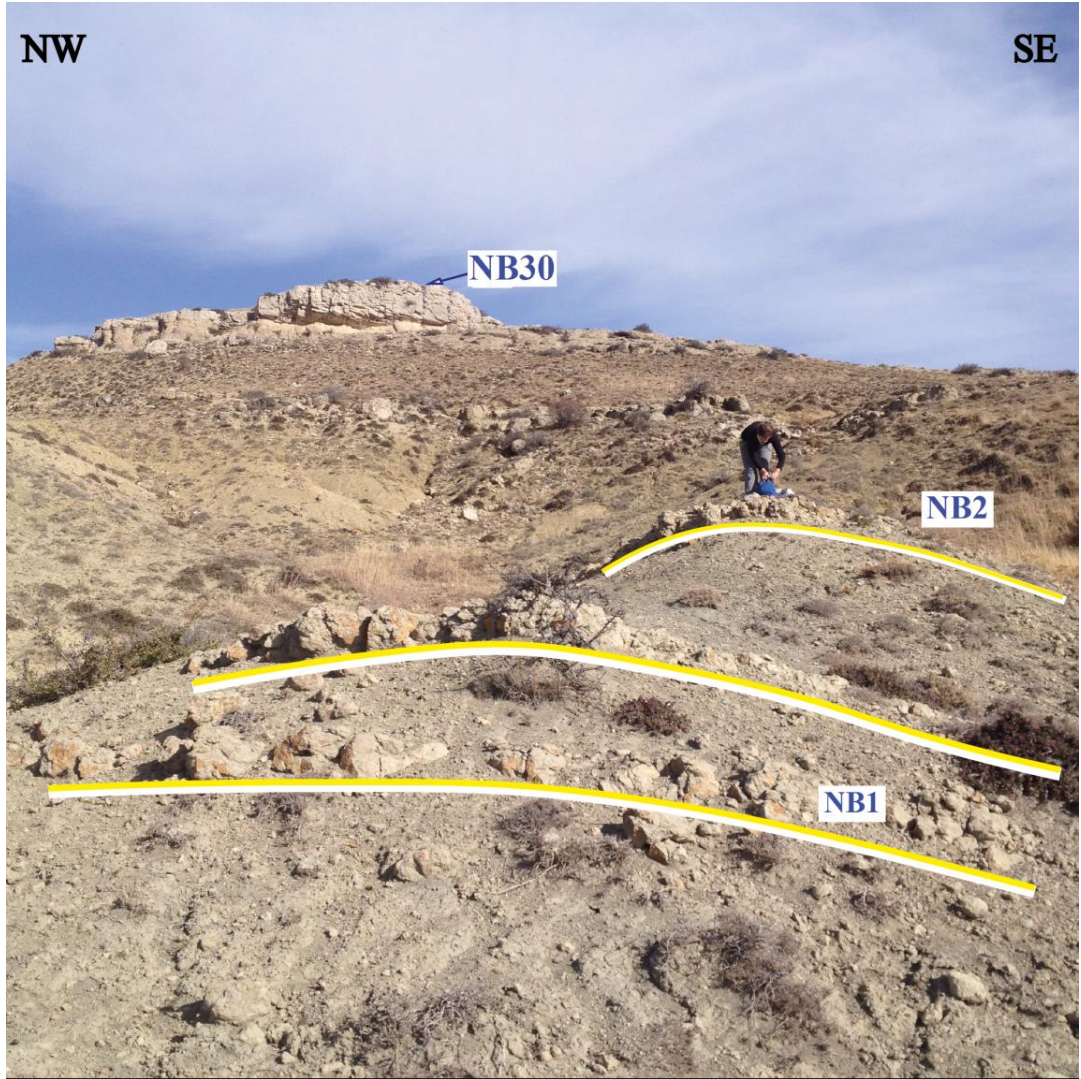


Figure 5: Field photograph of the studied section with the labeling of the sample numbers of the limestone.

1.3 Method of the Study

A section of 238 meters in total was measured for the study from the continuous succession of the Çayraz Formation. Sampling was carried out in three phases, and conducted by six fieldworks phases.

The first phase of the fieldwork, thirty samples from relatively resistant limestone units and two samples from sandstone have been collected. 110 meters of succession were elaborately examined and measured in the field. The sampling interval is determined

depending on the observable physical properties, such as; changes in the fossil content, the thickness of the bed and color. Relatively thin beds (around 1 meter) have been sampled only once. Two or three samples were taken from the relatively thick beds from bottom to top, in necessary cases from the middle of the single limestone bed, and also if there is change in the color or change in relief of the bed. At the first field work 30 samples of limestone and 2 sandstone samples were collected from the 110 meters sedimentary sequences. These samples are marked with green color in the figure 6. The sequence between limestone beds were also examined, however 35 meters of the measured section were not sampled at that fieldwork due to constricts of the topography. This area has been represented as covered interval in the measured section. Due to the high elevation and steep slope over the top of the hill, physically weathered rocks of the upper part of the succession are spread as talus of boulders. They have been disintegrated and/or remain as it is where they fall. Subsequent fieldwork was conducted with the similar sampling interval constraints. During the last two fieldwork phases, additional 26 samples of limestone were collected from various part of the study area including 70 meters of the upper part of the previously measured succession. These samples are marked with the lilac color in the figure 7.

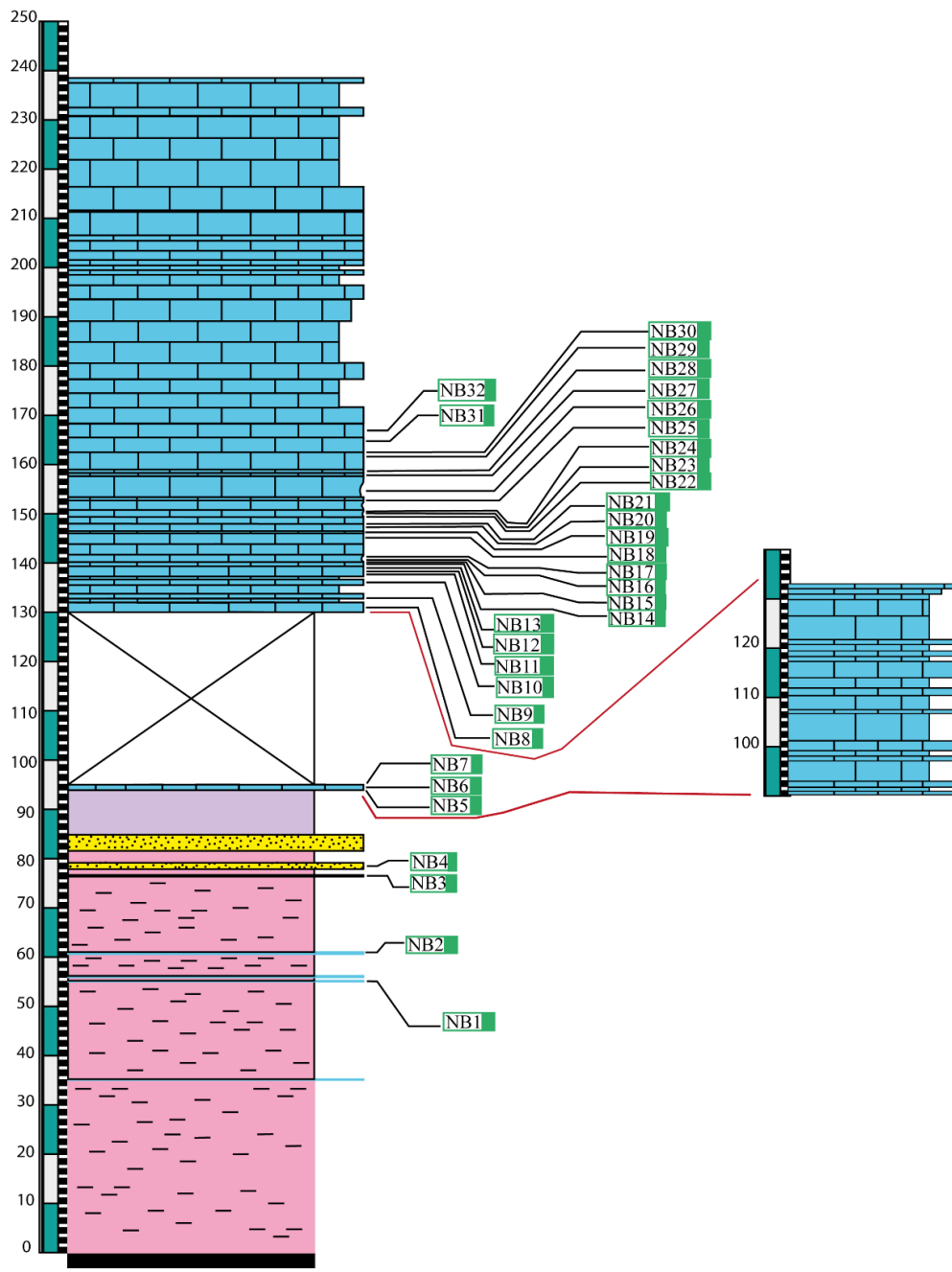


Figure 6: The positions of the limestone and sandstone samples that were collected during the first fieldwork phase. These samples are marked with green color.

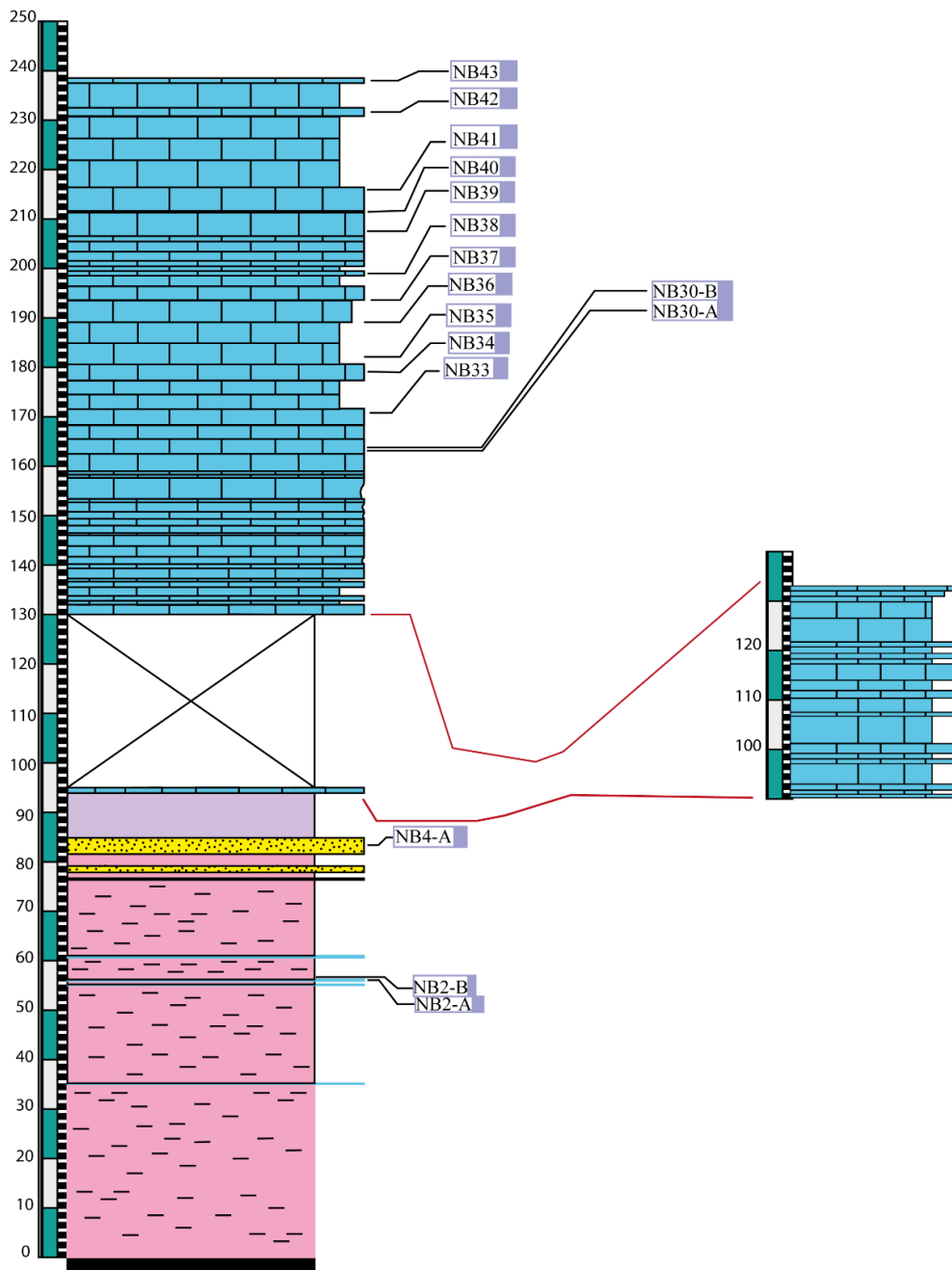


Figure 7: The positions of the limestone and sandstone samples that were collected during the second fieldwork phase. These samples are marked with lilac color.

In the second phase of the field work, mudstone samples have been collected from the top of the appointed sample locations. Additionally underlying mudstone lithology was measured and collected up to the NB1 sample location. The limestone packages readily observable according to the overall topography of the studied area. The rest of the sampling mostly is composed of mudstone and previously not sampled limestone lithology with low relief. The mudstone samples that immediately cover the limestone, have been taken just above the limestone beds. If the thickness of the succession where between two successive limestone packages is more than 1 meter, sampling was carried out at 2,2 m intervals from mudstone. At one sampling, after the NB2 limestone sample two mudstone samples were collected with 110 cm spacing. Moreover, the sampling interval between NB0-1 and NB0-2 was 5,5 meters and it continues up to the NB0-5. These collected samples are marked with pink color in the figure 8.

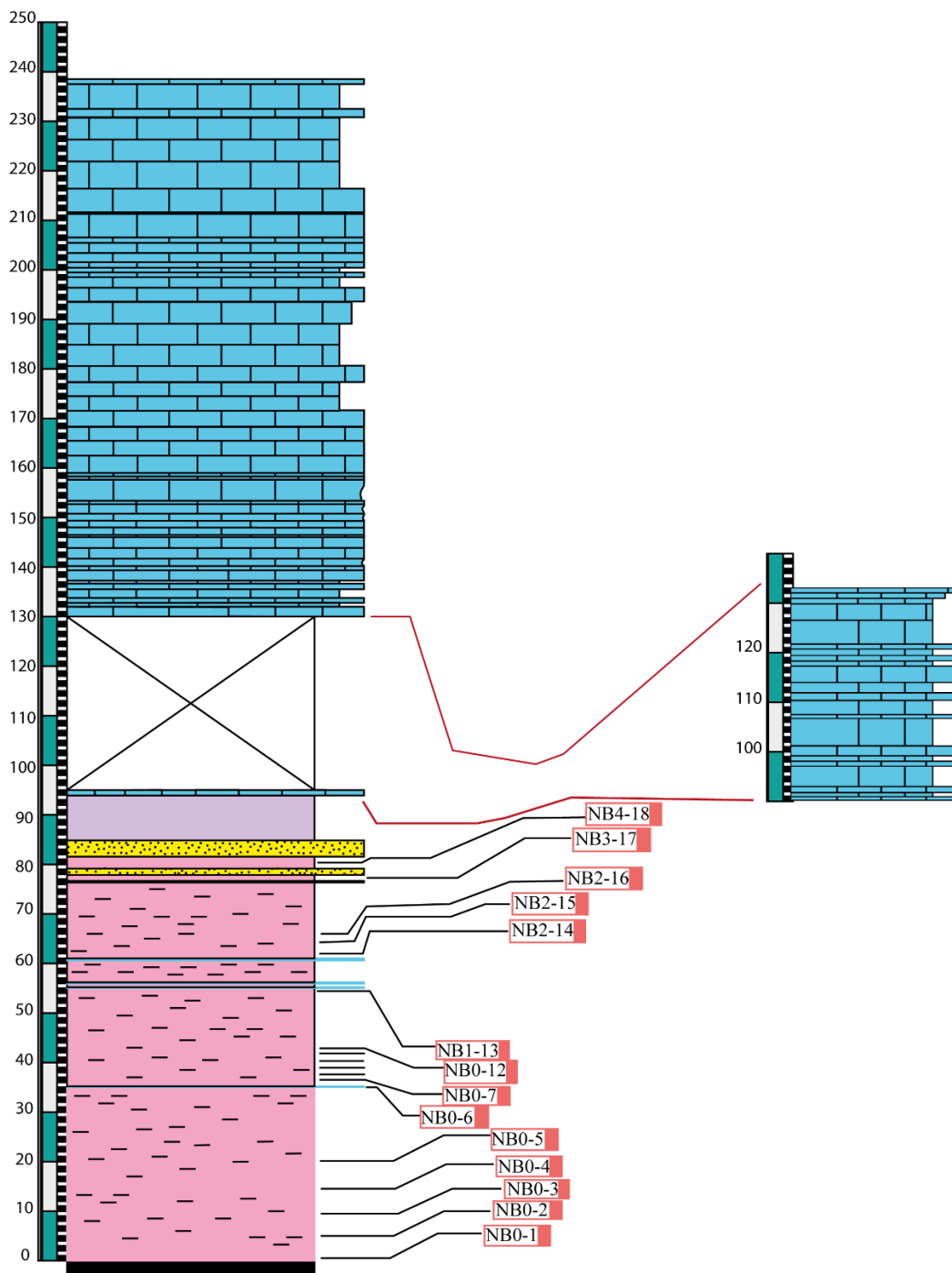


Figure 8: The positions of the samples were collected during the third fieldwork phase. These samples are marked with pink color.

The third phase of the fieldwork was done for the 35 meters covered area of the previously measured succession. The starting point of the measurement was determined by following the lateral continuation of the distinctive sandstone bed in the field. When it disappeared under the soil layer, successive lithology was followed and started from SE facing slope of the hill, without crossing but close to the river valley. Sampling was carried out from that point up to the already measured and sampled beds at the upper part of the succession. This section was assigned as NB-B section and it was approximately 40 m in thickness. Samples were numbered from NB-B-1 to NB-B-9. These samples are marked with yellow color in the figure 9.

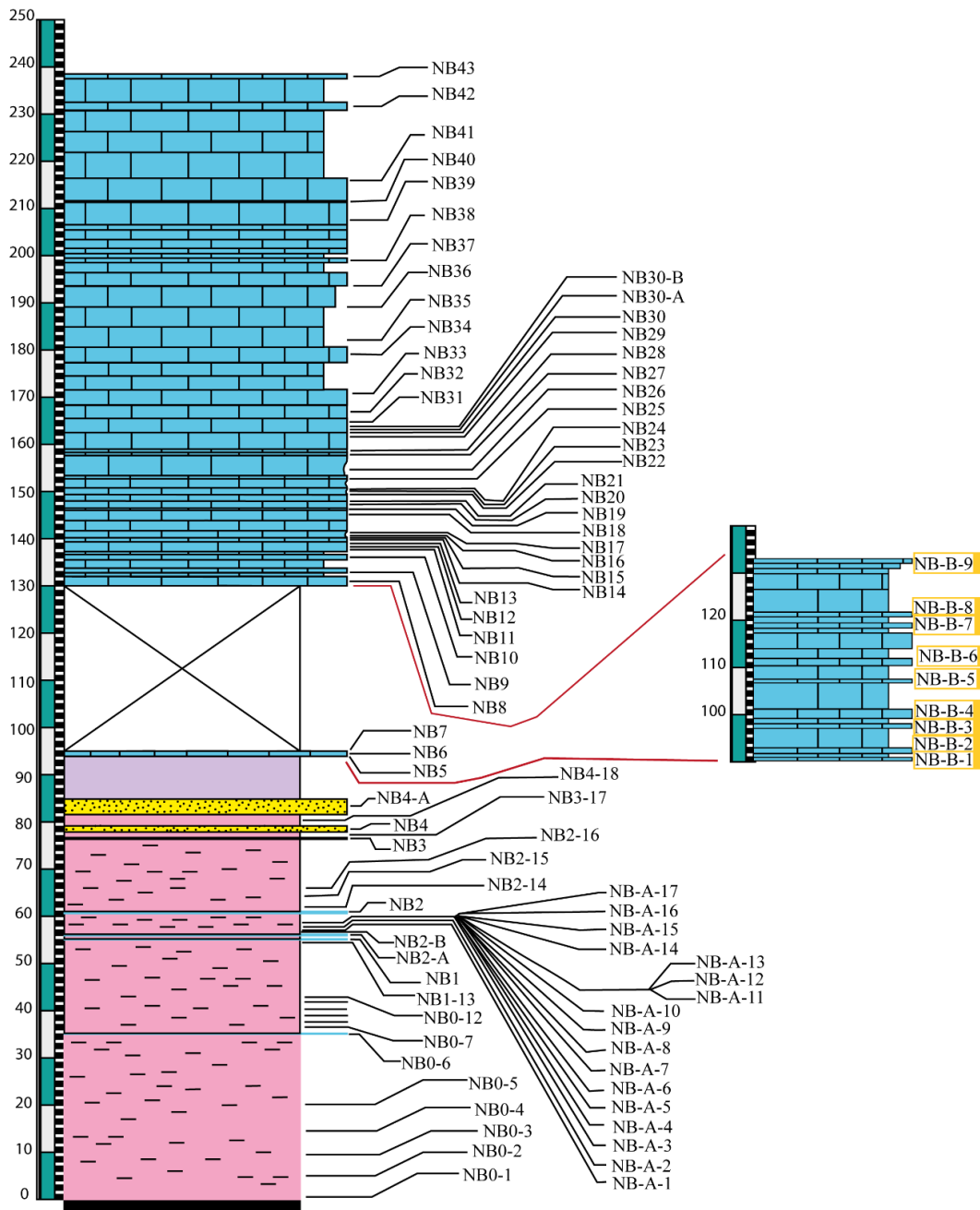


Figure 9: The positions of the samples that were collected during the fourth fieldwork phase. These samples are marked with yellow color.

The sampling method for the limestone and the mudstone beds were different. For the limestone units outcrop of the strata were broken and collected rock samples without any sign of weathering. A total of 56 samples of limestone and 2 sandstone samples have been collected from the 238 meters of succession. The samples of limestone are numbered from NB1 to NB43 with the addition of NB2-A, NB2-B, NB4-A, NB30-A,

and NB30-B to the measured section. These five samples are collected from the upper part of the succession where they have been named after the previously collected samples as “NB#-A”. If there is one more sample collected after that (NB#-A) sample without reaching any previously determined sample at the measured section, following sample was determined as “NB#-B” with same “#” in the determination of the name of the sample as preceding NB#-A sample (Figure 7).

Thin sections were made from collected limestone and sandstone samples. The sampling method for the mudstone units was different, which is the less resistant rock to the weathering, therefore it was covered by a few centimeters of soil layer. The soil layer has been removed from the point of sampling, and some more centimeters was dug, then the fresh mudstone pieces have been collected from this wedge-shaped opening from each point of sampling.

Samples of mudstone have been numbered as “NB#-(mudstone sampling number)”. While “#” is referring to the preceding collected sample of limestone, in order to show after which limestone sample this particular sample was taken. If there is more than one sample have been taken, they were designated with the same “#” of preceding limestone lithology and following number from the mudstone sampling number, such as; NB#-1, NB#-2, NB#-3, in order to create unity between mudstone samples. Another sampling of mudstone lithology is conducted with very short sampling space. It was carried where in between NB1 and NB2 samples. A total of 17 samples were collected. These samples are marked with orange color (Figure 10). This part of the succession is named as NB-A part of the depositional sequence. The interval between samples was about 32 cm. Additionally, three samples were collected right after each other where in between NB-A-10 and NB-A-14 samples where the lithology change from mudstone to sandstone at one part of the NB-A section (Figure 11). A total number of 33 mudstone, 58 limestone, and 3 sandstone samples were collected for this study.

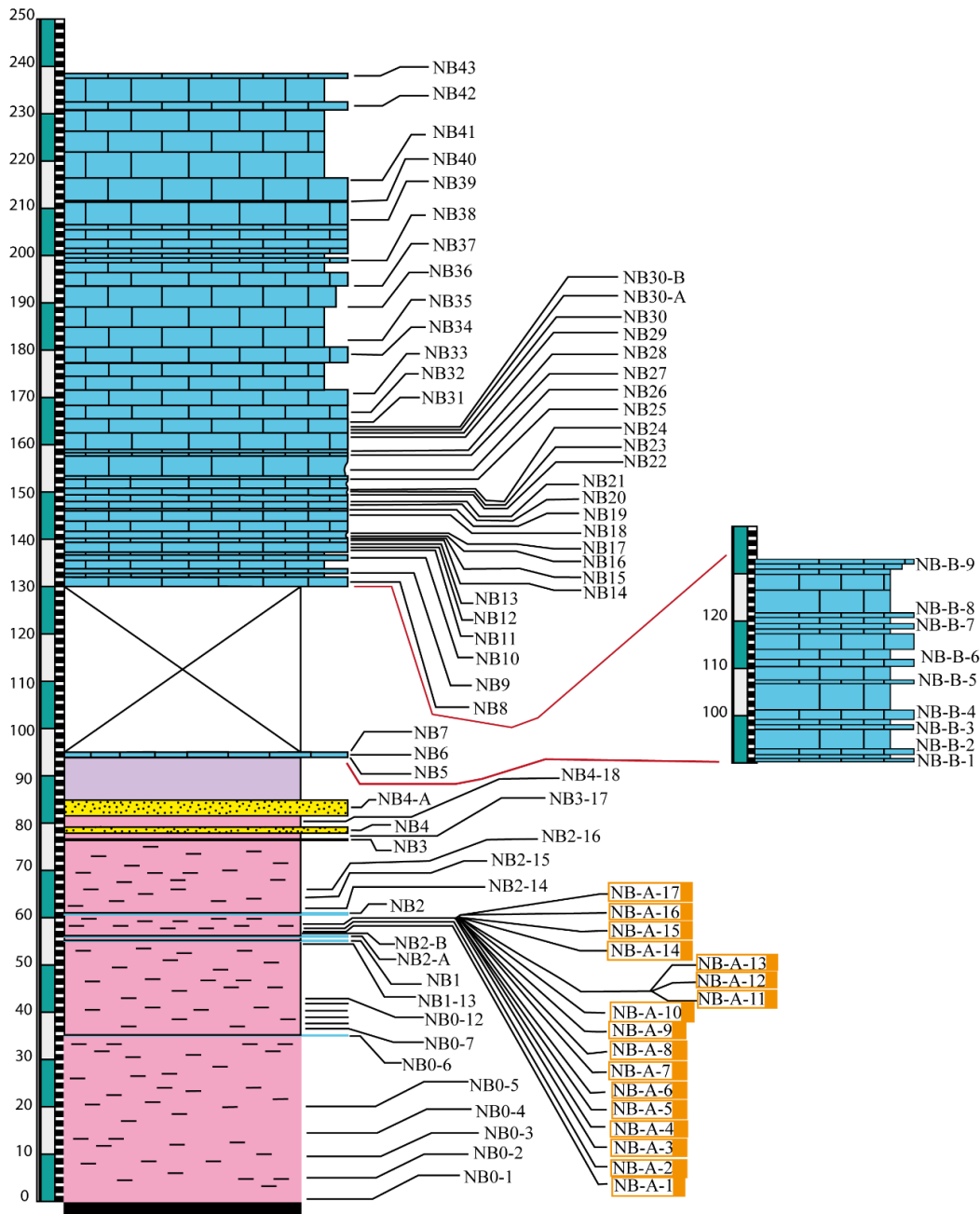


Figure 10: NB-A section part of the measured section. The positions of the samples that were collected during the fifth fieldwork phase. These samples are marked with orange color.

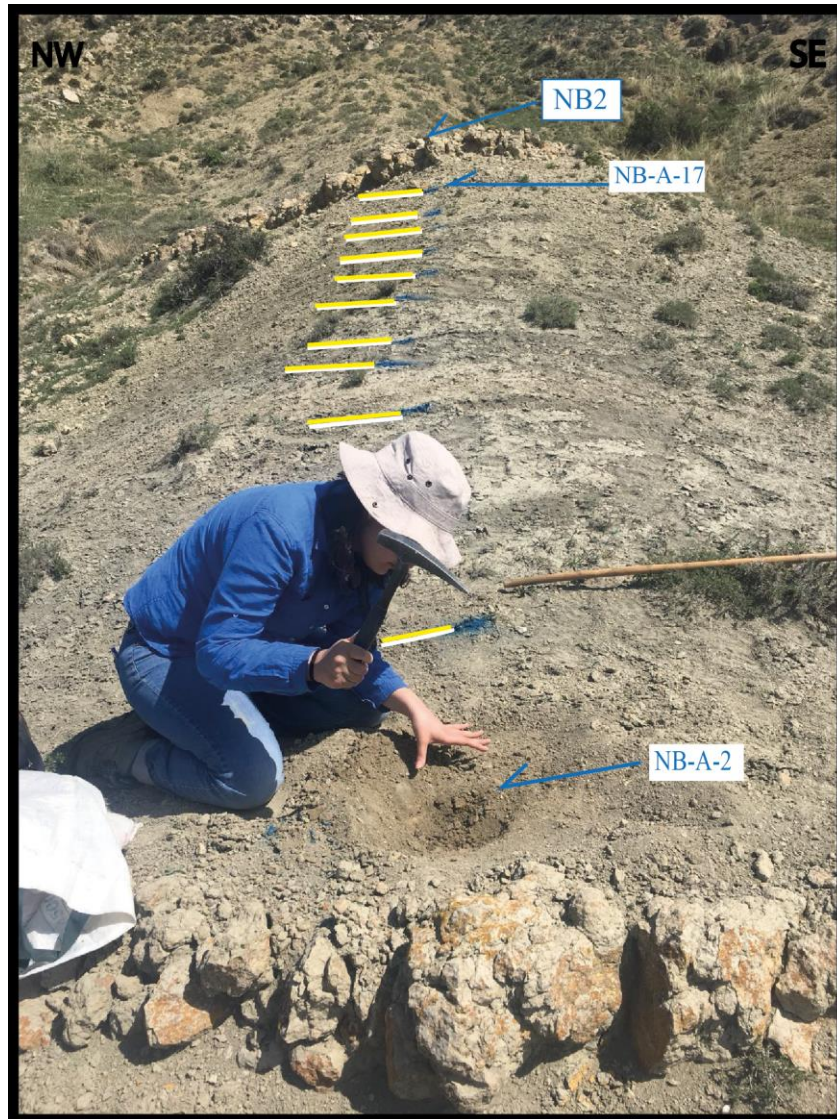


Figure 11: NB-A part the NB stratigraphic sequence

The main method for studying the samples is the thin section analysis under the light microscope since the main lithology of the sedimentary sequence is limestone, besides washing method were also considered for the softer lithology. Thin sections for each sample were prepared in the Thin Section Laboratory of Geological Engineering Department, Middle East Technical University and examined under the polarized light microscope (Figure 12).



Figure 12: Image of the thin section preparation in the laboratory.

Wash samples were subjected to an experiment in order to find out which washing method was suitable for these lithologic units. 100 ml of H_2O_2 solution with 100grams of dry and similar sized samples. All samples were broken into small pieces and subjected to the acid and the reaction time for the samples varied from 10 minutes to 120 minutes depending on the composition and the hardness of the lithology. After the reaction, the sample was washed under tap water and cleaned from the acid solution and clay-sized particles with gentle stir and light rubbing motion while passing them through sieves with the help of water.

The fractions of the sieves were 425, 250, 106 and 63-micron meters. The residue of the particles on the sieves was transferred to the evaporation dishes by using distilled water in order to prevent any precipitation of mineral on the sample. Mudstone samples were used for the age determination. Figure 13 shows the washing sample processes.



Figure 13: Image of washing samples 250-106-63-micron meters fraction and planktonic foraminifera.

1.4. Previous Works

The earliest studies of the Haymana Basin were conducted by Chaput (1932, 1935a, b), who identified the Cretaceous and Eocene rocks in the Haymana Basin. The geological studies in the Haymana Basin were done to understand the stratigraphic and structural evolutionary history of the region carried out by Lokman and Lahn (1946), Lahn (1949), Egeran and Lahn (1951), Rigo de Righi and Cortesini (1959), Reckamp and Özbey (1960), and Schmidt (1960). The main aim of these studies was to study the petroleum potential of the basin. They established the stratigraphic framework of the region (Figure 21).

Yüksel (1970) studied the Haymana region and established geological map and cross-section of the studied area. He also studied and define sedimentological characteristics and the relationship between the basin infilling units based on paleontological dating (Figure 21). Norman and Rad (1971) conducted a sedimentological study on the Harbor Formation, turbiditic characteristic of the succession has been described.

Comprehensive studies of the Haymana Basin were carried out by Sirel (1975) and Ünalán et al. (1976). These studies established the Formations of the Haymana Basin. Sirel (1975) worked and established the lithostratigraphic and biostratigraphic framework of Paleocene- Eocene successions of the Haymana Basin, and determined biozones of the time interval.

Ünalán et al. (1976) carried out an extensive study which established Upper Cretaceous- Cenozoic lithostratigraphic framework of the Haymana Basin with a comprehensive correlation chart with the earlier works. The pre-Upper Cretaceous basement rocks were determined as the Temirözü Formation and Mollaresul Formation. The units of Haymana Basin were distinguished to 11 members by Ünalán (1976) as; Temirözü Fm., Dereköy Fm., Beyobası Fm., Çaldağ Fm. followed by the northwest and the eastern part reaches its depositional limit. At the southeast of the area the Yeşilyurt Fm is exposed and continued with the Kırkkavak formation and the Iğnıkdere formation. Iğnıkdere Fm is covered by the Eskipolatlı formation. Eskipolatlı formation followed by the Çayraz formation southwest of the region Yamak Fm is deposited. Beldede, Çayraz, and Yamak formations are age equivalent to each other, the only difference between them is the depositional environment. Çayraz formation is followed by the Neogene deposits with the presence of the unconformity surface between them. The Çaldağ and Dereköy formations were described by Sirel (1975). Gökçen (1976a, 1976b, 1977) carried out extensive paleogeographic and sedimentologic study in the southern part of the Haymana Basin. The presence of oil saturated deep channels in the turbidite-bearing Haymana formation had been investigated by many researchers to determine the petroleum potential of the region (Gez, 1957; Druitt and Reckamp, 1959; Reckamp and Özbey, 1960; Schmidt, 1960; Akarsu, 1971; Arıkan, 1975 and Ünalán and Yüksel, 1985). Şenalp and Gökçen (1978) carried out a sedimentological study of the oil-saturated sandstones of the Haymana basin. They interpreted oil saturated turbidite facies as channel fill sediments deposited in the lower part of the submarine fans which gradually merge into the abyssal plain. Şenalp and Gökçen (1978) also studied the bottom sedimentary structures and interpreted a deep marine basin fill deposit as a depositional environment.

Gökçen (1978), Gökçen and Kelling (1983), Çetin et al. (1986) carried out sedimentology studies of the Haymana Basin. By doing petrographical and mineralogical analyses. They suggested that a single source area with two different lithologies and provided evidence for N to S feeding direction with exception of E to W paleoflow direction determined by Çetin et al. (1986) for the middle Eocene shallow marine units.

Research on petroleum reservoir rock quality of the Mollaresul formation which is composed of Jurassic-Lower Cretaceous aged limestones within the Haymana -Polatlı basin was carried out by Özdemir (2019).

The first paleontological investigation of the region started with Dağar *et al.*, (1963) and continued with some other planktonic, benthic and nannoplankton fossil studies. Dizer (1964, 1968) carried out studies about the Eocene by working on *Nummulites* and *Alveolina* type foraminifers. Toker (1975, 1977, 1979, 1980) carried out planktonic foraminifera studies and with his work biozones were designated for the Beyobası Formation of the Haymana Basin. Benthic foraminifera specially *Nummulites* spp., *Assilina* spp. and *Alveolina* species were studied taxonomically by Sirel and Gündüz (1976) and the biostratigraphy of Paleocene- Eocene age units were determined. After Sirel (1976), nannoplanktons in the Campanian- Lutetian age formations were studied by Toker (1979) and thanks to this study the compatibility between these nannoplanktons and planktonic fossils has been presented. Paleontological and stratigraphic studies in the Haymana Basin were continued with Meriç and Görür (1979-1980), Özcan and Özkan-Altınar (1997), Sirel (1999), Özcan *et al.* (2001, 2007). These authors documented the results of their paleontology studies conducted on upper Cretaceous to Eocene units of the Haymana Basin. Planktonic and benthic foraminifera were studied by Özcan and Özkan-Altınar (1997,1999a,1999b), Özkan-Altınar and Özcan (1999) and the Latest Cretaceous age was assigned to the studied sequence. Eocene larger benthic foraminifera were worked by Dinçer (2016) in terms of stable isotopes. Planktonic foraminiferal works were continued by Özkan-Altınar and Özcan (1999), Huseynov (2007), Amirov (2008), Esmeray (2008), Esmeray-Senlet et al. (2015) on the parts of Upper Cretaceous- Middle Eocene deposits of the region. Paleontologic studies on the benthic and planktonic foraminifera were conducted on taxonomical and biostratigraphic purposes by Sirel

(1976a, 1976b, 1976c, 1998, 1999), Sirel and Gündüz (1976), Matsumaru (1997,1999), Özcan et al. (2001), Özcan (2002), Çolakoğlu and Özcan (2003). Geyikçioğlu Erbaş (2008), worked on Paleocene-Eocene larger benthic foraminifera and meter scale cycles in the Eocene Çayraz formation and response of the foraminifers to cyclicity. Tanık (2017) worked on Upper Paleocene- Lowermost Eocene planktonic foraminiferal biostratigraphy and record of Paleocene- Eocene boundary. Karabeyoğlu (2017) and Vardar (2018) worked on planktonic foraminiferal and deep sea benthic foraminiferal diversity and abundance changes across Cretaceous- Paleocene boundary beds respectively. The most recent paleontological study in the Haymana Basin belongs to Özcan et al. (2020) worked on larger benthic foraminifera and planktonic foraminifera of the Eocene units of the basin in order to reassess the age and depositional environments of the units. The Çayraz formation was subdivided into three units based on their lithological feature and fossil content. The lower and upper units are mostly dominated by larger benthic foraminifera accumulations, while the middle unit consists of thick bedded to massive marl and siltstone beds with pelagic fauna. The lower unit was interpreted as a major shallowing-upward sequence characteristics of a deep setting in the outer-ramp at its base and the inner ramp as its upper part. The shallow marine deposition end abruptly after the *Alveolina*-bed at the top of the lower unit and deeper pelagic sedimentation starts with marly/silty beds. The middle unit (the marly/silty beds) of the Çayraz Formation contains planktonic foraminifera, suggestive of the P9 Zone, and implies a transitional age across the Ypresian-Lutetian boundary. The dating of the middle marly unit by pelagic fauna clarifies the stratigraphy of the lower and the middle units for the first time.

Görür et al. (1984, 1998), Koçyiğit (1991), Koçyiğit et al. (1988,2003), Rojay and Süzen (1997), Kaymakçı (2000) suggested that fore-arc type development for the evolution of the basin, by comparing the tectonic position and stratigraphic record of the Haymana Basin with other Central Anatolian basins. Gülyüz (2015) worked on tectono-stratigraphic and thermal evolution of the Haymana Basin. Stratigraphical and sedimentological studies revealed that; Santonian to middle Eocene continuous deposits of the Haymana Basin comprises four depositional sequences, as represented by contemporaneous sedimentation in continental to deep marine environment.

Özkaptan (2016) worked on Post-Late Cretaceous rotational evolution of Neotethyan sutures around the Ankara region. The paleomagnetic results show, that the region underwent strong clockwise and counterclockwise rotations resulting the present geometry of the suture zones.

Okay et al. (2001) studied the Haymana Basin from upper Cretaceous to lower Eocene and suggested the initiation of the continent-continent collision being reflected as the Paleocene uplift which they observed in the Central Sakarya and the northwestern Haymana Basins, while the southern parts of the Haymana still under the sea level and deposition continued until the middle- Eocene. These findings have restrained the continental collision, from the Paleocene to early Eocene time interval. Nairn et al. (2012) worked on the central Anatolia basins including Haymana Basin. Hypothesizing a diachronic closure, the formation of the İzmir- Ankara- Erzincan suture started by the collision of the Niğde- Kırşehir Massif and Pontide active margin during the Late Cretaceous, while the oceanic crust still remained the west and the east and continued to subducting during the late Paleocene- early Eocene. Okay and Altner (2016) studied Upper Jurassic- Lower Cretaceous benthic and planktonic foraminifera in the carbonate successions and stated that the Haymana Basin was a deep marine sedimentation site during the Cretaceous.

Sequence stratigraphy and cyclicity of the early -Middle Eocene shallow marine carbonates and clastic sequences were studied by Çiner et. al. (1993a, b, 1996a, b) and by Çiner (1993, 1996). Sequence stratigraphic perspective executed in these studies; clastic deposits in Beldede Fm., nummulitic bank in Çayraz Fm. and submarine fan deposits in Eocene deposits and sequence stratigraphic units were suggested in these formations (Çiner et al., 1993a), and also the formation mechanism of these formations have been examined. They suggested high rate of subsidence and tectono- eustatic mechanism for the time interval. Huseynov (2007) carried out a study on the Early to Middle Campanian of the Haymana Formation, concluding that tectonic effect is exceeding eustasy during that time interval.

1.5. Regional and Geological Setting

The Haymana basin is located approximately 70 km SW of Ankara, Turkey. It is geologically situated nearly 45 km northeast of the İzmir-Ankara suture (Okay and Altner 2016) (Figure 13). It was developed within a continental collision regime along the northern branch of the Neo-Tethys. Starting from the Cretaceous, the northern branch of Neo-Tethys began to close, and was subducted under the Eurasian Plate (Şengör and Yılmaz 1981, Görür et al. 1984).

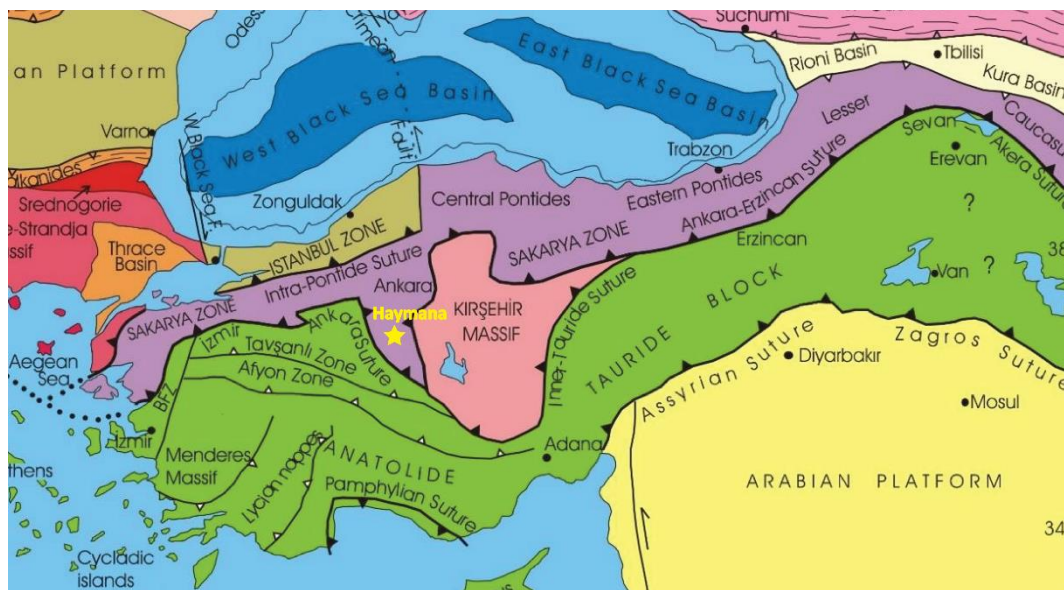


Figure 14: Main tectonic units of Turkey and the location of the Haymana Basin (yellow star). Image modified after Okay and Tüysüz (1999).

At that time, the Pontides were an active margin and grew southward by the addition of accretionary complexes (Okay and Altner 2016). Subduction initiated Albian, and the arc volcanism started in the Turonian and became widespread in the Santonian (Okay and Altner 2016). This volcanism was considered as submarine character because of its volcanoclastic deposits intercalated with deep marine limestones (Okay and Altner 2016) (Figure14). At the end of Campanian, volcanism faded out and carbonate deposition prevailed in the northern, and siliciclastic turbidites were deposited in the southern part of the Pontides through Maastrichtian. the Haymana Basin was opened as a fore-arc basin during the convergence of the Anatolide-Tauride

Platform and the Pontides (Görür et al. 1984, Koçyiğit et al. 1988, Koçyiğit 1991) (Figure 14).

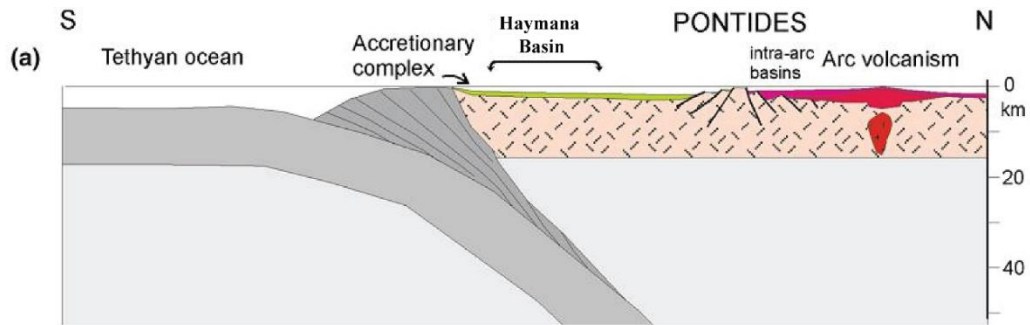


Figure 15: Development of the Haymana Basin as a fore-arc position due to subduction of the Northern Branch of Neo-Tethys beneath the Pontides. Image modified after Okay and Altner (2016).

The basement of the Haymana region is made up of Triassic Karakaya Complex. It is unconformably overlain by Middle Jurassic-Lower Cretaceous carbonates (Bilecik and Soğukçam limestones) and Upper Cretaceous flysch (i.e. Haymana Formation) (Okay 1989, Okay and Altner 2016) (Figure 14). The Bilecik Limestone is covered by pelagic deposits of the Soğukçam Limestone. From Albian to Cenomanian, both Bilecik and Soğukçam limestones are unconformably overlain by breccias and glauconite and radiolaria-bearing limestones of the Akkaya Formation. Then, these deposits are unconformably covered by pelagic limestones and shales of the Kocatepe Formation of the Turonian-Santonian age. Subsequently, flyschoidal deposits of the Haymana Formation covers the whole basin starting from the Campanian (Okay and Altner 2016) (Figure 17).

The Haymana formation is composed of mudstone, sandstone and conglomerate lenses. This sedimentation represents the turbiditic flyshoidal sedimentation of the deep marine system. The lateral and vertical continuation of the Haymana Fm is the Beyobası Formation, which is composed of sandstone, conglomerate, conglomeratic limestones and sandy marls. It represents shallower environment of deposition. The Kartal, Çaldağ and Yeşilyurt Formations are the age equivalent formations. They are

deposited during the Early Paleocene. The Kartal Formation is composed of red conglomerate, sandstone and marl. The Çaldağ formation is composed of algal limestone. The Yeşilyurt Formation is composed of marl with limestone blocks. The Yeşilyurt Fm. has a relatively deeper environment than it's lateral continuations and the Kartal formation represents relatively shallower environment that is close to land. Provided facies maps by Ünalán et al. (1976) lead him to make paleogeographical interpretations. A sketch cross section of the paleogeographical setting that provided by Ünalán et al. (1976) shows the setting and relative sea level while these formations are deposited (Figure 15). The shelf deepens southeastward and forms an arc shape.

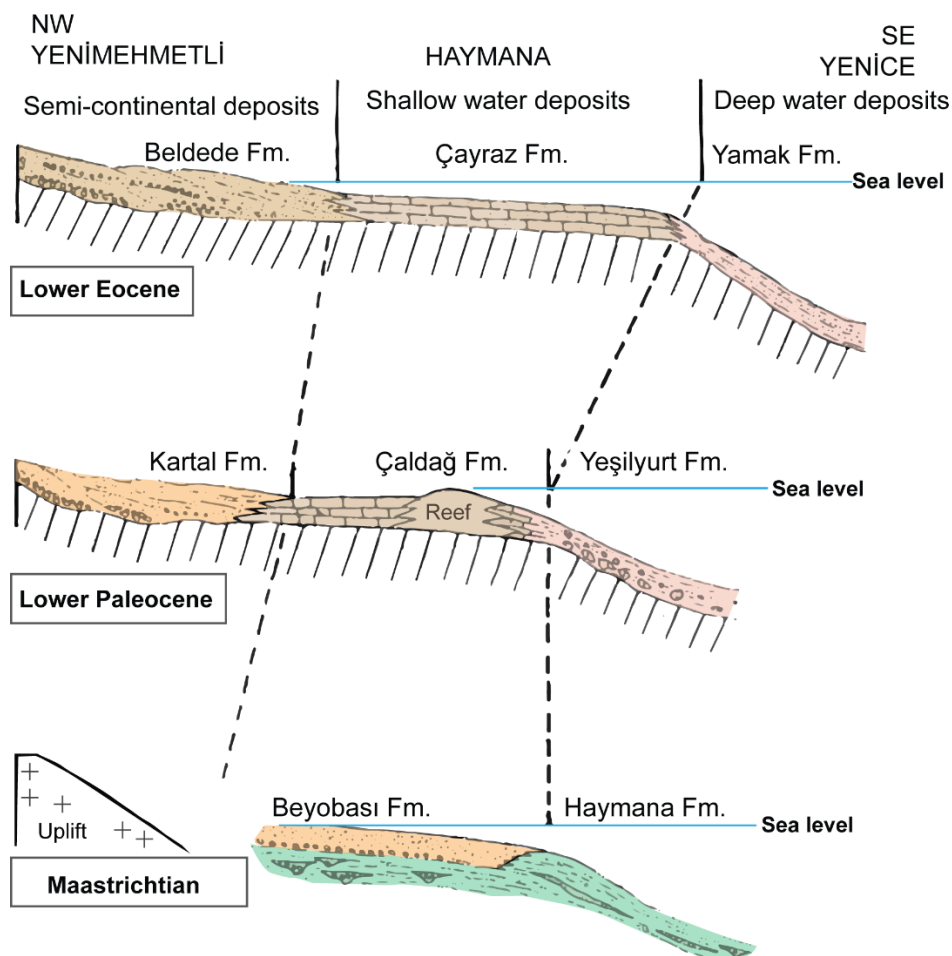


Figure 16: Sketch cross section of the Haymana Basin (showing the lateral relationships of the same aged units) during the Maastrichtian, Lower Paleocene and Lower Eocene showing the paleogeographical setting (modified after Ünalán et al., 1976)

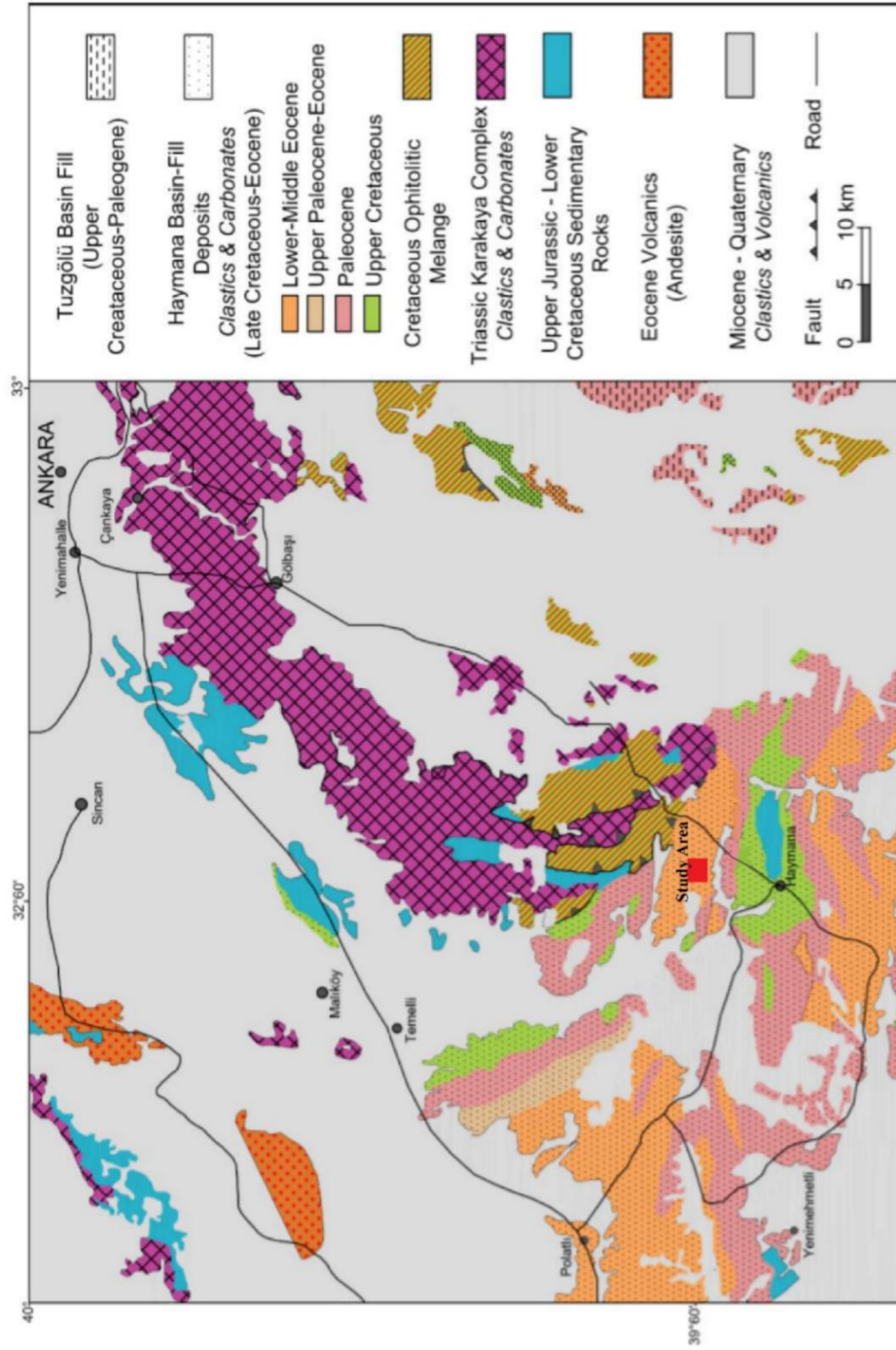


Figure 17: Geological map of the Haymana Region and location of the study area (red square) (Modified after 1/500,000 Map of MTA and Rojay 2013).

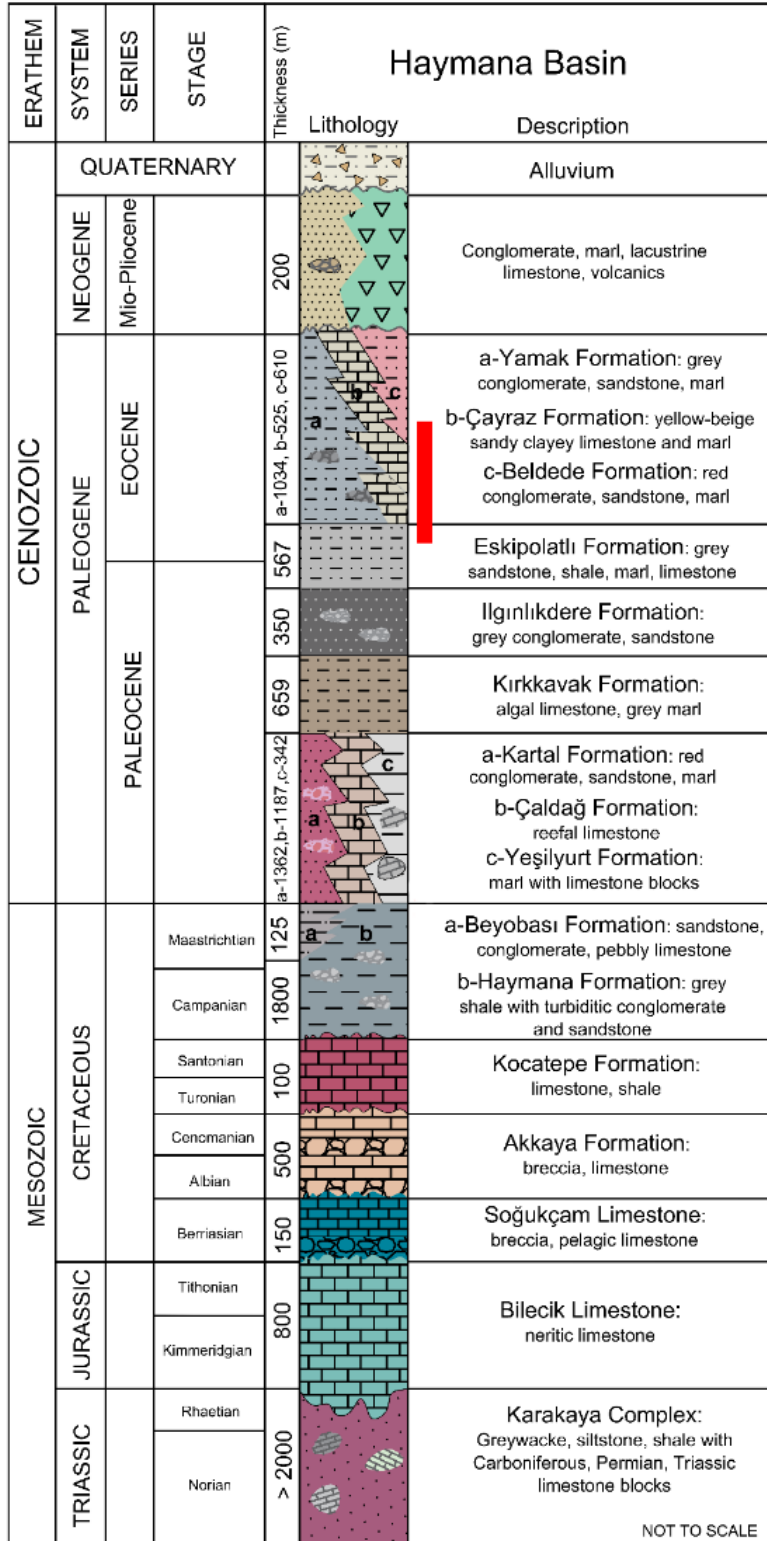


Figure 18: Generalized columnar section of the Haymana Basin modified from Ünalan et al. (1976) and Okay and Altınır (2016). (red line indicate the approximate location of the measured section covering the Çayraz Formation)

These three formations are covered by the Kırkkavak formation which is composed of algal limestones and grey marls. It has conformable boundaries with underlying formations. The age of the Kırkkavak formation is Thanetian. The Kırkkavak Formation is followed by the Ilgınlıkdere formation which is composed of conglomerate, and sandstone, with intercalations of shale. The age of the Ilgınlıkdere formation is Ilerdian. The thickness of conglomerate and sandstone beds is decreasing while the shale thickness is increasing to the top of the formation. The Ilgınlıkdere Formation is covered by the Eskipolatlı formation which is composed of shale with sandstone and limestone intercalations. Ilerdian to Causian aged (Ünalın et al,1976) Eskipolatlı formation's shale succession includes some limestone beds toward the top of the succession. The Çayraz Formation nummulitic limestone beds are both conformably and unconformably overlying the Eskipolatlı Formation (Ünalın et al, 1976). At the SE of the region the Yamak formation are deposited, and in the NW of the region semi continental deposits of the Beldede formation were deposited (Ünalın et al., 1976). The Beldede, Çayraz and Yamak formations are also age equivalent to each other like the Kartal, Çaldağ and Yeşilyurt formations.

The Beldede Formation is represented by shallow red clastics composed of conglomerate, sandstone and marl. The Çayraz Formation consists of the sandy limestones with highly abundant *Nummulites*, *Assilina* and *Alveolina*. The Yamak Formation is composed of grey conglomerate, sandstone and marl. All these formations are unconformably overlain by volcanoclastics and lacustrine limestones, conglomerate and marls in the Neogene age. The geological map of the Haymana Region and location of the study area are shown in the Figure 16. This thesis study is focused on the Çayraz Formation.

CHAPTER 2

STRATIGRAPHY

2.1. Lithostratigraphy

The deposits of the Haymana basin are mainly characterized by from Upper Cretaceous to Eocene marine sequences and the total thickness of these deposits is about 5000 m (Ünalán et al. 1976) (Figure 17). The Eocene aged Çayraz Formation is the main target of this thesis work, and is characterized by sandy limestones with larger benthic foraminifers, such as nummulites, assillinids and alveolinids. The Çayraz Formation is laterally and vertically passed into the Beldede and Yamak formations (Ünalán et al., 1976). The Beldede Formation consists of conglomerates, marls, and limestones in the north and west of the basin. The Yamak Formation is composed of sandstones southeast of the region. The Çayraz Formation is underlain by the Eskipolatlı Formation, and unconformably overlain by Neogene units.

The Eocene successions of the Haymana Basin is represented as sandy limestone units with abundant and diverse species of *Nummulites*, *Assilina* and *Alveolina*. These carbonate rocks with *Nummulites* sp. are characteristic for the shallow marine deposition of the Çayraz Formation of the Haymana Basin. The lower boundary is conformable with the Eskipolatlı Formation (Ünalán et al., 1976) (Figure 19). The Paleocene- Eocene Boundary is located in the Eskipolatlı formation depositional units (Tanık, 2017).

2.1.1. Çayraz Formation

The Çayraz Formation has been first defined by Schmidt (1960). The type locality of this formation is around Çayraz village north of the Haymana town (Figure 1, 2). The type section of the formation is west of the Çayraz Village. In the type section, the formation is represented by limestones with *Nummulites*, and *Alveolina* with marly

intercalations, containing abundant large *Nummulites* and *Assilina* at its base, and sandstones and marls with *Nummulites* at its top. The total thickness of the Çayraz Formation is approximately 400 meters (Çiner et al., 1996a). The formation conformably overlies the Eskipolatlı Formation except for the local unconformity in the northwest of the Yeşilyurt and is terminated by the Ophiolitic Mélange. The age of the formation is determined as Cuisian-Lutetian. By using *Alveolina canavari* Checchia-Rispoli (1905), *Alveolina bayburtensis* (Sirel, 1976), *Alveolina cayrazensis* Dizer (1964) the lower part of the Çayraz Formation has been assigned as Causian, by using *Nummulites laevigatus* Bruguiere, *Nummulites lehneri* Schaub, *Nummulites helveticus* Kaufmann, *Assilina spira* de Roissy, *Assilina exponensis* Sowerby, the upper part of the formation has been dated as Lutetian (Sirel and Gündüz, 1976).



Figure 19: Type locality of the Çayraz formation (NW of the Çayraz Village).

In addition, the age of the formation was studied by Özcan (2007) based on orthofragmines (*Discocyclina fortisi* cf. *cayrazensis* D. *spliti polatliensis* Özcan, *D. senegalensis*, *Nemkovella evae karitensis* Özcan, and *Orbitoclypeus varians ankaraensis* Özcan and *D. trabayensis* cf. *trabayensis* and a Late Ypresian- Middle

Lutetian have been assigned to the formation. The depositional environment of the formation is described as shallow water based on the lithological and paleontological data. According to Çiner (1993), the Çayraz Formation represents a shelf environment upon which laterally extensive nummulitic banks developed.

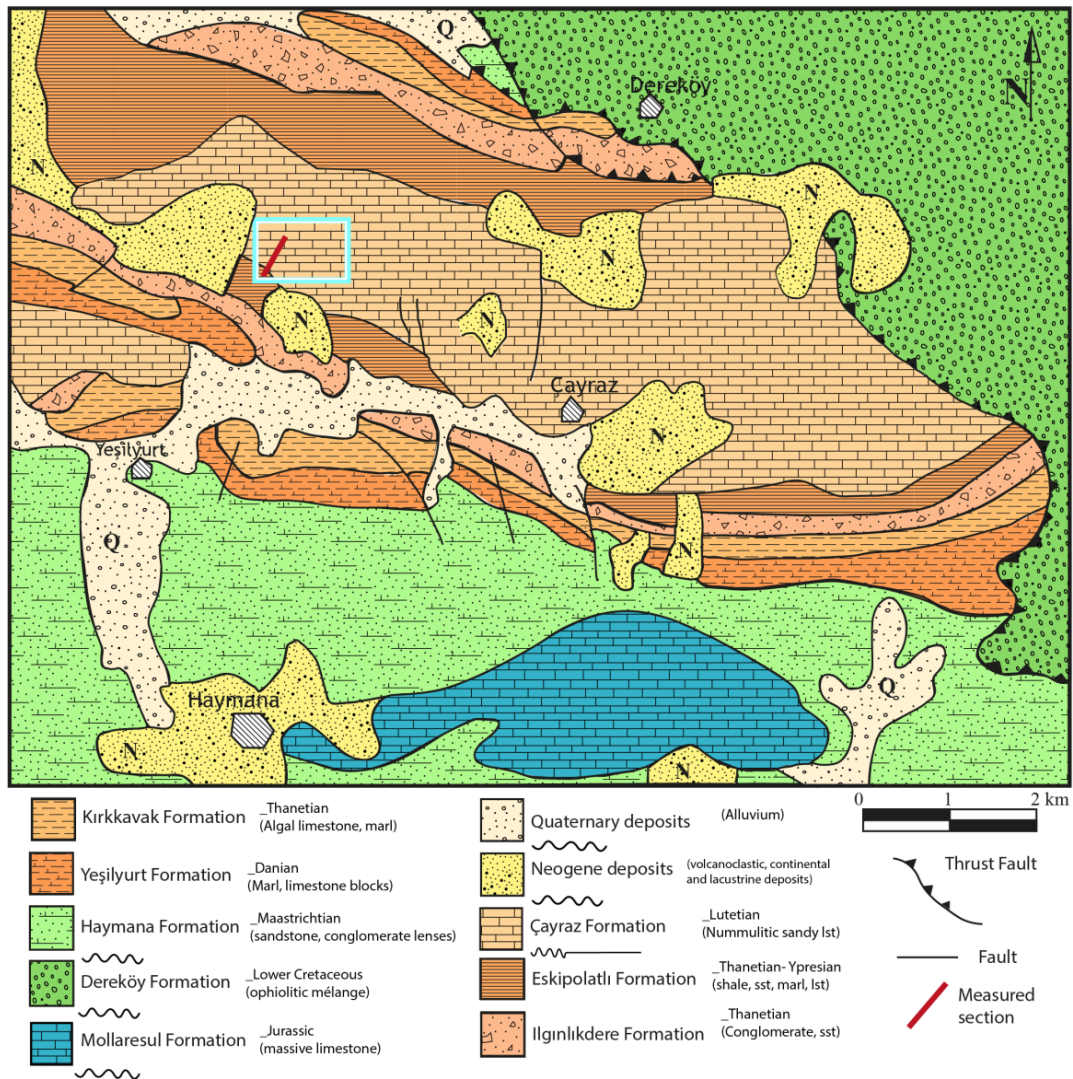


Figure 20: Generalized geological map of the Çayraz region with the subunits of the Haymana formation. (The red line shows the approximate location of the measured section, the white/blue rectangle shows the study area) (modified from Çiner, 1996).

The lateral and vertical relationships are also mentioned above. These lateral and vertical relationships of the formations illustrated by Ünalın et al. (1976) are used to create facies maps and made paleogeographic interpretations of the units. These interpretations have been made as the sea level interpretation of the settings. In this

thesis, the work of Ünalán et al. (1976) and Çiner et al. (1996a) has been taken as the base for this study. The formations of the Haymana basin have been distinguished by Ünalán et al. (1976) from the Upper Cretaceous to middle Eocene successions (Figure 15, 17). As shown in the generalized geological map (Figure 19), the Çayraz formation has contact with the Eskipolatlı Fm, however there are mentioned unconformity surfaces between Eskipolatlı and Çayraz formations (Ünalán et al., 1976). There is also conformable boundary between two formations (Ünalán et al., 1976; Çiner, 1996), it's approximately located near the study area of this study. The approximate location of the studied section of the Çayraz Formation is also given at the Generalized Columnar section of the Haymana Basin (Figure 17).

The studied section has been measured from the region extended from the 4km NW to the Çayraz village and 2km NE of the Yeşilyurt village (Figure 1, 21). The exposures are trending from NW to SE. According to the paleogeographical interpretation of Ünalán et al. (1976), the paleo land was on the northwestern side. Çiner et al. (1996a) suggested two shelf systems by the associations of basic sequences. These sequences are from bottom to top 1-) limestone- sandy limestone alternation, 2-) limestone sandy limestone marl alternation, 3-) thick monotonous marl horizon 4-) thick limestone sandy limestone marl alternation.,

The limestones can be classified as grainstones because their main components are large up to 3 centimeters foraminifers, especially *Nummulites* and *Alveolina*, *Assilina*. Moreover, sandy limestone and mudstone layers can be defined as packstone and wackestone. The nummulitic limestone levels of the formation are described as nummulite banks (Çiner et al. 1996a). Çiner et al.(1996a) assign these shelves as the lower shelf (first shelf) and the upper shelf systems. The measured section is located at the lower in other words first shelf system of the Çayraz formation. It started near the Eskipolatlı Formation and continued up to the end of the first shelf system. The section starts with the mudstone units with thin intercalations of limestone and sandstone. The thicknesses of the mudstones are decreasing and the thicknesses of the limestone bands are increasing.

Mudstone horizons between two shelves are interpreted as distal equivalent of shallow- marine limestones. Because of the decrease in the fossil content and lack of the large fossil content. Nummulitic banks are the proximal equivalent of the mudstone. Therefore, at the middle part of the two shelf systems can be sums up as shallow marine, shallow marine to slope, slope to front and another shallow marine in the sequences near the Çayraz Village.

2.1.1.1 The measured section of the Çayraz Formation

The measured section starts with mudstone lithology and continues with thin limestone units within these thick stacked mudstone packages (Figure 23). This indicates sea level fluctuation it caused the changes in lithologic properties of the units from the open marine mud to the shallow marine carbonate lithology. At first, it is sandy and fossiliferous in content, and its thickness is approximately in 50 meters. The fossil content and the relative abundance of fossils in a sequence vary so this is an indicator of the difference in the depositional environment of the lithology.



Figure 22: Close up view of the study area taken from Google Earth with measured section indicated. NB section showed with yellow lines and NB-B section showed with blue lines

After the alternation of fine sandy limestones and mudstones, two separated sandstone layers, i.e., fossiliferous sandstone, and sandstone levels are recorded. The succession is continued with several meters thick mudstone units, then it is followed by fossiliferous calcareous sandstone/ sandy limestone layer and then followed by fossiliferous limestone. After this point, the section is covered by 35 meters of a thick debris. After the end of the covered part, thick limestone units are observed and the content of the limestone gradually turned into the clayey fossiliferous limestone

(mainly composed of *Alveolina*, *Nummulites*, and *Assilina*). At the upper part of the succession, it turns into sandy limestone that is mainly composed of *Nummulites*, *Assilina*, and *Discocyclina* again.

The samples are taken at 5 m intervals. Pelecypods and gastropods and small *Nummulites* are readily observed as fossil contents in the first limestones unit (NB1) at the outcrop. In the third sample (NB3), sandstone with increasing particle size is observed. However, in the fifth sample (NB5), *Discocyclina* is recorded. *Assilina* and *Nummulites* are observed in the uppermost part of the section, and their relative abundances of these larger benthic foraminifers change from bed to bed. *Alveolina* is observed in the upper part of the studied succession.

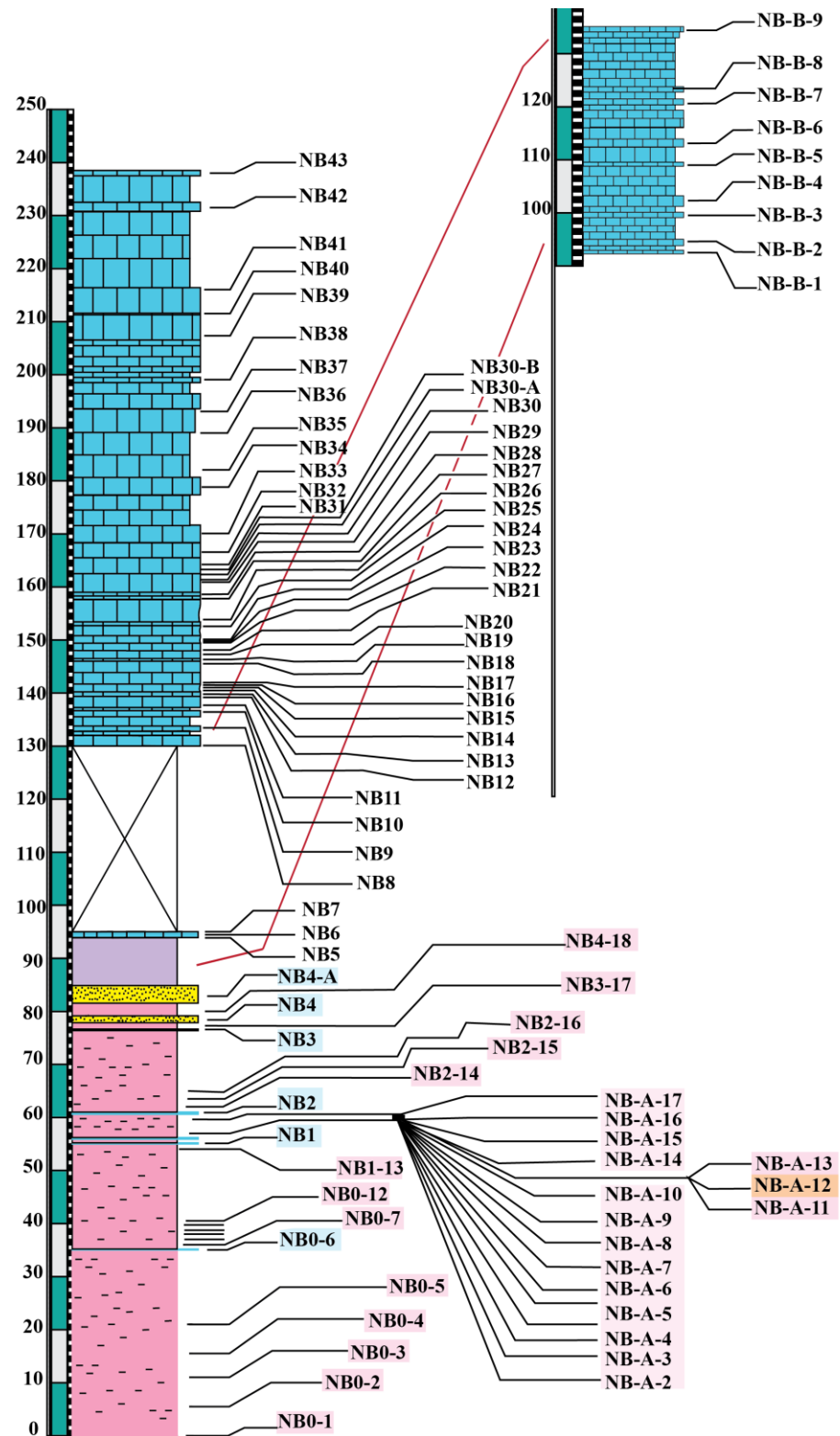


Figure 23: The Studied NB and NB-B Sections from the Çayraz Formation.

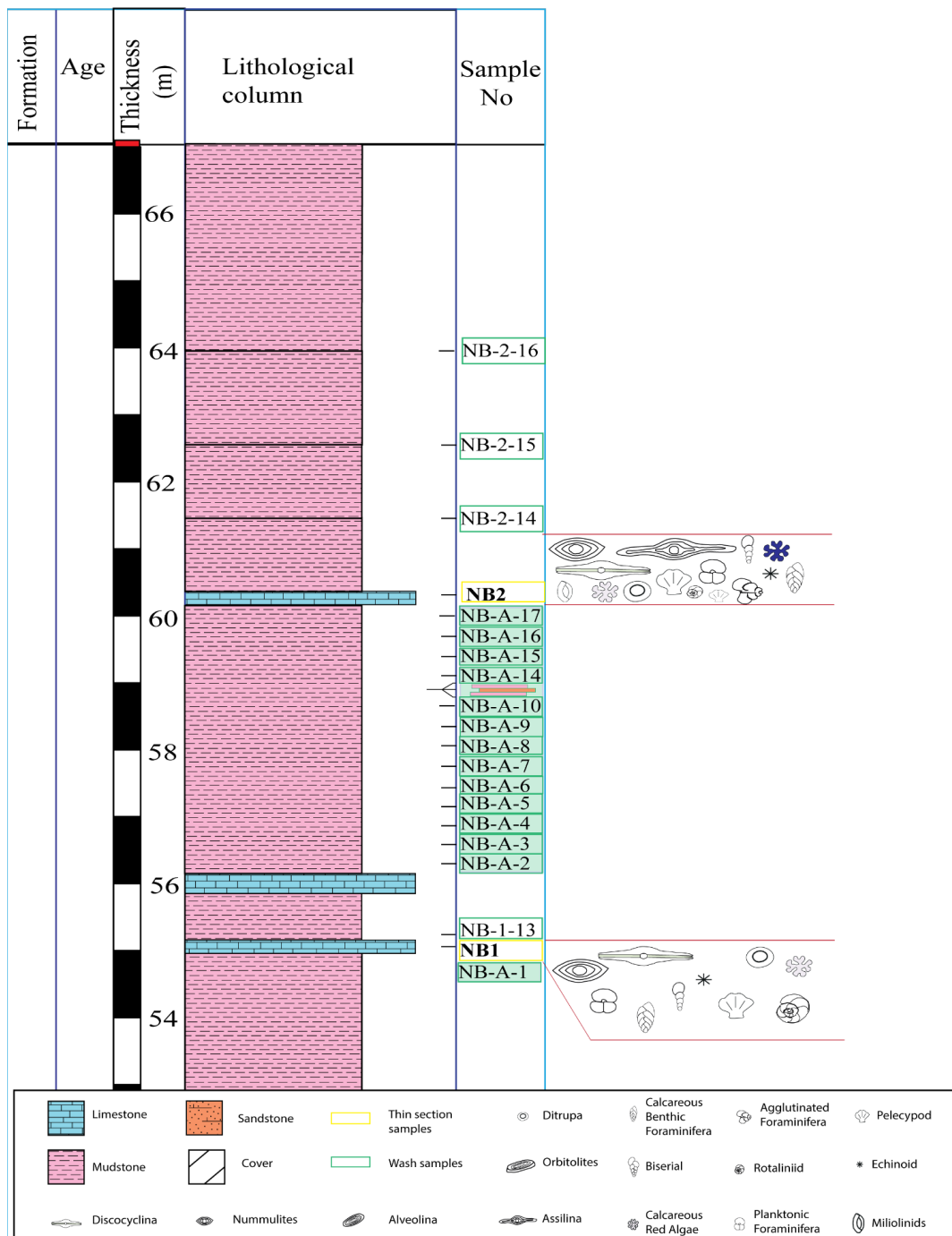


Figure 24: Detailed columnar section showing the taken samples NB1, NB2, limestone samples and NB-A-2, NB-A-3, NB-A-4, NB-A-5, NB-A-6, NB-A-7, NB-A-8, NB-A-9, NB-A-10, NB-A-14, NB-A-15, NB-A-16, NB-A-17, NB2-14, NB2-15, NB2-16 mudstone samples' location from the measured section.

From bottom to top of the measured section; the first sample (NB1) is a sandy limestone with small size *Nummulites* (Figure 24). A 4-meters thick mudstone succession between limestones is observed while continuing upward in the section. A total of 17 samples (NB-A-2 to NB-A-17) were taken from this part of the section at 32 cm intervals (Figure 24). Second limestone unit (NB2) is thicker (40cm) than the previous limestone unit (NB1), with small to medium *Nummulites* specimens. Foraminifers and pelecypods are recorded in these limestones. This sample is overlain by thick mudstone succession, 3 mudstone samples were taken with 110 cm intervals. After that point (NB2-16) the area is covered by vegetation and debris over the mudstones up to the following sample which is sandstone (NB3) (Figure 25).

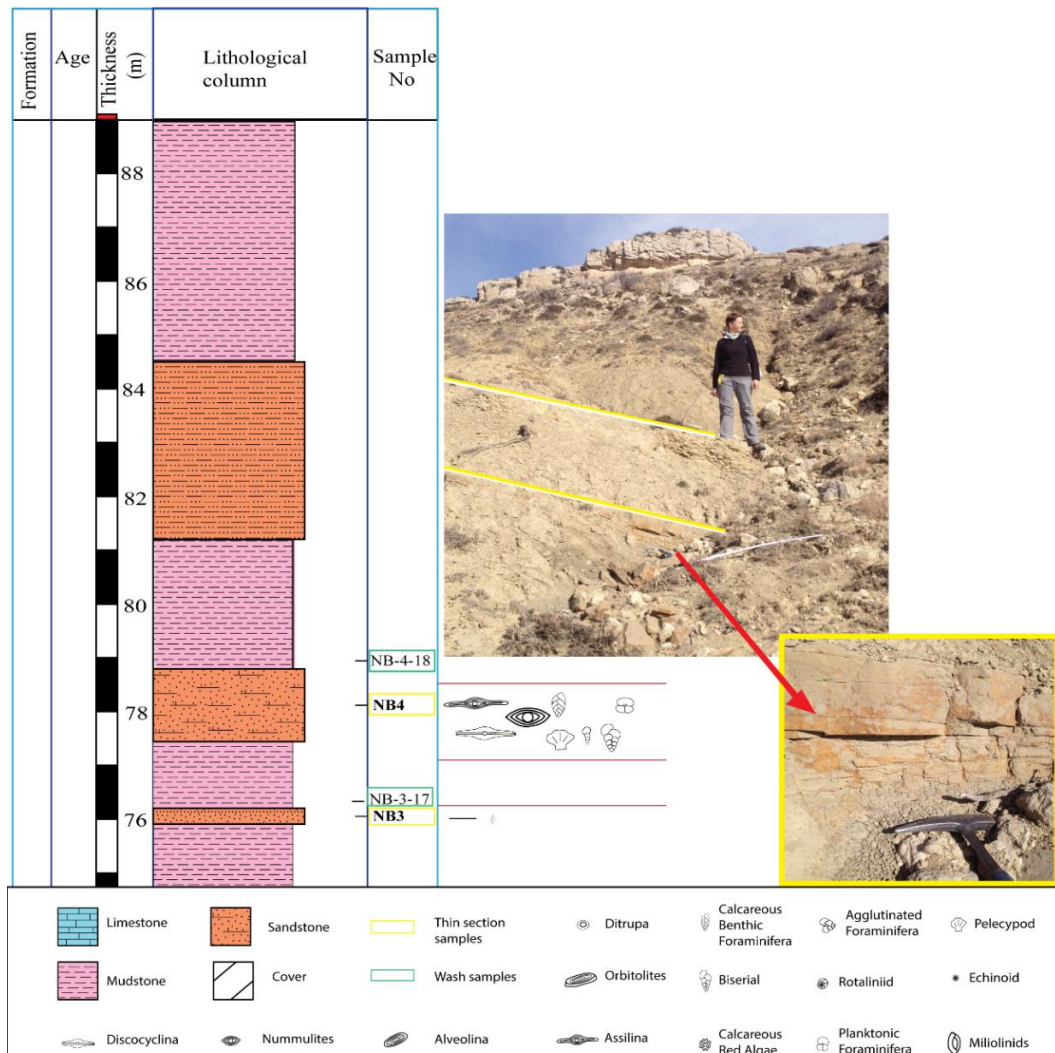


Figure 25: Detailed columnar section showing the taken samples NB3, NB4 location from the measured section.

The fossil content of this sandstone sample (NB3) is characterized by one fossil which is a suspension feeder worm like fossil which is called *Ditrupa* sp. After the non-fossiliferous sandstone level, the following lithology is the mudstone, the deposition is continued as 240 cm mudstone which is followed by the 330 cm sandstone (NB4) and continued by the 900 cm calcareous mudstone.

The next sample (NB5) was collected from the bottom of the 110 cm thick limestone layer after this thick calcareous mudstone (Figure 26). There are abundant medium-large *Nummulites* sp., pelecypoda, and *Ditrupa* sp., which a tube shape worm like fossil, and also abundantly coralline red algae (CRA). The following sample (NB6) was taken from the middle of the 110 cm thick limestone bed. It is characterized by very abundant *Nummulites* and *Assilina*. The NB6 sample is the first sample of the limestones that contains *Assilina*. The preservation of fossils in this sample is not the same or good in the previous sample.

Although the following sample (NB7) seems to have a relatively less fossil abundance in the field, the presence of benthic foraminifera are existed. The first occurrence of the *Alveolina* is also recorded in this sample (Figure 26). These three samples (NB5, NB6 and NB7) represent the first record of the changes in the depositional environment. These changes affect the preservation potential and the abundance of fossils in the samples. The relatively proximal units of the shelf are recognized on top of the relatively the distal units.

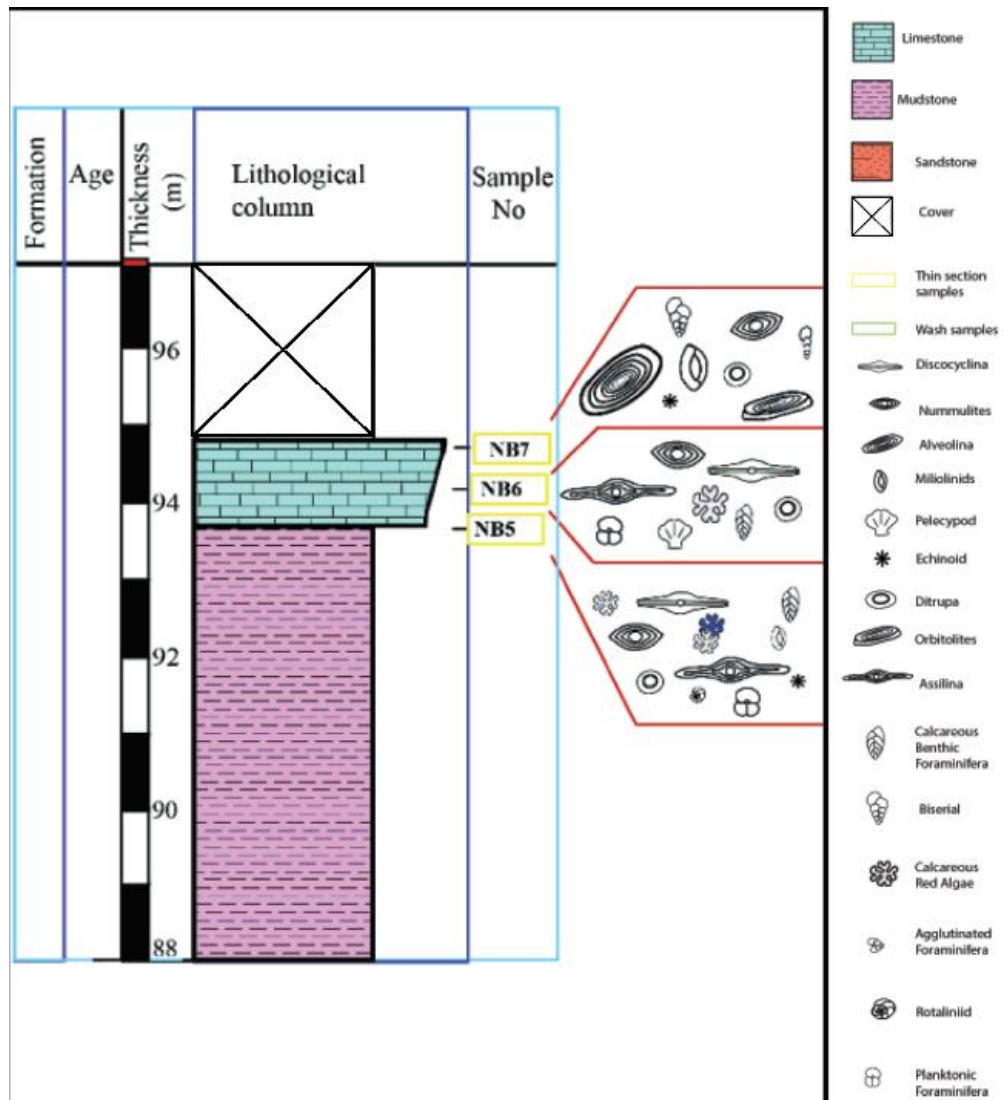


Figure 26: Detailed columnar section showing the taken samples NB5, N6 and NB7 location from the measured section.

After taking the last sample (NB7), there is a covered zone of 35 meters in thickness in the section (Figure26). This covered zone is shown in the whole stratigraphic section (Figure 23). While continuing upward in the section, the clastic input into the depositional environment is still continuing. This may indicates the fact that there was a river close proximate that feeds the shallow marine deposits. Moreover, the decrease in the presence of the small benthic foraminifers in the depositional environment in this particular sample also indicates that high energy levels even if the feeding mechanism of a stream does not exist, small benthic foraminifera has not preferred

this environment, which can be caused by the energy level of the area. Some of the *Nummulites* sp. and *Assilina* sp. are broken into the pieces.

Assilina sp. is still present in the following two samples (NB8 and NB9) (Figure 27). While the sand content is still high as in the previous sample, it becomes less sandy in the subsequent layers (NB10, NB11, NB12).

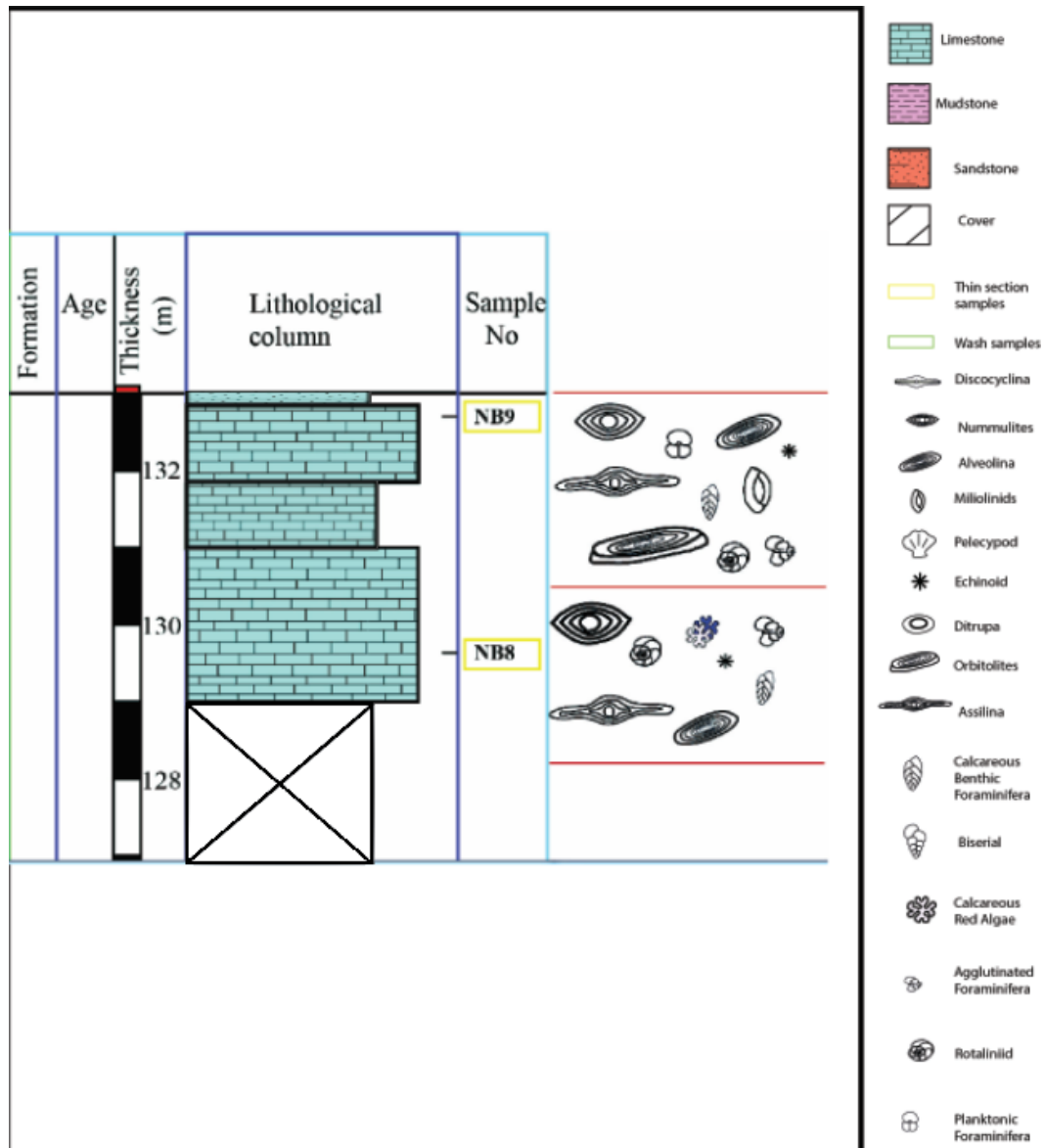


Figure 27: Detailed columnar section showing the taken samples NB8 and NB9 location from the measured section.

All the samples taken from the first continuous thick limestone succession are presented as follows (NB8- NB20). The limestone samples were taken from a thick limestone package that has no mud or any clastic intercalation recorded (Fig. 27, 28, 29). The thickness of this limestone stack which is approximately 20 meters, consist of multiple layers. The sample NB9 contains *Alveolina* sp., and they were observed in the field for the second time, while the sand amount has decreased considerably compared to the previous samples (NB7, NB8).

Alveolina sp. became the dominant fossils group in the part of the succession while continuing upwards through the section, starting from in the middle of this 20 meters measured part (NB12- NB17) (Figure 28). While going upward, the limestone layer, the last three samples (NB17, NB18, NB19) were taken from a highly jointed beds 430 centimeters thick.

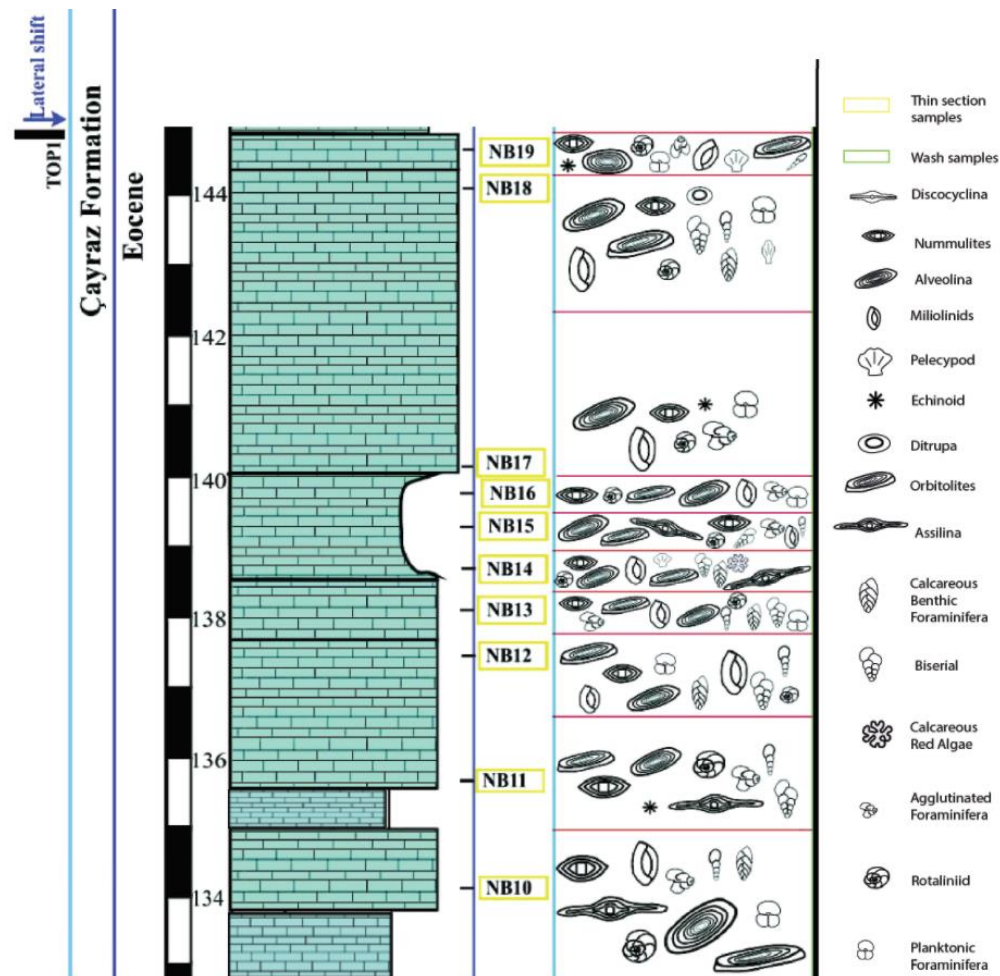


Figure 28: Detailed columnar section showing the taken samples NB10, NB11, NB12, NB13, NB14, NB15, NB16, NB17, NB18 and NB19 location from the measured section.

The next sample (NB20) is the limestone with clay composition and abundant fossil content. At this fossiliferous limestone, the clay content was first observed in the field. Therefore, it is considered as the changes in the depositional environment. Even if there is no observable difference in the rock type (Figure 29), still environment of deposition change is possible.

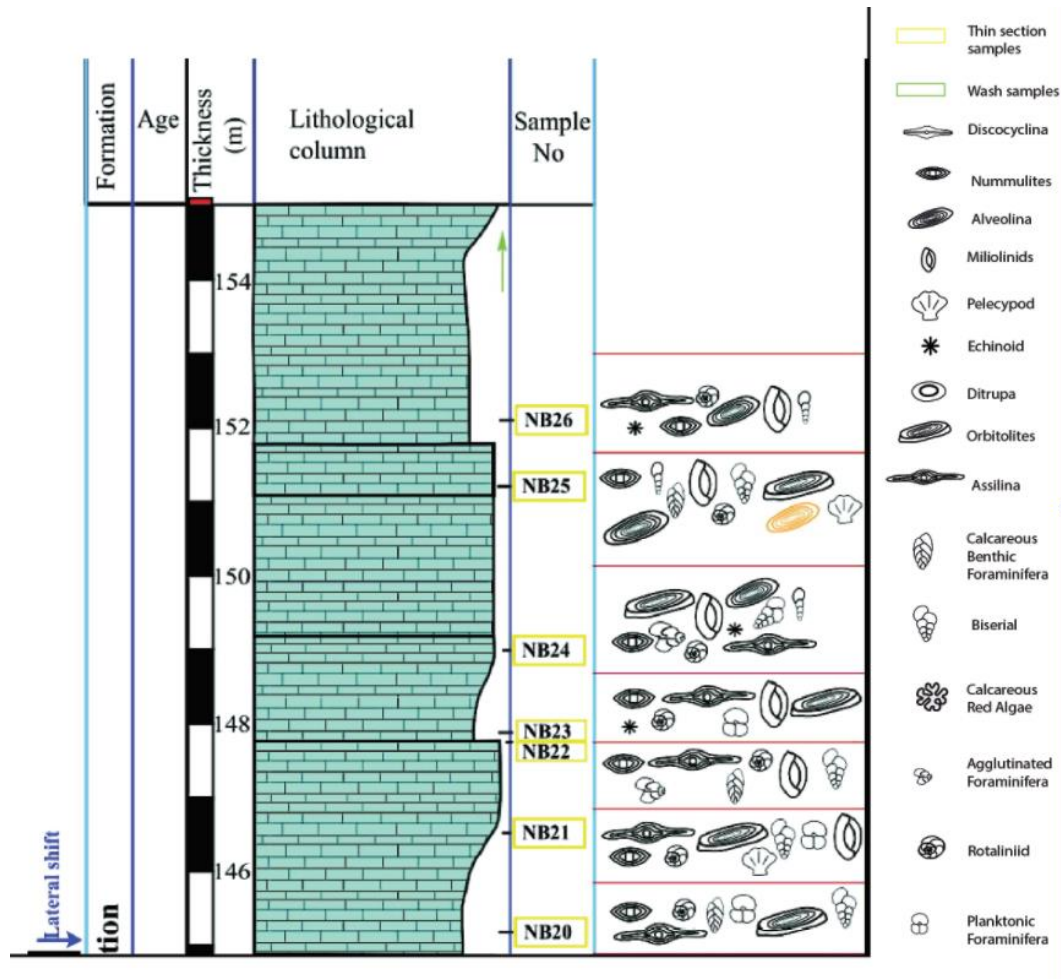


Figure 29: Detailed columnar section showing the taken samples NB20, NB21, NB22, NB23, NB24, NB25 and NB26 location from the measured section.

The following few samples (NB21- NB26) are characterized by a very similar composition and fossil occurrences. After that near at the top of the hill, the limestone unit with gastropods, pelecypods (only depending on the field observation) was observed. This bed (NB25) is thin compared to its successive beds. It has the larger benthic foraminifers such as; *Alveolina* and *Orbitolites*. An increase in the amount of clay through the sequence was observed until the samples (NB27-NB30). The subsequent samples were taken (NB30-A, NB30-B) after the top of the hill.

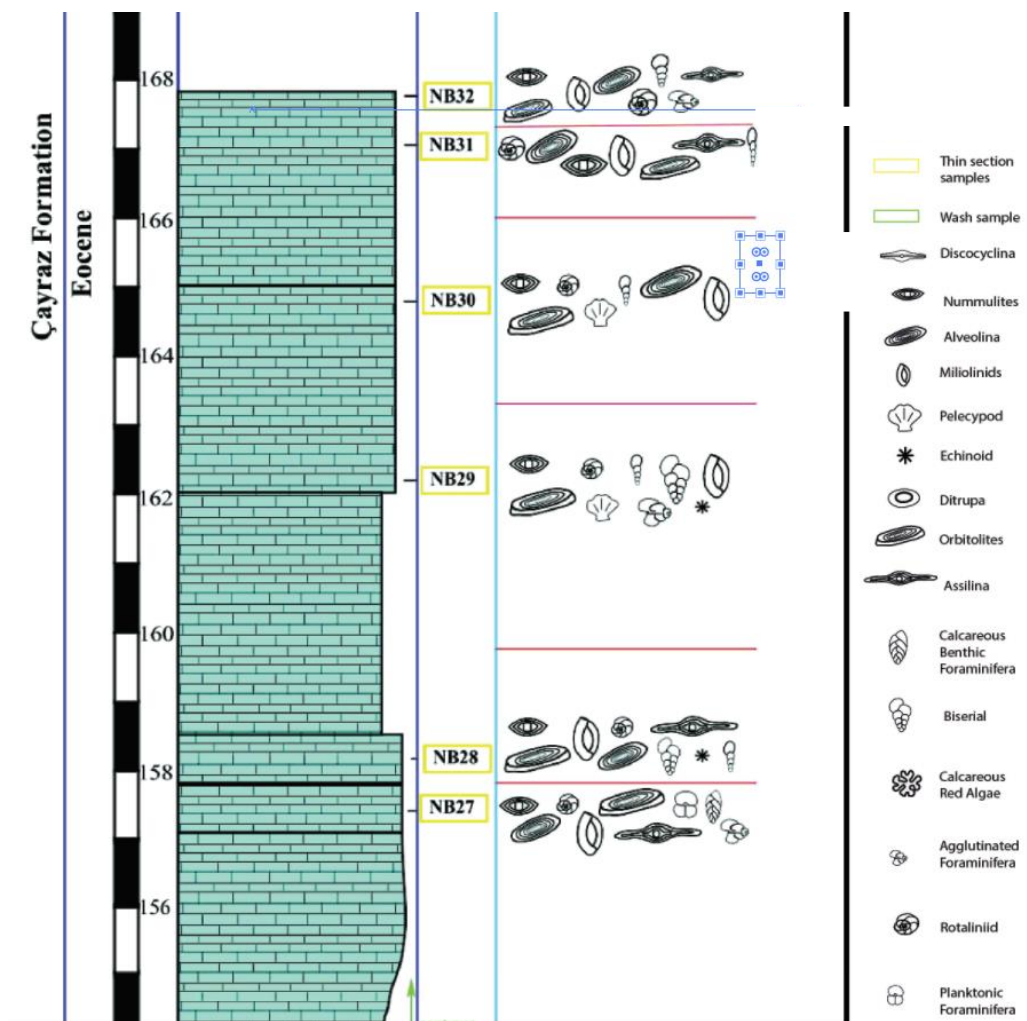


Figure 30: Detailed columnar sections showing the taken samples NB27, NB28, NB29, NB30, NB31 and NB32 location from the measured section.

The following samples (NB31 and NB32) (Figure 30) contain *Orbitolites* sp. and *Alveolina* sp. along with the miliolids, *Assilina* sp., and *Nummulites* sp.. The samples collected from the SE side of the hill are NB33 to NB43. These two samples (NB33 and NB34) contain *Assilina*, *Nummulites* and *Alveolina*. *Assilina* was not observed in the NB35 and NB36 samples. The following sample NB37 consist of *Nummulites*, *Assilina* and *Alveolina* again. The main fossil content of the NB38 was *Nummulites*, with absence of the *Alveolina* and *Assilina*. NB39 was the sample the *Alveolina*, *Assilina* and *Nummulites* recorded in the sample again. The following samples NB 40 and NB41 were the last samples that *Alveolina* was recorded. In the sample NB42,

large *Assilina*, *Discocyclina*, and *Nummulites* were recorded in the rock sample. The last sample of the measured section was NB43. The NB43 sample was characterized by the presence of *Discocyclina* and *Assilina*.

CHAPTER 3

MICROFACIES

For the purpose of determining the depositional models and recognizing facies zone, microfacies analyses are essential (Flügel, 2010). The term microfacies is previously defined only petrographic and paleontological criteria studied in thin sections. However, today this term is referred to all sedimentological and paleontological data determined from rock samples, polished slabs and thin sections (Flügel, 2010). Microfacies studies reflect the history and depositional environments of carbonate rocks (Flügel, 2010). Facies models service and support the understanding of the depositional environments. Changes in biological and sedimentological criteria across the shelf-slope basin transects form the basis of generalized models for carbonate platforms, ramps, and shelves. The distribution of the RMF and the bio zonation patterns reflect the facies belts (Flügel, 2010). Major criteria for classifying allochthonous limestones are depositional fabric, the abundance of grain categories, and the type of fine-grained matrix and types of carbonate cements associated with the grains (Flügel, 2010). Each lithofacies indicates a specific hydrodynamic environment. Microfacies types of carbonate rocks are not restricted to specific time intervals. Therefore, Wilson (1975) established the term standard microfacies types (SMF types) which can describe major depositional and biological controls. A total of 24 standard microfacies types have been distinguished by Wilson (1975). Flügel (2010) described 30 microfacies types for the carbonate ramps as ramp microfacies types (RMF) (Figure 36), and also classified 26 standard microfacies types (SMF) (Figure 35) for rimmed carbonate platforms.

In this study, the carbonate rocks are named according to the Dunham Classification (1962) and 12 different microfacies in the measured section are determined by the analysis of bioclastic components, and sedimentological features observed in the thin sections. Microfacies types distinguished in the studied rocks are summarized in Table 1. The main microfacies types are bioclastic packstone, bioclastic packstone to

wackestone, bioclastic wackestone, bioclastic grainstone, bioclastic packstone to grainstone, and grainstone.

3.1. Microfacies Types

Microfacies analyses have been done through detailed examinations of thin-sections of samples. In order to conduct the study, polarized light microscope has been used. In order to determine of the facies, several parameters were taken into consideration, such as; broken or intact representation of the fossil, absence or presence of the fossil, matrix composition, ratio of the fossils to the matrix, change in the abundance of specific microfossil groups, ratio of one fossil groups to another.

Dunham's classification is on the recognition of the depositional texture. Embry and Klovan have expanded and revised Dunham's classification (Figure 31) (Dunham, 1962; Embry and Klovan, 1971; Wright, 1992; Flügel, 2010).

CLASSIFICATION OF LIMESTONES (DUNHAM 1962)

DEPOSITION TEXTURE RECOGNIZABLE				Original components were bound together during deposition as shown by intergrown or lamination contrary to gravity, sediment-floored cavities that are roofed over by organic or questionable organic matter and are too large to be interstices	DEPOSITIONAL TEXTURE NOT RECOGNIZABLE
Contains mud (particles of clay and fine silt size)		Grain-supported	Lacks mud and is grain-supported		
Mud-supported					
less than 10% grains	more than 10% grains				CRYSTALLINE CARBONATE (Subdivide according classification designed to bear on physical texture or diagenesis)
MUDSTONE	WACKESTONE	PACKSTONE	GRAINSTONE	BOUNDSTONE	

EXPANDED CLASSIFICATION (EMBRY and KLOVAN 1971)









ALLOCHTHONOUS LIMESTONE ORIGINAL COMPONENTS NOT ORGANICALLY ORIGINAL BOUND DURING DEPOSITION					AUTOCHTHONOUS LIMESTONE COMPONENTS ORGANICALLY BOUND DURING DEPOSITION			
Less than 10% > 2 mm components contains lime mud (< 0.03 mm)		no lime mud		Greater than 10% > 2 mm components		by organisms which		
Mud supported		Grain-supported		Matrix-supported	> 2 mm component supported	build a rigid framework	encrust and bind	act as bafflers
less than 10% grains (> 0.03 mm and < 2 mm)	greater than 10% grains							
MUDSTONE	WACKESTONE	PACKSTONE	GRAINSTONE	FLOATSTONE	RUDSTONE	FRAMESTONE	BINDSTONE	BAFFLESTONE

REVISED CLASSIFICATION (WRIGHT 1992)

DEPOSITIONAL				BIOLOGICAL			DIAGENETIC			
Mixed supported (clay and silt grains)		Grain-supported		In situ organisms			Non-oblitative			Oblitative
< 10% grains	> 10% grains	with matrix	no matrix	rigid organisms dominant	encrusting binding organisms	organisms acted to baffle	main component in cement	many grain contacts micro-stylolites CONDENSED	most grain ascontacts are micro-stylolites FITTED	crystals > 10 µm
CALCI-MUDSTONE	WACKESTONE	PACKSTONE	GRAINSTONE	FRAMESTONE	BOUNDSTONE	BAFFLESTONE	CEMENTSTONE	GRAINSTONE		SPARSTONE
	FLOATSTONE	RUDSTONE								Crystals < 10 µm MICRO-SPARSTONE
	Grains > 2 mm									

Figure 31: Original, expanded and revised Dunham classification (Embry and Klovan, 1971) (The ones that were observed in the study have been indicated by red square) (gathered from Flügel, 2010)

Folk's classification system is another system to be used for the classification of carbonate rocks (Figure 32, Figure 33). This classification depends on the evaluation of the hydrodynamic conditions. Whether it is deposited in high energy environment or not. The ratio of the matrix is the main parameter for the Folk's Classification. However, the lack of specific name usage in the Folks Classification would make all the signed micro facies will be called as same name (packed biomicrite).

	Over 2/3 Lime Mud Matrix				Subequal Spar and Lime Mud	Over 2/3 Spar Cement		
	0 - 1 %	1 - 10 %	10 - 50 %	over 50%		Sorting poor	Sorting good	Rounded and abraded
Percent Allochems								
Representative Rock Terms	Micrite	Fossil- iferous Micrite	Sparse Biomicrite	Packed Biomicrite	Poorly washed Biosparite	Unsorted Biosparite	Sorted Biosparite	Rounded Biosparite
								
1959 Terminology	Micrite	Fossil- iferous Micrite	Biomicrite		Biosparite			
Terrigenous Analogues	Claystone		Sandy Claystone	Clayey or Immature Sandstone	Submature Sandstone	Mature Sandstone	Supermature Sandstone	



 Lime Mud Matrix
  Sparry Calcite Matrix

Figure 32: Folk's Textural Classification of Carbonate Sediments (The ones that were observed in the study have been indicated by red square) (Flügel,2010, after Folk,1959)

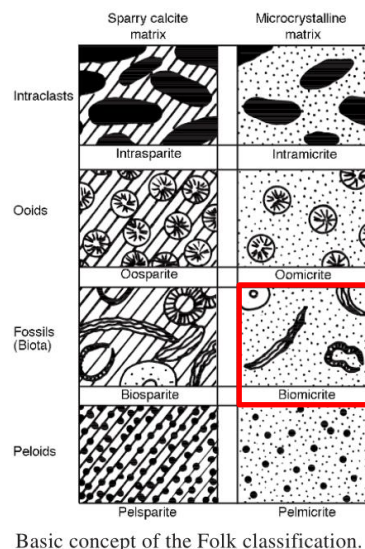


Figure 33: Folk's Textural Classification of Carbonate Sediments (The one that was observed in the study have been indicated by red square) (Flügel,2010, after Folk,1959)

When microfacies analysis is performed, all parameters such as particle type, matrix, the average ratio of properties, deposition texture, and fossil types should be observed. (Flügel, 2010). Dunham's classification of carbonate rocks (1962) is considered to be the main source, where the relationships between micro and macrofossils, field observations on outcrop rock, and lithological changes are considered together. This classification was used in the classification of carbonate rocks of the Çayraz Formation. According to Dunham (1962), there are two main types, one with carbonate, which is bonded with each other during deposition, which is called boundstone, and the other main group is not initially bound, which is called packstone (Figure 34). The second distinction is related to how these particles stand together if they are supported by particles, packstone or grainstone. If the particles are resting on each other, and if the support is provided from sludge (matrix), it is called mudstone or wackestone. Depending on the types of matrix, such as micrites or sparry, this naming is also differentiated. Figure 34 shows the original version of the Dunham classification of carbonate rocks system.

Carbonates					
Dunham (1962)					
Groundmass:			+ spar		sparry cement
Fine carbonate matrix					Bioconstruction
Matrix-supported		Grain-supported			
Grains: < 10%	> 10%				
MUDSTONE	WACKESTONE	PACKSTONE	GRAINSTONE	BOUNDSTONE	
Folk (1959, 1962)					
Allochems:					
< 1%	1-10%	10-50%	packed	> 50%	
fossiliferous	sparse			poorly washed	
MICRITE	BIOMICRITE			BIOSPARITE	BIOLITHITE
Terrigenous					
Matrix-supported			Grain-supported		
Sand: < 10%	10-25%	> 25%			
sandy			WACKE	SUBWACKE	ARENITE
MUDSTONE			SANDSTONE		

Figure 34: Fossiliferous limestone classification after Dunham (1962) and Folk (1959, 1962). (The ones that were observed in the study have been indicated by red square) (gathered from Flügel, 2010)

These Folks's and Dunham classifications distinguish allochthonous limestones (mudstone, wackestone, packstone, grainstone) from autochthonous limestones (here called boundstone or biolithite), Limestones whose components were deposited as

discrete grains are grouped according to mud-support or grain- support and the abundance of the grains. The Dunham classification stresses the depositional fabric, the Folk Classification tries to evaluate hydrodynamic conditions. Both classifications consider the dominating groundmass types.

The main expected microfacies types according to the samples encountered during the sampling of the Çayraz formation and subsequent thin section investigations are; bioclastic packstone, bioclastic packstone/wackestone, bioclastic wackestone, and wackestone. In the limestone samples taken, almost all of the formation was defined as packstone in the field and then the possibility of some of the sand-containing ones being grainstone was taken into consideration in the laboratory investigations. Sparry calcite was not observed in the samples in the field. Only two samples (NB20 and NB21) contained sparry calcite in the laboratory investigation. They have occurred after the rock formation, therefore, there is no reason to take them into consideration as the depositional environment indicator.

The two of the most frequently used microfacies models were proposed by Wilson (1975) and Flügel (2010) (Figure 35, Figure 36). Both of these detailed microfacies models have been examined. Wilson (1975) proposed a conceptual model and defined 9 Standard Facies Zones (FZ) which describe facies belts along an abstract transect from an open marine deep basin across a slope, a platform marginal rim including reefs and sand shoals, and an inner platform to the coast (Figure 35). This model of Wilson (1975) was revised and modified by Flügel (2010). 26 Standard Microfacies Types (SMF) have been proposed for the rimmed type carbonate shelves. Flügel also designed a conceptual facies models for unrimmed, ramp-type carbonate platforms. 30 Ramp Microfacies type (RMF) have been proposed for the ramp type carbonate platform (Figure 36). Carbonate ramps are carbonate platforms that have a very low gradient depositional slope (commonly less than 0.1 ~ from a shallow-water shoreline or lagoon to a basin floor (Burchette & Wright 1992).

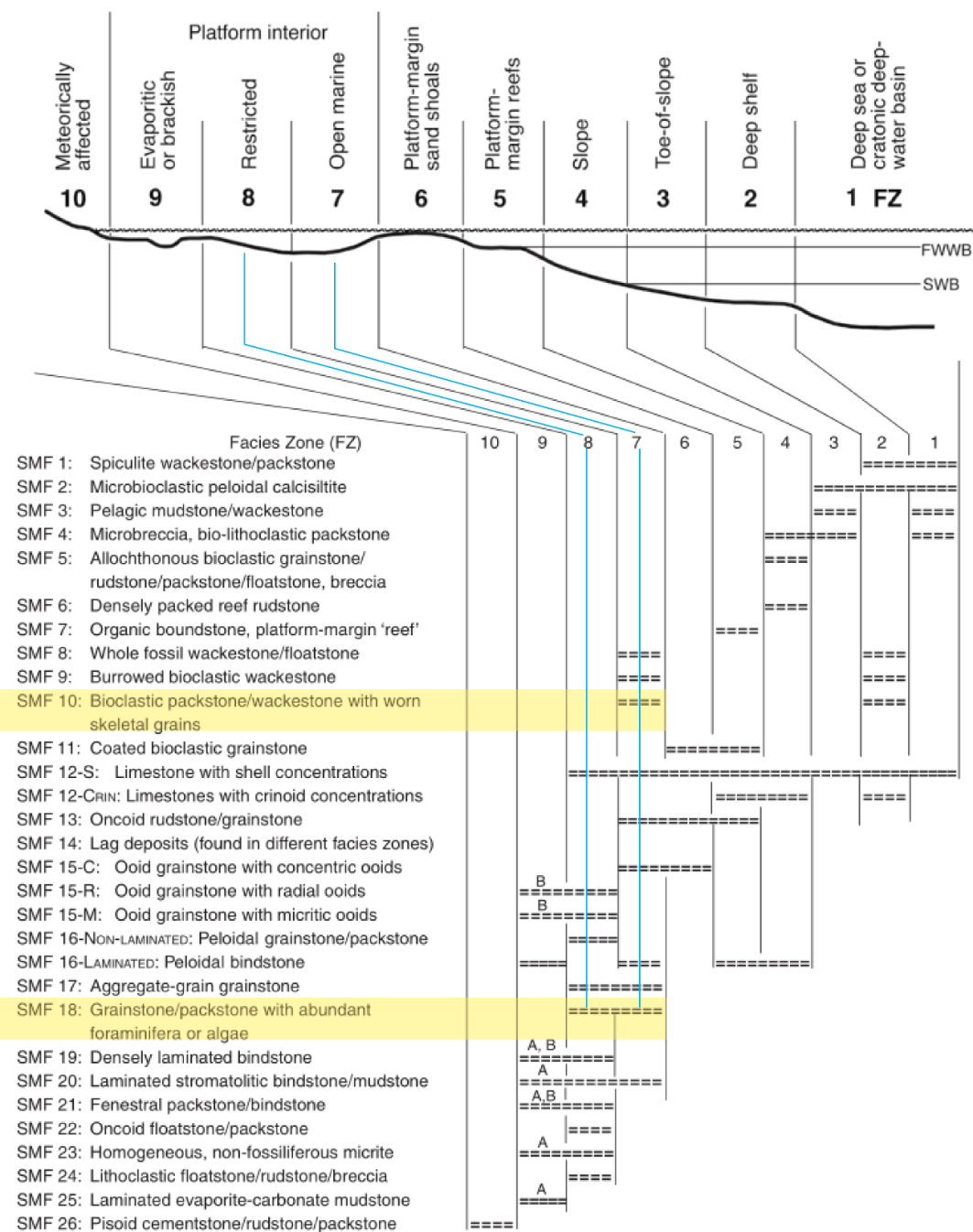


Figure 35: Distribution of the Standard Microfacies (SMF) types in the Facies Zones (FZ) of the rimmed carbonate platform model (Flügel, 2010) (A: evaporitic, B: brackish). The ones that were observed in the study have been indicated by yellow highlights.

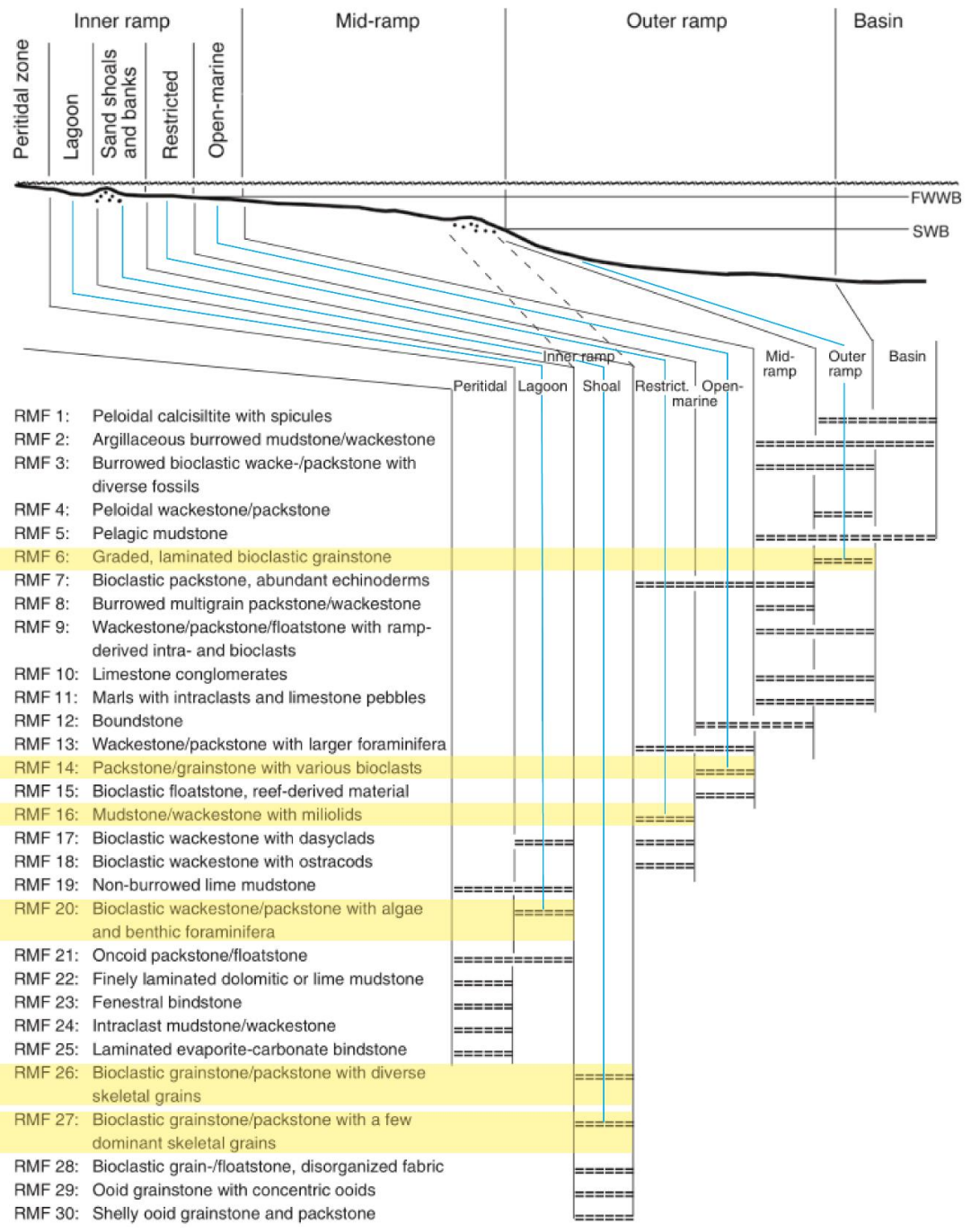


Figure 36: Generalized distribution of microfacies types in different parts of a homoclinal carbonate ramp (Flügel, 2010). The ones that were observed in the study have been indicated by yellow highlights.

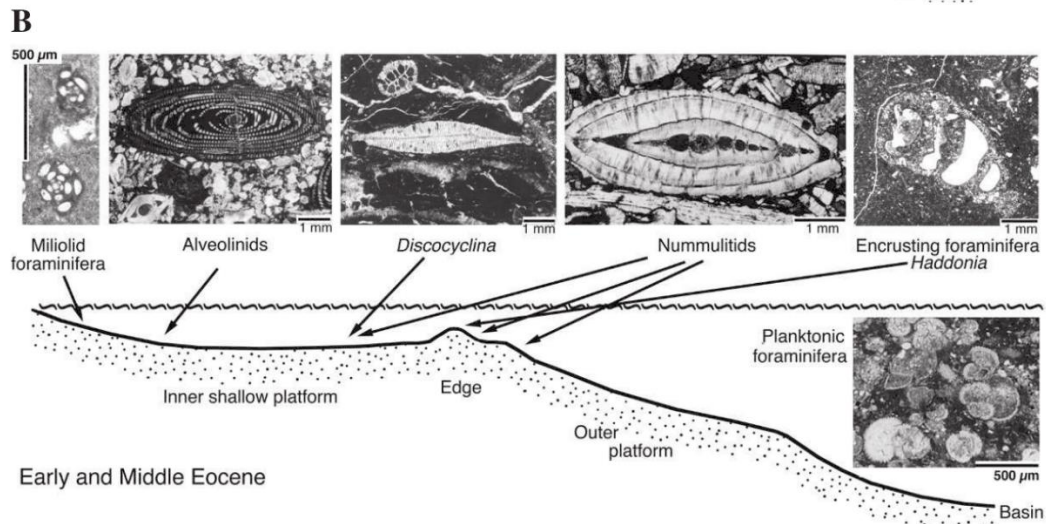


Figure 37: Early and Middle Eocene depositional platform model for large benthic foraminifera, and the distribution of the fossils over the platform (Flügel, 2010).

Figure 37 shows the Early and Middle Eocene depositional platform model for large benthic foraminifera and the generalized distribution of the fossils over the platform (Flügel, 2010). According to this model, miliolid foraminifers predominantly occur on the inner shallow platform near the coast. Alveolinids predominantly occur on the inner shallow platform. *Discocyclina* and nummulitids predominantly occur on the inner shallow platform near the edge. Nummulitids (*Nummulites*, *Assilina*) are also predominantly present on the edge which can be shoal and sand banks depositional environment of the homoclinal ramp, or platform-margin sand shoals of the rimmed platform model. Encrusting foraminifers such as *Haddonia* predominantly occur on the edge. This model summarizes foraminifera distribution during the Eocene on an idealized carbonate ramp from the shallowest to the deepest part of the ramp. Sartorio and Venturi (1988) also use a similar depositional model for the platform carbonates of Tale- Zang Formation at the type section and Kialo section, Zagros Basin, SW Iran.

Nummulites sp., *Assilina* sp., *Discocyclina* sp., alveolinids., miliolids, coralline red algae, increase or decrease of the abundance of planktonic foraminifers, uniserial or biserial agglutinated fossils, echinoderm fragments, increase or decrease in the sizes of gastropod, ostracod, varieties of these fossils, abundance and associations of the

fossil groups, quartz fragments, presence of micrite. That is the examination that can be carried out in thin-sections.

In this study, the main microfacies types that are encountered through the thin section analyses are; MF1 miliolinid, alveolinid, orbitolitid, bioclastic packstone, MF2 orbitolitid, alveolinid, miliolinid, bioclastic packstone to wackestone, MF3 nummulitid, alveolinid, miliolinid, bioclastic packstone to wackestone, MF4 nummulitid, orbitolitid, bioclastic packstone to grainstone, MF5 nummulitid, assilininid, bioclastic packstone, MF6 nummulitid, discocyclinid, assilininid, bioclastic packstone to wackestone, MF7 assilininid, nummulitid, bioclastic grainstone, MF8 discocyclinid, nummulitid, assilininid, planktonic foraminiferal, bioclastic packstone to wackestone, MF9 discocyclinid, nummulitid, bioclastic grainstone, MF10 discocyclinid, nummulitid, planktonic foraminiferal, bioclastic packstone, MF11 grainstone (very rare fossil composition with broken fossil fragments), MF12 small benthic foraminiferal, planktonic foraminiferal wackestone.

In some samples (NB5) fossils, bioclasts, appear clean, while others have various problems in the preservation of bioclasts. The reason for these differences is entirely related to the depositional environment. As they have been deposited at different times, the increase or decrease of the sea level naturally causes the living groups to change, and the increase in the energy level of the environment also affects the preservation of the tests of the dead organisms.

Sea level is one of the most important environmental conditions. As mentioned before, one of the events observed in the thin sections examined is the increase of planktonic foraminifers in the rock compared to the changing sea level. Planktonic foraminifera can be lived in the photic zone as they are suspended in water. Benthic foraminifera is also known to live in close relationship with the seafloor, but depth affects them more than planktonic foraminifera. Therefore, the increase of planktonic foraminifers in the rock is provided by the decrease of benthic foraminifers.

Lagoon Facies

3.1.1 MF1, Miliolinid, alveolinid, orbitolitid, bioclastic packstone

MF1 microfacies is mainly composed of miliolids, alveolinid, together with orbitolitid, nummulitid, also agglutinated foraminifers. They are listed based on their abundances, from the most abundant to relatively less abundant. In other words the relatively most abundant foraminifer in the facies is miliolid. The second most abundant foraminifer is alveolinid, and the third most abundant foraminifer is orbitolit. This facies corresponds to RMF20 (Flügel, 2010). Since the RMF20 corresponds to the bioclastic wackestone and packstone with calcareous algae and benthic foraminifera. This microfacies indicates inner ramp, near coast depositional environment, and brackish water (Flügel, 2010). The depositional environment is a lagoon. Microfacies 1 (MF1) is shown in the figure 39. This is most proximal microfacies in the carbonate ramp model that is determined in the sample NB7 (Figure 38) from the measured section. This microfacies is recorded in the samples NB7, NB17, NB18, NB19. Bioclastic packstone and grainstones microfacies with similar test fragments of porcelaneous foraminifera have been observed in the Eocene Succession, at Hamzeh-Ali Area, North- Central Zagros Iran (Moghaddam et al., 2002).

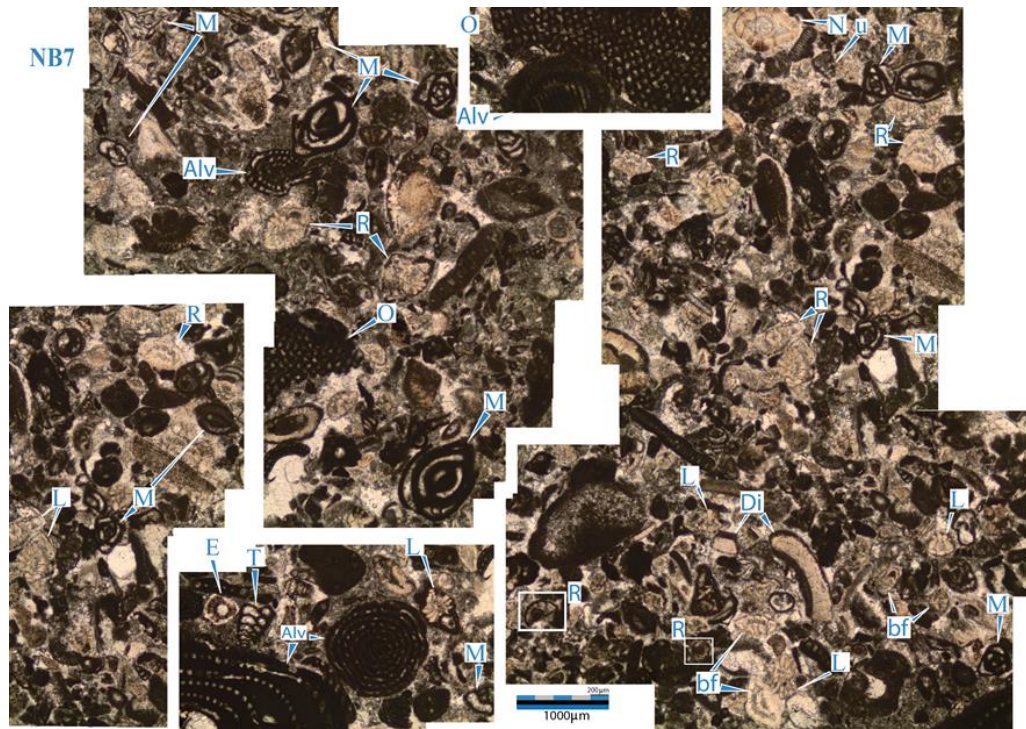


Figure 38:Photomicrograph of MF1 (sample NB7).

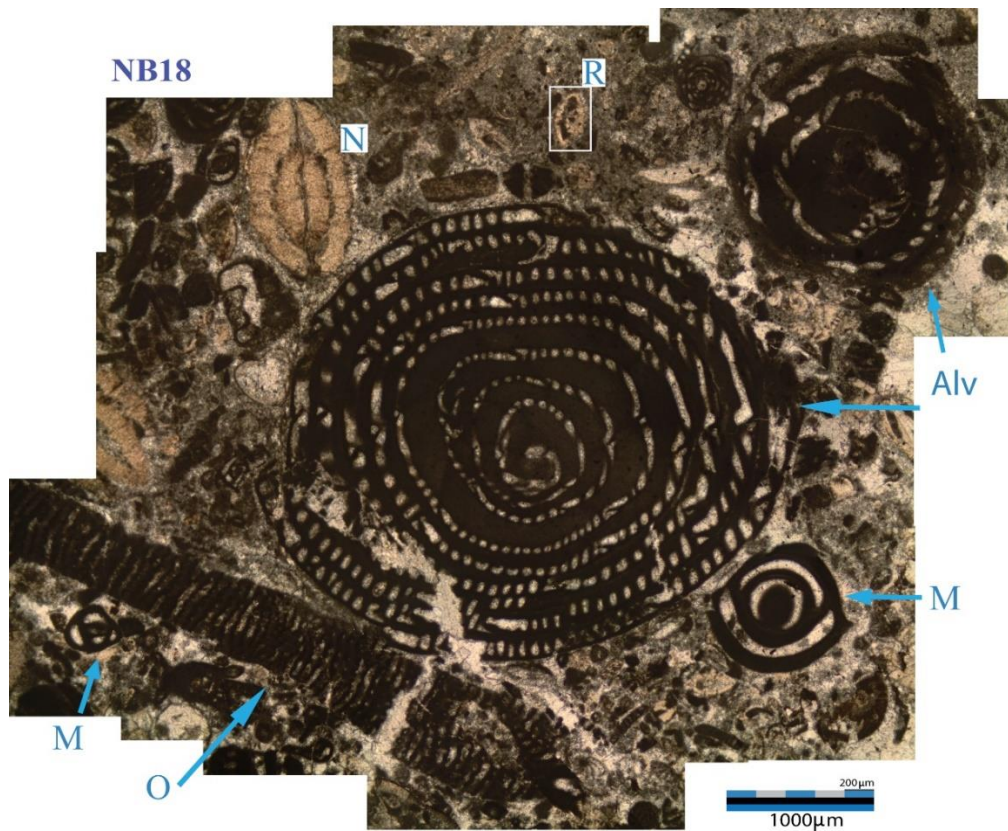


Figure 39: Photomicrograph of the MF1 (sample NB18).

3.1.2 MF2, Orbitolitid, alveolinid, miliolinid, bioclastic packstone to wackestone

MF2 microfacies mainly consists of *Orbitolites* sp., alveolinids, miliolids, *Nummulites* sp., and *Assilina* sp.. *Orbitolites* is the most abundant foraminifer in this microfacies. Alveolinids and miliolinids abundance are also high with respect to the other foraminifers. Therefore, the microfacies is named as orbitolitid, alveolinid, miliolinid, bioclastic packstone to wackestone. Abundance of *Orbitolites* sp., alveolinids, and miliolids respectively presents itself in decreasing trend. Microfacies 2 (MF2) is shown in the figure 40, 41. This facies corresponds to RMF20 (Flügel, 2010). Since the RMF20 corresponds to the bioclastic wackestone and packstone with calcareous algae and benthic foraminifers. MF2 indicates an inner ramp through the lagoon depositional environment. Orbitolinid abundance increase and also respectively decrease of the miliolid foraminifers differs MF2 from MF1. This microfacies is recorded in samples NB12, NB16, NB25, NB27, NB28, NB30-B, NB31, NB36, NB39.

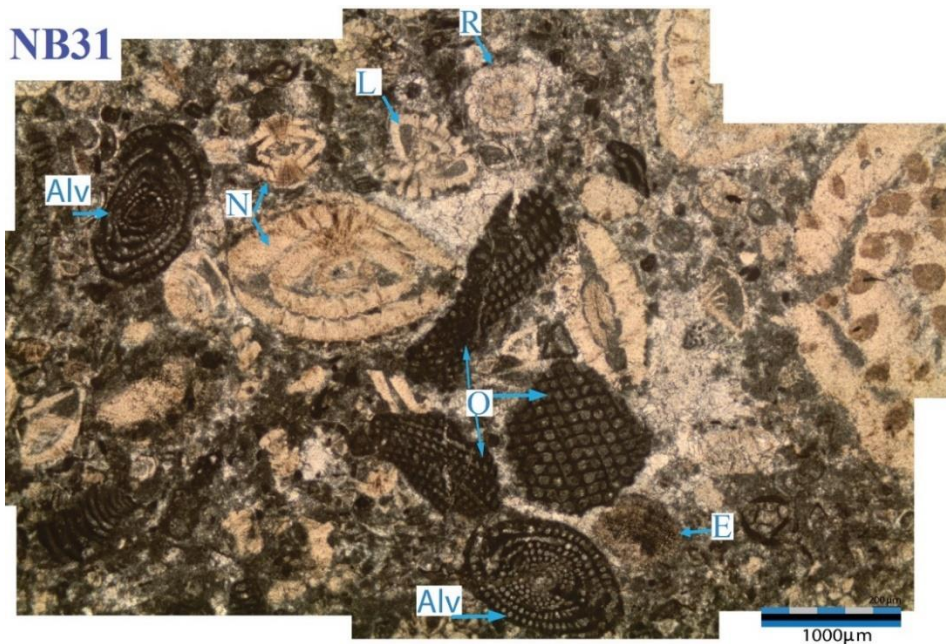


Figure 40: Photomicrograph of the MF2. (sample number NB31. *N*: *Nummulites* sp., *R*: Rotaliniid, *O*: *Orbitolites* sp., *Alv*: *Alveolina* sp., *L*: *Lockhartia* sp. *E*: Echinoid fragment.)

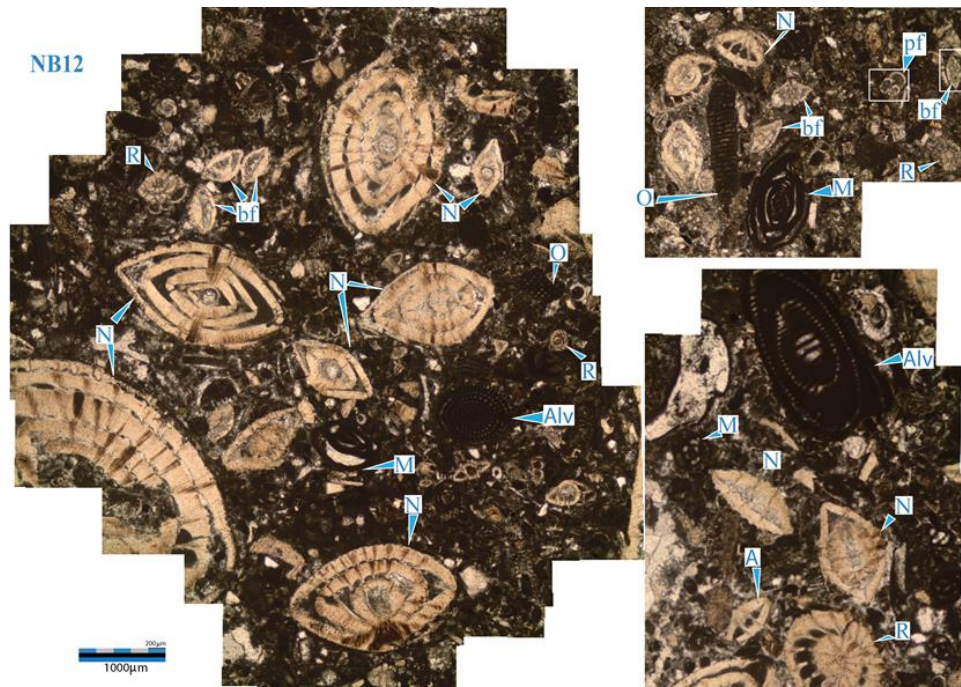


Figure 41: Photomicrograph of MF2 (sample number NB12. *N*: *Nummulites* sp., *R*: Rotaliniid, *O*: *Orbitolites* sp., *M*: Miliolinid, *Alv*: *Alveolina* sp., *L*: *Lockhartia* sp. *E*: Echinoid fragment, *bf*: benthic foraminifera, *pf*: planktonic foraminifera.)

3.1.3 MF3, Nummulitid, alveolinid, miliolinid, bioclastic packstone to wackestone
 MF3 microfacies is mainly composed of *Nummulites* sp., alveolinid, miliolids, and agglutinated foraminifers. . The order of the constituents within the name of the microfacies is based on their relative abundances of them; from the most abundant foraminifer to the least abundant foraminifers respectively. Abundance of *Alveolina* sp., and miliolid respectively decrease, with an increase in the *Nummulites* sp. presents itself. Microfacies 3 (MF3) is shown in the figure 42. This facies corresponds to RMF20 (Flügel, 2010). Since the RMF20 corresponds to the bioclastic wackestone and packstone with calcareous algae and benthic foraminifera. MF3 indicates the inner ramp and lagoon depositional environment. An increase in the abundance of nummulitid makes this microfacies to be different from the MF2. This microfacies is recorded in the samples NB-B-6, NB-B-9, NB14, NB15, NB24, NB26, NB30, NB30-A, NB32, NB35, and NB37.

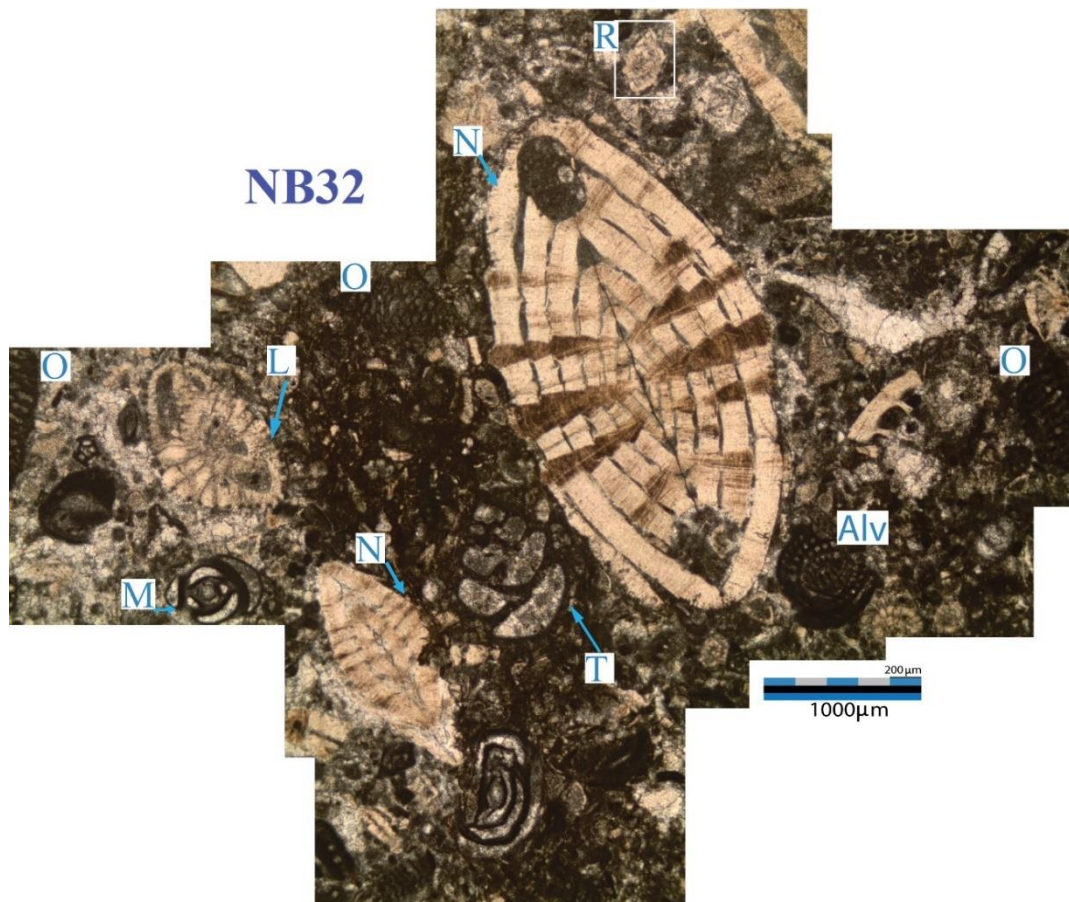


Figure 42: Photomicrograph of the Microfacies 3 (sample NB32. A: *Assilina* sp., Alv: *Alveolina*, L: *Lochartia* sp., M: *Milionid*, N: *Nummulites* sp., O: *Orbitolites* sp., R: *Rotaliniid*.sp., T: *textularina*.)

3.1.4 MF4, Nummulitid, orbitolitid, bioclastic packstone to grainstone

MF4 microfacies is mainly composed of *Nummulites* sp. and *Orbitolites* sp.. This microfacies is named by using the relative abundances of the constituents; the first is the most abundant foraminifer which is *Nummulites* in the facies then the second most abundant foraminifer which is *Orbitolites*. Thus the name is nummulitid, orbitolitid, bioclastic packstone to grainstone. This facies corresponds to RMF 20 (Flügel, 2010). Since the RMF20 corresponds to the bioclastic wackestone and packstone with calcareous algae and benthic foraminifers. this microfacies indicates an inner ramp and lagoonal depositional environment at the near shoal part. The bioclastic packstone to grainstone microfacies is differentiated from packstone only by the amount of the grains in the matrix being more than packstone. The abundance of the microfossils of *Nummulites* sp., *Orbitolites* sp. in the microfacies 4 (MF4) is shown in the figure 43.

At the sample NB9 (Figure 42) there is a good example of the small and larger benthic foraminifers. Observed fossils are (LBF) *Discocyclina*, *Nummulites*, *Assilina*, *Operculina*, *Lockhartia*, and Rotaliniid, *Ditrupa*, miliolid, coralline red algae (CRA), planktonic foraminifers, benthic foraminifera, agglutinated foraminifers, uniserial and or biserial ones, echinoid fragments, alveolinid fragments. Mostly the preservation of the fossil is good, however there are some samples that is not the case. The increase in abundance of the nummulitid and orbitolitid and also the decrease in the abundance of alveolinid and miliolinid differs this microfacies MF4 from MF3. This microfacies is recorded in the samples NB-B-2, NB7-A, NB9, NB11, NB13, and NB29.

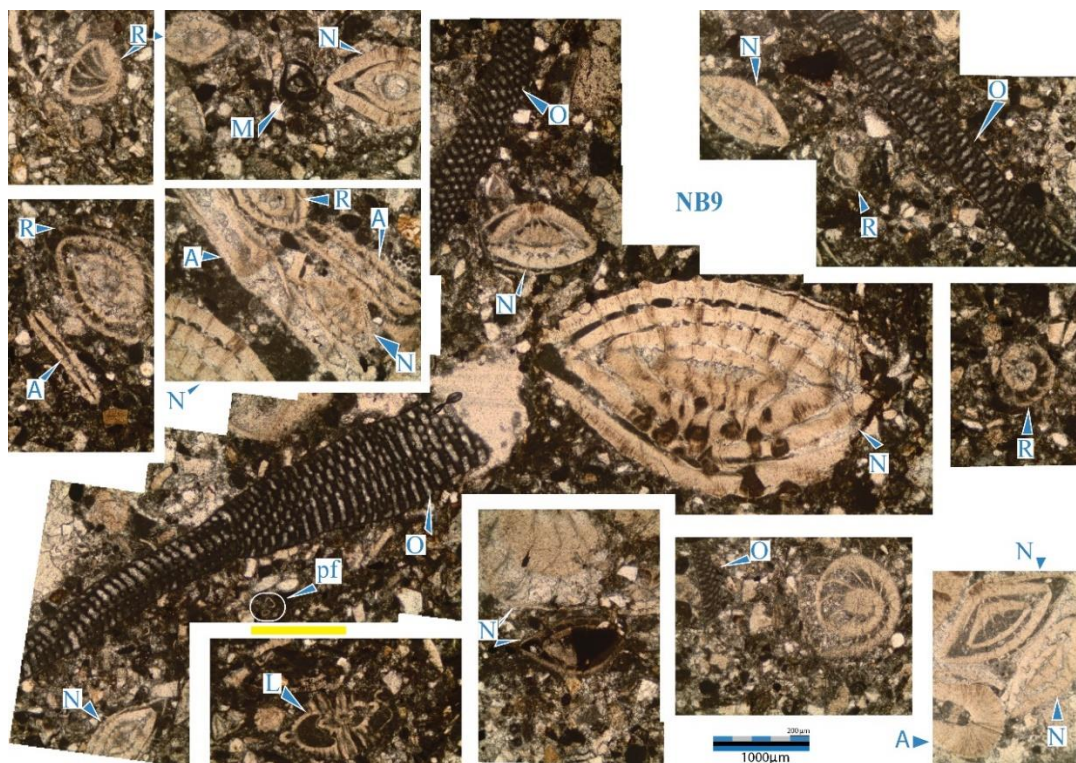


Figure 43: Photomicrograph of the microfacies MF4. (sample NB9. A: *Assilina* sp., bf: benthic foraminifera, D: *Discocyclina* sp., pf: planktonic foraminifera, N: *Nummulites* sp., O: *Orbitolites* sp., R: *Rotaliniid*.sp., L: *Lockhartia* sp.)

Shoal Facies

3.1.5 MF5, Nummulitid, assilinitid, bioclastic packstone

MF5 microfacies is mainly composed of *Nummulites* sp., *Assilina* sp.. Relatively highest abundant foraminifers are *Nummulites* and the second one is *Assilina*. Thus, the name of the microfacies is nummulitid, assilinitid, bioclastic packstone. This facies

corresponds to RMF27 (Flügel,2010). Since the RMF27 corresponds to the bioclastic grainstone and packstone that is composed of a few dominant skeletal grains, this microfacies indicates sand shoal and bank depositional environment. MF5 is shown in the figure 44. An increase in the abundance of *Nummulites* and decrease in the abundance of the orbitolite differs MF5 to MF4. This microfacies is recognized into the samples NB4-A, NB-B-5, NB-B-7, NB-B-8, NB10, NB20, NB21, NB22, NB23, NB33, NB34, NB38, and NB40. Bioclastic extraclastic packstone in the Upper Eocene shallow water carbonates from Rodnei mountains N Romania (Sahy et al., 2008) has also similar characteristics with this sample such as nummulitids, other benthic genera, and fragments of coralline algae, however differs with nodosariids and echinoids.

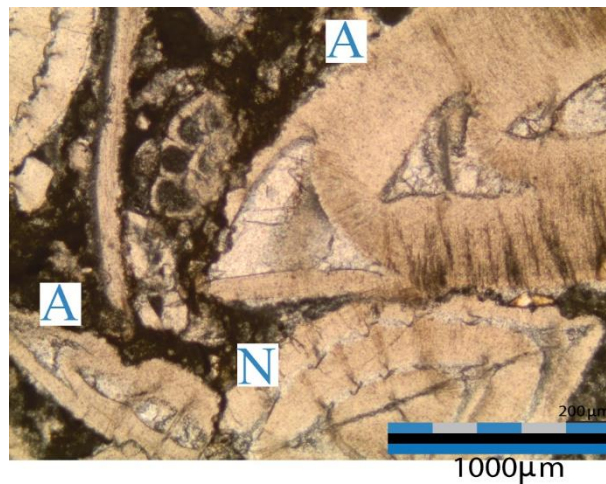


Figure 44: Photomicrograph of the MF5 (sample NB-B-7. MF7 A: *Assilina* sp., N: *Nummulites* sp.).

3.1.6 MF6, Nummulitid, discocyclinid, assilinid, bioclastic packstone

MF6 microfacies is mainly consist of *Nummulites* sp., *Discocyclina* sp., *Assilina* sp.. Relatively the most abundant foraminifers are *Nummulites*. The second most abundant foraminifers are *Discocyclina*, and the third most abundant foraminifers are *Assilina*. Therefore, the name of the microfacies is based on the relative abundance of these foraminifers; nummulitid, discocyclinid, assilinid, bioclastic packstone to wackestone. This facies corresponds to RMF27 (Flügel, 2010). Since the RMF27 corresponds to the bioclastic grainstone and packstone composed of a few dominant skeletal grains, this microfacies indicates inner ramp; sand shoal and bank depositional environment. An algal overproduction as seen in the photomicrographs of the MF6 is related to the

moderate to high energy, but mostly with high energy level (Wray, 1977). NB5 shows *Nummulites* sp. samples with intact and broken samples present together, CRA at the upper right of the photomicrograph, and there is a secondary crystallization of the upper part of the pelecypoda, bivalve (Figure 45). NB5, NB-B-4, are the samples in which this microfacies are recorded.

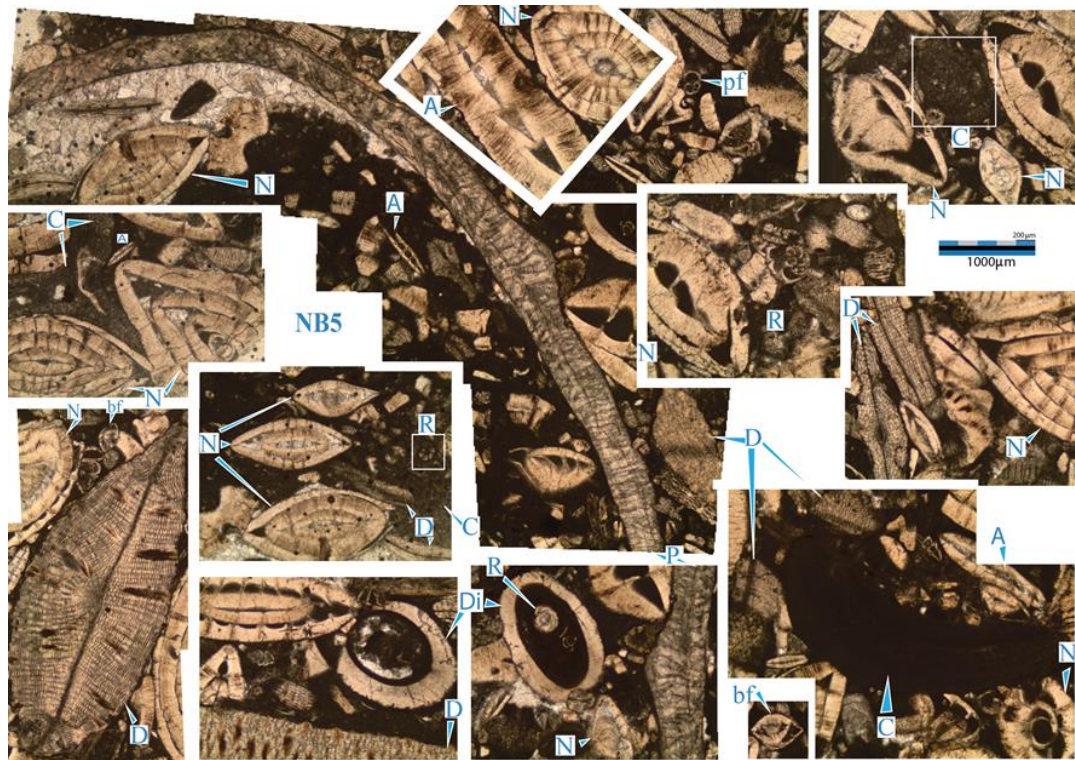


Figure 45: Photomicrograph of the MF6 (the sample NB5. P: pelecypoda surrounded with calcite crystal, C:LCRA and CRA. N: *Nummulites*, A: *Assilina* sp., R: *Rotaliniid*, pf: Planktonic foraminifera, Di: *Ditrupa* sp., D: *Discocyclina*, C: Coralline Red Algae (CRA)).

3.1.7 MF7, Assilinid, nummulitid, bioclastic packstone to grainstone

MF7 microfacies is mainly composed of *Assilina* sp., *Nummulites* sp., *Assilina* is the most abundant foraminifers in this microfacies. The second most abundant foraminifers is *Nummulites*. Therefore, the name of the microfacies is assigned as assilinid, nummulitid, bioclastic packstone to grainstone. This facies corresponds to RMF27 (Flügel, 2010). Since the RMF27 corresponds to the bioclastic grainstone and packstone composed of a few dominant skeletal grains, this facies indicates the inner ramp and sand shoal and bank depositional environment. MF7 is characterized by the

lack of micritic matrix and grain support presented, it has a high amount of bioclastic content. In sample NB8, there are very big forms of the *Assilina* (Figure 46). Such a big form indicates the warm-water condition (Flügel, 2010). An increase in the abundance of assilinid differs MF7 from MF5. This facies are recorded into samples NB8, NB41. Nummulitid grainstone microfacies with similar test fragments have been observed in the Eocene Ziarat formation, eastern Alborz zone, NE Iran (Hadi et al., 2021).

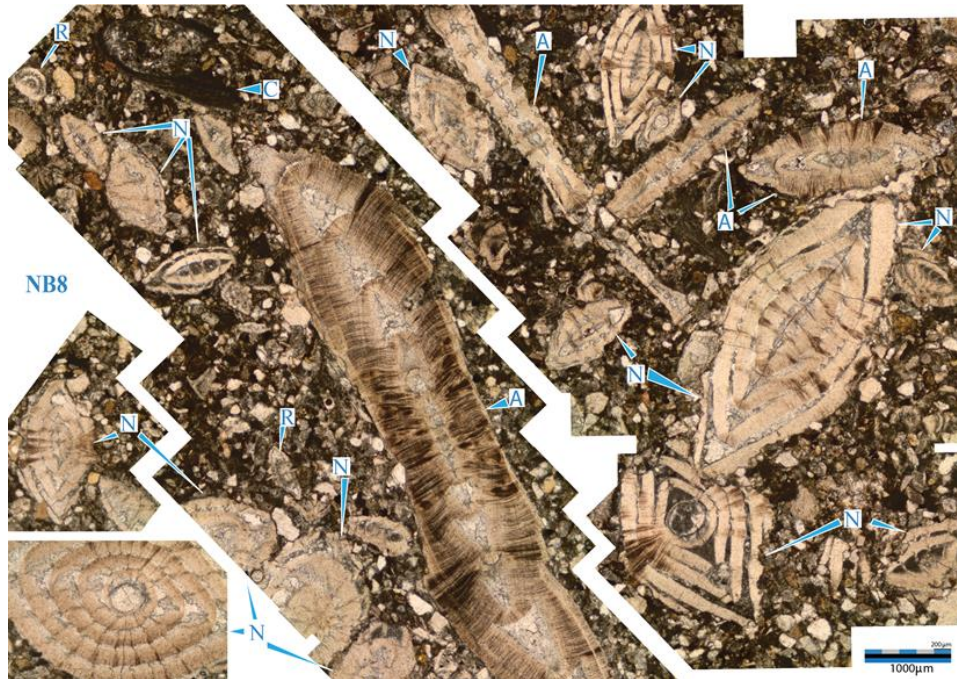


Figure 46: Photomicrograph of the MF7. (the sample NB8. A: *Assilina* sp., C: Coralline Red Algae, N: *Nummulites* sp., R: Rotaliniid, sand grains).

3.1.8 MF8, Discocyclinid, nummulitid, assilinid, planktonic foraminiferal, bioclastic packstone to wackestone

MF8 microfacies is mainly composed of *Discocyclina* sp., *Nummulites* sp., *Assilina* sp. Relatively most abundant foraminifers are *Discocyclina*. The second most abundant foraminifers are *Nummulites*. The third abundant foraminifers are *Assilina*. Thus, the name of the microfacies is assigned as discocyclinid, nummulitid, assilinid, planktonic foraminiferal, bioclastic packstone to wackestone. This facies corresponds to RMF27 (Flügel, 2010). Since the RMF27 corresponds to the bioclastic grainstone

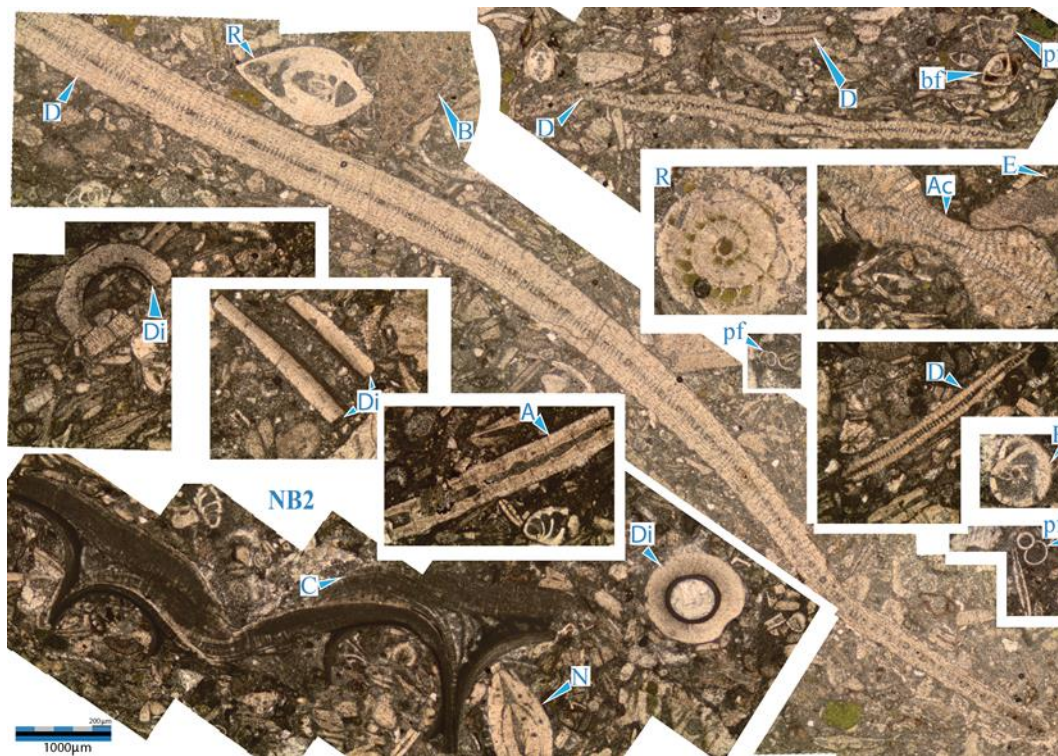


Figure 48: Photomicrograph of the MF8 (the sample NB2 , A: *Assilina* sp., Ac: *Actinocyclus* sp., D: *Discocyclina* sp., Di: *Ditrupa* sp., E: Echinoid plate, pf: Planktonic foraminifera, bf: Benthic foraminifera, N: *Nummulites* spp., C: Coralline Red Algae).

Shallow open marine facies

3.1.9 MF9, Discocyclinid, nummulitid, bioclastic grainstone

MF9 microfacies is mainly composed of *Discocyclina* sp. *Nummulites* sp.. Relatively the most abundant foraminifers are *Discocyclina*, and the second most abundant foraminifers are *Nummulites*. Therefore, the name of the microfacies is assigned as discocyclinid, nummulitid, bioclastic grainstone. This facies corresponds to RMF14. Since the RMF 14 corresponds to the bioclastic packstone or wackestone with skeletal grains this microfacies indicates the inner ramp, shallow open marine depositional environment. In the sample NB4, the grain support is provided by sand grains (Figure 49). In some of the samples, coralline red algae itself is the grain support factor. The size of *Discocyclina* and *Nummulites* are varied in the sample NB-4 (Figure 49). This microfacies is recorded in the NB2-A, NB4, NB-B-1, and NB-B-3. Bioclastic packstone microfacies with similarly large and flat nummulitids and discocyclinids

has been observed in the Eocene Succession, at Hamzeh-Ali Area, North- Central Zagros Iran (Moghaddam et al., 2002). Bioclastic extra-clastic grainstone (A3) microfacies also similar to this microfacies in the Upper Eocene shallow-water carbonates from Rodnei mountains at N Romania (Sahy et al.,2008) it is represented by discocyclinids alongside the nummulitids.

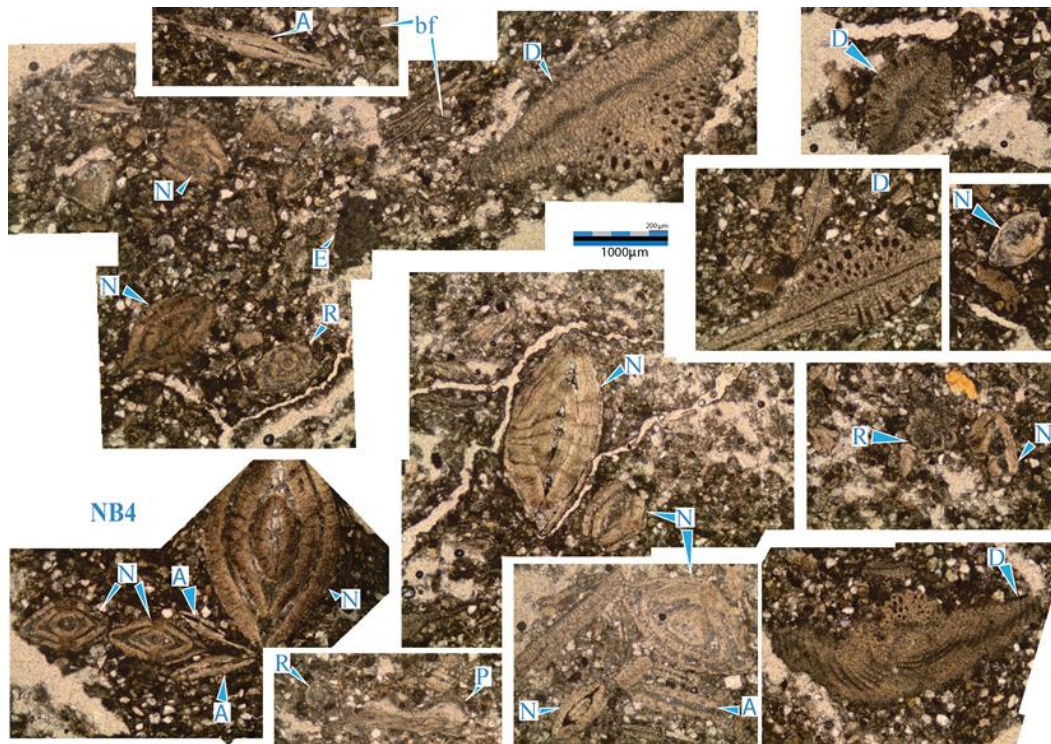


Figure 49: Photomicrograph of the MF9 (the sample NB4. MF11, A: *Assilina* sp., B: Benthic foraminifera C: Rotaliniid,, D: *Discocyclina* sp., E: echinoid fragment, pf: planktonic foraminifera, N: *Nummulites* sp., P: pelecypods).

3.1.10. MF10, Discocyclinid, nummulitid, planktonic foraminiferal, bioclastic packstone

MF10 microfacies is mainly composed of *Discocyclina* sp., *Nummulites* sp.. Relatively the most abundant foraminifers are *Discocyclina*. The second most abundant foraminifers are Nummulites. The third abundant foraminifers are planktonic foraminifers. Therefore the name of the microfacies is assigned as discocyclinid, nummulitid, planktonic foraminiferal, bioclastic packstone. This facies corresponds to RMF14 (Flügel, 2010). Since the RMF 14 corresponds to the bioclastic

packstone or wackestone with skeletal grains, this microfacies indicates the inner ramp, shallow open marine depositional environment. The first limestone sample (NB1) of the studied section is represented by bioclastic packstone microfacies. The fossil groups of the NB1; *Discocyclus* sp., *Nummulites* sp., pelecypods, small benthic foraminifers, planktonic foraminifers, ostracods, *Ditrupa* sp. in the NB1 sample (Figure 50). An increase in *Discocyclus* sp. and nummulitid abundance differs this microfacies from MF9 and MF8. This microfacies are recognized in the samples NB1, NB42, and NB43. Bioclastic packstone and wackestone microfacies with similar larger benthic foraminifers such as *Nummulites*, *Discocyclus* and also *Assilina*, *Operculina*, *Asterocyclus* has been observed in the Eocene Succession, at Hamzeh-Ali Area, North- Central Zagros Iran (Moghaddam et al., 2002).

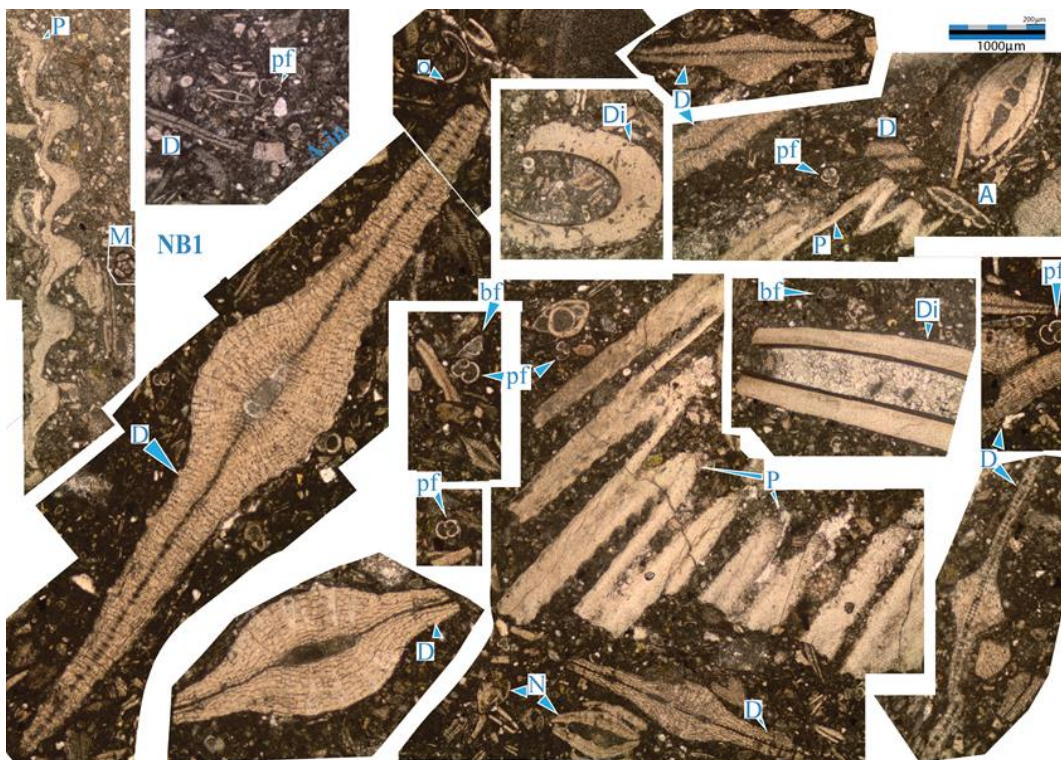


Figure 50: Photomicrograph of the MF10 (the sample NB1, D: *Discocyclus* sp., Di: *Ditrupa* sp. pf: Planktonic foraminifera, P: Pelecypods (Bivalve fragment), o: Ostracoda, bf: Benthic foraminifera, N: *Nummulites* spp., M: miliolid).

3.1.11 MF11 Grainstone

The MF11 type microfacies of the studied section is very poor in bioclast content and it mainly depends on the grain support. NB3 is the only representative of the sandstone without any larger benthic foraminifers. The remnants of the various fossils; broken fragments of benthic foraminifers, echinoid spines and one rotaliniid is the only recorded fossils in the sample NB3 (Figure 51). There is various mineral growth present in this quartz sandstone. Matrix is lime mud. Except these fossils this sample is nearly barren in terms of the fossil. This facies corresponds to RMF6 (Flügel, 2010). Since the RMF6 corresponds to graded, laminated bioclastic grainstone, the depositional environment is assigned to the outer ramp, near midramp. NB3 is the only recorded sample of this microfacies.

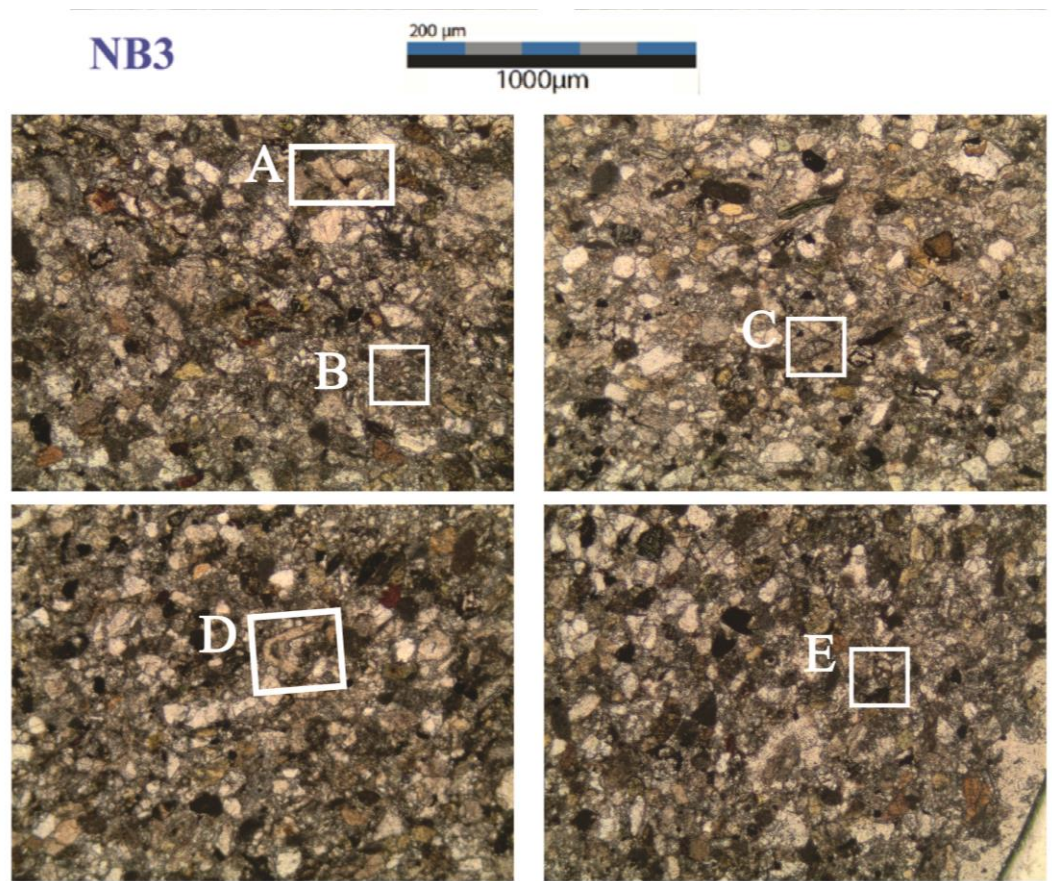


Figure 51: Photomicrograph of the Microfacies 11 (sample NB3, A & D: Broken benthic foraminifera fragment, B: echinoid spine, C: Rotaliniid, E: biserial.)

3.1.12 MF12 Small benthic foraminiferal, planktonic foraminiferal wackestone

The MF12 type microfacies of the studied section, is highly abundant in small benthic foraminifers and few planktonic foraminifers. This facies corresponds to RMF5 (Flügel, 2010). Since the RMF5 corresponds to wackestone with abundant benthic foraminifers and a few planktonic foraminifers, the depositional environment is assigned as the outer ramp, near midramp. This microfacies is recorded into the samples NB0-1, NB0-2, NB0-3, NB0-4, NB0-5, NB0-7, NB0-8, NB0-9, NB0-10, NB0-11, NB0-12, NB1-13, NB-A-1, NB-A-2, NB-A-3, NB-A-4, NB-A-5, NB-A-6, NB-A-7, NB-A-8, NB-A-9, NB-A-10, NB-A-11, NB-A-12, NB-A-13, NB-A-14, NB-A-15, NB-A-16, NB-A-17, NB2-14, NB2-15, NB2-16, NB3-17, and NB4-18.

3.1. 6. Microfacies and Depositional Environment

Determined microfacies types are divided into five main groups based on the Dunham's classification of carbonate rocks (1976). These main groups are; grainstone, bioclastic grainstone, bioclastic packstone, bioclastic packstone to grainstone, bioclastic packstone to wackestone. These microfacies indicate that the depositional environments are lagoon, sand shoals and barriers, restricted and shallow open marine environments. Based on the distribution of the RMF types, the depositional environments of these samples are suggested as shallow marine carbonate ramp type (Figure 36, 52).

Ćosović (2004) studied the paleoenvironmental model for Eocene foraminiferal limestones of the Adriatic carbonate platform, Istrian Peninsula. The Orthopragminae-bearing parts of the foraminiferal limestones are recognized in terms of larger foraminiferal faunal associations similar to this study. Relative abundance of planktonic foraminifers, limitations of algal endosymbionts, foraminiferal lamellar thickness and flattening of test shapes. Similar to this study, the microfacies-I contains nummulitids, assilinids, and asterocyclinids.

Özgen-Erdem et al. (2005) also studied microfacies of Paleocene-Eocene carbonate rocks in the Kastamonu region, Northern Turkey. Microfacies analysis was carried out

with respect to the distribution of depositional components and biota. Similar to this study, *Nummulites*, *Assilina* and *Orbitolites* have been recognized as well as other forms. Hence, the Lutetian units were deposited into the platform margin through fore-slope to deep marine shelf paleoenvironments. In the Safranbolu section, the Lutetian level is represented by grainstone and packstone with abundant *Nummulites*, *Assilina*, *Discocyclina* in sparitic cement. In other sections, bioclastic wackestone and FZ 3-SMFZ 3-4 facies types are observed.

Similar to this study, Adabi (2008) studied Eocene deposits in Zagros Basin, SW Iran, which are carbonate sequences of the Tale-Zang Formation that mainly consist of large benthic foraminifera such as *Nummulites* and *Alveolina*. Microfacies analysis led to recognition of ten microfacies that are related to four facies belts such as tidal flat, lagoon, shoal, and open marine. An absence of turbidite deposits, reefal facies, gradual facies changes, and widespread tidal flat deposits indicate that this sequence was deposited in a carbonate ramp environment.

Bagherpour and Vaziri (2012) studied a Lower Eocene succession which is characterized by 10 microfacies types, which are dominated by diverse larger foraminifera such as alveolinids, orbitolitids, and nummulitids. The Taleh Zang Formation at the Sarkan and Maleh kuh sections represents sedimentation on a carbonate ramp similar to this study.

Mirza (2015) studied microfacies of Eocene-aged Kohat formation, Gumbat section, Himalayan fold and thrust belt, Northern Pakistan. Four microfacies and eight subfacies have been identified in the section. Benthic foraminiferal wackestone facies, and benthic foraminiferal packstone facies are very similar to the facies described in our study. These subfacies are alveolinid wackestone facies, nummulites-alveolinia wackestone facies, nummulites-alveolina-miliolid wackestone facies, nummulites-miliolid wackestone facies, nummulites-alveolina packstone facies, nummulites-assilina packstone facies.

Similar to this study; Hadi et al., (2016) studied nummulites from the Eocene Ziarat formation of Western Alborz (NW Iran). Five microfacies types are defined within the shallow-water carbonate deposits of the Ziarat formation in the western Alborz zone.

Özcan (2020) studied the depositional environments of the Eocene Çayraz formation, as a reference unit for Tethyan larger benthic foraminifera. Three sections were measured and one of these sections is measured close to our study area and shows similarities in microfacies and depositional environments. Since this thesis study focus on the lower unit of the Çayraz Formation and also Özcan (2020) worked on the lower unit of the Çayraz formation in section YEŞ the interpretations are very similar. From the work of Özcan (2020) the lower unit, in general, is a regressive unit, dominated by quartz-orthophragminid (locally with *Nummulites*) wackestone to packstone facies at its base and, alveolinid-nummulitid wackestone-packstone facies at its top immediately below the pelagic marls. Therefore, the whole sequence records the stratigraphic development from outer to inner ramp setting. Abundant orthophragminids (represented by *Discocyclina*, *Orbitoclypeus* and *Asterocyclina*) and sporadic planktonic foraminifera at the basal beds of the lower unit suggest open marine depositional conditions such as middle to outer-ramp. The middle part of the lower unit is mostly characterized by cyclic deposits of larger benthic foraminifera (LBF) deposits, of various LBF wackestone-packstone facies characterizing shallowing-upward cycles and deposited in the middle to inner ramp settings. Moreover, the lower unit presents notable lateral facies and faunal changes westward and is characterized by a silici-clastic sequence (sandstone and conglomerate) with very poor fauna (only rare tests of *Nummulites* or *Assilina*). Different from our study they observed conglomerates. The predominance of *Alveolina* in most levels in westerly section (YEŞ), alveolinid-nummulitid wackestone-packstone and nummulites-assilina grainstone facies, also shows that the lower unit has been deposited in a shallower palaeoenvironment (inner-ramp) compared to easterly sections (ÇAYB, ÇAYA). The upper part of the lower unit is dominated by Dasycladalean algal-bivalve mudstone and Alveolinid-nummulitid wackestone-packstone facies. The dominant occurrence of *Alveolina*, *Orbitolites* and dasycladalean algae below the pelagic marls of the middle unit is very characteristic

feature for the development of succession. These beds are interpreted to have deposited in an inner-ramp setting. This thesis study is also interpreted the depositional environment as inner-ramp to outer ramp setting.

Hadi et al. (2021) studied microfacies of the Eocene Ziarat Formation (eastern Alborz zone, NE Iran). Similar to this study the biotic communities are characterized by larger benthic foraminifera (LBF), coralline algae, corals, and bivalves as the major carbonate facies components. The microfacies gradients and paleoenvironmental analysis suggest deposition in shallow-marine oligotrophic ramp environment within two platform stages. Both these stages indicate an increase in water depth from the inner to the middle ramp setting with the spatial distribution of the larger benthic foraminifers (LBF) and other benthic components.

Fahad et al. (2021) studied microfacies of Early Eocene aged Chorgali Formation exposed at eastern salt range, upper Indus basin, Pakistan. Four microfacies are identified by using *Nummulites*, *Lockhartia*, *Assilina*, and miliolinids similar to this study. The determined microfacies are as follows; Foraminiferal bioclastic wackestone microfacies (CF-1), Benthonic foram-rich wackestone microfacies (CF-2), Bioclastic wackes-packstone microfacies (CF-3), Miliolidal bioclastic wackestone microfacies (CF-4). Open marine platform conditions existed during the Early Eocene time (Ghazi et al. 2014). The *Nummulites* accumulations are the evidence of high sediment production rates in middle ramp waters (Pomar 2001; Barattolo et al 2007) and the *Lockhartia* sp. represents inner to middle ramp settings (Racey 1994). The association of *Nummulites* sp. with *Assilina* sp. indicates deeper inner to middle ramp depositional conditions (Buxton and Pedley 1989; Racey 2001; Beavington-Penney and Racey 2004; Vaziri-Moghaddam et al 2006; Adabi et al 2008; Payros et al 2010). Based on the detailed microfacies analysis coupled with the association of faunal assemblage of larger benthic foraminifera and other fossils, the inferred environment of deposition of the Chorgali Formation at the study area is a homoclinal ramp of middle to inner ramp settings.

A list of the determined microfacies of this study and depositional environments are shown in table 1. Determined RMF types are also listed below (Figure 52). RMF types and their depositional environments are shown in table 1. Composite depositional model of the studied area is shown in figure 53.

Outer ramp,

RMF6: Mudstone, wackestone or packstone with abundant miliolid foraminifera (SMF18-FOR)

Open inner ramp environments,

RMF13: Bioclastic wackestone and packstone with abundant larger foraminifera (e.g. orbitolinids) (SMF18-FOR)

RMF14: Bioclastic packstone and wackestone with skeletal grains, various amounts of intraclasts and some ooids (near-shoal)

RMF16: Mudstone, wackestone or packstone with abundant miliolid foraminifera (SMF18-FOR)

Lagoonal environment,

RMF20: Bioclastic wackestone and packstone with calcareous algae and benthic foraminifera.

Carbonate sand shoals and banks,

RMF26: Medium- and coarse grained bioclastic grainstone and packstone with various benthic skeletal grains

RMF27: Bioclastic grainstone and packstone composed of few dominant skeletal grains (e.g. predominantly echinoderms, or predominantly foraminifera)

Figure 52: Determined RMF types in this study.

Table 1 Microfacies main groups, Determined microfacies and environment of deposition.

Microfacies	Depositional Environment	RMF	Description	Sample #
MF1 Miliolimid, alveolimid, orbitolimid, bioclastic packstone	inner ramp, lagoon	RMF20	Bioclastic packstone with calcareous algae and benthic foraminifera	NB7, NB17, NB18, NB19
MF2 Orbitolimid, alveolimid, miliolimid, bioclastic packstone to wackestone	inner ramp, lagoon	RMF20	Bioclastic wackestone and packstone with calcareous algae and benthic foraminifera	NB12, NB16, NB25, NB27, NB28, NB30-B, NB31, NB36, NB39
MF3 Nummulitid, alveolimid, miliolimid, bioclastic packstone to wackestone	inner ramp, lagoon	RMF20	Bioclastic wackestone and packstone with calcareous algae and benthic foraminifera	NB-B-6, NB-B-9, NB14, NB15, NB24, NB26, NB30, NB30-A, NB32, NB35, NB37
MF4 Nummulitid, orbitolimid, bioclastic packstone to grainstone	inner ramp, lagoon	RMF20	Bioclastic wackestone and packstone with calcareous algae and benthic foraminifera	NB-B-2, NB7-A, NB9, NB11, NB13, NB29
MF5 Nummulitid, assilimid, bioclastic packstone	inner ramp, shoal	RMF27	Bioclastic grainstone and packstone composed of few dominant skeletal grains	NB4-A, NB-B-5, NB-B-7, NB-B-8, NB10, NB20, NB21, NB22, NB23, NB33, NB34, NB38, NB40
MF6 Nummulitid, discoicyclid, assilimid, bioclastic packstone	inner ramp, shoal	RMF27	Bioclastic grainstone and packstone composed of few dominant skeletal grains	NB5, NB-B-4

Table 1 (Continued) Microfacies main groups, Determined microfacies and environment of deposition.

MF7 Assilimid, nummulitid, bioclastic packstone to grainstone	inner ramp, shoal	RMF27	Bioclastic grainstone and packstone composed of few dominant skeletal grains	NB8, NB41
MF8 Discocyclinid, nummulitid, assilimid, planktonic foraminiferal, bioclastic packstone to wackestone	inner ramp, shoal	RMF27	Bioclastic grainstone and packstone composed of few dominant skeletal grains	NB2, NB2-B, NB6
MF9 Discocyclinid, nummulitid, bioclastic grainstone	inner ramp, shallow open marine	RMF14	Bioclastic packstone or wackestone with skeletal grains	NB2-A, NB4, NB-B-1, NB-B-3
MF13 Discocyclinid, nummulitid, planktonic foraminiferal, bioclastic packstone	inner ramp, shallow open marine	RMF14	Bioclastic packstone or wackestone with skeletal grains	NB1, NB42, NB43
MF11 Grainstone	outer ramp, near midramp	RMF 6	Graded, laminated bioclastic grainstone	NB3
MF12 Small benthic foraminiferal, planktonic foraminiferal wackestone	outer ramp, near midramp	RMF 5	Wackestone with abundant benthic foraminifera and a few planktonic foraminifera	NB0-1, NB0-2, NB0-3, NB0-4, NB0-5, NB0-7, NB0-8, NB0-9, NB0-10, NB0-11, NB0-12, NB1-13, NB-A-1 to NB-A-17, NB2-14, NB2-15, NB2-16, NB3-17, NB4-18

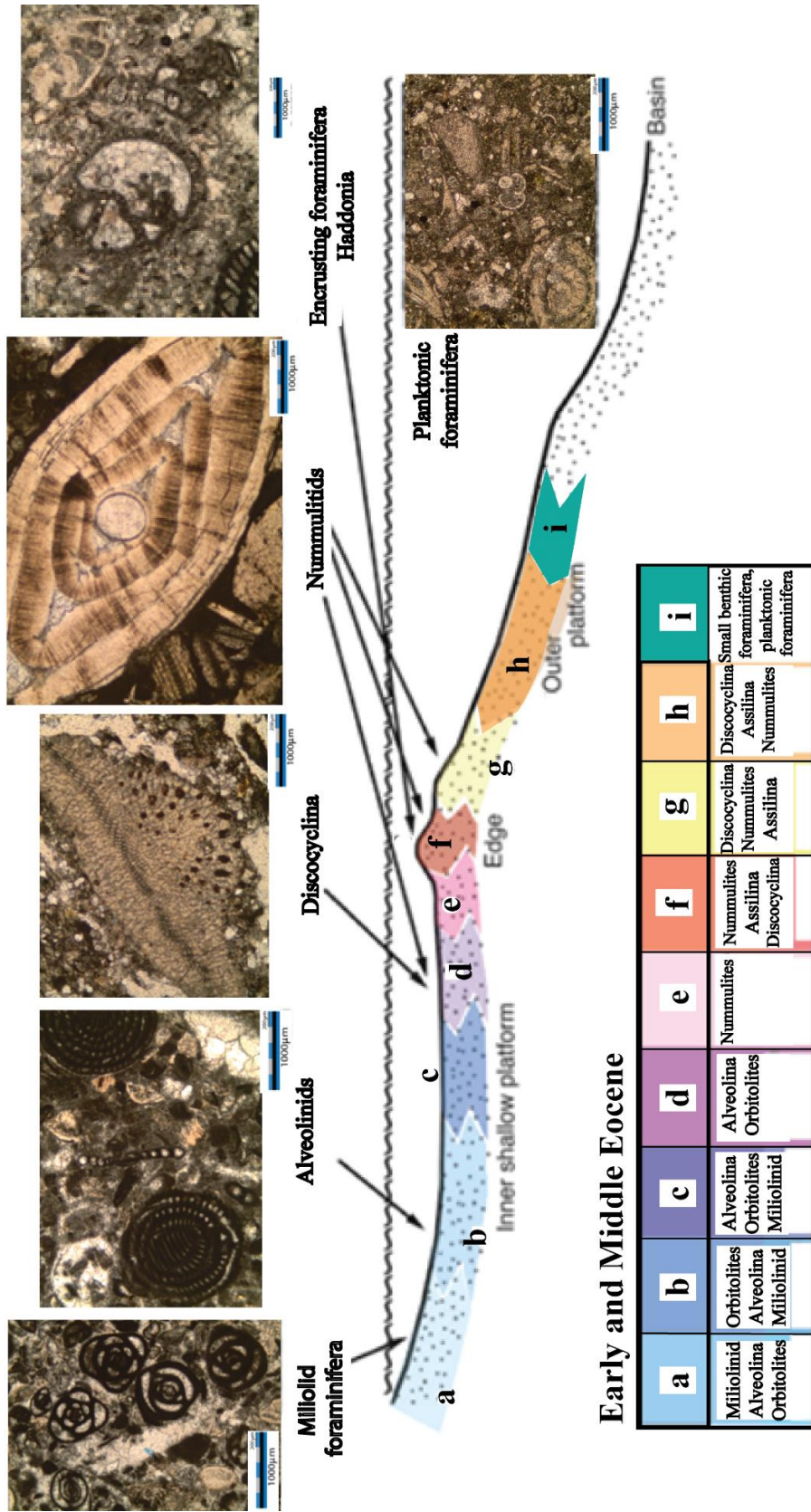


Figure 53: Early and Middle Eocene depositional platform model for large benthic foraminifera, and the distribution of the fossils over the platform (modified from Flügel, 2010), and determined bio-associations from this work (a, b, c, d, e, f, h, i). Microfacies distribution with bio-associations. The order of the list of fossil in the figure indicates the possibility of the occurrence in the depositional environment is high then the others. The preferences of the fossils are depending of the depositional environment condition. (BouDagher-Fadel, 2018a).

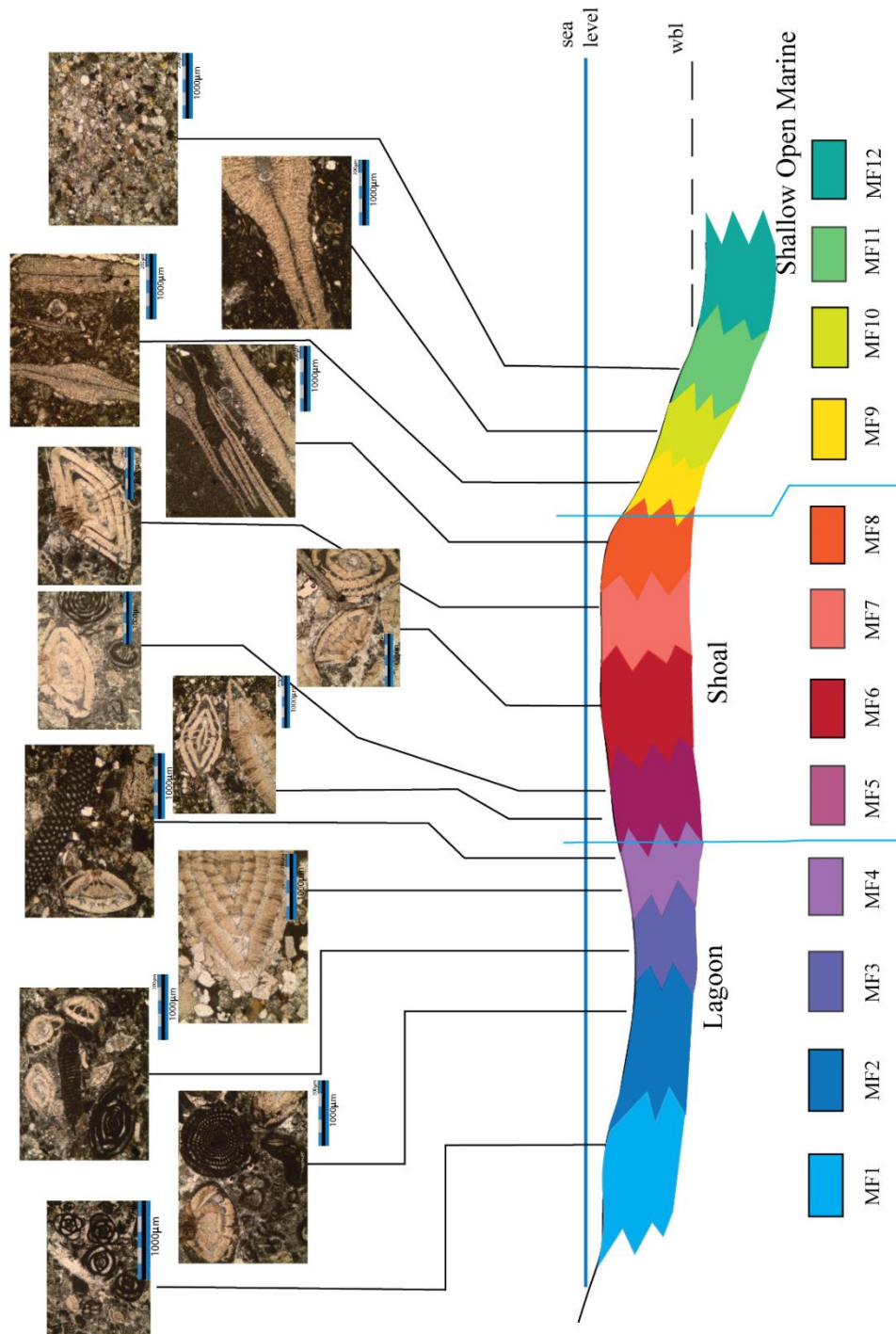


Figure 54: Composite depositional model of the studied area.

3.2. Microfacies Analyses dependent on fauna relationship

In order to determine the depositional environment of the studied samples of the sequence, the fossil varieties and abundances have been used. The most common fossil assemblages that have been recorded in samples are benthic foraminiferal assemblages.

3.2.1 Foraminiferal Assemblages used in the detection of the fossil associations

Larger benthic foraminiferal assemblages are useful tools to obtain information about the sea level change. Because of their benthic mode of life, they are very sensitive to environmental changes, in particular, to sea-level changes. They give us valuable information to construct sea-level change chart. Moghaddam et. al. (2002) studied on Eocene succession in Hamzeh-Ali Area, North-Central Zagros, Iran. They have used biofacies in order to understand paleoecology and sedimentary environments in association with the occurrence of foraminifera and suggested shelf model. By using these information They have recognized depositional sequences in the studied succession. Similar to this study they used *Nummulites* sp., *Discocyclina* sp., *Alveolina* sp., *Orbitolites* sp., Miliolids, differently *Somalina* sp. has been used.

The most common Eocene benthic foraminifers are readily identified as morphologically larger miliolines and rotaliines (especially nummulitids and orthophragmiids. The miliolines included large fusiform alveolinids, and the discoid soritids that became prominent throughout the Eocene. Another highly abundant foraminifers are rotaliinids. Some rotaliines are characterized by a complex system of marginal cords, characteristic of nummulitids. These latter exhibited high evolutionary rates and became very abundant in the Eocene.

The microfossils have been recognized in the thin sections of the studied samples have been briefly explained below:

CLASS FORAMINIFERA
ORDER ROTALIIDA Delage and Herouard, 1896
Superfamily NUMMULITOIDEA de Blainville, 1827
Family Nummulitidae de Blainville, 1827
Subfamily Nummulitinae de Blainville, 1827
Genus Nummulites Lamarck, 1801

Nummulites sp. Lamarck, 1801

Plate 1

Type species: *Camerina laevigata* Bruguere, 1792

- Nummulites* Lamarck, 1801
- Camerina* Bruguere, 1792
- Phacites* Blumenbach, 1799
- Egeon* de Montfort, 1808
- Helicites* de Blainville, 1824
- Nummulina* d'Orbigny, 1826
- Nummularia* Sowerby and Sowerby, 1826
- Nummulita* Fleming, 1828
- Discospira* Morris, in Mantell, 1850
- Camerina* (*Bruguieria*) Prever, 1902
- Camerina* (*Laharpeia*) Prever, 1902
- Lenticulina* (*Hantkenia*) Prever, 1902
- Paronaea* Prever, 1903
- Paronia* Chelussi, 1903
- Palaeonummulites* Schubert, 1908
- Verbeekia* A. Silvestri, 1908
- Operculinella* Yabe, 1918
- Operculina* (*Operculinella*) Yabe and Hanzawa, 1929
- Operculinoides* Hanzawa, 1935
- Pseudonummulites* A. Silvestri, 1937
- Paraspiroclypeus* Hanzawa, 1937

Pseudonummulites Thalmann, 1941

Eoassilina S. N. Singh, 1957

Planocamerinoides Cole, 1958

Craterocamerina Omara and Kenawy, 1979

Diagnostic features &Remarks:

Nummulites are taxonomically classified into Order Rotaliida because of the radially hyaline, perforate wall. The test is lenticular, and biconvex in shape. The chambers are tightly coiled as planispiral, and involute with numerous whorls. Chambers are simple with distinct marginal cord on the periphery. Septa are annular in more advanced forms and there are septal canal trabeculae but without secondary septa forming chamberlets (Flügel, 2010; BouDagher-Fadel, 2018a). *Nummulites* shown in figure 55. It is abundant in Palaeocene to Upper Eocene sediments (e.g. Loucks et al., 1998; Sinclair et al., 1998; Allen et al., 2001; Pomar, 2001).

Stratigraphic range: Paleocene to Holocene and abundant in Eocene (BouDagher-Fadel, 2018a).

Occurrence: This genus shows occurrence between NB1 to NB2-B and NB4 to NB42.

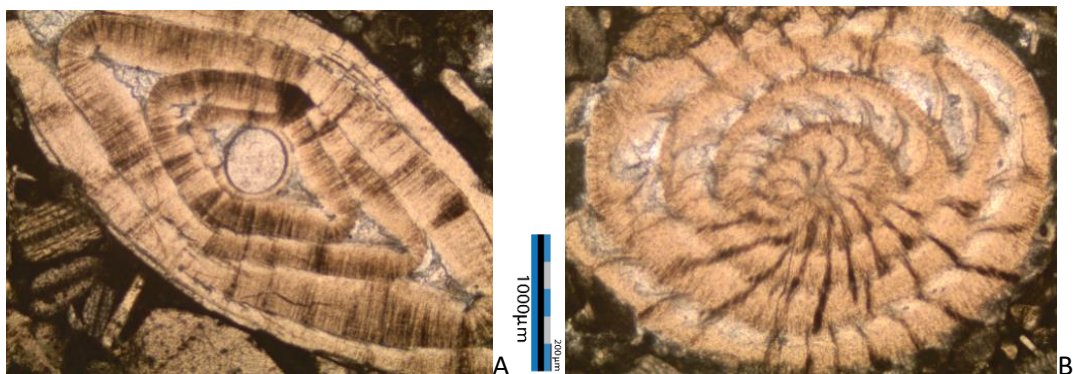


Figure 55: Thin section photomicrographs of *Nummulites* sp.. from sample NB5 (A:axial section; B: oblique section)

Genus *Assilina*. d'Orbigny, 1839

Assilina sp. d'Orbigny, 1839

Plate 2

Type species: *Assilina depressa* d'Orbigny, 1850 = *Nummulites spira* de Roissy, 1805

Nummulina (*Assilina*) d'Orbigny, 1839

Assilina d'Orbigny, 1846

Nummulites (*Assilina*) Reuss, 1862

Operculina (*Frilla*) de Gregorio, 1894

Neooperculinoides Golev, 1961

Operculina (*Assilina*) Schaub, 1981

Diagnostic features &Remarks:

Assilinids are taxonomically classified into Order Rotaliida because of the radially hyaline, perforate wall. The test is discoidal and flattened in shape. The chambers are tightly coiled as planispiral, and evolute. Chambers are simple and numerous per whorl. The rate of whorl growth is slow. The marginal cord on the periphery is thick with a coarse canal system. Septa are radial, and trabeculae are absent. Size range of the test gives some information on stratigraphic age. For instance, large size in the sample points to Middle Eocene age (Flügel, 2010; BouDagher-Fadel, 2018a).. *Assilina* shown in figure 56.

Stratigraphic range: M. Paleocene to Holocene (BouDagher-Fadel, 2018a).

Occurrence: This genus shows occurrence between NB2, NB2-B, NB4, NB4-A, NB5, NB6, NB-B1, NB-B-3 to NB-B9, NB8 to NB16, NB19 to NB28, NB31 to NB34, NB37, NB39, NB40, NB42 and NB43

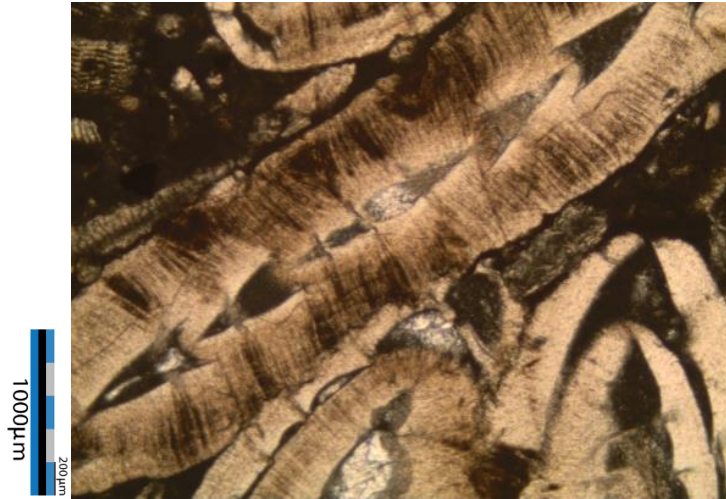


Figure 56: Thin section photomicrograph of *Assilina* sp. from sample NB5 (axial section).

CLASS FORAMINIFERA d'Orbigny, 1826
ORDER ROTALIIDA Delage and Herouard, 1896
Family Orthophragminidae Vedekind, 1937
Subfamily Discocyclininae Galloway, 1928
Genus Discocyclina. Gümbel 1870

***Discocyclina* sp. Gümbel 1870**

Plate 3

Type species: *Orbitolites prattii* Michelin, 1846

Orbitoides (Discocyclina) Gümbel, 1870

Orbitoides (Rhipidocyclina) Gümbel, 1870

Orthophragmina Munier-Chalmas, 1891

Orbitoides (Orthophragmina) Checchia-Rispoli, 1907

Orthophragmina (Nodocyclina) Heim, 1908

Orthophragmina (Discocyclina) Heim, 1908

Discocyclina H. Douville, 1922

Discocyclina (Eudiscodina) van der Weijden, 1940

Discocyclina (Umbilicodiscodina) van der Weijden, 1940

Discocyclina (Eudiscodina) Thalmann, 1943

Discocyclina (Umbilicodiscodina) Thalmann, 1943

Hexagonocyclina Caudri, 1944

Bontourina Caudri, 1948

Diagnostic features &Remarks:

Discocyclinids are taxonomically classified into Order Rotaliida because of the radially hyaline, perforate wall. They are informally called as Orthophragminid foraminifera. They were first classified based on the general shape of their test, the pillar-lateral chamberlet network and size of their pillars (Brönnimann, 1951). The test is discoidal, flat, with an equatorial layer of concentric rings of rectangular chamberlets, those of successive cycles alternating in position. The growth in *Discocyclina* is both cyclical and involute. Lateral chambers are connected with the equatorial layer by vertical stolons (BouDagher-Fadel, 2018a). Annular stolons occur at the proximal end of the radial walls and connect adjacent chambers (BouDagher-Fadel, 2018a). A median layer of chambers is differentiated from lateral chambers (Flügel, 2010). It has radiating pillars which give rise to granules of the outer surface (BouDagher-Fadel, 2018a). *Discocyclina* shown in figure 57.

Stratigraphic range: Middle Paleocene to Late Eocene (BouDagher-Fadel, 2018a).

Occurrence: This genus shows occurrence between NB1 to NB2-B, NB4, NB5, NB6, NB-B-1, NB-B-3, NB-B-4, NB42 and NB43.

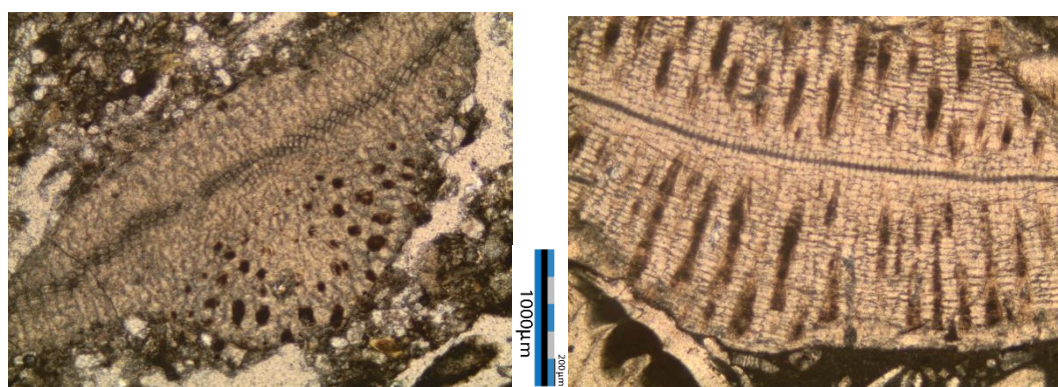


Figure 57: Thin section photomicrograph of *Discocyclina* sp. from samples NB4 and NB5 (nearly axial / tangential sections)

ORDER MILIOLIDA Delage and Herouard, 1896

Superfamily ALVEOLINOIDEA Ehrenberg, 1839

Family Alveolinidae Ehrenberg, 1839

Genus Alveolina d'Orbigny, 1826

***Alveolina* sp. d'Orbigny, 1826**

Plate 4

Type species: *Oryzaria boscii* Defrance, in Bronn, 1825

Alveolina d'Orbigny, 1826

Fasciolites Parkinson, 1811

Alveolites Defrance, 1816

Oryzaria Defrance, in Bronn, 1825

Flosculina Stache, 1880

Alveolina (*Flosculina*) Schwager, 1883

Flosculina (*Semiflosculina*) Doncieux, 1905

Alveolina (*Fasciolites*) A. Silvestri, 1928

Alveolina (*Eoalveolinella*) A. Silvestri, 1928

Borelis (*Fasciolites*) Yabe and Hanzawa, 1929

Borelis (*Alveolina*) Yabe and Hanzawa, 1929

Borelis (*Flosculina*) Yabe and Hanzawa, 1929

Flosculina (*Checchiaites*) Sorrentino, 1935

Flosculina (*Checchiaites*) Thalmann, 1936

Fasciolites (*Microfasciolites*) Gaemers, 1978

Diagnostic features &Remarks:

Alveolinds are taxonomically classified into Order Miliolida because of the porcelaneous and imperforated wall. Test is large, planispiral to fusiform, subcylindrical or globular in shape. The chambers are enrolled along an elongate axis, initially planispiral or streptospiral, or milioline with chambers added in varying planes. Chambers are subdivided into chamberlets by longitudinal partitions (septula) perpendicular to the main septa, and connected by passages below the apertural face. The basal layer is thick, as deposition of secondary calcite (flosculinisation) fills most

of the chamber lumen. . Successive chambers communicate with post- and pre-septal passages. The final chamber has two rows of apertures alternating in position (Flügel, 2010; BouDagher-Fadel, 2018a). *Alveolina* shown in figure 58.

Stratigraphic range: Late Paleocene to Eocene (BouDagher-Fadel, 2018a).

Occurrence: This genus shows occurrence between NB7 , NB-B-2 to NB-B-9, NB9 to NB19, NB24 to NB28, NB30 to NB37, NB39 to NB41.

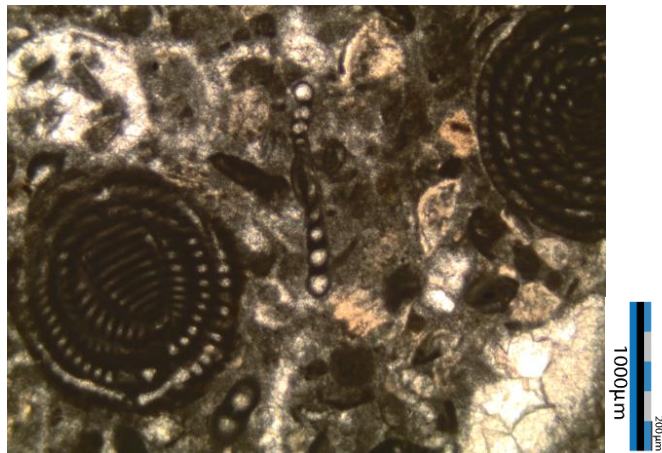


Figure 58: Thin section photomicrograph of *Alveolina* sp. from sample NB 18 (oblique section)

ORDER MILIOLIDA Delage and Herouard, 1896

Superfamily MILIOLOIDEA Ehrenberg, 1839

Family MILIOLIDAE Ehrenberg, 1839

Miliolid

Plate 5

Type family: Miliolidae d'Orbigny, 1839

Miolina Ehrenberg, 1839

Miolida Schultze, 1854

Miolitidae Parker, 1858

Miolidea Reuss and Fritsch, 1861

Miolidee Schwager, 1876

Miliolidina Bütschli, in Bronn, 1880
Milioletta Haeckel, 1894
Miliolinidae Rhumbler, 1895
Miliolinae Delage and Herouard, 1896
Armiliolidia Rhumbler, 1913

Diagnostic features & Remarks:

Miliolids are taxonomically classified into Order Miliolida because of the porcelaneous and imperforated wall. The test is multichambered which are coiling in varying planes with two chambers per whorl, with the axis of coiling normal to the apertural axis and rotated, so that several angles exist between the median planes of consecutive chambers. The test may become uncoiled, cylindrical or compressed with partial partitions. The proloculus is followed by a spiral passage (BouDagher-Fadel, 2018a). Miliolids shown in figure 59. Miliolina are abundant in warm waters of normal salinity, and may occur up to the hypersaline waters.

Stratigraphic range: Carboniferous to Holocene (Flügel, 2010).

Occurrence: This genus shows occurrence between NB2, NB2-B, NB5, NB7, NB-B-1, NB-B3 to NB-B-5, NB-B-9, NB9 to NB19, NB21 to NB33, NB35 to NB37 and NB39 to NB41

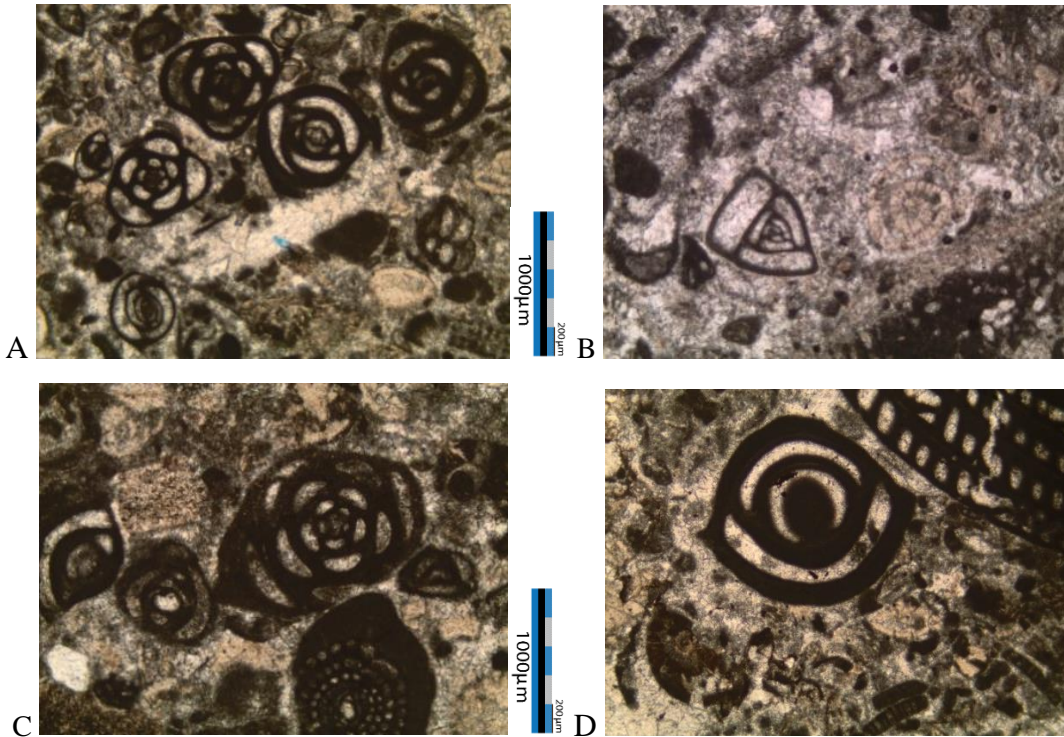


Figure 59: Thin section photomicrographs of miliolids from samples A&D: NB18, B&C:NB19 (A, B, C: equatorial sections; D: oblique section)

ORDER MILIOLIDA
Superfamily SORITOIDEA
Family Soritidae
Genus Orbitolites Lamarck, 1801

***Orbitolites* sp. Lamarck, 1801**

Plate 6

Type species: *Orbitolites complanatus* Lamarck 1801

Discolites de Montfort, 1808

Discolites concentricus de Montfort, 1808

Diagnostic features &Remarks:

Orbitolitids are taxonomically classified into Order Miliolida because of the porcelaneous and imperforated wall. Test is large, discoidal, very slightly biconcave, large proloculus and second chamber forming an inflated nucleoconch. The later cyclic chambers are subdivided into small numerous chamberlets with curved thickened walls. Those of successive cycles alternating in position. Adjacent chambers are not interconnected with stolons, but the connections are between the obliquely adjoining chamberlets. Annular chambers are less defined in the later stage and chamberlets separated by thickened oblique walls. It has found in the restricted environment abundantly (Flügel, 2010; BouDagher-Fadel, 2018a). *Orbitolites* shown in figure 60.

Stratigraphic range: Early to M. Eocene (BouDagher-Fadel, 2018a).

Occurrence: This genus shows occurrence between NB7, NB-B-1 to NB-B-5, NB-B-7, NB-B-9, NB9 to NB16, NB18 to NB21, NB23 to NB25, NB27 to NB37, and NB39 to NB41.

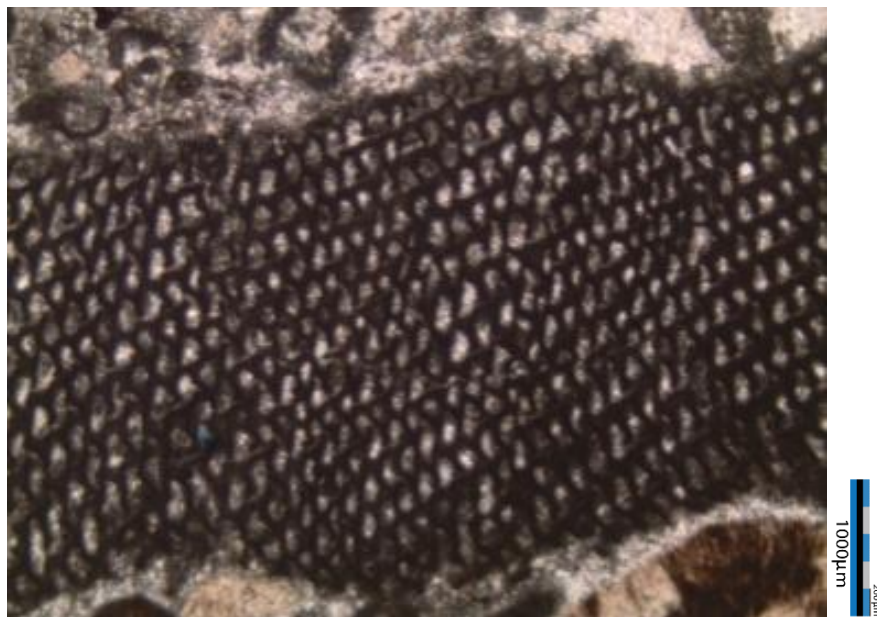


Figure 60: Thin section photomicrograph of *Orbitolites* sp. from sample NB19.

Division Rhodophyta Wettstein, 1901
Class Rhodophyceae Rabenhorst, 1863
Order Corallinales Silva & Johansen, 1986

Coralline Red Algae

The red algae belong to the division Rhodophyta within which the coralline algae form the order Corallinales.

They are characterized by a thallus that is hard because of calcareous deposits contained within the cell walls. The colors of these algae are most typically pink, or some other shade of red, but some species can be purple, yellow, blue, white, or gray-green. Coralline algae play an important role in the ecology of coral reefs. Many are typically encrusting and rock-like, found in marine waters all over the world. A close look at almost any intertidal rocky shore or coral reef will reveal an abundance of pink to pinkish-grey patches, distributed throughout the rock surfaces.

Coralline red algae (CRA) is found in the thin sections as the surrounding species of the other fossils such as *Assilina* sp., *Nummulites* sp, *Discoyclina* sp.. Coralline red algae shown in figure 60.

Occurrence: This genus shows occurrence between NB1, NB2, NB2-B, NB5, NB6, NB-B-5, NB-B-7, NB-B-8, NB8, NB12, NB14, NB19, NB22, NB30-B, NB33, NB34, NB37, and NB38.

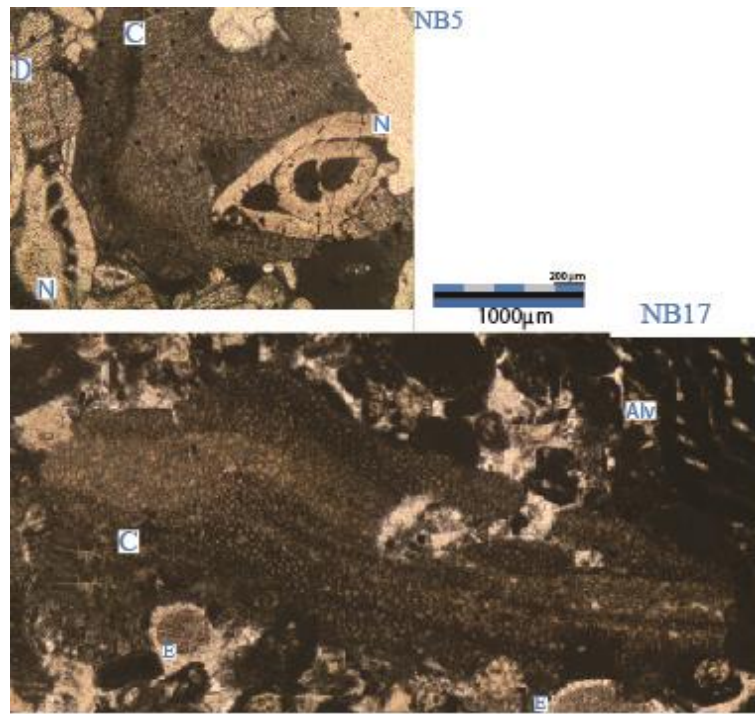


Figure 61: Thin section photomicrograph of CRA from samples NB5, NB17.

3.3 Bio-associations

Bio-associations give us the needed information to construct ancient sea-level change chart. These fossils are not the only fossils that are recorded in the thin section studies. However, their relationship gives data about which part of the ramp was the depositional environment for our measured section samples. These fossils are of rock-building importance. All the interpretations are done by using the ramp model (BouDagher-Fadel, 2018a). These interpretations and the ramp model shown in the figure 53. Bio-associations of the samples are seen in the figure 62.

Bio-association A

These foraminiferal associations predominantly consist of miliolid, *Alveolina* sp., together with *Orbitolites* sp. and also agglutinated foraminifera, which indicates inner ramp, near coast depositional environment and brackish water (Flügel, 2010), since the preferences of the fossil fauna co-existed in the area that we can generate a solution that this is most proximal microfacies in carbonate ramp model that in the measured section of thin section samples. The environment of deposition is the lagoon. The samples NB18, NB30-B, NB31, NB32 are the ones in which this bio-association A was recorded (Figure 62).

Bio-association B

These foraminiferal associations predominantly consist of *Orbitolites* sp., *Alveolina* sp., miliolinid, *Nummulites* sp., and *Assilina* sp.. This association indicates the inner ramp through the lagoon near the coastal depositional environment. *Orbitolites* sp., *Alveolina* spp., and miliolid respectively are abundant. The samples NB9, NB11 to NB17, NB19, NB28 to NB30-A, NB33, NB36, NB37, NB39, NB40, and NB41 are the ones in which this bio-association B was recorded (Figure 62).

Bio-association C

These foraminiferal associations predominantly consist of *Alveolina* sp., *Orbitolites* sp., miliolinid, and agglutinated foraminifera, which indicates inner ramp and lagoon depositional environment. *Orbitolites* sp., *Alveolina* sp., and miliolid respectively are

abundant, with an increase in abundance of the *Nummulites* sp. present itself. The samples NB20 (one part of the thin section), NB24, NB25, NB27, NB34, and NB35 are the ones in which this bio-association C was recorded (Figure 62).

Bio-association D

These foraminiferal associations predominantly consist of *Alveolina* spp., *Orbitolites* sp., *Nummulites* sp. and *Assilina* sp. indicating the inner ramp and lagoon depositional environment at the near shoal part. The abundance of the fossils of *Nummulites* sp., and *Assilina* sp. respectively decrease in the abundance of *Orbitolites* sp., *Alveolina* sp. and miliolids. The samples NB7, NB-B-6, NB-B-7, NB-B-9, NB20 (the other part of the thin section), NB21, NB22, NB23, NB26, and NB38 are the ones in which this bio-association D was recorded (Figure 62).

Bio-association E

These foraminiferal associations predominantly consist of *Nummulites* sp. and *Assilina* sp. indicating inner ramp at shoal depositional environment. *Nummulites* sp. and *Assilina* sp., *Orbitolites* sp., *Alveolina* sp., and miliolids respectively are abundant; from most abundant to relatively less abundant. The samples NB-B-2, NB-B-5, NB-B-8, NB8, and NB10 are the ones in which this bio-association E was recorded (Figure 62).

Bio-association F

These foraminiferal associations predominantly consist of *Nummulites* sp. and *Assilina* sp. indicates inner ramp at shoal depositional environment to the mid-ramp transition. *Nummulites* sp., *Assilina* sp., and *Discocyclina* sp. respectively are abundant. The samples NB1, NB2, NB5, NB6, NB-B-1, NB-B-3, NB-B-4, and NB42 are the ones in which this bio-association F was recorded (Figure 62).

Bio-association G

These foraminiferal associations predominantly consist of *Discocyclina* sp., *Assilina* sp., and *Nummulites* sp. indicates inner ramp at the mid ramp transition. *Discocyclina* sp., *Assilina* sp., and *Nummulites* sp. respectively are abundant. The samples NB0-6,

NB2-A, NB2-B, NB2-16, NB4, and NB43 are the ones in which this bio-association G was recorded (Figure 62).

Bio-association H

These foraminiferal associations predominantly consist of *Discocyclina* sp., *Nummulites* sp., and *Assilina* sp. indicating the inner ramp, shallow open marine depositional environment. *Discocyclina* sp., *Assilina* sp., small benthic foraminifers, and planktonic foraminifers respectively are abundant. The samples NB0-1 to NB0-5, NB0-7, NB0-8, NB0-12, NB0-13, NB2-A, NB2-14, NB2-15, NB3-17, NB4-A, and NB4-18 are the ones in which this bio-association H was recorded (Figure 62).

Bio-association I

These foraminiferal associations predominantly consist of small benthic foraminifers and planktonic foraminifers indicating the inner ramp, shallow open marine depositional environment. The samples NB0-9, NB0-10, and NB0-11 are the ones in which this bio-association I was recorded (Figure 62).

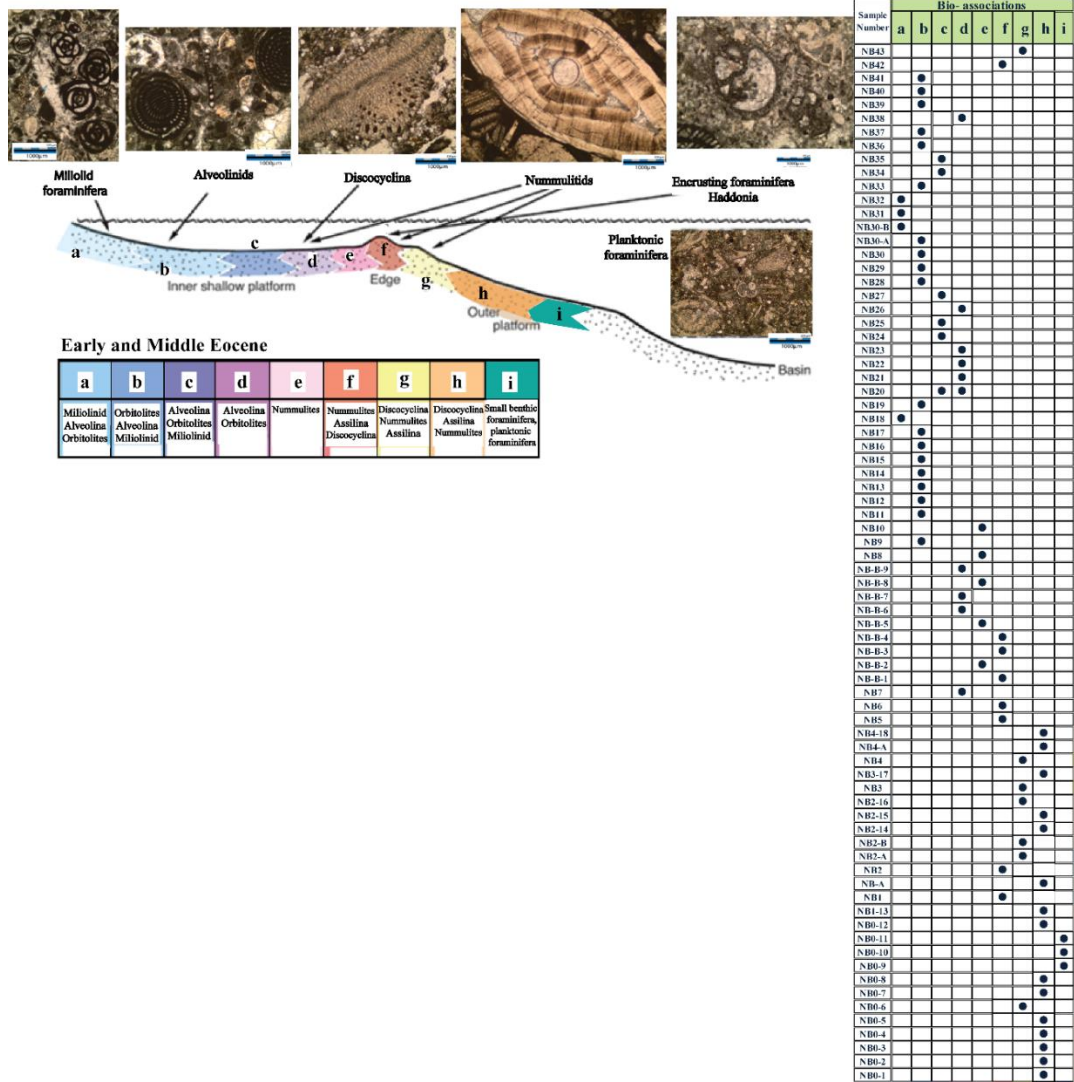


Figure 62: Distribution of bio-associations in the studied samples.

CHAPTER 4

SEQUENCE STRATIGRAPHY

4.1. Historical Background of Sequence Stratigraphy

Sequence stratigraphy is the most intriguing concept in geology. It has been developed after the seismic stratigraphy with the work of Vail et al. (1977). Seismic stratigraphy is a geological approach to seismic data (Vail and Mitchum, 1977). The seismic stratigraphy is a way of approaching depositional units under the surface. Depositional sequence as a stratigraphic unit is composed of relatively conformable succession. The depositional sequence as a stratigraphic unit composed of relatively conformable succession of genetically related strata and bounded at its top and bottom by their correlative conformities or unconformities (Mitchum et al., 1977). The seismic stratigraphy is in close relationship with the outcrop data as well (Posamentier et al. 1988; Van Wagonner et al., 1988). Sequence stratigraphy is widely used as a method of stratigraphic analysis and has become a very successful technique in natural searches (Catuneanu, 2002).

Sequence stratigraphy is defined as the study of rock relationships within a chronostratigraphic framework of repetitive and genetically related strata bounded by the surface of erosion, non-deposition, or their correlative conformities (Van Wagonner et al., 1988). The sequence is the fundamental unit of sequence stratigraphy. A sequence can be subdivided into system tracts which are composed of depositional systems (Van Wagonner et al., 1988). System tracts are defined by stacking patterns of parasequence sets or cycles (Van Wagonner et al., 1988).

4.2. Meter-scale shallowing upward cycles (Parasequences)

Shallowing upward cycles are named as parasequences. The parasequences are the building blocks of the sequence stratigraphy. The parasequence is a relatively conformable succession of beds or bedsets bounded by marine flooding surfaces (Van Wagoner et al., 1988). Shallow marine carbonates are the best indicators of sea-level changes since their deposition is dependent on the parameters such as; water depth, energy, and fossil content (Goldhammer et al., 1990). Parasequences tend to be

systematically arranged within parasequence sets. Stacking patterns of the meter-scale cycles can be used to define large-scale sequences, system tracts, and long-term relative sea-level changes (Osleger and Read, 1991; Goldhammer et al., 1990).

In this study, a section was measured to define the shallowing upward meter-scale cycles in Lower Eocene succession in the Haymana Basin. The measured section is 238 m and represented by twenty-one cycles. Lithostratigraphic and microfacies details of these cycles are given in the following sections.

4.1.1. Types of shallowing upward cycles (Parasequences)

According to vertical association and bio-associations of different microfacies, eight main types and twenty sub-types are recognized in this study. The discrimination of the cycles is based on the superimposed sub-environments.

4.1.1.1 A-Type Cycles

A-type cycles characterized by small benthic foraminiferal, planktonic foraminiferal wackestone (MF12) microfacies as its base and shallowing upward to the top. They are dominant in the lower part of the measured section. The cycles begin with small benthic foraminiferal, and planktonic foraminiferal wackestone (MF12) facies. This microfacies is followed upward and capped with grainstone (MF11), discocyclinid, nummulitid, planktonic foraminiferal, bioclastic packstone (MF10), discocyclinid, nummulitid, bioclastic grainstone (MF9), discocyclinid, nummulitid, assilinitid, planktonic foraminiferal, bioclastic packstone to wackestone (MF8), nummulitid, discocyclinid, assilinitid, bioclastic packstone to wackestone (MF6), nummulitid, assilinitid, bioclastic packstone (MF5). In this type of cycle, most distal shallow open marine facies changes into more proximal shallow open marine facies or the shoal facies. There are six different variation of A type cycles. These are A1 (cycle 1), A2 (cycle 2 and cycle 3), A3 (cycle 4), A4 (cycle 5), A5 (cycle 6) and A6 (cycle 7).

A1 type cycle (Cycle 1) is the first cycle in the measured section (Figure 63). This cycle includes the interval of the sample numbers NB0-7/NB1-13 and NB1. The interval between NB0-7 and NB1-13 samples are represented by small benthic foraminiferal, planktonic foraminiferal wackestone (MF12) facies. NB1 sample is represented limestone with *Discocyclina* and *Nummulites*. This cycle starts with small

benthic foraminiferal, planktonic foraminiferal wackestone (MF12) and is capped with discocyclinid, nummulitid, planktonic foraminiferal bioclastic packstone (MF10). The cycle represents a shallow open marine facies variation.

A2 type cycle (Cycle 2) is the second cycle in the measured section (Figure 64). This cycle includes the interval between samples NB2-A and NB2-B. The sample NB2-A consist of limestone with *Discocyclina* and *Nummulites*. NB2-B sample is represented by bioclastic wackestone with *Discocyclina* and *Nummulites* and planktonic foraminifera. This cycle starts with small benthic foraminiferal, planktonic foraminiferal wackestone (MF12). The facies follow upward with discocyclinid, nummulitid, bioclastic grainstone (MF9) and finally the cycle capped with discocyclinid, nummulitid, assilid, planktonic foraminiferal, bioclastic packstone to wackestone (MF8). The cycle represents a shallow open marine conditions change into shoal conditions.

A2 type cycle (Cycle 3) is the third cycle in the measured section (Figure 65). This cycle includes the interval of the sample numbers NB-A-2 / NB-A- 17 and NB2. NB2 sample contains *Discocyclina*, *Nummulites* and *Assilina*. This cycle starts with small benthic foraminiferal, planktonic foraminiferal wackestone (MF12) with intercalation of sandstone lithology. This microfacies is capped with discocyclinid, nummulitid, assilid, planktonic foraminiferal, bioclastic packstone to wackestone (MF8). The cycle corresponds to shallow open marine turns into shoal conditions.

A3 type cycle (Cycle 4) is the fourth cycle in the measured section (Figure 66). This cycle includes sample numbers NB2-14, NB2-15, NB2-16 and NB3. NB3 sample represents non-fossiliferous sandstone. This cycle starts with small benthic foraminiferal, planktonic foraminiferal wackestone (MF12) and is capped with grainstone (MF11). The cycle represents a shallow open marine facies variation.

A4 type cycle (Cycle 5) is the fifth cycle in the measured section (Figure 67). This cycle includes sample numbers NB3-17 and NB4. NB4 sample contains *Discocyclina*, *Assilina* and *Nummulites*. This cycle starts with small benthic foraminiferal, planktonic foraminiferal wackestone (MF12) and is capped with discocyclinid, nummulitid, bioclastic grainstone (MF9). The cycle is a shallow open marine variation.

A5 type cycle (Cycle 6) is the sixth cycle in the measured section (Figure 68). This cycle includes sample NB4-18 and NB4-A. NB4-A sample is represented by *Nummulites*. This cycle starts with small benthic foraminiferal, planktonic foraminiferal wackestone (MF12) and is capped with nummulitid, assilinitid, bioclastic packstone (MF5). The cycle shows a return from shallow open marine conditions to inner ramp shoal depositional environment conditions.

A6 type cycle (Cycle 7) is the seventh cycle in the measured section (Figure 69). This cycle includes only sample NB5. NB5 sample is represented by *Nummulites*, *Assilina* and *Discocyclusina*. This cycle starts with small benthic foraminiferal, planktonic foraminiferal wackestone (MF12) and is capped with nummulitid, discocyclinid, assilinitid, bioclastic packstone to wackestone (MF6). The cycle shows a return from shallow open marine depositional environment to inner ramp shoal conditions.

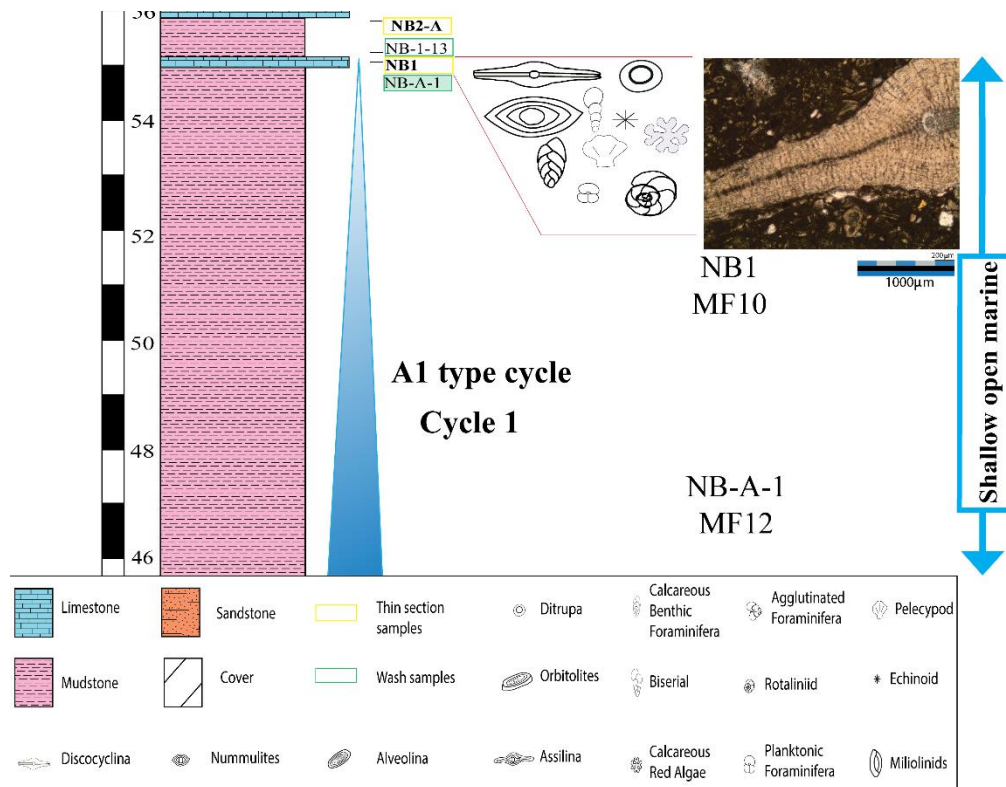


Figure 63: A1 type cycle (Cycle 1) of the measured section and photomicrographs of microfacies deposited within this cycle.

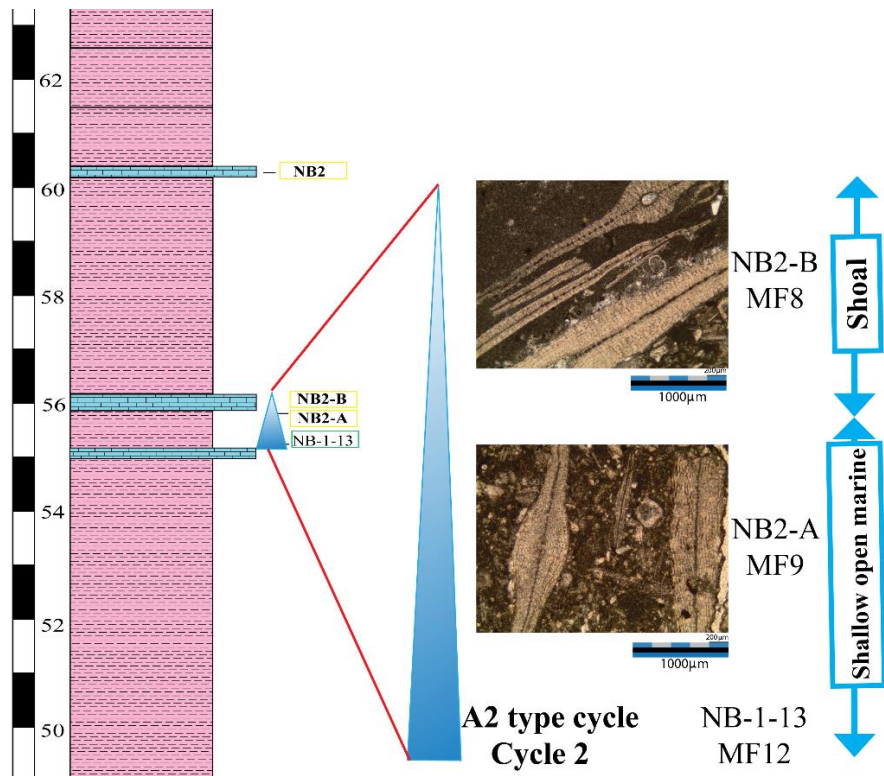


Figure 64: A2 type cycle (Cycle 2) of the measured section and photomicrographs of microfacies deposited within this cycle.

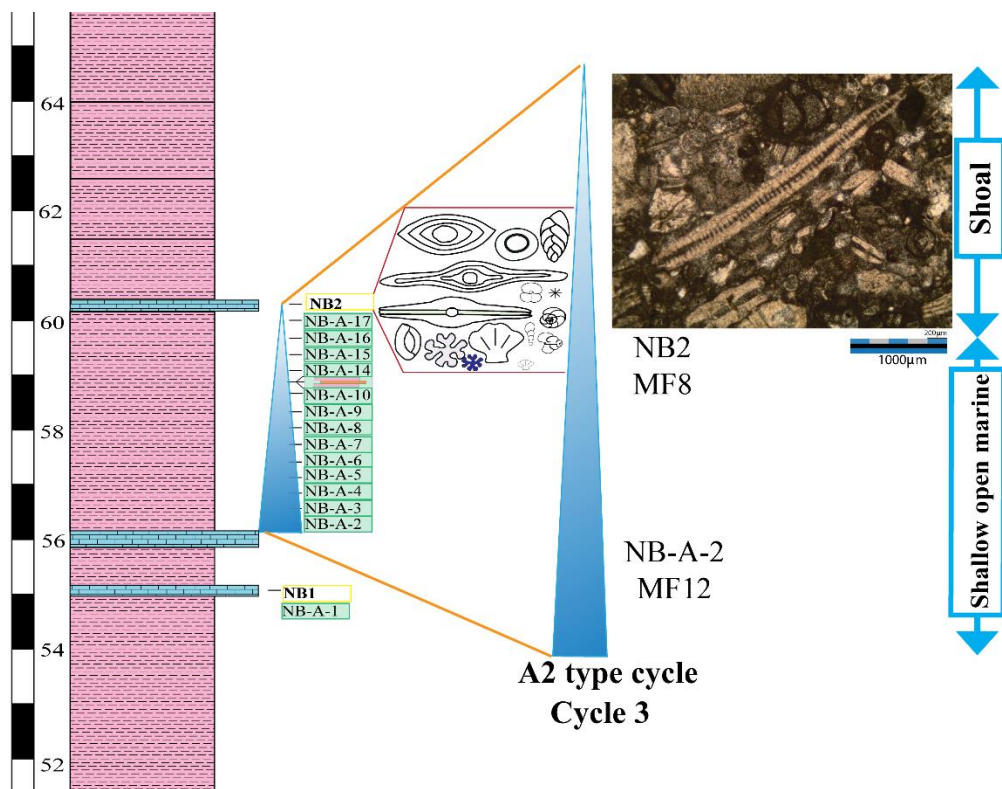


Figure 65: A2 type cycle (Cycle 3) of the measured section and photomicrographs of microfacies deposited within this cycle.

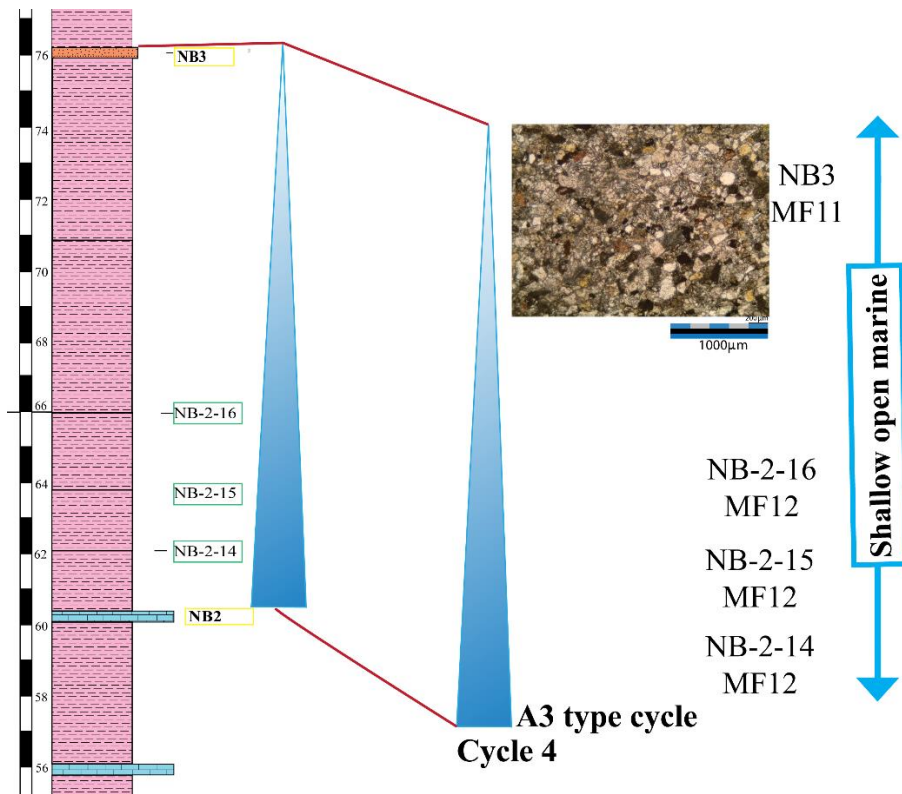


Figure 66: A3 type cycle (Cycle 4) of the measured section and photomicrographs of microfacies deposited within this cycle.

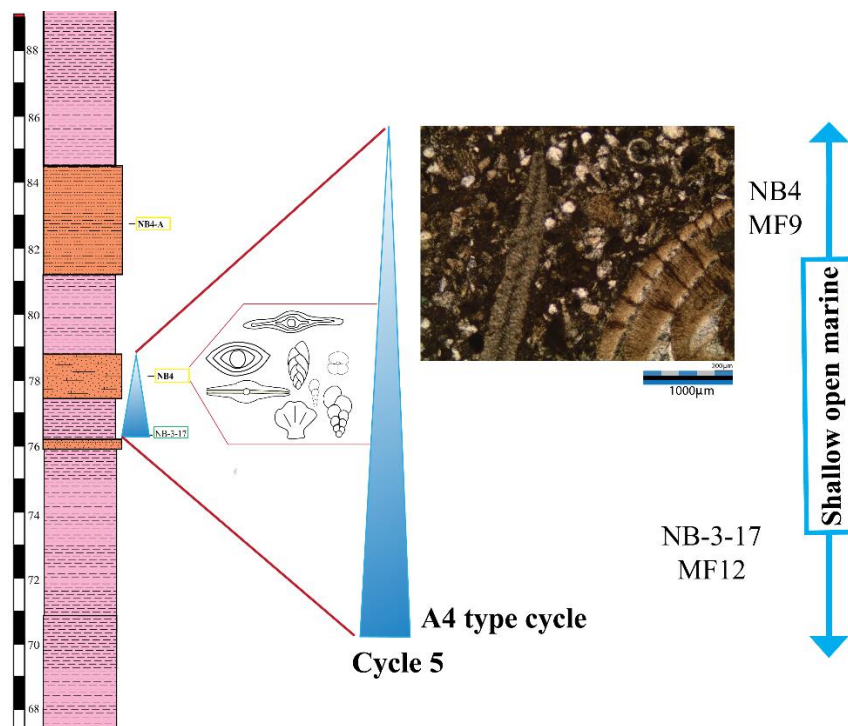


Figure 67: A4 type cycle (Cycle 5) of the measured section and photomicrographs of microfacies deposited within this cycle.

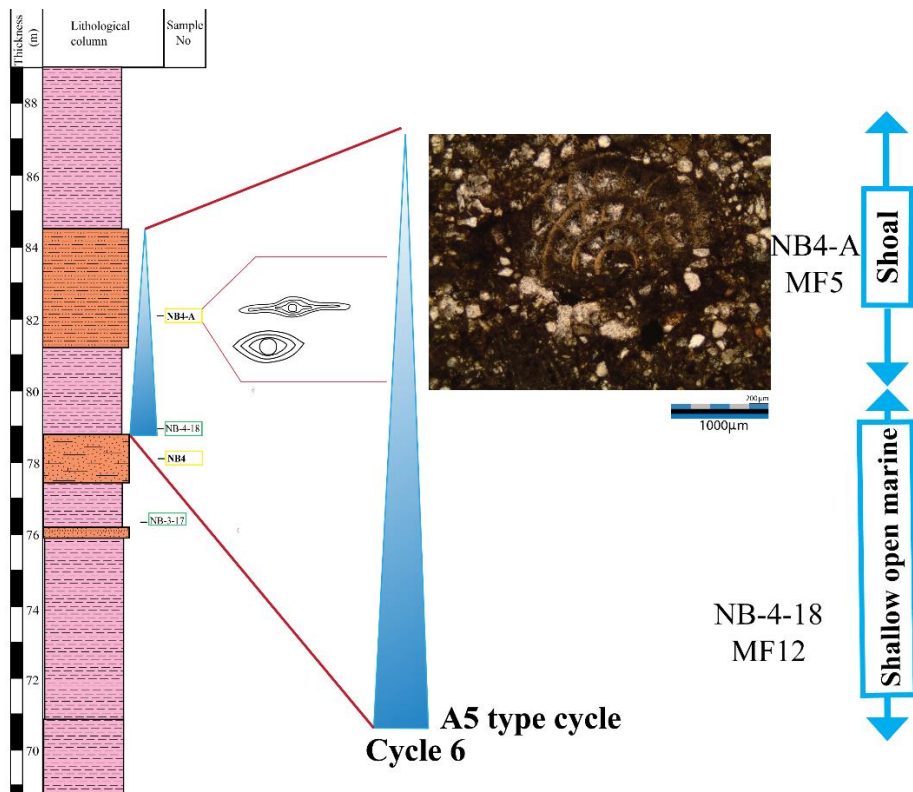


Figure 68: A5 type cycle (Cycle 6) of the measured section and photomicrographs of microfacies deposited within this cycle.

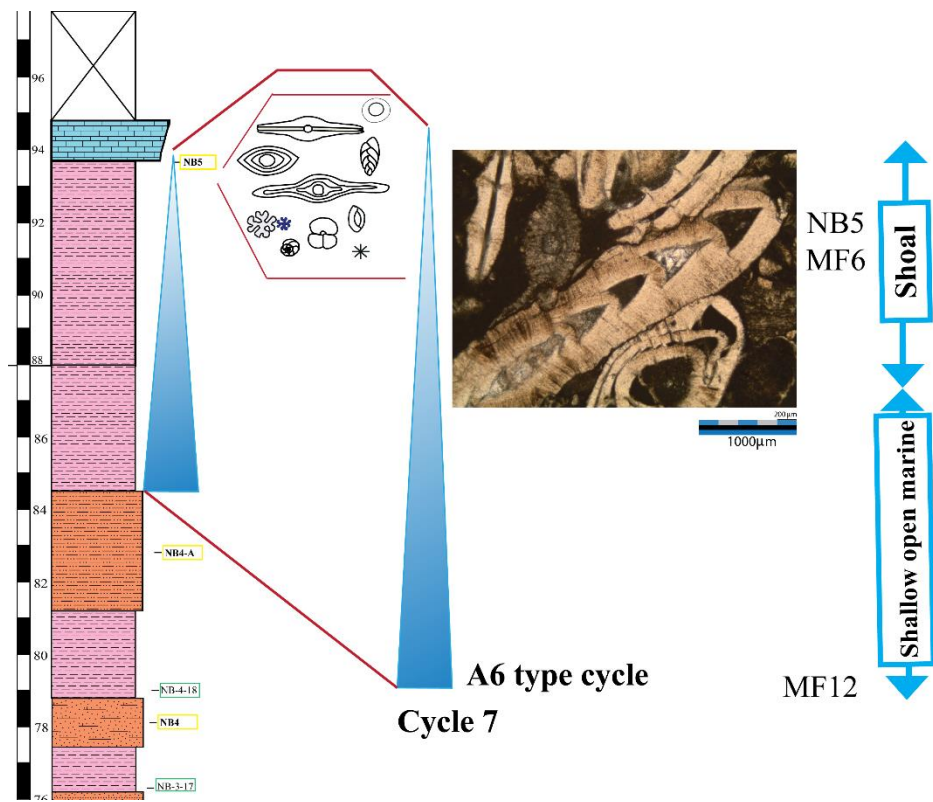


Figure 69: A6 type cycle (Cycle 7) of the measured section and photomicrographs of microfacies deposited within this cycle.

4.1.1.2 B-Type Cycles

B-type cycles are characterized by discocyclinid, nummulitid, assilid, planktonic foraminiferal, bioclastic packstone to wackestone microfacies (MF8) as its base and shallowing upward to the top. This microfacies is followed upward and is capped with miliolinid, alveolinid, orbitolitid, bioclastic packstone (MF1). In this type of cycle, most distal shoal facies change into most proximal lagoon facies. There is only one B-type cycle present in the studied section. The B-type cycle is represented by the cycle 8.

B-type cycle (Cycle 8) is the 8th cycle in the measured section (Figure 70). This cycle includes sample numbers NB6 and NB7. NB6 sample is represented by *Discocyclina*, *Nummulites* and *Assilina*. NB7 sample is represented by *Nummulites* and *Alveolina*. The cycle shows a return from inner ramp shoal conditions to inner ramp lagoon depositional conditions.

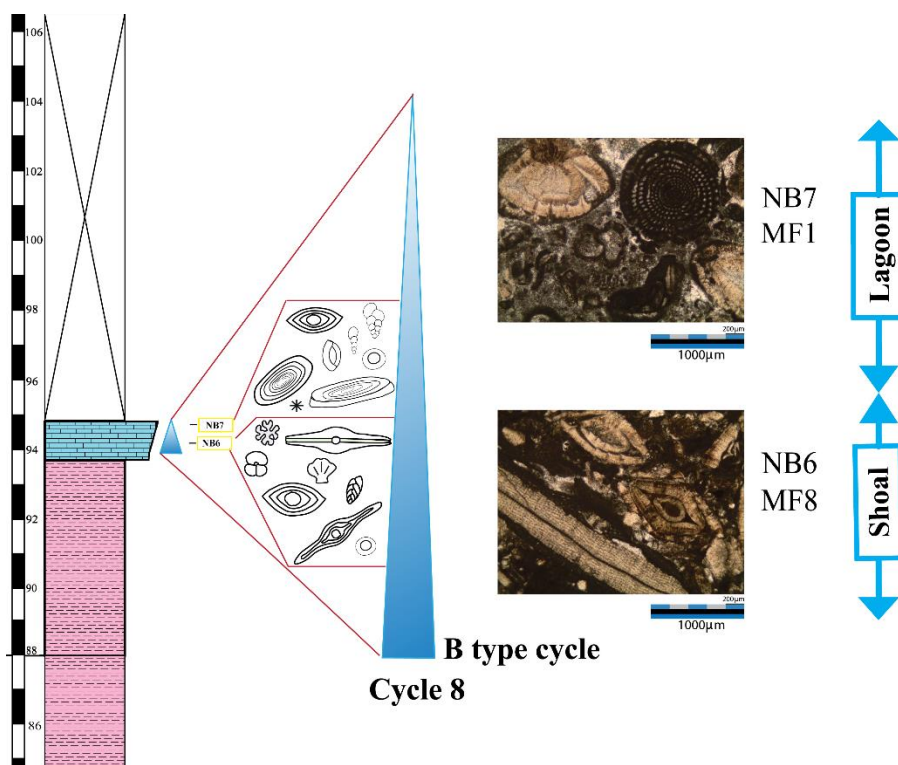


Figure 70: B type cycle (Cycle 8) of the measured section and photomicrographs of microfacies deposited within this cycle.

4.1.1.3 C-Type Cycles

C-type cycles are characterized by discocylinid, nummulitid, bioclastic grainstone (MF9) microfacies as its base and shallowing upward to the top. This microfacies is followed upward and is capped with nummulitid, orbitolitid, bioclastic packstone to grainstone microfacies (MF4), nummulitid, discocylinid, assilid, bioclastic packstone to wackestone microfacies (MF6), nummulitid, assilid, bioclastic packstone microfacies (MF5) and is capped with nummulitid, alveolinid, miliolinid, bioclastic packstone to wackestone microfacies (MF3). In this type of the cycle, shallow open marine facies is followed upward with the shoal facies and the shoal facies is capped with lagoon facies. In one variation shoal facies are missing. There are two different variations of C-type cycles. These are C1 (cycle 9) and C2 (cycle 10).

C1 type cycle (Cycle 9) is the ninth cycle in the measured section (Figure 71). It is composed of fossiliferous sandy limestone lithology. This cycle includes sample numbers NB-B-1 and NB-B-2. NB-B-1 sample is represented by *Discocyclus* and *Nummulites*. NB-B-2 sample is represented by *Nummulites* and *Orbitolites*. This cycle starts with discocylinid, nummulitid, bioclastic grainstone (MF9) and is capped with nummulitid, orbitolitid, bioclastic packstone to grainstone (MF4). The cycle shows a return from open marine conditions to inner ramp lagoon depositional environment conditions.

C2 type cycle (Cycle 10) is the tenth cycle in the measured section (Figure 72). It is composed of fossiliferous sandy limestone lithology. This cycle includes the interval of the sample numbers NB-B-3/ NB-B-6. NB-B-3 sample is represented by *Assilina*, *Nummulites* and *Discocyclus*. NB-B-4 sample is represented by *Nummulites*, *Discocyclus* and *Orbitolites*. NB-B-5 sample is represented by *Nummulites*, *Assilina* and *Alveolina*. NB-B-6 sample is represented by *Nummulites*, *Alveolina* and *Assilina*. This cycle starts with discocylinid, nummulitid, bioclastic grainstone microfacies (MF9) and continues with nummulitid, discocylinid, assilid, bioclastic packstone to wackestone microfacies (MF6). The nummulitid, assilid, bioclastic packstone microfacies (MF5) follow these facies and the cycle finally finished with nummulitid,

alveolinid, miliolinid, bioclastic packstone to wackestone microfacies (MF3). The cycle shows the return of the inner ramp open marine facies to inner ramp shoal facies and finally to the return of shoal conditions to the inner ramp lagoon depositional environment conditions.

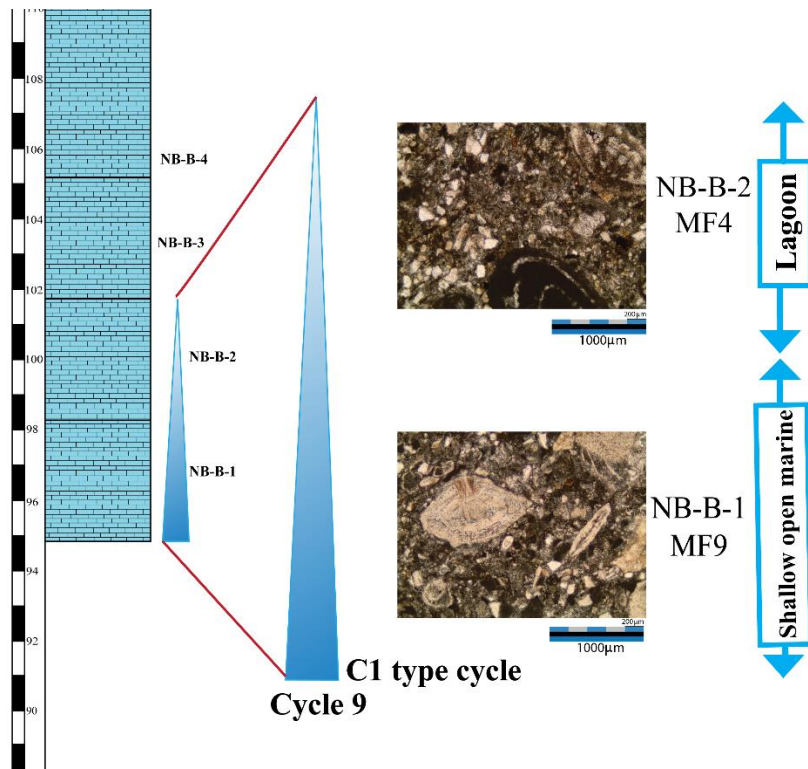


Figure 71: C1 type cycle (Cycle 9) of the measured section and photomicrographs of microfacies deposited within this cycle.

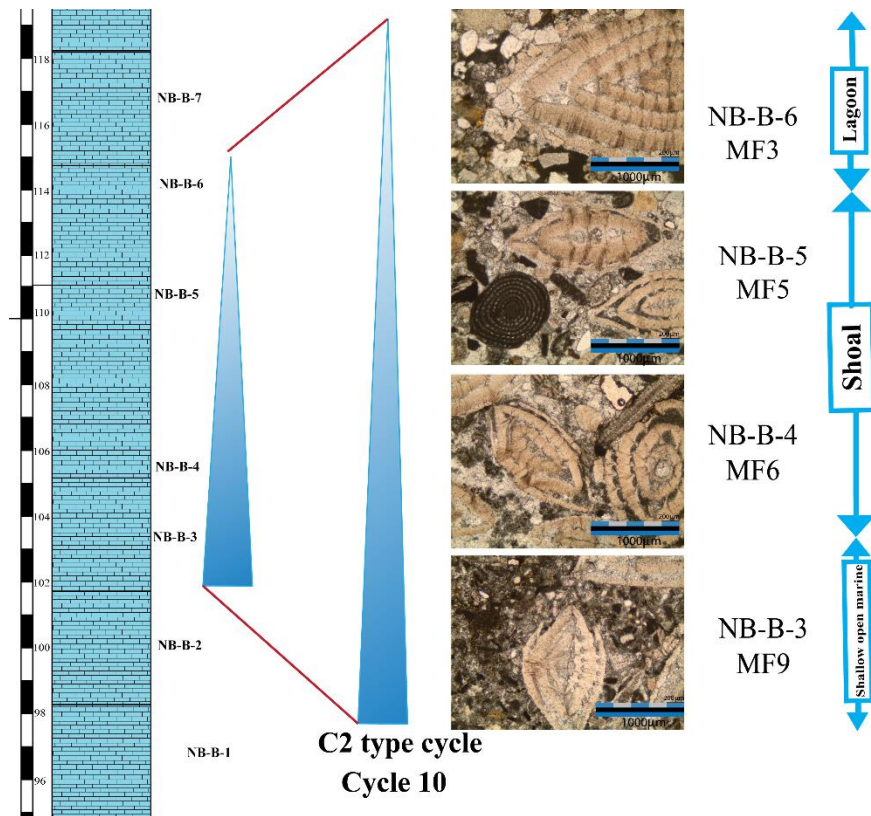


Figure 72: C2 type cycle (Cycle 10) of the measured section and photomicrographs of microfacies deposited within this cycle.

4.1.1.4 D-Type Cycles

D-type cycles are characterized by nummulitid, assilid, bioclastic packstone (MF5) microfacies as its base and shallowing upward to the top. This microfacies is followed upward and capped with nummulitid, alveolinid, miliolinid, bioclastic packstone to wackestone microfacies (MF3). In other variation this microfacies is followed upward with nummulitid, orbitolitid, bioclastic packstone to grainstone (MF4) and is capped with orbitolinid, alveolinid, miliolinid, bioclastic packstone to wackestone (MF2). In this type of cycle, shoal facies change into lagoon facies. There are five different variations of D-type of cycles. These are D1 (cycle 11), D2 (cycle 13), D3 (cycle 15), D4 (cycle 18) and D5 (cycle 19).

D1 type cycle (Cycle 11) is the 11th cycle in the measured section (Figure 73). It is composed of fossiliferous limestone lithology. This cycle includes the interval of sample numbers NB-B-7/NB-B-9. NB-B-7, NB-B-8, and NB-B-9 samples are represented by *Nummulites*, *Assilina* and *Alveolina* with an increase in the alveolinid content. This cycle starts and continues with nummulitid, assilid, bioclastic

packstone microfacies (MF5). The cycle is capped with nummulitid, alveolinid, miliolinid, bioclastic packstone to wackestone microfacies (MF3). The cycle shows the inner ramp shoal conditions change gradually to more landward shoal conditions and finally reach to inner ramp lagoon depositional environment conditions.

D2 type cycle (Cycle 13) is the 13th cycle in the measured section (Figure 74). This cycle includes sample numbers NB10, NB11, and NB12. NB10 sample is represented by *Nummulites*, *Assilina* and miliolid. NB11 and NB12 samples are represented by *Orbitolites*, *Nummulites* and *Alveolina*. This cycle starts with nummulitid, assilid, bioclastic packstone (MF5) and continues with nummulitid, orbitolitid, bioclastic packstone to grainstone (MF4) and is finally capped with orbitolinid, alveolinid, miliolinid, bioclastic packstone to wackestone (MF2). The cycle shows the inner ramp shoal conditions change gradually more inward shoal conditions and finally capped with inner ramp lagoon depositional environment conditions.

D3 type cycle (Cycle 15) is the 15th cycle in the measured section (Figure 75). This cycle includes the interval of sample numbers NB20 and NB25. NB20 sample is represented with *Nummulites*, *Assilina* and rotalinid. NB21 sample is represented with *Assilina*, *Nummulites* and rotalinid. NB22 and NB23 samples are represented with *Nummulites*, rotalinid and *Assilina*. NB24 sample is represented with *Nummulites*, rotalinid and miliolinid. NB25 sample is represented with *Nummulites*, miliolinid and *Orbitolites*. This cycle starts with nummulitid, assilid, bioclastic packstone (MF5) and continues with nummulitid, alveolinid, miliolinid, bioclastic packstone to wackestone (MF3). It is capped with orbitolitid, alveolinid, miliolinid, bioclastic packstone to wackestone microfacies (MF2). The cycle shows the inner ramp shoal depositional environment conditions change into inner ramp lagoon conditions and finalize with inner ramp lagoon depositional environment conditions.

D4 type cycle (Cycle 18) is the 18th cycle in the measured section (Figure 76). This cycle includes sample numbers NB33, NB34. NB33 sample is represented by *Nummulites*, *Assilina* and rotalinid. NB34 sample is represented by *Assilina*, *Nummulites* and *Alveolina*. This cycle starts with nummulitid, assilid, bioclastic packstone (MF5). The cycle shows an inner ramp shoal facies variation.

D5 type cycle (Cycle 20) is the 20th cycle in the measured section (Figure 77). This cycle includes sample numbers NB38 and NB39. NB38 sample is represented by rotalinid and *Nummulites*. NB39 sample is represented by *Orbitolites* and miliolid. This cycle starts with nummulitid, assilimid, bioclastic packstone (MF5). It is capped with orbitolitid, alveolinid, miliolinid, bioclastic packstone to wackestone (MF2). The cycle shows the inner ramp shoal depositional environment conditions change into inner ramp lagoon conditions.

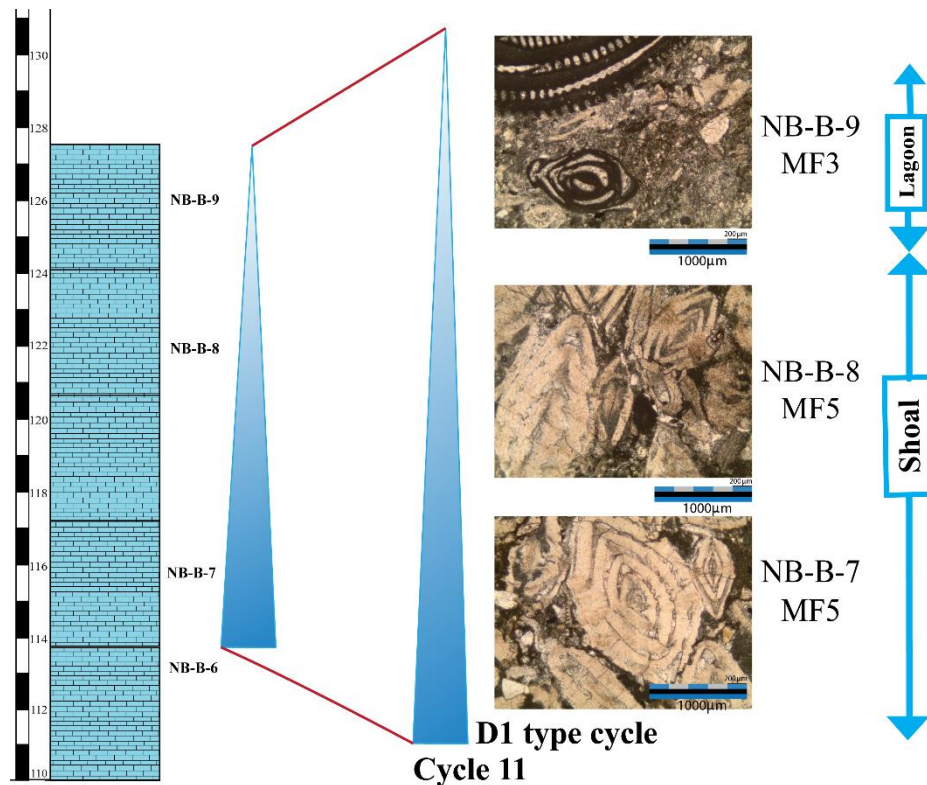


Figure 73: D1 type cycle (Cycle 11) of the measured section and photomicrographs of microfossils deposited within this cycle.

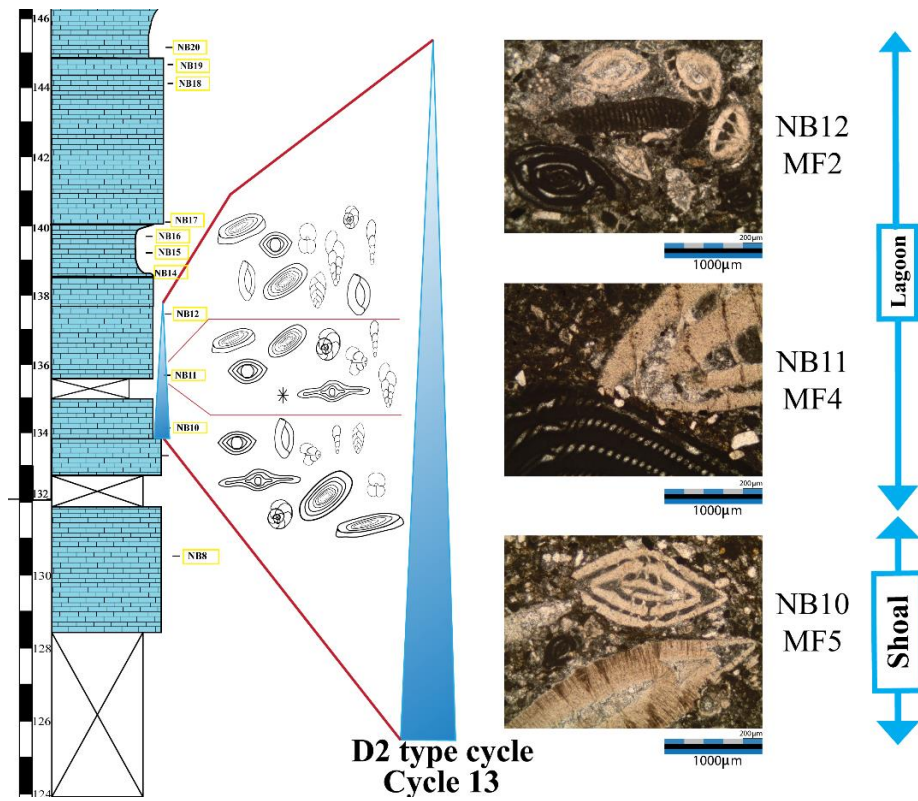


Figure 74: D2 type cycle (Cycle 13) of the measured section and photomicrographs of microfacies deposited within this cycle.

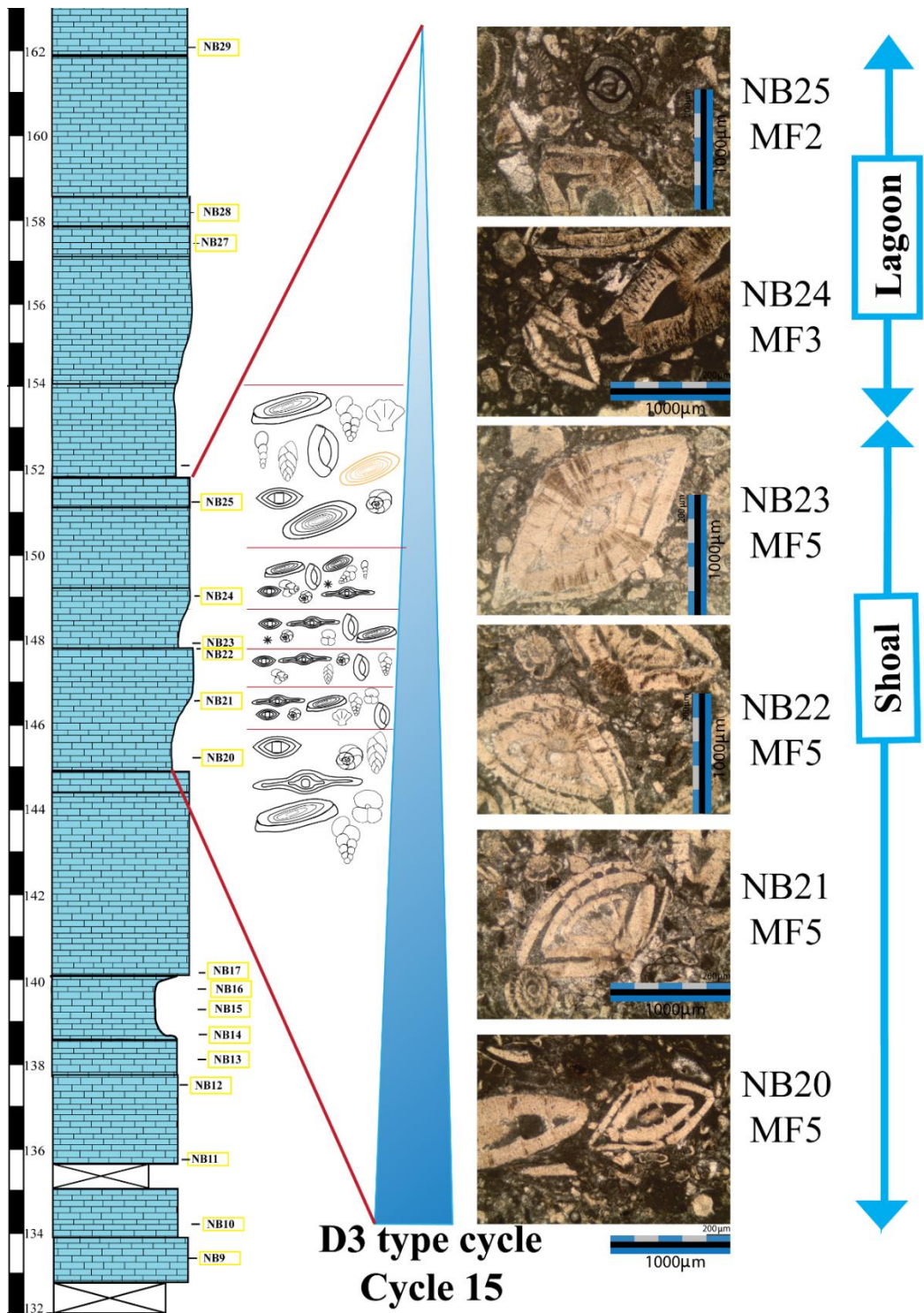


Figure 75: D3 type cycle (Cycle 15) of the measured section and photomicrographs of microfacies deposited within this cycle.

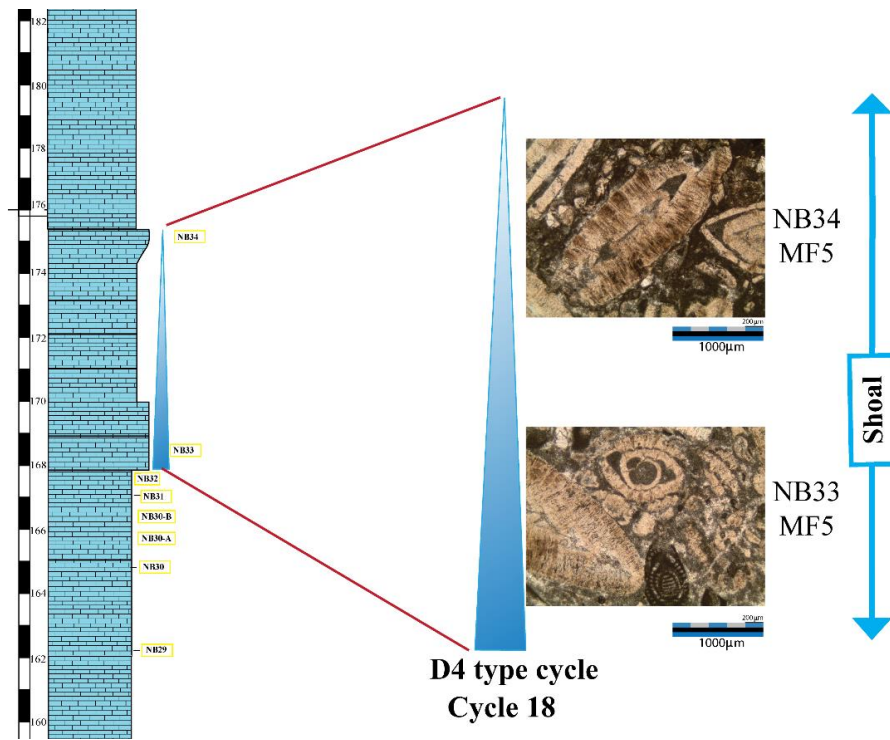


Figure 76: D4 type cycle (Cycle 18) of the measured section and photomicrographs of microfacies deposited within this cycle.

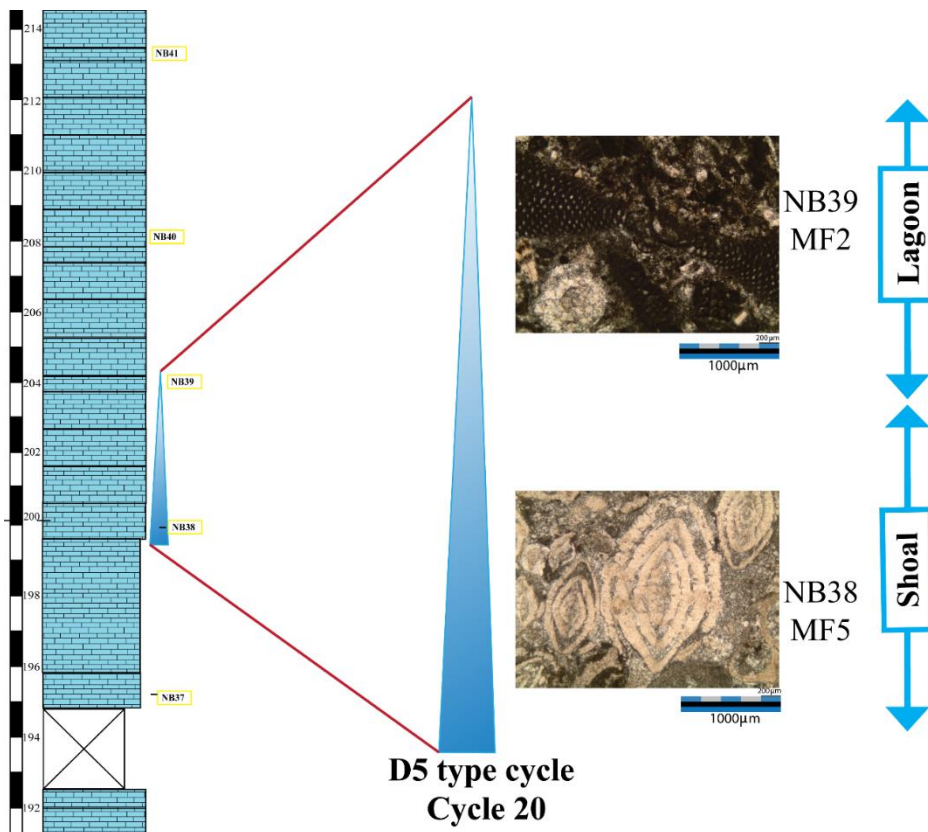


Figure 77: D5 type cycle (Cycle 20) of the measured section and photomicrographs of microfacies deposited within this cycle.

4.1.1.5 E-Type Cycles

E-type cycles are characterized by assilinitid, nummulitid, bioclastic grainstone (MF7) microfacies as its base and shallowing upward to the top. This microfacies is followed upward and is capped with nummulitid, orbitolitid, bioclastic packstone to grainstone (MF4). In this type of cycle, shoal facies is capped with lagoon facies. There is only one E-type cycle is present in the studied section. The E type cycle is represented by the cycle 12.

E type cycle (Cycle 12) is the 12th cycle in the measured section (Figure 78). This cycle includes sample numbers NB8 and NB9. NB8 sample is represented by *Nummulites* and *Assilina*. NB9 sample is represented by *Nummulites*, *Assilina* and *Orbitolites*. The cycle shows the inner ramp shoal conditions change to inner ramp lagoon conditions.

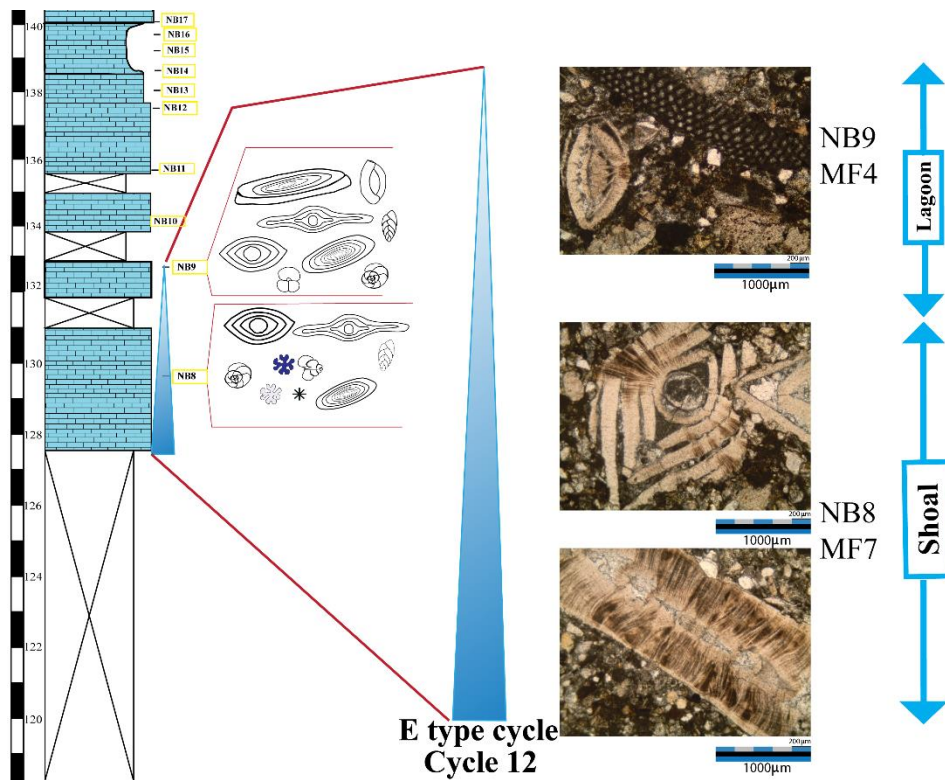


Figure 78: E type cycle (Cycle 12) of the measured section and photomicrographs of microfacies deposited within this cycle.

4.1.1.6 F-Type Cycles

F-type cycles are characterized by nummulitid, orbitolitid, bioclastic packstone to grainstone microfacies (MF4) as its base and shallowing upward to the top. This microfacies is followed upward and is capped with nummulitid, alveolinid, miliolinid, bioclastic packstone to wackestone microfacies (MF3), orbitolinid, alveolinid, miliolinid, bioclastic packstone to wackestone (MF2), miliolinid, alveolinid, orbitolitid, bioclastic packstone (MF1). In this type of cycle, only lagoonal facies and the variation of this lagoon facies are present. There are two variations of the F-type cycle. These are F1 (cycle 14) and F2 (cycle 17).

F1 type F cycle (Cycle 14) is the 14th cycle in the measured section (Figure 79). This cycle includes the interval of sample numbers NB13 and NB19. NB13 sample is represented *Nummulites*, *Orbitolites* and miliolinid. NB14 sample is represented by *Nummulites*, *Orbitolites* and *Alveolina*. NB15 is represented by *Alveolina*, *Orbitolites* and *Assilina*. NB16 sample is represented by *Orbitolites*, *Nummulites* and *Alveolina*. NB17 sample is represented by *Alveolina*, miliolinid and *Nummulites*. NB18 and NB19 samples are represented by miliolinid, *Alveolina* and *Nummulites*. This cycle starts with nummulitid, orbitolinid, bioclastic packstone to grainstone microfacies (MF4) and continues with nummulitid, alveolinid, miliolinid, bioclastic packstone to wackestone microfacies (MF3) in two beds. The orbitolitid, alveolinid, miliolinid, bioclastic packstone to wackestone (MF2) follow these microfacies in two beds, and is finally capped with miliolinid, alveolinid, orbitolitid, bioclastic packstone (MF1). The cycle shows the inner ramp lagoon conditions and is finally capped with inner ramp lagoon depositional environment near coastward.

F2 type cycle (Cycle 17) is the 17th cycle in the measured section (Figure 80). This cycle includes sample numbers NB29, NB30, NB30-A, NB30-B, NB31 and NB32. NB29 sample is represented by *Nummulites*, rotalinid and *Orbitolites*. NB30 sample is represented by *Nummulites*, *Orbitolites* and rotalinid. NB30-A sample is represented by *Nummulites*, *Alveolina* and *Orbitolites*. NB30-B sample is represented by *Alveolina*, *Nummulites* and *Orbitolites*. NB31 sample is represented by *Alveolina*, rotalinid and *Nummulites*. NB32 sample is represented by *Nummulites*, *Alveolina* and

miliolinid. This cycle starts with nummulitid, orbitolinid, bioclastic packstone to grainstone (MF4). It is continued with nummulitid, alveolinid, miliolinid, bioclastic packstone to wackestone (MF3). The orbitolitid, alveolinid, miliolinid, bioclastic packstone to wackestone microgacies (MF2) follows these microfacies. Finally, it is capped with nummulitid, alveolinid, miliolinid, bioclastic packstone to wackestone (MF3). The cycle represents an inner ramp lagoon facies variation.

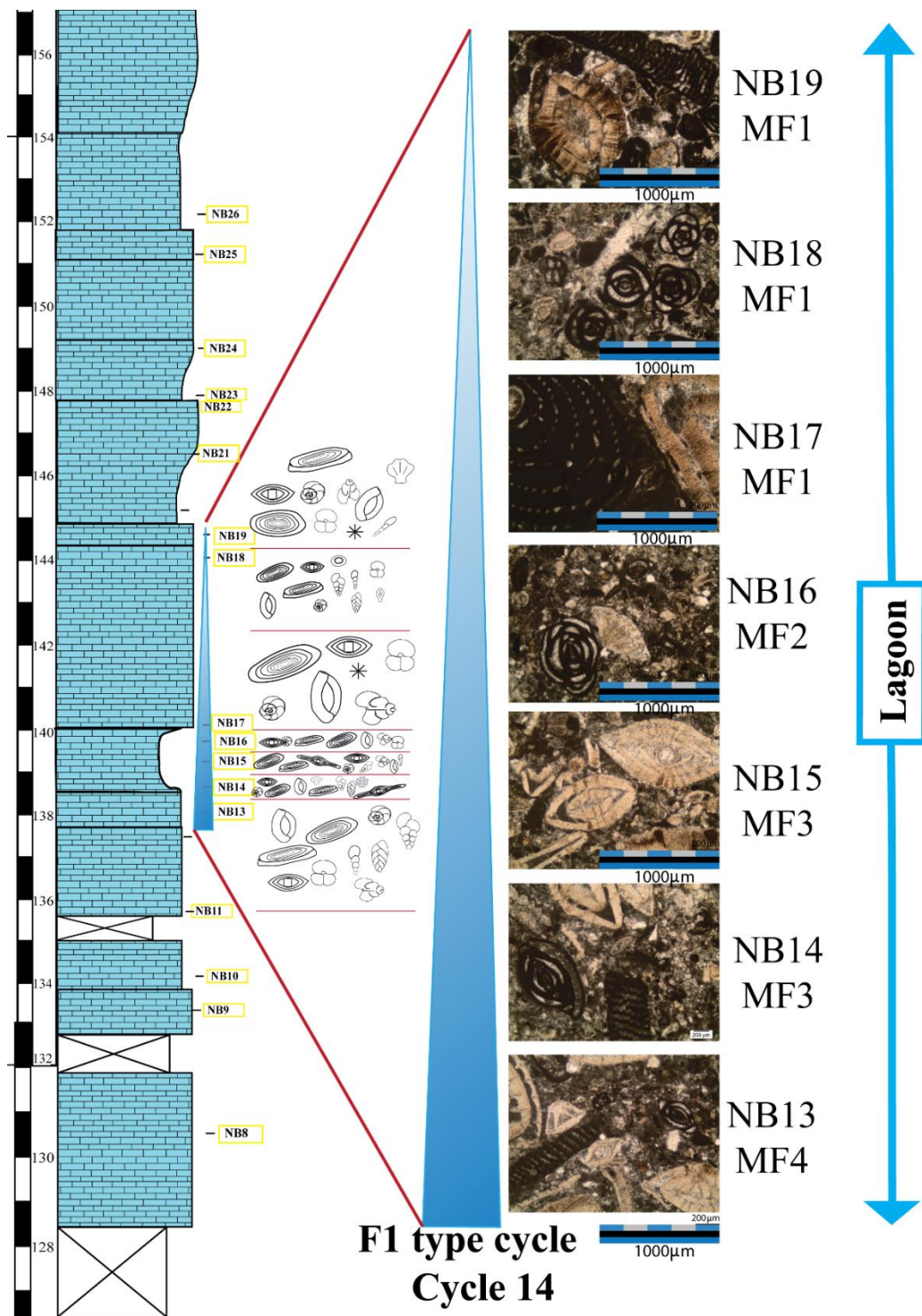


Figure 79: F1 type cycle (Cycle 14) of the measured section and photomicrographs of microfacies deposited within this cycle.

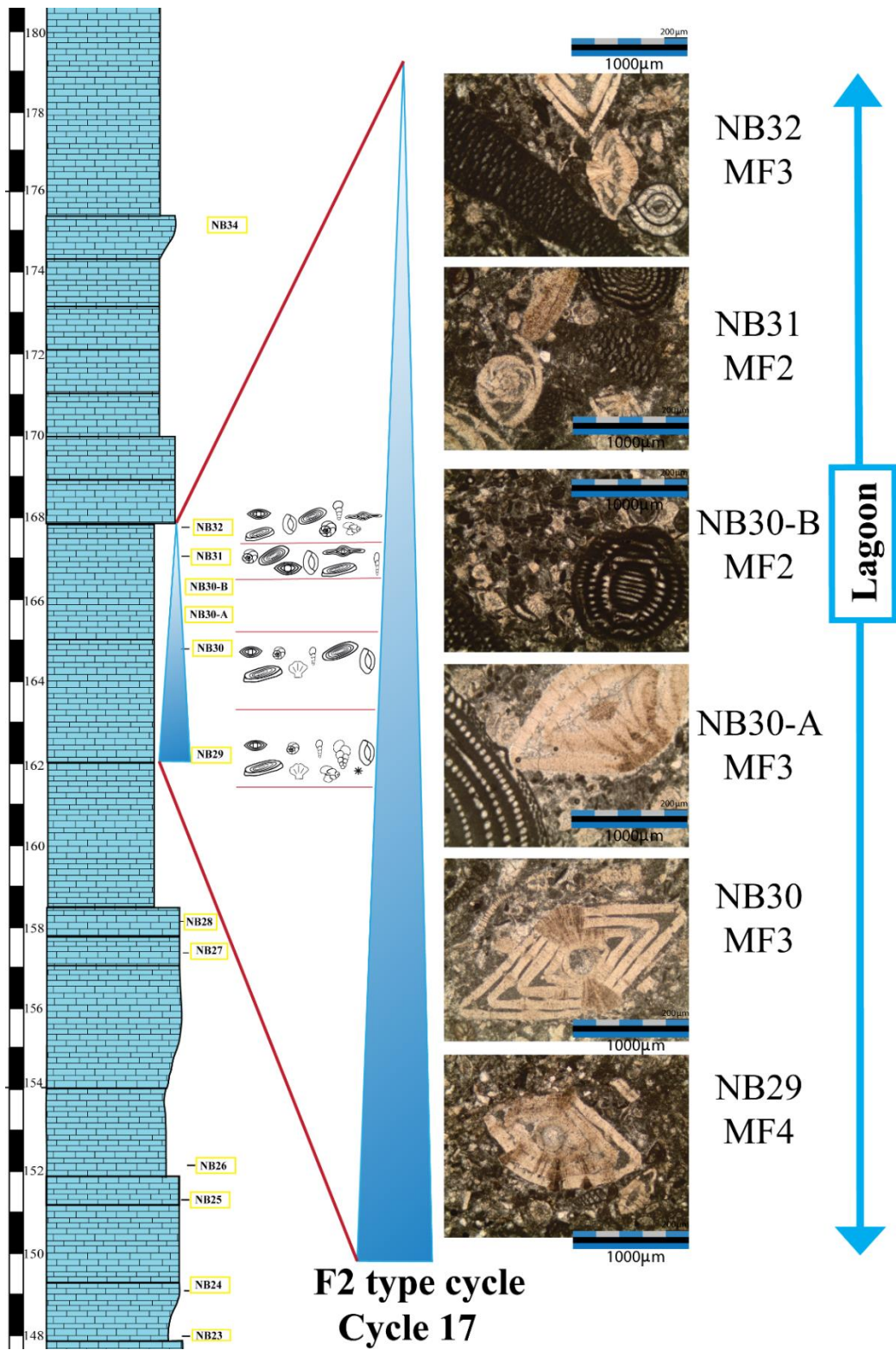


Figure 80: F2 type cycle (Cycle 17) of the measured section and photomicrographs of microfossils deposited within this cycle.

4.1.1.7 G-Type Cycles

G-type cycles are characterized by nummulitid, alveolinid, miliolinid, bioclastic packstone to wackestone microfacies (MF3) as its base and shallowing upward to the top. This microfacies is followed upward and is capped with orbitolinid, alveolinid, miliolinid, bioclastic packstone to wackestone (MF2). In this type of cycle, lagoonal facies variation is present. There are two variations of the G type cycle. These are G1 (cycle 16) and G2 (cycle 18).

G1 type cycle (Cycle 16) is the 16th cycle in the measured section (Figure 81). This cycle includes sample numbers NB26, NB27 and NB28. NB26 sample is represented by *Nummulites*, *Assilina* and rotalinid. NB27 sample is represented by *Nummulites*, *Alveolina* and *Orbitolites*. NB28 sample is represented by *Nummulites*, *Orbitolites* and *Alveolina*. This cycle starts with nummulitid, alveolinid, miliolinid, bioclastic packstone to wackestone microfacies (MF3). It is continued with orbitolitid, alveolinid, miliolinid, bioclastic packstone to wackestone (MF2) and is capped with the same microfacies (MF2) with an increase in the orbitolinid content in the sample. The cycle represents an inner ramp lagoonal facies variation.

G2 type cycle (Cycle 19) is the 19th cycle in the measured section (Figure 82). This cycle includes sample numbers NB35, NB36, and NB37. NB35 sample is represented by *Nummulites*, *Orbitolites* and *Alveolina*. NB36 sample is represented by *Alveolina*, *Orbitolites* and rotalinid. NB37 is represented by *Alveolina*, *Assilina* and *Nummulites*. The cycle starts with nummulitid, alveolinid, miliolinid, bioclastic packstone to wackestone (MF3). This microfacies is followed by the orbitolitid, alveolinid, miliolinid, bioclastic packstone to wackestone microfacies (MF2). Finally, it is capped with nummulitid, alveolinid, miliolinid, bioclastic packstone to wackestone (MF3). The cycle starts with and is capped with inner ramp lagoon facies.

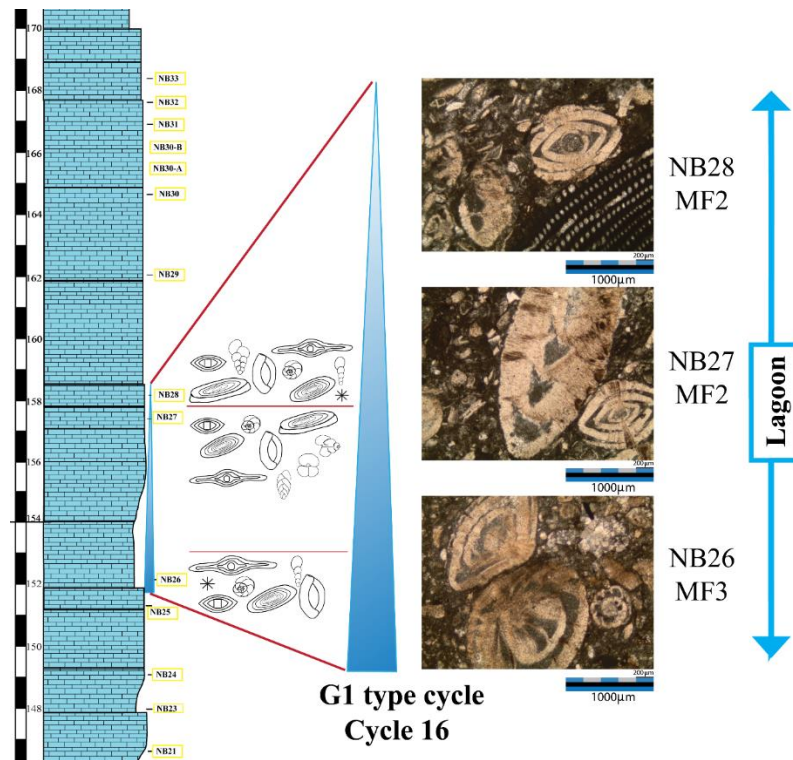


Figure 81: G1 type cycle (Cycle 16) of the measured section and photomicrographs of microfacies deposited within this cycle.

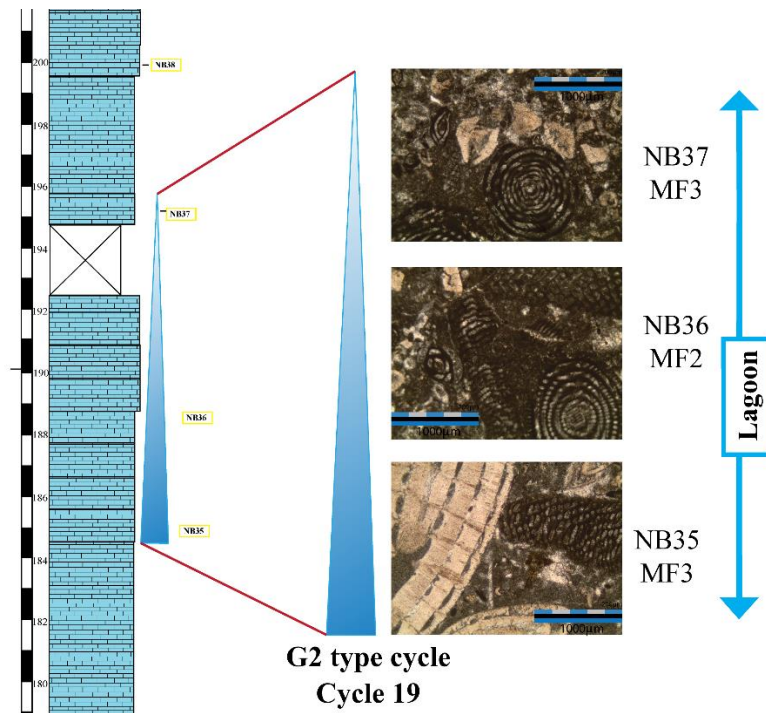


Figure 82: G2 type cycle (Cycle 19) of the measured section and photomicrographs of microfacies deposited within this cycle

4.1.1.8 H-Type Cycles

H-type cycles are characterized by nummulitid assilinid bioclastic packstone (MF5) as its base and deepening upward to the top. This microfacies is followed upward with assilinid nummulitid bioclastic grainstone (MF7) and is capped with discocyclinid, nummulitid, planktonic foraminiferal bioclastic packstone (MF10). In this type of cycle, the shoal facies changes into shallow open marine facies. The H-type cycle is represented by the cycle 21.

H-type cycle (Cycle 21) is the 21th cycle in the measured section (Figure 83). This cycle includes sample number NB40, NB41, NB42 and NB43. NB40 sample is represented by *Nummulites* and rotalinid. NB41 sample is represented by *Nummulites*, *Assilina* and *Alveolina*. NB42 sample is represented by *Assilina*, *Discocyclina* and *Nummulites*. NB43 sample is represented by *Discocyclina* and *Assilina*. This cycle starts with nummulitid assilinid bioclastic packstone (MF5) and is continued with assilinid nummulitid bioclastic grainstone (MF7). The discocyclinid, nummulitid, planktonic foraminiferal, bioclastic packstone (MF10) follows and capes the cycle. The cycle shows inner ramp shoal conditions return to inner ramp shallow open marine conditions.

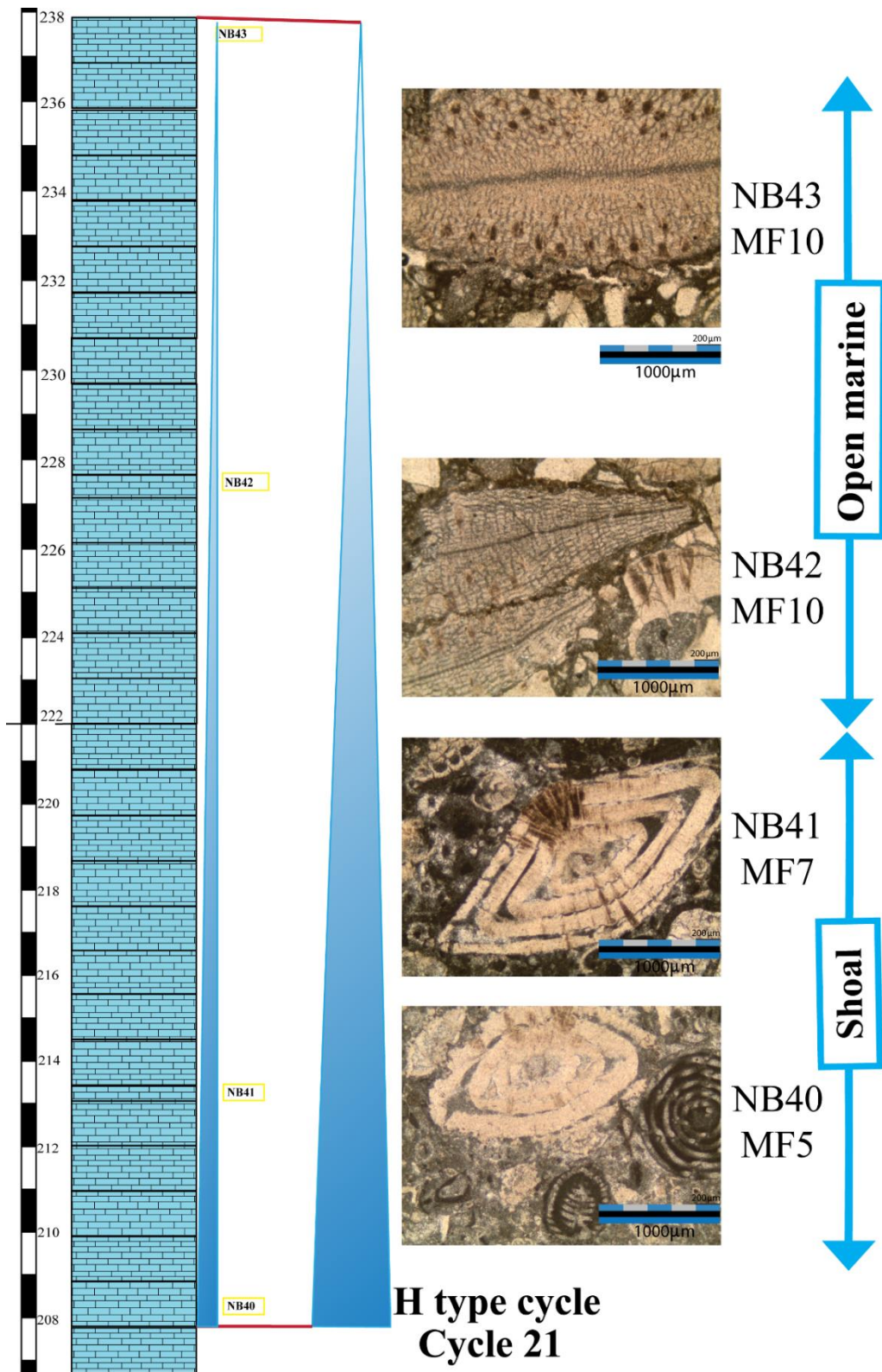


Figure 83: H type cycle (Cycle 21) of the measured section and photomicrographs of microfossils deposited within this cycle.

4.2. Sequence Stratigraphic Interpretation

In order to interpret sequential patterns, firstly types of microfacies for each sample have been determined and the depositional model has been suggested of that microfacies. It was possible to determine the microfacies and obtain relevant information for carbonate ramp deposits with highly abundant fossil content.

Sequence stratigraphic analyses started with the repositioning of the depositional area of shallow marine carbonate ramp deposits in time and space, with this way it was possible to see the trend of the depositions and the relationship between sequent deposits. A total of 58 limestones and 2 sandstone samples were collected from 238 meters thick sequence. The data gathered from thin-sections of the samples and the fieldwork notes taking into consideration, their vertical association have been studied and six 3rd order depositional sequences have been determined. Figure 84 illustrate the levels and the components that have been used for the interpretation. The whole lithology of the sequence is probably not limited to the listed lithology. Sampling space varied due to the topography, and the accessibility of the rock.

The depositional environments of each sample of the measured section have been determined by using the microfacies data. Vertical distributions of depositional environments have been brought together throughout the measured section (columnar section). The lateral distributions of the depositional environments of the samples have been already known (Flügel 2010, Bou Dagher, 2018a). Therefore, it is possible to make sequence stratigraphical interpretations for the studied sequence.

For instance, the sample NB5 has a matrix that is micrite, therefore, the NB5 sample has been named as bioclastic packstone. The depositional environment is low energy and the depth of water is relatively shallow. Most of the biotic fragments are intact and well preserved in this sample, because of the presence of the CRA all over the section. On the other hand, when the sample NB8 was examined under the polarized light microscope, broken fossil fragments and a high amount of quartz particles which are large in size have been observed. It may point to still shallow water conditions and a high-energy environment (and even siliciclastic influx). There might also be reworked fossils in the samples. A comparison of the successive samples also signifies

the change in the record of the depositional environment. As a result of the inferences made in this way, the framework of the whole section has been made.

When all of the sequence boundary and sequence interpretations have been done, we have recognized sequences of the Early Eocene Ypresian aged shallow marine carbonate ramp deposits of the Çayraz Formation. All of the divided sequences have been shown in figure 84. Six sequences and seven sequence boundaries have been identified by the presence of shallowing upward meter scale cycles and the bio-associations of the microfacies (Figure 84).

Deepening and shallowing depositional structure must be observed in order to construct depositional sequence in the depositional model. The concept of microfacies of the strata has already been known. The Highstand System Tracts (HST) and Transgressive System Tracts (TST) depositional patterns have also been known from the Vail et al.'s works (1977 and 1988). Highstand System Tracts can be seen as aggradational to progradational patterns. After the maximum flooding surface (mfs) bound which is basically ended the TST, progradation of the land represents the HST deposits.

Sequence 1 is between samples NB0-1 and NB7 and includes samples NB0-1 to NB4-18 and NB1 to NB7 approximately 95 meters. It includes possible TST in the wackestone stacking pattern and HST starts with NB0-6 with the shallowing trend of the regressive depositional pattern up to the NB7 sample. The sequence boundary is placed above the NB7 sample. From sample NB0-6 to NB7, it is possible to see the parasequences A1, A2, A3, A4, A5, A6 and B-type cycles and the aggradation and progradation pattern of the cycles from the microfacies chart.

Sequence 2 is represented by the C1, C2, and D1 type cycles. After the sequence boundary 2 transgressive depositional patterns have been observed in the measured NB-B section. C1 type cycle is represent the TST. The shallowing upward C2 and D1 type cycles are represent the HST of the sequence 2.

The sequence boundary 3 is recognized below the NB8 sample which is represent a shift from shallower part of the ramp (MF3) to the deeper part of the ramp (MF7). We can observe thin TST within the E-type cycle. After that, we can observe HST within the D2 and F1 types of cycles and the regressive trend of the microfacies from the chart. Sequence 3 is represented with these parasequences and the samples are NB8 to NB19. When the microfacies reach the shallowest part of the ramp with NB19 (MF1), a sequence boundary is placed.

The sequence boundary 4 is recognized between samples NB19 and NB20 since there is a shift from NB19 (MF1) inner ramp lagoon to the NB20 (MF5) inner ramp shoal facies. At the upper part of sequence boundary 4, we can observe thin TST within the D3 type cycle and the HST within the G1 and F2 type cycles as the TST and HST of the sequence 4. Sequence 4 is represented by the NB20- NB23 samples as the transgressive depositional pattern and NB 24 to NB31 regressive depositional trend. When we reach the NB31 (MF2) there is a shift from inner ramp lagoon NB32 (MF3) to the NB33 (MF5) inner ramp shoal facies. The sequence boundary is placed between NB31 and NB32 samples.

Sequence 5 starts with the D4 type cycles of TST, and continues with the HST represented by the G2 and D5 types of cycles. NB33 and NB34 represent the transgression in the depositional pattern. NB35 to NB39 represent the regression of the depositional record. NB39 (MF2) is in the inner ramp lagoon facies and near the shallowest part of the ramp. Subsequent sample NB40 (MF5) represents the inner ramp shoal facies and it is in the deeper part of the ramp. A sequence boundary is placed between these samples as sequence boundary 6.

Sequence 6 is represented by only with the TST as the H type cycle. The sequence 6 is approximately 30 meters thick depositional sequence between samples 40 and 43, and including samples NB40 to 43. For this sequence, it is not possible to divide higher order sequences and/or parasequences, since the control of the lithology (thin section samples) only presents itself near the sequence boundaries. However, it can be

possible with more resolution and more sampled sequences. For instance; sequence 1, it is possible to divide higher order sequences and even parasequences.

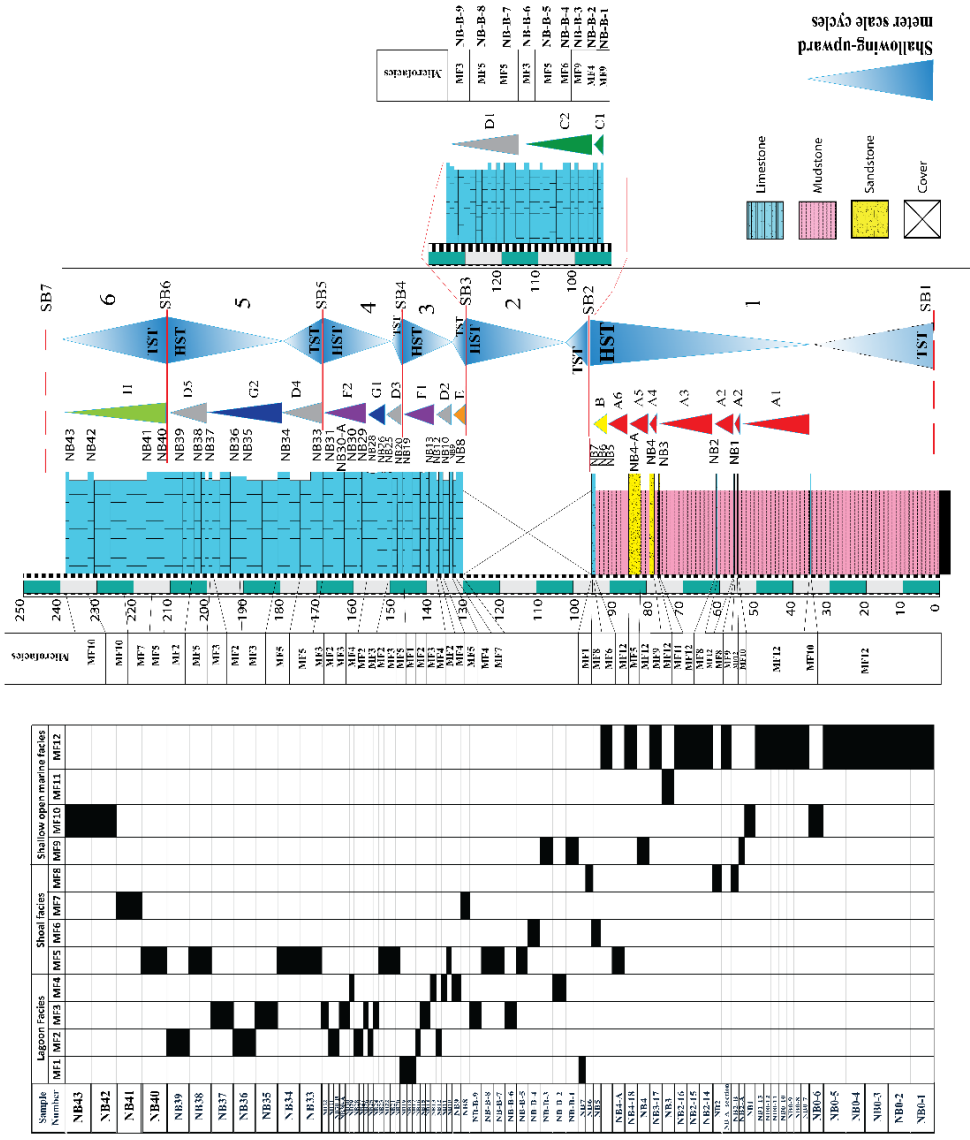


Figure 84: Sequence Structure: TST: Transgressive System Tract, HST: Highstand System Tract, (SB: Generalized Measured Section and Interpreted Sequence Boundaries with MF

“Planktonic foraminifers which has wide geographic range, archived through the Late Mesozoic and in the Cenozoic, is combined with a short stratigraphic time range due to their rapid evolutionary characteristic, they make excellent index fossils at family, generic and species levels (BouDagher-Fadel, 2015).”

In order to understand the eustatic control on the Çayraz Formation, time lines have been needed. It is already known that the deposition of the Çayraz Formation was started during Illerian (Ünalán et al., 1976; Çiner et al., 1996). However more a specific time interval is needed, in order to do this comparison. The first and last mudstone samples have been investigated by Tanık, G.. She has already studied the Eskipolatlı formation which is overlain by the Çayraz Formation and P/E boundary has been recorded in this formation (Tanık, 2017). The findings are as follows;

Sample NB0-1:

This sample was collected from the first mudstone level at the base of the measured section. The larger fraction (>250 microns) of samples were mainly investigated. While benthic foraminiferal assemblages are dominant, and planktonic foraminifers are very low abundant. Morozovellid abundance is very low. The planktonic foraminiferal assemblage is composed of *Morozovella aequa*, *M. acuta*, *M. edgari*, *M. gracilis*; *Parasubbotina inaequispira*; *Acarinina coalingensis*, *A. soldadoensis*, *A. angulosa*, *A. wilcoxensis/pseudotopilensis* lineage; *Pearsonites lodoensis*; *Subbotina roesnaensis*, *S. velascoensis*

Age for NB0-1 is assigned as E2 zone.

Sample NB 4-18:

This sample was collected from the last mudstone level at the top of the measured section. The larger fraction (>250 microns) of samples were mainly investigated. While benthic foraminiferal assemblages are dominant, and planktonic foraminifers are very low abundant. Morozovellid abundance is very low. The planktonic foraminiferal assemblage is composed of *Morozovella crater*, *M. aequa/lensiformis(?)*, *Acarinina angulosa*, *A. wilcoxensis/pseudotopilensis* lineage, *A. quetra*, *A. pentacamerata*, *A. esnehensis*, *A. coalingensis/primitiva* lineage, *A. interposita*, *Subbotina patagonica*, *S. eocaena?*, *Pearsonites lodoensis*.

Age for NB4-18 is assigned as E5-6 zone due to *M. lensiformis* occurrence.

The first sample location seems very close to the units of the Eskipolatlı Formation. The foraminiferal assemblage also agrees with an age assignment of E2. The last sample NB4-18 is about 80 m above the first sample. Planktonic foraminiferal zones from P4c to E2 is equivalent to nearly 30m thick sequence which was deposited into 2 my. E2 zone has already been determined by Tanık (personal communication). Therefore; 80 meters from E2 to E6 is possible in 4 my. These Nummulite banks are probably rapidly deposited. P9 (Berggren et al. 1995) equals E7 (Berggren and Pearson, 2005) equals E7a (Wade et al. 2011) spans around 1.2 my. According to Emery 1996 (Advanced Stratigraphy 2 book; chapter 10; figure 10.4) Apennine platforms show a sedimentation rate of 100 m per my, and recent reefs show a rate of 1000 m per my, so having 140 m Nummulitic bank in just 1.2 my is not very unlikely.

The ages from E2 to E5-6, respectively, have been given to the samples NB0-1 and NB4-18 of mudstone samples. Using this data and Eustatic sea level curve (Snedden and Liu, 2010). The control over the depositional history will be found out.

Another time constraint is found in order to control the sequences at both ends of the time interval. The mud deposits between the lower shelf and upper shelf are described and determined by Çiner et al.(1996). The planktonic foraminifera between two shelves of the Çayraz formation gives P9 (Berggren et al., 1995) from the study of Özcan E. et al. (2018, 2020). That is confined to the sample NB43, discocyclinid, numulitid, assilinitid packstone unit. It's probable lateral continuity of the formation, since it is approximately 4 km away, it is possible to see these lateral facies change.

When we compare the results of the sequence boundaries of this study with the Snedden and Liu (2010) eustatic curve (Figure 85), there are several similarities between some of the boundaries coinciding with the given sequence boundaries, however, some of them do not coincide as an SB of the 3rd order sequences. It looks like the higher order sequences of the 3rd order sequence boundary.

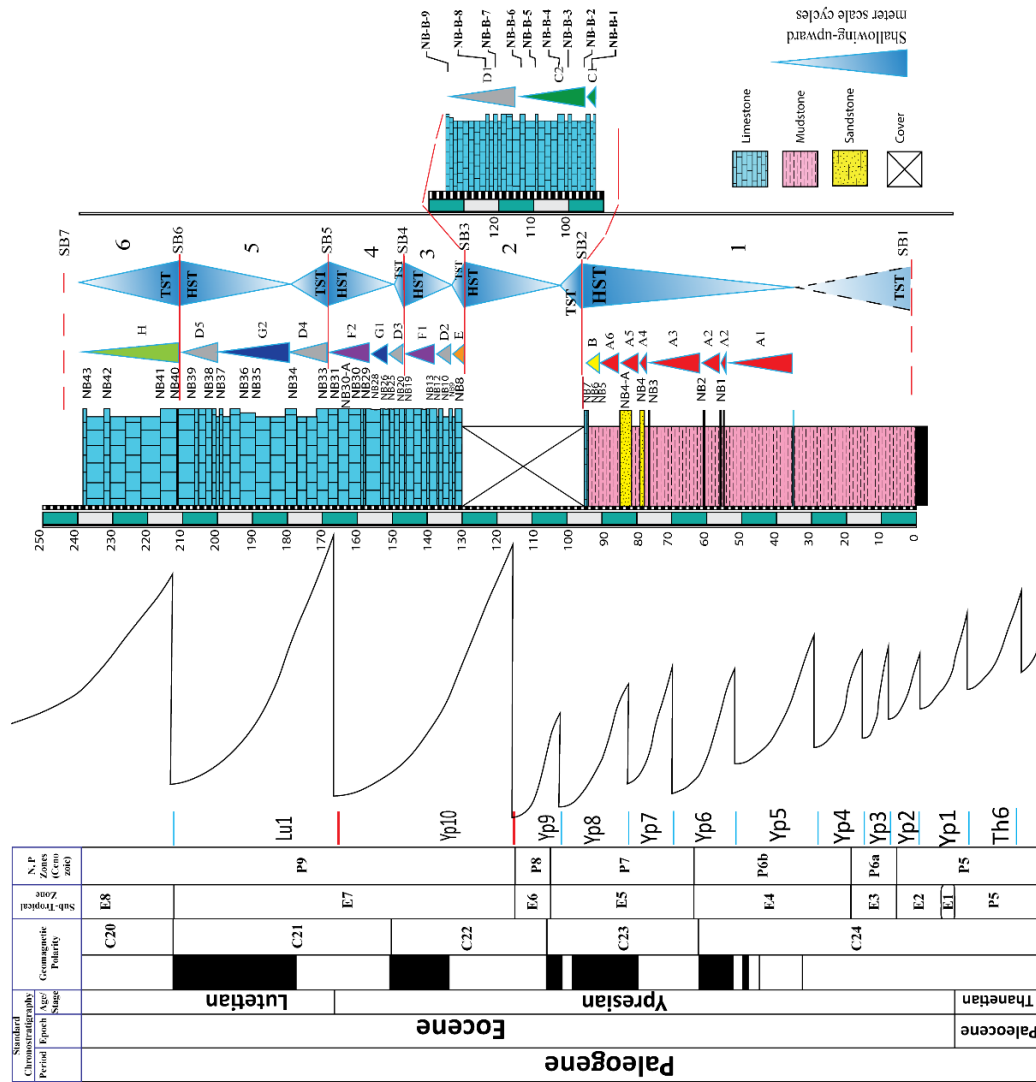


Figure 85: Generalized measured section showing sequence boundaries and comparison with Sneddan and Liu (2010) eustatic sea level curve.

CHAPTER 5

DISCUSSION AND CONCLUSION

In the Haymana Basin, a stratigraphic section that is 238 meters in thickness was measured throughout the Early to Middle Eocene aged Çayraz Formation is mainly composed of carbonates and calcareous mudstones. The aim of this study is to investigate the sedimentary cyclicity and depositional sequences in the Eocene successions of the Haymana Basin.

The stratigraphical section has been measured within the lower shelf system of the Çayraz Formation (Çiner 1993). The main stratigraphic section is the NB section which is total of 238 meters in thickness. Because of the 35 meters covered part on the NB-section, the orientation of the section was laterally shifted along the strike of the known bed. Then, the NB-B section that is continued of the NB section has been measured. The NB section begins with thick mudstone beds and continues with thin sandy limestone beds with *Nummulites* and *Discocyclina*. The section continues with alternations of gradually thickening sandy limestone beds and gradually thinning mudstone beds up to the sandstone bed. After that point, alternations of mudstone beds and fossiliferous sandy limestone beds with *Nummulites*, *Assilina*, and *Discocyclina* alternations are observed. The stratigraphic section is measured upward within limestones with *Nummulites* and *Alveolina*, then, the sequence is covered by soils. This covered part is nearly 35 meters in thickness. The closed area was measured and recorded from the lateral continuations of the limestone beds as the NB-B section. This section is started with sandy limestone beds with *Discocyclina* and *Nummulites* and continues with clayey limestone with *Nummulites* and *Alveolina*. The NB section continues upward with limestone with *Assilina* and *Nummulites*. Then, the section continues up with clayey limestone bearing *Nummulites* and *Alveolina* changes into limestone with *Nummulites* and *Assilina*, and finishes with limestone with *Discocyclina* and *Nummulites* and *Assilina*. A total of 58 limestone samples, 2

sandstone samples, and 35 mudstone samples have been collected. Thin-sections of limestone and sandstone samples have been examined under a polarized light microscope.

Detailed microfacies analyses have been carried out on the samples collected from the studied section in order to determine the depositional model of the formation. Twelve different microfacies types are defined based on the larger benthic foraminifera (LBF); miliolinid, alveolinid, orbitolite, bioclastic packstone (MF1); orbitolite, alveolinid, miliolinid, bioclastic packstone to wackestone (MF2); nummulite, alveolinid, miliolinid, bioclastic packstone to wackestone (MF3); nummulite, orbitolite, bioclastic packstone to grainstone (MF4); nummulite, assilinite, bioclastic packstone (MF5); nummulite, discocyclinid, assilinite, bioclastic packstone to wackestone (MF6); assilinite, nummulite, bioclastic grainstone (MF7); discocyclinid, nummulite, assilinite, planktonic foraminiferal, bioclastic packstone to wackestone (MF8), discocyclinid, nummulite, bioclastic grainstone (MF9); discocyclinid, nummulite, planktonic foraminiferal, bioclastic packstone (MF10); grainstone (MF11); small benthic foraminiferal, planktonic foraminiferal wackestone (MF12).

Based on the detailed microfacies analyses and their vertical distribution, a composite depositional model is suggested. According to this model, three major facies associations are distinguished, from deepest to shallowest, shallow open marine, sand shoal and banks, and lagoon. These three environments are represented by twelve microfacies. The shallow open marine part is characterized by small benthic foraminiferal, planktonic foraminiferal wackestone (MF12); grainstone (MF11); discocyclinid, nummulite, planktonic foraminiferal, bioclastic packstone (MF10); discocyclinid, nummulite, bioclastic grainstone (MF9). The sand shoal and bank part are represented by discocyclinid, nummulite, assilinite, planktonic foraminiferal, bioclastic packstone to wackestone (MF8); assilinite, nummulite, bioclastic grainstone (MF7); nummulite, discocyclinid, assilinite, bioclastic packstone to wackestone (MF6); nummulite, assilinite, bioclastic packstone (MF5). The lagoon part is characterized by the nummulite, orbitolite, bioclastic packstone to grainstone (MF4); nummulite, alveolinid, miliolinid, bioclastic packstone to wackestone (MF3);

orbitolite, alveolite, miliolite, bioclastic packstone to wackestone (MF2); miliolite, alveolite, orbitolite, bioclastic packstone (MF1).

In this study, bio-associations of foraminifers and microfacies data of shallowing upward cycles (parasequences) are used for sequence stratigraphic interpretation. Based on the vertical changes of microfacies and the stacking pattern of the meter-scale cycle types within the NB and NB-B sections, a total of 21 cycles and six sequences are determined in the measured section. The presence of a total of six 3rd-order sequences is distinguished from the change in the composition of the rock and intercalating nature of the development of the vertical section. Moreover, changes in the composition also indicate lower-order parasequences.

Nummulites are the most abundant foraminiferal group in the measured section and show a good response to cyclicity. As well as the *Nummulites*, the other abundant foraminiferal groups which are *Discocyclina*, *Assilina*, *Alveolina*, *Orbitolites*, and miliolids show good response to cyclicity. *Nummulites*, *Discocyclina*, and *Assilina* show a decreasing trend toward the top of the cycle in the shallowing upward cycles and an increasing trend toward the top of the cycle in the deepening upward cycle. *Alveolina*, *Orbitolites*, and miliolids show an increasing trend toward the top of the cycle in the shallowing upward cycles.

The sequences presented in the studied area may result from the sea-level variation. In order to understand the driving force for the sequence formation, the data that have been recognized in this study and the eustatic sea-level curve (Snedden and Liu, 2010) are correlated with the eustatic sea-level curve of Snedden and Liu (2010) by using the age data from the planktonic fossils.

The Çayraz Formation conformably overlies the Eskipolatlı Formation. Tanık (2017) studied the planktonic foraminifers of the Eskipolatlı Formation including the Paleocene/Eocene boundary which took place in 56 Ma. The youngest age data from the Eskipolatlı Formation is the planktonic foraminiferal E2 zone that corresponds to nearly the earliest Ypresian, Early Eocene (Tanık, 2017). The age control is made by using the data from the lowest (NB0-1) and uppermost (NB4-18) samples of the mudstone part of the studied section. The age of the sample NB0-1 that corresponds

to the last sample of the sequence of Tanik (2017) is assigned as the earliest Ypresian, Early Eocene by using planktonic foraminifera zone E2 (Tanik, 2017; Berggren & Pearson, 2005). The E2 zone corresponds to the latest part of the P5 zone (Berggren et al., 1995). However, the age of the sample NB4-18 that corresponds to the last level of mudstone part of the sequence is assigned as middle Ypresian, middle Early Eocene by using planktonic foraminifera zone E5 (Berggren & Pearson, 2005) which corresponds to the age P7 (Berggren et al., 1995) aged deposits at the beginning of the measured section. The mudstone level between the lower and upper shelf unit in the succession studied by Özcan et al. (2018, 2020) is confined to our last sample NB43 (discocyclinid, nummulitid, and assilinid packstone). This mudstone level is probable lateral continuity of the last part of the studied sequence. So the last sample NB43 has been dated as early Lutetian, early Middle Eocene by using planktonic foraminifera zone E7/P9 recorded by Özcan et al. (2018, 2020).

Transgressive-regressive cycles on all scales are controlled by eustatic variations, the degree of sea-floor subsidence, and the rate of deposition (Einsele et al., 1991). When the rate of maximum sea-level fall is lower than the rate of subsidence, sediment accumulation at the site is continuous, and no distinct sequence boundary is generated (Einsele et al. 1991). In that case, the sequence boundary generated is named a type-2 sequence boundary. All the sequence boundaries that are interpreted in this study is type-2 sequence boundary, since the sea-level fall is not exceeded by the subsidence rate. Therefore, during the field and the laboratory studies, any exposure/unconformity surface, in other words, the unconformity is not determined. The subsidence is continuous consequently the deposition is continuous at the time of sea level rise and even at the time of sea level fall.

The Haymana Basin was developed within a continental collision regime along the northern branch of the Neo-Tethys. Starting from the Cretaceous, the northern branch of the Neo-Tethys began to close and was subducted under the Eurasian Plate (Şengör and Yılmaz 1981, Görür et al. 1984). The type of carbonate platform is interpreted as a ramp-type platform by using the microfacies analysis data. Since the subduction is still continuous at the time of deposition of the Eocene Çayraz Formation, the ramp is

still under the control of the tectonism. Therefore, the carbonate platform in active margin would be the right assumption for the Çayraz Formation development.

There was a stable warm tropical climate through the Eocene Epoch (Pearson et al., 2007). The Earth's climate cooled from the period of extreme warmth in the early Eocene Epoch (ca. 50 Ma) to the early Oligocene (ca. 33 Ma), when a large ice cap first appeared on Antarctica (Pearson et al., 2007). Since there were no large ice caps during the Eocene, the glacio-eustasy could not be mentioned as a driving mechanism behind the sea-level fluctuations during the Eocene. There might be aquifer-eustasy and thermo-eustasy which both could not create more than 10 meters of sea-level fluctuation (Ray et al. 2020). There must be different mechanisms behind the sea-level fluctuations, such as subsidence, the subduction which is still going on, compaction, or both sea-level and compaction together or without sea level change storm can shift the shoal from its place.

Çiner et al. (1996a) have also studied the cyclicity of the Çayraz Formation. They have measured 7 sections (Ç1, Ç2, Ç3, Ç4, Ç5, Ç6, and Ç7) in order to correlate them with each other and finally to interpret the geometry of the study area. The measured sections of Ç6 and Ç7 are very close to this study's area. Therefore, we can correlate them with the NB section. The cycles interpreted in the NB section are differentiated from each other with the type of cycles. There are eight different types of cycles present and they are cyclic in nature. The types of cycles are differentiated from the basic units in the Çiner et al. (1996a). There are four different basic units that are distinguished. From these basic units, there are six cycles interpreted in the Ç6 section, and six cycles are interpreted for the Ç7 section. Basic units are considered to be allocyclic transgressive-regressive cycles tuned to Milankovitch bands. At the scale of the basic sequences and shelf systems, the lateral and vertical distribution of the sequences, and the presence of onlap structures strongly suggest sea-level changes. In this study 21 cycles, are differentiated from the eight different types of cycles, and suggested seven sequence boundaries and six sequences. Since only one section was measured, the geometry of the basin could not be defined, the assumption is that the deeper part of the basin is in the SE of the studied area where the marl deposits outcropped between two shelf systems (Çiner et al, 1996a; Özcan et al., 2020). No

lateral distribution of the facies is observed because of the lack of the different section measurement, the vertical distribution of the sequences is suggested the short-term sea level change. Çiner et al. (1996a) suggested two shelf systems within the thick marl deposition. This study showed ramp type carbonate platform type and suggested a composite depositional model for the ramp type system. No marl level is observed in the NB section which corresponds to the first shelf system of the Çiner et al.'s work. In the upper part of the studied section, a deepening cycle is observed which corresponds to the H-type cycle. This transgressive part of sequence 6 is the TST of the sequence and is assumed to be the lateral continuation of the marl deposits with lateral facies change to the MF10 discocyclinid, nummulitid, planktonic foraminiferal bioclastic packstone.

Geyikçioğlu Erbaş (2008) has also studied meter-scale cycles of the Çayraz Formation near Çayraz Village. She measured one section, section 1 which is 44,55 meters in thickness, from the lower shelf of the Çayraz Formation. This section is approximately 4km (SE) away from our study's stratigraphic section. There is no contact present with the Ekipolatlı Formation with the section Geyikçioğlu Erbaş's (2008) section. Another section, section 2 which is 25,95 meters in thickness, is from the upper shelf of the Çayraz Formation. In the study of Geyikçioğlu Erbaş (2008), detailed microfacies analyses were carried out and 10 different microfacies were identified strictly based on the biofacies in order to define meter-scale cyclic sedimentation. In our study, only one section has been measured at 238 meters in thickness, with a contact between Ekipolatlı Formation. The section 1 from the Geyikçioğlu Erbaş's study is corresponds to the upper part of the NB stratigraphic section. Based on detailed microfacies analyses and the distribution of the vertical facies relationships a composite depositional model is suggested for Geyikçioğlu Erbaş's (2008) study. According to this model, three major facies associations were distinguished, from deepest to shallowest, as; shallow open marine, shoal, and lagoon facies. In our study, also a composited depositional model is suggested based on the detailed microfacies analyses. The findings are the same as Geyikçioğlu Erbaş's (2008) study, except twelve microfacies are used to determine these three major facies from shallowest to deepest lagoon, sand banks, and shoal, restricted and shallow open marine facies.

From Geyikçioğlu Erbaş's (2008) study the studied sections are composed of meter-scale cycles of upward both shoaling or deepening in character. Five cycles are determined for the Section 1, and six cycles are determined for the Section 2. Cycles of section 1 are represented by shallow open marine and lagoonal depositional environment and are represented by highstand system tract (HST). Section 2 is represented by a transgressive system tract (TST) backstep in a retrogradational parasequence set and the system tract progressively deepens upward and successively younger parasequences step farther landward. In our study eight different cycle types are differentiated and 21 cycles are determined. The transgressive system tracts are relatively thin in our study, around 1 meter, 5,5 meters, 7 meters, 7,5 meters, and also 30 meters transgressive system tracts are present in the measured section. The thickness of the transgressive system tracts is progressively increasing. A total of six, one possible, and five determined TST are present in the measured section. A total of five highstand system tracts are recognized in the measured section. The thicknesses of the highstand system tracts are around 60 meters, 33 meters, 14,5 meters, 13 meters, and 32,5 meters. The thicknesses of the HST are decreasing for a while and increase again in the sequence 5. Based on the stacking pattern of the meter-scale cycles two sequence boundaries are identified in Geyikçioğlu Erbaş's (2008) study. In our study, a total of seven; two possible, five type-2 sequence boundaries are determined. Geyikçioğlu Erbaş (2008) are documented the responses of the benthic foraminiferal groups to the sedimentary cyclicity by quantitative and statistical analysis to understand the shallowing upward cycles.

The short-term sea level change could be created by a possible mechanism in behind, such as; aquifer-eustasy, thermo-eustasy, and dynamic topography (Sames et al., 2016). Aquifer-eustasy and thermo-eustasy are effect 10 meters each in the geological record. The effect

of the dynamic topography is much more intense than the aquifer-eustasy and the thermo-eustasy. Dynamic topography is the subduction, and subsidence rate of the regional geography. It can create more than 10 meters of accommodational space for the carbonate factory that is present in the studied area. The general trend of the microfacies when we look up close to the microfacies chart (Figure 84) regression

trend can be seen at first from NB0-6 to the NB19 and then turn into the transgression phase from NB20 up to the NB43. This is interpreted as a long-term higher-order sequence. It is possible to divide short-term sea-level changes as sequences and even parasequences thanks to the sampling interval intensity at the middle part of the measured NB and NB-B sections.

Difficulties in the interpretation of the sequence stratigraphy of the studied section might be related to the following: lack of information on the geometry of the studied area such as onlap and down lap surfaces; lack of seismic data; or the presence of only one measured section instead of many sections close to each other to construct the geometry of the basin.

In order to improve the interpretation of sequence stratigraphy of the studied section, some further studies might be made in the future, such as mineralogical analyses on the wackestone samples. These recommended studies will probably help to understand the stacking pattern of these facies.

None of these analyses have been done for this study due to time and budget constricts. Nevertheless, all these do not abate the value of the thesis.

In a conclusion, in this study, a stratigraphic section (NB section and NB-B part of the NB section) was measured,

- A total of 58 limestone, 2 sandstone, and 35 mudstone samples were collected;
- Detailed microfacies analyses have been carried out;
- Twelve microfacies have been determined by using the relative abundance of fossil content, in particular, larger benthic foraminifers;
- A composite depositional model has been suggested based on the detailed microfacies analyses and the vertical distribution of the microfacies;
- Three major facies associations have been distinguished from shallowest to deepest, as lagoon, sand shoal and banks, and shallow open marine;
- The bio-associations of foraminifers and microfacies data of shallowing upward cycles (parasequences) A total of 21 cycles (parasequences) have been determined;

- Based on the data, the stacking pattern of eight different cycle types, a total of seven as; two possible and five of type 2 sequence boundaries have been determined;
- Between these sequence boundaries, six sequences are recognized;
- The age of the sample NB0-1 has been assigned as the earliest Ypresian, Early Eocene by using planktonic foraminifera zone E2/P5 (Tanık, 2017; Berggren& Pearson, 2005).
- The age of the latest mudstone sample NB4-18 has been assigned as middle Ypresian, middle Early Eocene by using planktonic foraminifera zone E5-E6/P7 (Berggren& Pearson, 2005). The E5-6/P7zone has been defined by the presence of *M. lensiformis* (Gamze Tanık, personal communication).
- The age of the last sample of the studied sample has been assigned as early Lutetian, early Middle Eocene by using planktonic foraminifera zone E7/P9 (Özcan et al., 2020).
- These ages have been used for the correlation of the sequence boundaries with the eustatic sea-level curve (Snedden and Liu, 2010).
- The type of carbonate platform in the composite section has been defined as carbonate ramp type.
- However, the ramp associated with the active margin is more suitable for this study area. The difference between sequence boundaries and the eustatic curve of Snedden and Liu (2010) might have resulted from the dynamic topography of the ramp margin, the subsidence rate, and tectonics.

REFERENCES

- Adabi, M. H., Zohdi, A., Behdad, A., Amiri, H., (2008). Applications of nummulitids and other larger benthic foraminifera in depositional environment and sequence stratigraphy: An example from the Eocene deposits in Zagros Basin, SW Iran. *Facies* 54(4), 499-512.
doi: 10.1007/s10347-008-0151-7
- Akarsu, İ., (1971). II. Bölge AR/TPO/747 nolu sahanın terk raporu. Pet. İş. Gen. Md., Ankara. Dergisi, 85, 17-38.
- Amirov, E., (2008). *Planktonic foraminiferal biostratigraphy, sequence stratigraphy and foraminiferal response to sedimentary cyclicality in the Upper Cretaceous-Paleocene of the Haymana Basin (Central Anatolia, Turkey)*. Ankara: MSc. Thesis, Middle East Technical University.
- Arıkan Y., (1975). Tuzgözü havzasının jeolojisi ve petrol imkanları. MTA Dergisi, 85, 17-38
- Bagherpour, B., Vaziri, M. R., (2012). Facies, paleoenvironment, carbonate platform and facies changes across Paleocene Eocene of the Taleh Zang Formation in the Zagros Basin, SW-Iran. *Historical Biology*, V:24(2).
<https://doi.org/10.1080/08912963.2011.587185>
- Barattolo, F., Bassi, D., Romano, R., (2007). Upper Eocene larger foraminiferal - Coralline algal facies from the Klokova Mountain (southern continental Greece). *Facies* 53(3): 361-375
doi: 10.1007/s10347-007-0108-2
- Beavington-Penney, S. J., Racey, A., (2004). Ecology of extant nummulitids and other larger benthic foraminifera: applications in palaeoenvironmental analysis. *Earth Sci Rev* 67:219–265
- Berggren, W. A. (1977). Atlas of Palaeogene Planktonic Foraminifera: Some Species of the Genera Subbotina, Planorotalites, Morozovella, Acarinina and Truncorotaloides. In e. A.T.S. Ramsay, *Oceanic Micropaleontology* (pp. 205-300). London: Academic Press.
- Berggren, W. A., Kent, D. V., Flynn, J. J. , and van Couvering, J. A. (1985). Cenozoic geochronology: Geological Society of America Bulletin, v. 96, p. 1407–1418, doi:10.1130 /0016-7606(1985)96<1407:CG>2.0.CO;2.
- Berggren, W. A., and Miller, K. G. (1988). Paleogene tropical planktonic foraminiferal biostratigraphy and magnetobiochronology. *Micropaleontology*, vol. 34, no. 4, pp. 362-380.
- Berggren, W. A. (1992). 31. Paleogene planktonic foraminifer magnetobiostratigraphy of the southern Kerguelen Plateau (Sites 747-749).

In S. W. Wise, & R. e. Schlich, *Proceedings of the Ocean Drilling Program, Scientific Results, Vol. 120* (pp. 551-568). Texas: Ocean Drilling Program.

- Berggren, W. A., Kent, D. V., Swisher III, C. C., and Aubry, M.P. (1995b). A revised Cenozoic geochronology and chronostratigraphy, In: Berggren, W.A., Kent, D.V., Aubry, M.-P., Hardenbol, J. (Eds.), *Geochronology, Time Scales and Global Stratigraphic Correlation: A Unified Temporal Framework for a Historical Geology: SEPM Special Publication*, vol. 54, pp. 129–212.
- Berggren, W. A., and Norris, R. D. (1997). Taxonomy and Biostratigraphy of (Sub)tropical Paleocene Planktonic Foraminifera. *Micropaleontology, Supplement 1*, 43, pp. 1-116.
- Berggren, W. A., and Ouda, K. (2003a). Upper Paleocene-lower Eocene planktonic foraminiferal biostratigraphy of the Dababiya section, Upper Nile Valley (Egypt). *Micropaleontology*, vol. 49, pp. 61-92.
- Berggren, W. A., and Ouda, K. (2003b). Upper Paleocene-lower Eocene planktonic foraminiferal biostratigraphy of the Qreiya (Gebel Abu Had) section, Upper Nile Valley (Egypt). *Micropaleontology*, vol. 49, pp. 105-122.
- Berggren, W. A., and Pearson, P. N. (2005). A revised tropical to subtropical Paleogene planktonic foraminiferal Zonation. *Journal of Foraminiferal Research*, v. 35, no. 4, p. 279-298.
- BouDagher-Fadel, M. K. (2015). *Biostratigraphic and Geological Significance of Planktonic Foraminifera, Updated 2nd Ed.* London: UCL Press.
- BouDagher-Fadel, M.K. (2018a). *Evolution and Geological Significance of Larger Benthic Foraminifera.* UCL Press, London. 639 p.
- Brönnimann, P. (1951). A model of the Internal Structure of *Discocyclina* s.s.. *Journal of Paleontology*, Vol. 25. No. 2. pp. 208-211.
- Burchette, T.P., Wright, V.P. (1992): Carbonate ramp depositional systems. – *Sed. Geol.*, **79**, 3-57
- Buxton M, Pedley H (1989) Short paper: a standardized model for Tethyan Tertiary carbonates ramps. *J Geol Soc* 146:746–748
- Çetin, H., Demirel, İ. H., and Gökçen, S.L., (1986). Haymana'nın (SW Ankara) doğusu ve batısındaki Üst Kretase-Alt Tersiyer istifinin sedimentolojik ve sediment petrolojik incelemesi. *TJK Bülteni*, 29/2, 21-33.
- Catuneanu O (2006) *Principles of sequence stratigraphy.* Elsevier, New York, p 386.
- Catuneanu O. et al., (2008). Towards the standardization of Sequence stratigraphy. *Earth Science Reviews* (2008).
- Catuneanu, O., Abreu, V., Bhattacharya, J.P., Blum, M.D., Dalrymple, R.W., Eriksson, P.G., Fielding, C.R., Fisher, W.L., Galloway, W.E., Gibling, M.R.,

Giles, K.A., Holbrook, J.M., Jordan, R., Kendall, C.G.S.T.C., Macurda, B., Martinsen, O.J., Miall, A.D., Neal, J.E., Nummedal, D., Pomar, L., Posamentier, H.W., Pratt, B.R., Sarg, J.F., Shanley, K.W., Steel, R.J., Strasser, A., Tucker and M.E. and Catuneanu, O., Galloway, W.E., Kendall, C.G.S.T.C., Miall, A.D., Posamentier, H.W., Strasser, A. and Tucker, M.E. (2011). Sequence Stratigraphy: Methodology and Nomenclature. *Newsletters on Stratigraphy*, 44, 173-245.

<http://dx.doi.org/10.1127/0078-0421/2011/0011>

Chaput E., (1932). Observations géologiques en Asie Mineure: Le Crétacé supérieur dans l'Anatolie Centrale. *C. R. A. S.*, 194, 1960-1961.

Chaput E., (1935a). L'Eocene du plateau de Galatie (Anatolie Centrale). *C. R. A. S.*, 200, 767-768.

Chaput E., (1935b). Les plissements Tertiaires de l'Anatolie Centrale. *C.R. A. S.*, 201, 1404- 1405.

Checchia-Rispoli, G. (1905). Sopra alcune Alveoline eoceniche della Sicilia. *Palaeontographia Italica*. 11: 147-167.

Ćosović, V., Drobne, K. & Moro, A., (2004). Paleoenvironmental model for Eocene foraminiferal limestones of the Adriatic carbonate platform (Istrian Peninsula). *Facies* 50, 61–75

<https://doi.org/10.1007/s10347-004-0006-9>

Çiner A. (1993). Geology of Haymana Basin (U. Cretaceous – M. Eocene); Central Anatolia, Turkey. 6th International Meeting and Training School on IGCP Project 269, Middle East Technical University, Field Trip Guide Book, 21 s.

Çiner A. (1996). Distribution of small scale sedimentary cycles throughout several selected Basins, *Tr. J. of Earth Sciences*, 5, 25-37.

Çiner A., Deynoux M., Koşun E. ve Gündoğdu N. (1993b). Yamak türbidit karmaşığının (YTK) sekansiyel stratigrafik analizi: Haymana Baseni (Orta Eosen). *Sekans Stratigrafisi, Sedimentoloji Çalışma Grubu Özel Yayını*, 1, 53-70.

Çiner A., Deynoux M., Koşun E. ve Gündoğdu N. (1993a). Beldede örgülü-delta karmaşığının (BÖDK) sekans stratigrafik analizi: Polatlı-Haymana baseni (Orta Eosen) Orta Anadolu. *Yerbilimleri*, 16, 67-92.

Çiner A., Deynoux M., Ricou S. ve Koşun E. (1996a). Cyclicity in the Middle Eocene Çayraz Carbonate Formation, Haymana Basin, Central Anatolia *Palaeogeography, Palaeoclimatology, Palaeoecology*, 121, 313-329.

- Çiner A., Deynoux M. ve Koşun E. (1996b). Cyclicity in the Middle Eocene Yamak turbidite complex of the Haymana basin, Central Anatolia, Turkey. *Geol. Rundschau.*, 85, 669- 682.
- Çolakoğlu, S., & Özcan, E. (2003). Orthophragminid foraminiferal assemblages from an Ilerdian-early Cuisian reference section (Sakarya section, Haymana-Polatlı Basin, Central Anatolia-Turkey). *Rivista Italiana di Paleontologia e Stratigrafia*, vol. 109, no. 1, ta. 3, pp. 1-17.
- Dağer Z., Öztümer E., Sirel E. ve Yazlak Ö. (1963). Ankara civarında birkaç stratigrafik kesit. TJK Bülteni, 8/1-2, 84-95.
- Dinçer, F. (2016). Eocene benthic foraminiferal assemblages from Central Anatolia (Turkey): biostratigraphy, stable isotope data, paleoenvironmental and paleontological interpretations. *Journal of African Earth Sciences*, 114, pp. 143-157.
- Dizer, A., (1964). Sur quelques alveolines de l'Eocene de Turquie. *Revue de Micropaleontologie*, 7, 265-279.
- Dizer, A., (1968). Etude micropaleontologique du nummulitique de Haymana (Turquie). *Revue de Micropaleontologie*, 11, 13-21.
- Dunham, R.J. (1962). Classification of carbonate rocks according to depositional texture. In: Ham, W.E. (eds.): *Classification of carbonate rocks. A symposium of American Associated Petroleum Geologist Memoir*, 1, 108-171.
- Druitt C. E. ve Reckamp, J. U., (1959). Çaldağ columnar section TPAO Arşivi, Ankara.
- Einsele, G., Ricken, W. and Seilacher, A. (Eds.), (1991), *Cycles and Events in Stratigraphy*, Springer-Verlag, Berlin Heidelberg.
- Egeran N. ve Lahn E., (1951). Kuzey ve Orta Anadolu'nun tektonik durumu hakkında not. MTA Bülteni, 41, 23-28.
- Emery, D. (1996). Chapter Ten Carbonate Systems. In Emery, D. and Myers, K. (eds). *Sequence Stratigraphy*. Blackwell Publishing.
- Esmeray, S. (2008). *Cretaceous/Paleogene boundary in the Haymana Basin, Central Anatolia, Turkey: micropaleontological and sequence stratigraphic approach*. Ankara: MSc. Thesis, Middle East Technical University.
- Esmeray-Senlet, S., Özkan-Altın, S., Altın, D., and Miller, K. G. (2015). Planktonic foraminiferal biostratigraphy, microfacies analysis, sequence stratigraphy and sea-level changes across Cretaceous across the Cretaceous-Paleogene boundary in the Haymana Basin, Central Anatolia, Turkey. *Journal of Sedimentary Research*, v. 85, pp. 489-508.

- Fahad, M., Khan, M., Hussain, J., Ahmed, A., Yar, M., (2021). Microfacies analysis, depositional settings and reservoir investigation of Early Eocene Chorgali Formation exposed at Eastern Salt Range, Upper Indus Basin, Pakistan. *Carbonates and Evaporites* 36(3).
- doi: 10.1007/s13146-021-00708-7
- Flügel, E. (2010). *Microfacies of Carbonate Rocks, Analysis, Interpretation and Application*. Springer-Verlag, Berlin, 996 p.
- Folk, R.L., 1959, Practical petrographic classification of limestones: American Association of Petroleum Geologists Bulletin, v. 43, p. 1-38.
- Folk, R.L. (1962). Spectral subdivision of limestone types. In: *Classification of carbonate rocks*. (Ed. by Ham, W.E.), American Association of Petroleum Geologist Memoirs 1, Tulsa, pp. 62–84.
- Galloway, J. J. (1928). A revision of the family Orbitoididae. *Journal of Paleontology*. 2: 45-69.
- Geyikçiöđlu, Erbař, B. (2008). *Meter scale cycles in the Eocene Çayraz Formation (Haymana Basin) and response of foraminifers to cyclicity*. Ankara: MSc. Thesis, Middle East Technical University.
- Gez, S., (1957). Dereköy- Haymana- Elifköy stratigrafik profilleri hakkında. MTA Enstitüsü, Rapor no. 2748, Ankara
- Ghazi, S., Ali, A., Hanif, T., Sharif, S., Sajid, Z., Aziz, T., (2014). Microfacies and depositional setting of the early Eocene Chorgali Formation, Central Salt Range, Pakistan. Institute of Geology, Punjab University, Quaid-e-Azam Campus, Lahore Pakistan. *J Sci*, vol 66.
- Goldhammer, R. K., Dunn, P. A. and Hardie, L. A. (1990). Depositional cycles, composite sea-level changes, cycle stacking patterns, and their hierarchy of stratigraphic forcing: examples from Alpine Triassic platform carbonates. *Geol. Soc. of Am. Bull.*, 102, 663.
- Gökçen, S. L. (1976a). Ankara - Haymana güneyinin sedimantolojik incelenmesi I: stratigrafik birimler ve tektonik. Hacettepe Üni. Yer Bilimleri Ens. Yayın Organı, C. 2, No. 2, pp. 161-199.
- Gökçen, S. L. (1976b). Ankara-Haymana güneyinin sedimantolojik incelenmesi II: sedimantoloji ve paleoakıntılar. Hacettepe Üni. Yer Bilimleri Ens. Yayın Organı, C. 2, No. 2, pp. 201-235.
- Gökçen, S. L. (1977). Ankara-Haymana güneyinin sedimantolojik incelenmesi III: bölge tortullařma modeli ve paleocoğrafya. Hacettepe Üni. Yer Bilimleri Ens. Yayın Organı, C. 3, No. 1, 2, pp. 13-23.
- Görür, N., Oktay, F. Y., Seymen, İ., & Şengör, A. C. (1984). Paleotectonic evolution of the Tuzgölü Basin complex, central Turkey: Sedimentary record of the neotethyan closure. In J. Dixon, & A. F. Robertson, *The Geological Evolution of*

- the Eastern Mediterranean (pp. 467–481). London: Geological Society of London, Special Publications, 17.
- Görür, N., Tüysüz, O., and Celal Şengör, A. M. (1998). Tectonic evolution of the central Anatolian basins. *International Geology Review*, 40(9), 831–850.
<https://doi.org/10.1080/00206819809465241>
- Gülyüz, E., (2015). *Tectono-Stratigraphic and Thermal Evolution of the Haymana Basin, Central Anatolia, Turkey*. Ankara: MSc. Thesis, Middle East Technical University.
- Hadi, M., Mosaddegh, H., Abbassi, N., (2016). Microfacies and biofabric of nummulite accumulations (Bank) from the Eocene deposits of Western Alborz (NW Iran), *Journal of African Earth Sciences*
doi: 10.1016/j.jafrearsci.2016.09.012.
- Hadi, M., Sarkar, S., Vahidinia, M., Bayet-Goll, A. (2021). Microfacies analysis of Eocene Ziarat Formation (eastern Alborz zone, NE Iran) and paleoenvironmental implications, *All Earth* V:33:1 66–87
<https://doi.org/10.1080/27669645.2021.1956175>
- Hallock, P.(1981). *Production of Carbonate Sediments by Selected Large Benthic Foraminifera on Two Pacific Coral Reefs. SEPM Journal of Sedimentary Research, Vol. 51.*
doi:10.1306/212f7cb1-2b24-11d7-8648000102c1865d
- Hallock P., Glenn E., 1986. Larger foraminifera: a tool for paleoenvironmental analysis of Cenozoic depositional facies. *Palaios* 1:55–64.
- Hottinger, L. (1983). Processes determining the distribution of larger foraminifera in space and time. *Utrecht Micropaleontol Bull* 30:239–253.
- Hottinger, L. (1989). Conditions for generating carbonate platforms: *Memorie della Società Geologica Italiana*, v. 40, p. 265–271
- Hottinger, L. (1997). Shallow benthic foraminiferal assemblages as signals for depth of their deposition and their limitations. *Bull Soc Geol Fr* 168:491–505.
- Hottinger, L. (1998). Shallow benthic foraminifera at the Paleocene– Eocene boundary. *Strata* 9:61–64.
- Huseynov, A. (2007). *Sedimentary cyclicity in the Upper Cretaceous Successions of the Haymana Basin (Turkey): depositional sequences as response to relative sea-level changes*. Ankara: MSc. Thesis, Middle East Technical University.
- Karabeyoğlu, A. U., (2018). *Planktonic Foraminiferal Diversity and Abundance Changes Across Cretaceous-Paleocene Boundary Beds in the Haymana Basin and New Observations on the Extinction Horizon*. Ankara: MSc. Thesis, Middle East Technical University.

- Kaymakçı, N., 2000. Tectono-stratigraphical evolution of the Çankırı Basın (Central Anatolia, Turkey). *Geologica Ultraictina*, no. 190, 247 p.
- Ketin, İ., (1966). Anadolu'nun Tektonik Birlikleri, Maden Tetkik ve Arama (MTA) Dergisi, cilt 66, sayı 66, 20.
- Koçyiğit A. (1991). An example of an accretionary fore –arc basin from northern Central Anatolia and its implications for the history of subduction of Neo–Tethys in Turkey. *Geol Soc Am Bull*, 103, 22 - 36.
- Koçyiğit A., Özkan, S., Rojay F.B. (1988). Examples from the fore-arc basin remnants at the active margin of northern Neo –Tethys; development and emplacement ages of the Anatolian nappe, Turkey. *J Pure Appl Sci Ankara*, 21, 183- 210.
- Lahn E., (1949). Orta Anadolu'nun jeolojisi hakkında, TJK Bülteni, 1, 1
- Lokman K. ve Lahn D., (1946). Haymana bölgesi jeolojisi. MTA Dergisi, 36, 292-300.
- Matsumaru, K., (1997). On Pseudorbitoides Trechmanni Douville (orbitoidal foraminifera) from Turkey. *Revue de Micropaleontologie*, 40, 339-346.
- Matsumaru, K., (1999). Multiple Fission in Alveolina oblonga D'Orbigny in Turkey. *Revue de Micropaleontologie*, vol. 42, no. 3, pp. 245-251.
- Meriç E. ve Görür N., (1979-80). Haymana-Polatlı havzasındaki Çaldağ kireçtaşının kireçtaşının yaş konağı. MTA Dergisi, 93/94, 137-142.
- Mirza, K., (2015) Microfacies Analysis and Paleoenvironmental Interpretation of the Eocene Kohat Formation, Gumbat Section, Himalayan Fold and Thrust Belt, Northern Pakistan. EGU General Assembly 2015, Vol 17, EGU2015-2278
- Mitchum, R. M., Vail, P. R. and Thomson, S. (1977). Seismic stratigraphy and global changes of sea level, part 2: The depositional sequences as a basic unit of for stratigraphic analysis. Applications to Hydrocarbon Exploration: Association of Petroleum Geologist Memoir, 26, 53-62.
- Norman, T., Rad, M. R., (1971). Çayraz (Haymana) Civarındaki Harhor (Eosen) Formasyonunda Alttan Üste Doğru Doku Parametrelerinde ve Ağır Mineral Bolluk Derecelerinde Değişmeler. Türkiye Jeoloji Kurumu Bülteni, 14-2, 205-225.
- Okay A.I., Tansel, İ. & Tüysüz, O., (2001). Obduction, subduction and collision as reflected in the Upper Cretaceous-Lower Eocene sedimentary record of western Turkey. *Geological Magazine*, 138, 117-142.
- Okay, A. I., and Altıner, D. (2016). Carbonate sedimentation in an extensional active margin: Cretaceous history of the Haymana region, Pontides. *International Journal of Earth Sciences (Geologische Rundschau)*, 105, pp. 2013-2030.

- Orbigny, A. d' 1826. Tableau me ´thodique de la classe des Ce ´phalopodes. Annales des Sciences Naturelles, 7, 245–314.
- Osleger, D. and Read, J. F. (1991). Relation of eustacy to stacking patterns of meter-scale Carbonate cycles, late Cambrian, U.S.A. Journal of Sed. Pet., 61 (7), 1225-1252.
- Özcan, E., (2002). Cuisian orthophragminid assemblages (*Discocyclina*, *Orbitoclypeus* and *Nemkovella*) from the Haymana-Polatlı Basin (central Turkey): biometry and description of two new taxa. Eclogae Geol. Helv., 95,75-97.
- Özcan, E., Özkan-Altın S., (1997). Late Campanian – Maastrichtian evolution of orbitoidal foraminifera in Haymana Basin successions (Ankara, Central Turkey). Revue Paleobiol., Geneve, 16, (1), 271 – 290.
- Özcan, E., Özkan-Altın S., (1999a). The genera *Lepidorbitoides* and *Orbitoides*: evolution and stratigraphic significance in some Anatolian basins. Geological Journal, 34, 275 – 286.
- Özcan, E., Özkan-Altın S., (1999b). The Genus *Lepidorbitoides*: Evolution and Stratigraphic Significance in some Anatolian Basins (Turkey). Revue de Micropaleontologie, 42, 111-131.
- Özcan, E., Özkan-Altın S., (2001). Description of an early ontogenetic evolutionary step in *Lepidorbitoides*: *Lepidorbitoides bisambergensis asymmetrica* subsp. n., Early Maastrichtian (central Turkey) Rivista Italiana di Paleontologia e Stratigrafia, 107, 137-144.
- Özcan, E., Sirel E., Özkan S.A. and Çolakoğlu, S. (2001). Late Paleocene Orthophragminae (foraminifera) from the Haymana – Polatlı Basin, (central Turkey) and description of a new taxon, *Orbitoclypeus haymanaensis* Micropaleontology, 47, 339- 357.
- Özcan, E., Gyorgy L., and Botond, K., (2007). Late Ypresian to Middle Lutetian Orthophragminid Record From Central and Northern Turkey: Taxonomy and Remarks on Zonal Scheme. Turkish Journal of Earth Sciences, vol. 16, pp. 281-318.
- Özcan, E., Hakyemez, A., Çiner, A., Okay, A. I., Soussi, M., (2020). Reassessment of the age and depositional environments of the Eocene Çayraz formation, a reference unit for Tethyan larger benthic foraminifera (Haymana Basin, central Turkey). Journal of Asian Earth Sciences, vol. 193, article. 104304.
- Özdemir, A. (2019). Mollaresul Formasyonunun (Haymana-Ankara) Petrol Hazne Kaya Özellikleri. Türkiye Jeoloji Bülteni , 62 (2) , 181-198 .
- doi: 10.25288/tjb.567893
- Özgen-Erdem, N., İnan, N., Akyazı, M., Tunoğlu, C., (2005). Benthonic foraminiferal assemblages and microfacies analysis of Paleocene–Eocene carbonate rocks in

the Kastamonu region, Northern Turkey. *Journal of Asian Sciences*, 25(3), 403-417.

<https://doi.org/10.1016/j.jseaes.2004.04.005>

Özkan-Altın S., Özcan, E., (1999). Upper Cretaceous planktonic foraminiferal biostratigraphy from NW Turkey: calibration of the stratigraphic ranges of larger benthonic foraminifera. *Geological Journal*, 34, 287 – 301.

Özkaptan, M., (2016). *Post-Late Cretaceous Rotational Evolution of Neotethyan Sutures around Ankara Region*. Ankara: MSc. Thesis, Middle East Technical University.

Payros, A., Pujalte, V., Tosquella, J., Orue-Etxebarria, X., (2010). The Eocene storm-dominated foralgal ramp of the western Pyrenees (Urbasa– Andia Formation): an analogue of future shallow-marine carbonate systems? *Sediment Geol* 228:184–204

Pearson, P. N., van Dongen, B. E., Nicholas, C. J., Pancost, R. D., Schouten, S., Singano, J. M., Wade, B. S., (2007). Stable warm tropical climate through the Eocene Epoch, *Geology*, 35 (3): 211-214.

<https://doi.org/10.1130/G23175A.1>

Pomar, L., (2001) Types of carbonate platforms: a genetic approach. *Basin Res* 13:313–334

Racey A (1994) Biostratigraphy and palaeobiogeographic significance of Tertiary nummulitids (Foraminifera) from northern Oman. In: Simmons MD (ed) *Micropalaeontology and hydrocarbon exploration in the Middle East*. Chapman and Hall, London, pp 343–370

Racey A (2001) A review of Eocene nummulite accumulations: structure, formation and reservoir potential. *J Pet Geol* 24:79–100

Ray, D. C., Simmons, M., van Buchem, F.S.P., Baines, G., Davies, A., Greselle, B., Robson, C. (2020). *Exploration Insights*, Oxfordshire, May.

Rojay, B., (2013). Tectonic evolution of the Cretaceous Ankara Ophiolitic Melange during the Late Cretaceous to pre-Miocene interval in Central Anatolia, Turkey, *J Geodyn*, 65, p. 66-81.

Reckamp, J., U., Özbey, S., (1960), *Petroleum geology of Temelli and Kuştepe structures, Polatlı area*. Pet. İş. Gen. Md., Ankara.

Rigo de Righi, M., Cortesini, A., (1959), *Regional studies in central Anatolian basin*. Progress Report 1, Turkish Gulf Oil Co., Pet. İş. Gen. Md., Ankara.

Sames, B., Wagreich, M., Wendler, J. E., Haq, B. U., Conrad, C.P., Melinte-Debrinescu, M. C., Hu, X., Wendler, I., Yılmaz, İ. Ö., Zorina, S. O., (2016). Review: Short-term sea-level changes in a greenhouse world- A view from the Cretaceous. *Paleogeography, Paleoclimatology, Paleoecology* 441, 393-411.

- Sarg J. F., (1988). Carbonate sequence stratigraphy. SEPM Spec Publ 42:155–188.
- Schmidt, G. C., (1960), AR/MEM/365-266-367 sahalarının nihai terk raporu. Pet. İş. Gen. Md., Ankara.
- Sirel, E. (1975). Polatlı (GB Ankara) güneyinin stratigrafisi / Stratigraphy of the south of Polatlı (SW Ankara). *Türkiye Jeoloji Kurumu Bülteni / Bulletin of the Geological Society of Turkey*, v. 18, pp. 181-192.
- Sirel, E. (1976a). Polatlı (GB Ankara) güneyinde bulunan Alveolina, Nummulites, Ranikothalia ve Assilina cinslerinin bazı türlerinin sistematik incelemeleri. TJK Bülteni, 19/2, p. 89- 103.
- Sirel, E. (1976b). Description of six new species of the Alveolina found in the South of Polatlı (SW Ankara) region. TJK Bülteni, 19, p. 19-22.
- Sirel, E. (1976c). Haymana (G Ankara) yöresi İlerdiyen, Küziyen ve Lütisiyen'deki Nummulites, Assilina ve Alveolina cinslerinin bazı türlerinin tanımlamaları ve stratigrafik dağılımları. TJK Bülteni, 19, p. 31-44.
- Sirel, E. (1998). *Foraminiferal description and biostratigraphy of the Paleocene-Lower Eocene shallow-water limestones and discussion on the Cretaceous-Tertiary boundary in Turkey*. General Directorate of the Mineral Research and Exploration, Monography Series, 2, 117 p.
- Sirel, E., (1999). Four new genera (*Haymanella*, *Kayseriella*, *Elazigella* and *Orduella*) and one new species of *Hottingerina* from the Paleocene of Turkey *Micropaleontology*, 42, 113 – 137.
- Sirel, E., Gündüz, H. (1976). Description and stratigraphical distribution of the some species of the genera Nummulites, Assilina and Alveolina from the Ilerdian, Cuisian and Lutetian of the Haymana region. Bull Geol Soc Turkey 19, 31 – 44.
- Snedden, J.W. and Liu, C. (2010). A Compilation of Phanerozoic Sea-Level Change, Coastal Onlaps and Recommended Sequence Designations. Search and Discovery, Article ID: 40594.
- Snedden, J.W. and Liu, C., (2011). Recommendation for a uniform chronostratigraphic designation system for phanerozoic depositional sequences. American Association of Petroleum Geologists Bulletin 95. 1095-1122.
- Şengör, A., & Yılmaz, Y. (1981). Tethyan evolution of Turkey: a plate tectonic approach. Tectonophysics, 75, pp. 181-241.
- Tanık, G., (2017). *Upper Paleocene-Lowermost Eocene Planktonic Foraminiferal Biostratigraphy and Record of the Paleocene- Eocene Thermal Maximum in the Haymana Basin (Ankara, Turkey)*. Ankara: MSc. Thesis, Middle East Technical University.

- Toker, V. (1975). *Haymana yöresinin (SW Ankara) planktonik foraminifera ve nannoplanktonlarla biyostratigrafik incelenmesi*. Ankara, PhD. Thesis: Ankara Üni. Fen Fak.
- Toker, V. (1977). Haymana ve Kavak formasyonlarındaki planktonik foraminifera ve nannoplanktonlar. *TÜBİTAK VI. Bilim Kongresi Tebliğleri*, pp. 57-70.
- Toker V., (1979). Upper Cretaceous Planktonic Foraminifera and the biostratigraphic investigations of the Haymana area. *Bulletin of the Geological Society of Turkey*, 22, 121 – 132.
- Toker, V. (1980). Haymana yöresi (GB Ankara) nannoplankton biyostratigrafisi. *TJK Bülteni*, 23/2, p. 165-178.
- Ünalın G., Yüksel V., Tekeli T., Gonenç O., Seyirt Z., Hüseyin S. (1976). Upper Cretaceous – Lower Tertiary stratigraphy and paleogeographic evolution of Haymana – Polatlı region (SW Ankara). *Turkish Geol Soc Bull*19,159 – 176.
- Ünalın G., Yüksel V., (1985). Haymana-Polatlı havzasının jeolojisi ve petrol olanakları. *MTA Petrol ve Jeotermal Enerji Dairesi Raporu*.
- Vail, P. R., Mitchum Jr., R. M., and Thompson III, S. (1977). Seismic stratigraphy and global changes of sea level: Part 3, Relative changes of sea level from coastal onlap: Section 2, Application of seismic reflection configuration to stratigraphic interpretation, in Payton, C. E. (ed.), *Seismic stratigraphy: Applications to hydrocarbon exploration: American Association of Petroleum Geologists Memoirs* 26, p. 63–81.
- Vail, P. R. (1987). Seismic stratigraphic interpretation using sequence stratigraphy. Part 1: Seismic stratigraphy interpretation procedure, in A. W. Bally, ed., *Atlas of Seismic Stratigraphy: American Association of Petroleum Geologists Studies in Geology*, v. 27-1, p. 1-10.
- Van Wagoner, J. C., Posamentier, H. W., Mitchum, R. M., Vail, P. R., Sarg, J. F., Loutit, T. S., and Hardenbol, J. (1988). An overview of the fundamentals of sequence stratigraphy and key definitions, in Wilgus, C. K., Hastings, B. S., Kendall, C. G. St. C., Posamentier, H. W., Ross, C. A. and Van Wagoner, J. C. (eds.), *Sea-level changes: An integrated approach: SEPM Special Publication* 42, p. 39–46.
- Vardar, E., (2018). *Deep Sea Benthic Foraminiferal Diversity and Abundance Change Across Cretaceous- Paleogene Boundary Beds in the Haymana Basin (Ankara, Turkey): Paleoenvironmental Implications*. Ankara: MSc. Thesis, Middle East Technical University.
- Vaziri-Moghaddam, H., Kimiagari, M., Taheri, A., (2006). Depositional environment and sequence stratigraphy of the Oligo-Miocene Asmari Formation in SW Iran. *Facies* 52(1): 41-51

doi: 10.1007/s10347-005-0018-0

- Wade, B.S., Pearson, P.N., Berggren, W.A. and Pälike, H. (2011). Review and revision of Cenozoic tropical planktonic foraminiferal biostratigraphy and calibration to the geomagnetic polarity and astronomical time scale. *Earth-Science Reviews*, 104(1- 3), pp.111-142.
- Wilson, J. L. (1975). *Carbonate Facies in Geologic History*: New York, Springer, 471 p.
- Weber M. E., Fenner J., Thies A. and Cepek P. (2001). Biological response to Milankovitch forcing during the Late Albian (Kirchrode I borehole, northwest Germany). *Paleogeography, Paleoclimatology, Palaeoecology*, 174, 269-286.
- Yüksel, S., 1970, *Etude géologique de la region d'Haymana (Turquie Centrale)*. Thèse Fac. Sci. Univ. De Nancy, p. 1-179.

APPENDICES

A. PLATES

PLATE 1

Nummulites sp.; nearly axial sections except h is equatorial section.

a: NB1

b: NB4

c, d, e, f, g, i: NB5

h: NB6

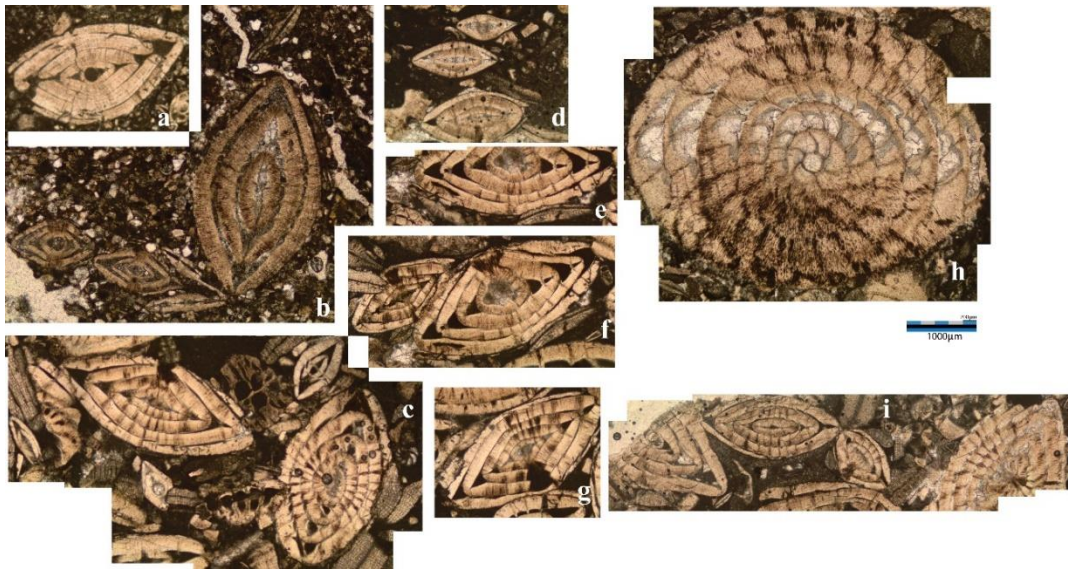


PLATE 2

Assilina sp.; nearly axial sections.

a: NB5

b: NB11

c: NB34

d: NB15

e: NB33



PLATE 3

Discoyclina sp.; nearly axial sections.

a: NB5

b: NB2-B

c: NB1

d: NB1

e: NB2-B

f: NB-B-1

g: NB1

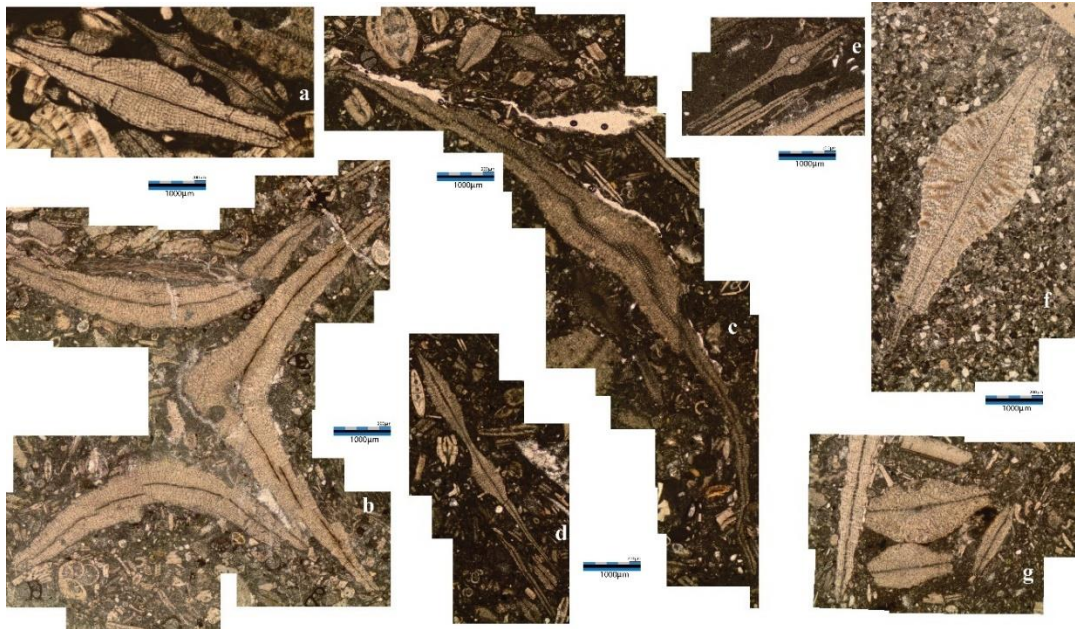


PLATE 4

Alveolina sp.; nearly axial sections ; except c is oblique section.

- a: NB34
- b: NB36
- c: NB36
- d: NB30-B
- e: NB18
- f: NB30-A

g: NB11

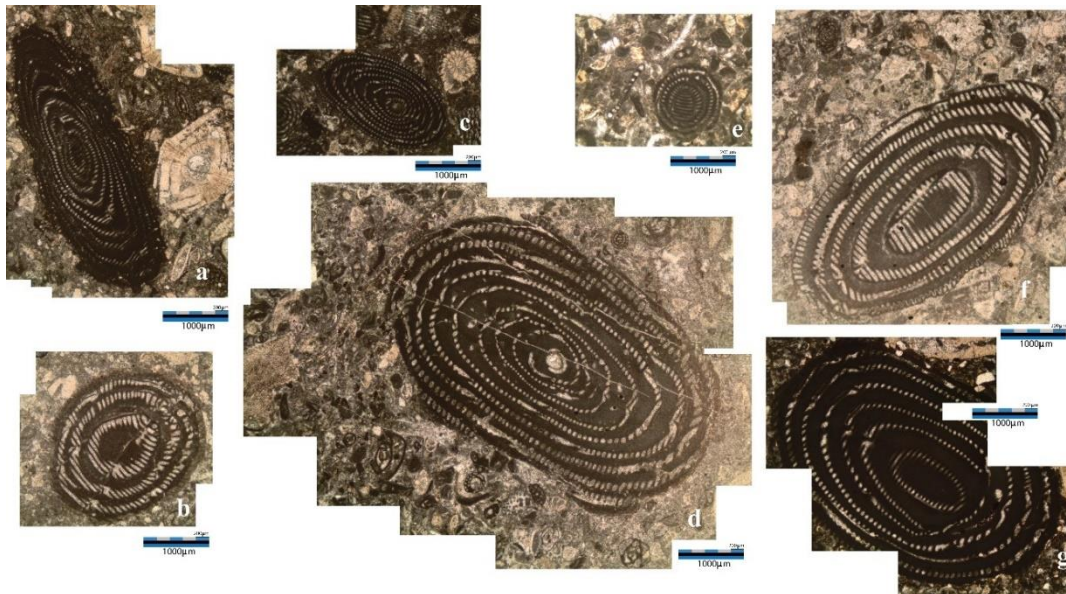


PLATE 5

Miliolid; equatorial sections (b, e, f, i); oblique sections (a, c, d, g); axial section (h).

a: NB18

b: NB19

c: NB7

d: NB17

e: NB19

f: NB7

g: NB18

h: NB7

i: NB19

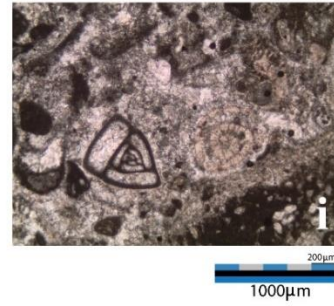
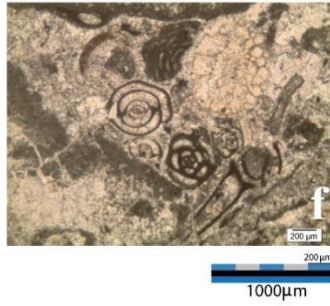
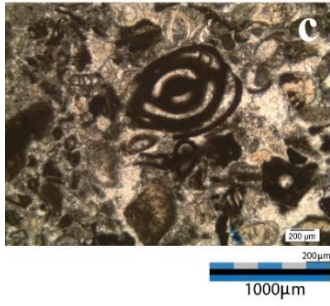
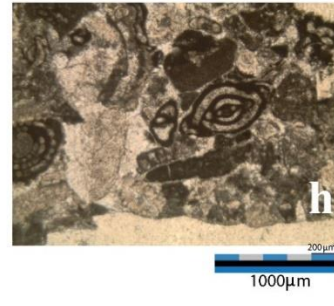
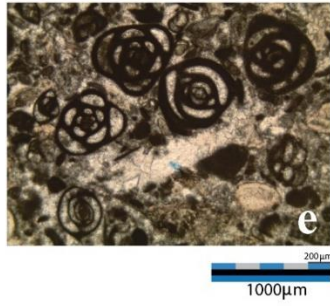
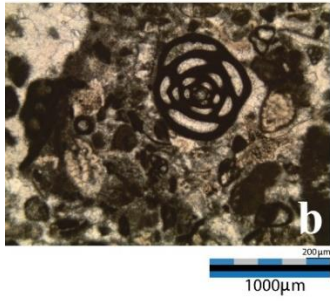
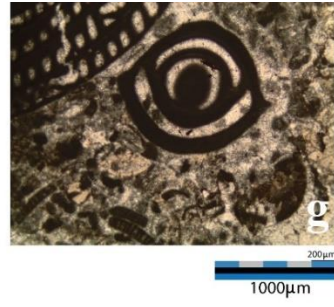
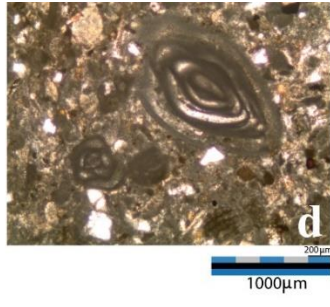
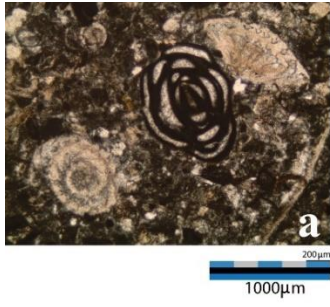


PLATE 6

Orbitolites sp.; oblique sections.

a: NB35

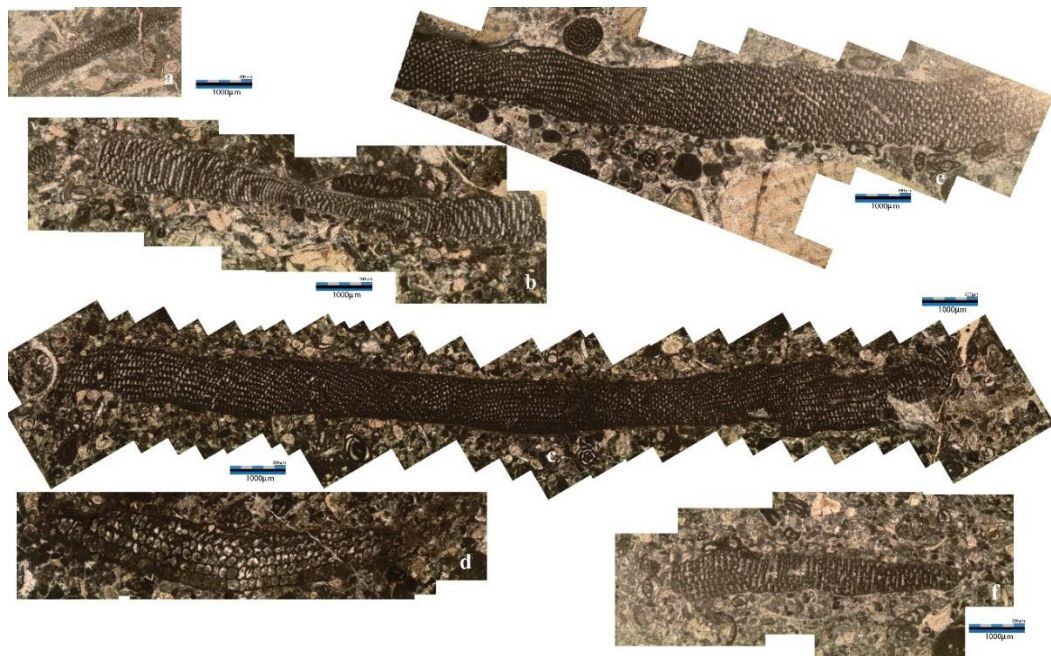
b: NB36

c: NB30-B

d: NB30-B

e: NB19

f: NB30-B



B. Stratigraphical distribution of fossil assemblages in the measured section

1. Stratigraphical & environmental distribution of fossil assemblages in the part of the measured from samples NB0 to NB7

D: *Discocyclus* sp., As: *Assilina* sp., N: *Nummulites* sp., Alv: *Alveolina* sp., O: *Orbitolites* sp., M: Miliolid, CRA: Coralline Red Algae, E: Echinoid, L: *Lockhartia* sp., R: Rotaliniid, bf: benthic foraminifera, pf: planktonic foraminifera, Agg: agglutinated foraminifera, Di: *Ditrupa* sp., Bi: Biserial (*Textularina* sp.), Uni: uniserial form, Pel: Pelecypods, Bry: Bryozoa, S: sand content, M: mineral growth

white square indicates presence of the fossil, light pink color: mudstone

light orange color: sandstone

light blue: limestone at shallow and restricted part of the ramp,

mid blue: limestone near shoal,

dark blue: limestone deposited at distal part of the ramp

3. Stratigraphical & environmental distribution of fossil assemblages in the part of the measured from samples NB8 to NB43

D: *Discocyclus* sp., As: *Assilina* sp., N: *Nummulites* sp., Alv: *Alveolina* sp., O: *Orbitolites* sp., M: Miliolid, CRA: Coralline Red Algae, E: Echinoid, L: *Lockhartia* sp., R: Rotaliniid, bf: benthic foraminifera, pf: planktonic foraminifera, Agg: agglutinated foraminifera, Di: *Ditrupa* sp., Bi: Biserial (*Textularina* sp.), Uni: uniserial form, Pel: Pelecypods, Bry: Bryozoa, S: sand content, M: mineral growth

white square indicates presence of the fossil,

light pink color: mudstone,

light orange color: sandstone,

light blue: limestone at shallow and restricted part of the ramp,

mid blue: limestone near shoal,

dark blue: limestone deposited at distal part of the ramp,

light purple: reappearance of the *discocyclus* sp. at the limestone sequence

Table 2 GPS data of the measured section from sample NB1 to NB43, gathered from "BasicAirData GPS Logger" application

Sample Number	North	East	Altitude (m)
NB1	39 4912	32 5012	1179
NB2-A	39 4912	39 5012	1182
NB2- B	39 4912	32 5012	1182
NB2	39 4912	32 5012	1183
NB3	39 4915	32 5013	1188
NB4	39 4915	39 5013	1189
NB8	39 4919	32 5018	1210
NB9	39 4920	32 5018	1211
NB10	39 4920	32 5018	1214
NB11	39 4920	32 5018	1214
NB12	39 4920	32 5018	1216
NB13	39 4921	32 5015	1216
NB28	39 4922	32 5016	1229
NB30-A	39 4923	32 5015	1218
NB30-B	39 4923	32 5016	1220
NB29	39 4923	32 5029	1221
NB30	39 4923	32 5029	1221
NB32	39 4923	32 5030	1224
NB33	39 4919	32 5040	1213
NB34	39 4920	32 5041	1219
NB35	39 4920	32 5042	1222
NB36	39 4920	32 5043	
NB37	39 4920	32 5044	1221
NB38	39 4919	32 5045	1228
NB39	39 4913	32 5051	
NB40	39 4910	32 5055	1233
NB41	39 4907	32 5059	1228
NB42	394907	325063	1223
NB43	394908	325065	1221

